Rôle des ribosomes et de la traduction dans la régulation post-transcriptionnelle de l'expression des gènes au cours de la réponse immunitaire

Emiliano P. Ricci

▶ **To cite this version:**

Emiliano P. Ricci. Rôle des ribosomes et de la traduction dans la régulation post-transcriptionnelle de l'expression des gènes au cours de la réponse immunitaire. Cellular Biology. École Normale Supérieure de Lyon, 2020. ⟨tel-04917624⟩

HAL Id: tel-04917624

https://hal.science/tel-04917624v1

Submitted on 28 Jan 2025

HAL is a multi-disciplinary open access archive for the deposit and dissemination of scientific research documents, whether they are published or not. The documents may come from teaching and research institutions in France or abroad, or from public or private research centers.

L'archive ouverte pluridisciplinaire **HAL**, est destinée au dépôt et à la diffusion de documents scientifiques de niveau recherche, publiés ou non, émanant des établissements d'enseignement et de recherche français ou étrangers, des laboratoires publics ou privés.

HAL Authorization

Mémoire d'habilitation à diriger des recherches

Rôle des ribosomes et de la traduction dans la régulation post-transcriptionnelle de l'expression des gènes au cours de la réponse immunitaire

Emiliano Ricci

CRCN Inserm
Laboratoire de Biologie et Modélisation de la Cellule (LBMC)
UMR5239 U1210 / ENS de Lyon / Université de Lyon

Jury

Dr. Caroline Goujon (Pré-rapporteur)
Dr. Stefania Millevoi (Pré-rapporteur)
Dr. Jérôme Cavaillé (Pré-rapporteur)
Dr. Olivier Namy
Dr. Pierre-Emmanuel Gleizes
Pr. Bertrand Mollereau

Table of contents

Curriculum Vitae....4
Research Supervision....9
Previous work and main achievements....11
I. Graduate work....11
1. Translational control of the genomic RNA from Human Immunodeficiency Virus Type 2 (HIV-2):....11
2. Dissecting the mechanism of action of microRNAs in repressing mRNA translation:....13
3. Translation stimulation of unspliced mRNAs by the Epstein-Barr virus nuclear-export factor protein EB2:....14
II. Postdoctoral work....16
1. Characterizing the role of the double-stranded RNA-binding protein Staufen1 in regulating gene expression:....16
2. Role of long non-coding RNAs in regulating the innate immune response:....18
Current Research and projects....19
A viral-derived protein delivery system to mediated efficient genome-editing in primary cells. .20
Assessing the role of ribosomes and mRNA translation in shaping the immune response....22
Aim 1. The atlas of ribosome-associated proteins in the course of macrophage stimulation and its impact on the inflammatory response:....25
Aim 2. Cross-talks between ribosomes and translation with mRNA decay pathways:....26
Aim 3. Coordination between cytosolic and mitochondrial translation during immune cell activation:....27
Methodology and preliminary results....27
Aim1. The atlas of ribosome-associated proteins in the course of macrophage stimulation and its impact on the inflammatory response:....27
Aim2. Cross-talks between ribosomes and translation with mRNA decay pathways:....31
Aim3. Testing the potential coordination between cytosolic and mitochondrial translation during immune cell activation:....37
General conclusion and perspectives....39
References....40
Selected Publications....45

Curriculum Vitae

Ricci Emiliano, Ph.D.

Date of birth: 02.10.1983
Citizenship: Italian
Current position: Chargé de Recherche classe normale - INSERM
Phone: 0783069389
e-mail: emiliano.ricci@ens-lyon.fr

EDUCATION

2006-2010 **Ph.D. : Molecular Biology and Virology**
Ecole Normale Supérieure de Lyon (France). Under the supervision of Dr. Théophile Ohlmann

2004-2006 **Master degree: Molecular and Cellular Biology (*Summa Cum laude*)**
Ecole Normale Supérieure de Lyon (France) / Imperial College London (Erasmus programme)

2001-2004 **Bachelor of Science: Molecular and Cellular Biology (Magna *Cum laude*)**
Université Claude Bernard Lyon / Ecole Normale Supérieure de Lyon (France).

RESEARCH EXPERIENCE

Since January 2019: **Chargé de Recherche (INSERM) & *Group leader "RNA metabolism in immunity and infection (RMI²)"*.** Laboratoire de Biologie et de Modélisation Cellulaire (LBMC UMR5239 – ENS Lyon).

2015-2018: **Chargé de Recherche (INSERM) – Team "Translation of Eukaryotic and Viral mRNAs" lead by Dr. Théophile Ohlmann.**
Centre International de Recherche en Infectiologie (CIRI U1111 – ENS Lyon).

2010-2014: **Postdoctoral associate: Post-transcriptional control of gene expression.**
University of Massachusetts Medical School (Worcester, MA. USA). Laboratory of Prof. Melissa Moore.

2006-2010: **Graduate student: Investigation of the molecular mechanisms of microRNA-mediated regulation of mRNA translation.**
Laboratoire de Virologie Humaine (U759 – ENS Lyon). Under supervision of Théophile Ohlmann.

AWARDS

2010: Graduate Student Prize* (Ecole doctorale BMIC – Lyon)*: 1500€

FUNDING

2019-2023: **Starting Grant – European Research Council, 1,5M€.** Assessing the role of ribosomes and mRNA translation in shaping the inflammatory response.

2019-2021: **ATIP-Avenir, No funds received but official program grantee.** Assessing the role of ribosomes and mRNA translation in shaping the inflammatory response.

2019-2010: **Fondation Finovi, appel d'offre n°13 (Associated partner), 10k€.** Epigenetic control of inflammatory response: role in the immunoregulation of severe infections.

2016-2018: **ANRS (PI), 125k€ + one postdoctoral position funded for 3 years.** Functional coupling of mRNA splicing and translation during the course of HIV-1 infection.

2016-2017: **Labex Ecofect (PI), 50k€.** Using modified virus-like particles from Murine Leukemia Virus to deliver the Cas9/sgRNA ribonucleoprotein in cultured cells and *in vivo*.

2016-2017: **Fondation FINOVI, accueil jeunes chercheurs (PI), 25k€:** Atlas of proteins and RNAs bound to the HIV-1 genomic RNA.

2016-2017: **Ligue contre le Cancer (Associated partner),10k€:** Inhibition of Nonsense Mediated mRNA Decay (NMD), and its impact on tumorigenesis *in vivo*.

2009-2010: **Fondation pour la Recherche Médicale:** 4th year Ph.D. fellowship.

2006-2009: **French Ministry for Research:** Ph.D. fellowship.

COMMISSIONS OF TRUST AND PEER-REVIEW DUTIES

2018-2020: **External ad honorem referee to the Academic Board of the PhD program in Biomedical Sciences, School of Medicine, University of Chile, Chile.**

2020: **Reviewer for the European Research Council (ERC Starting Grant).**

2019: **Reviewer for the National Science Center Poland (NCN) grant proposals.**

2014-2019, Reviewer for: **Nature Communications, Journal of Biological Chemistry, Journal of Proteomics, Gene Therapy, Frontiers Cellular and Infection Microbiology, Transactions of the Biochemical Society, Methods.**

2016-2020: **Member of the thesis committee of three Ph.D students.**

INVITED ORAL COMMUNICATIONS

December 8, 2016 **(CRISPR Therapeutics, Cambridge Massachusetts -USA: Invited by Dr. Tirtha Chakraborty):** Efficient delivery of the Cas9/guideRNA Ribonucleoprotein in primary cells and in vivo using modified Virus-like particles.

January 14, 2016 **(I-STEM: Institute for Stem cell Therapy and Exploration of Monogenic Diseases, Evry - France: Invited by Dr. Christian Pinset):** Transcriptome-wide analysis of translation dependent mRNA decay during T cell activation.

October 16, 2015 **(Université Toulouse III, Paul Sabatier - France: Invited by Dr. Pierre-Emmanuel Gleizes):** The dsRBP Staufen1 senses overall transcript secondary structure to regulate mRNA translation.

September 29, 2015 **(Universidad de Chile - Chile, The complex-life of mRNA Symposium: Invited by Dr. Ricardo Soto-Rifo):** Transcriptome-wide analysis of translation dependent mRNA decay during T cell activation.

September 24, 2015 **(Annual meeting of the Chilean Biochemistry and Molecular Biology Society - Chile. Invited by Dr. Marcelo Lopez-Lastra):** RIPiT-seq reveals the endogenous binding sites of the RNA Helicase DDX3.

September 25, 2014 **(Annual meeting of the Chilean Biochemistry and Molecular Biology Society - Chile. Invited by Dr. Marcelo Lopez-Lastra):** Dissecting microRNA mechanisms of action to better understand their role in disease.

PATENTS

1. Mangeot P, Ohlmann T, **Ricci EP.** Methods and products for genetic engineering. Publication number (2017). WO2017068077A1. (Prise de license en négociation).

2. **Ricci EP**, Heyer E, Ozadam H, Cenik C, Moore MJ. Compositions and Methods for Constructing cDNA Libraries that Allow for Mapping the 5' and 3' Ends of RNAs (2015). US20150099671A1.

PUBLICATIONS

1. **Ribosomes guide pachytene piRNA formation on long intergenic piRNA precursors.** Sun YH, Zhu J, Xie LH, Li Z, Meduri R, Zhu X, Song C, Chen C, **Ricci EP**, Weng Z, Li XZ. **Nat Cell Biol.** 2020 Feb.22(2):200-212.

2. **Staphylococcus aureus Small Colony Variants (SCVs): News From a Chronic Prosthetic Joint Infection.** Loss G, Simões PM, Valour F, Cortês MF, Gonzaga L, Bergot M, Trouillet-Assant S, Josse J, Diot A, **Ricci EP**, Vasconcelos AT, Laurent F. **Front Cell Infect Microbiol.** 2019 Oct.22;9:363.

3. **A cohesin/HUSH- and LINC-dependent pathway controls ribosomal DNA double-strand break repair.** Marnef A, Finoux AL, Arnould C, Guillou E, Daburon V, Rocher V, Mangeat T, Mangeot PE, **Ricci EP**, Legube G. **Genes Dev.** 2019 Sep.1;33(17-18):1175-1190.

4. **Senataxin homologue Sen1 is required for efficient termination of RNA polymerase III transcription.** Rivosecchi J, Larochelle M, Teste C, Grenier F, Malapert A, **Ricci EP**, Bernard P, Bachand F, Vanoosthuyse V. **EMBO J.** 2019 Aug 15;38(16):e101955.

5. **System-wide Profiling of RNA-Binding Proteins Uncovers Key Regulators of Virus Infection.** Garcia-Moreno M, Noerenberg M, Ni S, Järvelin AI, González-Almela E, Lenz CE, Bach-Pages M, Cox V, Avolio R, Davis T, Hester S, Sohier TJM, Li B, Heikel G, Michlewski G, Sanz MA, Carrasco L, **Ricci EP**, Pelechano V, Davis I, Fischer B, Mohammed S, Castello A. **Mol Cell.** 2019 Apr 4;74(1):196-211.e11.

6. **Genome editing in primary cells and in vivo using viral-derived Nanoblades loaded with Cas9-sgRNA ribonucleoproteins.** Mangeot PE*, Risson V, Fusil F, Marnef A, Laurent E, Blin J, Mournetas V, Massouridès E, Sohier TJM, Corbin A, Aubé F, Teixeira M, Pinset C, Schaeffer L, Legube G, Cosset FL, Verhoeyen E, Ohlmann T, **Ricci EP***. **Nat Commun.** 2019 Jan 3;10(1):45. * Corresponding authors.

7. **The long noncoding RNA CHROME regulates cholesterol homeostasis in primate.** Hennessy EJ, van Solingen C, Scacalossi KR, Ouimet M, Afonso MS, Prins J, Koelwyn GJ, Sharma M, Ramkhelawon B, Carpenter S, Busch A, Chernogubova E, Matic LP, Hedin U, Maegdefessel L, Caffrey BE, Hussein MA, **Ricci EP**, Temel RE, Garabedian MJ, Berger JS, Vickers KC, Kanke M, Sethupathy P, Teupser D, Holdt LM, Moore KJ. **Nat Metab.** 2019 Jan;1(1):98-110.

8. **PDZ domain-binding motif of Tax sustains T-cell proliferation in HTLV-1-infected humanized mice.** Pérès E, Blin J, **Ricci EP**, Artesi M, Hahaut V, Van den Broeke A, Corbin A, Gazzolo L, Ratner L, Jalinot P, Duc Dodon M. **PLoS Pathog.** 2018 Mar 22;14(3):e1006933.

9. **When mRNA translation meets decay.** Bicknell AA*, **Ricci EP***. **Biochem Soc Trans.** 2017 Apr 15;45(2):339-351. * Corresponding authors.

10. **microRNAs stimulate translation initiation mediated by HCV-like IRESes.** Mengardi C, Limousin T, **Ricci EP**, Soto-Rifo R, Decimo D, Ohlmann T. **Nucleic Acids Res.** 2017 May 5;45(8):4810-4824.

11. **An intimate look at the viral replication cycle through ribosome profiling.** Blin J, **Ricci EP***. Med Sci (Paris). 2016 Oct;32(10):849-860. * Corresponding author.

12. **A Long Noncoding RNA lincRNA-EPS Acts as a Transcriptional Brake to Restrain Inflammation.** Atianand MK, Hu W, Satpathy AT, Shen Y, **Ricci EP**, Alvarez-Dominguez JR, Bhatta A, Schattgen SA, McGowan JD, Blin J, Braun JE, Gandhi P, Moore MJ, Chang HY, Lodish HF, Caffrey DR, Fitzgerald KA. **Cell.** 2016 Jun 16;165(7):1672-1685.

13. **Biogenesis and function of tRNA fragments during sperm maturation and fertilization in mammals.** Sharma U, Conine CC, Shea JM, Boskovic A, Derr AG, Bing XY, Belleannee C, Kucukural A, Serra RW, Sun F, Song L, Carone BR, **Ricci EP**, Li XZ, Fauquier L, Moore MJ, Sullivan R, Mello CC, Garber M, Rando OJ. **Science.** 2016 Jan 22;351(6271):391-396.

14. **Integrative analysis of RNA, translation, and protein levels reveals distinct regulatory variation across humans.** Cenik C, Cenik ES, Byeon GW, Grubert F, Candille SI, Spacek D, Alsallakh B, Tilgner H, Araya CL, Tang H, **Ricci E**, Snyder MP. **Genome Res.** 2015 Nov;25(11):1610-21.

15. **An optimized kit-free method for making strand-specific deep sequencing libraries from RNA fragments.** Heyer EE, Ozadam H, **Ricci EP**, Cenik C, Moore MJ. **Nucleic Acids Res.** 2015 Jan;43(1):e2.

16. **HIV-2 genomic RNA accumulates in stress granules in the absence of active translation.** Soto-Rifo R, Valiente-Echeverria F, Rubilar PS, Garcia-de-Gracia F, **Ricci EP**, Limousin T, Décimo D, Mouland AJ, Ohlmann T. **Nucleic Acids Res.** 2014 Nov 10;42(20):12861-75.

17. **Post-transcriptional regulation of gene expression in innate immunity.** Carpenter S*, **Ricci EP***, Mercier BC*, Moore MJ, Fitzgerald KA. Nat Rev Immunol. 2014 Jun;14(6):361-76. * Equal contribution.

18. **Staufen1 senses overall transcript secondary structure to regulate translation. Ricci EP**, Kucukural A, Cenik C, Mercier BC, Singh G, Heyer EE, Ashar-Patel A, Peng L, Moore MJ. **Nat Struct Mol Biol.** 2014 Jan;21(1):26-35.

19. **RIPiT-Seq: a high-throughput approach for footprinting RNA:protein complexes.** Singh G, **Ricci EP**, Moore MJ. **Methods.** 2014 Feb;65(3):320-32.

20. **A long noncoding RNA mediates both activation and repression of immune response genes.** Carpenter S, Aiello D, Atianand MK, **Ricci EP**, Gandhi P, Hall LL, Byron M, Monks B, Henry-Bezy M, Lawrence JB, O'Neill LA, Moore MJ, Caffrey DR, Fitzgerald KA. **Science.** 2013 Aug 16;341(6147):789-92.

21. **miRNA repression of translation in vitro takes place during 43S ribosomal scanning.** **Ricci EP**, Limousin T, Soto-Rifo R, Rubilar PS, Decimo D, Ohlmann T. **Nucleic Acids Res.** 2013 Jan 7;41(1):586-98.

22. **The Andes hantavirus NSs protein is expressed from the viral small mRNA by a leaky scanning mechanism.** Vera-Otarola J, Solis L, Soto-Rifo R, **Ricci EP**, Pino K, Tischler ND, Ohlmann T, Darlix JL, López-Lastra M. **J Virol.** 2012 Feb;86(4):2176-87.

23. **Different effects of the TAR structure on HIV-1 and HIV-2 genomic RNA translation.** Soto-Rifo R, Limousin T, Rubilar PS, **Ricci EP**, Décimo D, Moncorgé O, Trabaud MA, André P, Cimarelli A, Ohlmann T. **Nucleic Acids Res.** 2012 Mar;40(6):2653-67.

24. **Activation of a microRNA response in trans reveals a new role for poly(A) in translational repression.** **Ricci EP**, Limousin T, Soto-Rifo R, Allison R, Pöyry T, Decimo D, Jackson RJ, Ohlmann T. **Nucleic Acids Res.** 2011 Jul;39(12):5215-31.

25. **The 3' untranslated region of the Andes hantavirus small mRNA functionally replaces the poly(A) tail and stimulates cap-dependent translation initiation from the viral mRNA.** Vera-Otarola J, Soto-Rifo R, **Ricci EP**, Ohlmann T, Darlix JL, López-Lastra M. **J Virol.** 2010 Oct;84(19):10420-4.

26. **Structural and functional diversity of viral IRESes.** Balvay L, Soto Rifo R, **Ricci EP**, Decimo D, Ohlmann T. **Biochim Biophys Acta.** 2009 Sep-Oct;1789(9-10):542-57.

27. **Translation of intronless RNAs is strongly stimulated by the Epstein-Barr virus mRNA export factor EB2.** **Ricci EP**, Mure F, Gruffat H, Decimo D, Medina-Palazon C, Ohlmann T, Manet E. **Nucleic Acids Res.** 2009 Aug;37(15):4932-43.

28. **Lentiviral RNAs can use different mechanisms for translation initiation.** **Ricci EP**, Soto Rifo R, Herbreteau CH, Decimo D, Ohlmann T. **Biochem Soc Trans.** 2008 Aug;36(Pt 4):690-3.

29. **In vitro expression of the HIV-2 genomic RNA is controlled by three distinct internal ribosome entry segments that are regulated by the HIV protease and the Gag polyprotein.** **Ricci EP**, Herbreteau CH, Decimo D, Schaupp A, Datta SA, Rein A, Darlix JL, Ohlmann T. **RNA.** 2008 Jul;14(7):1443-55.

30. **Back to basics: the untreated rabbit reticulocyte lysate as a competitive system to recapitulate cap/poly(A) synergy and the selective advantage of IRES-driven translation.** Soto Rifo R, **Ricci EP**, Décimo D, Moncorgé O, Ohlmann T. **Nucleic Acids Res.** 2007;35(18):e121.

TEACHING

2007-2010: Monitorat (64h per year L3 and M1 levels; ENS de Lyon).

Since 2015:

- Lecture on “Translational control of mRNAs” (4h per year L3 level; ENS Lyon).
- Tutorials on “RNA metabolism” (4h per year L3 level; ENS de Lyon).
- Lecture on “Translational control of viral infections” (2h per year M1 level, EPHE).

Research Supervision

Engineers

Since January 2020	David Cluet, PhD (IR1, CNRS) **Project title :** Role of translation-dependent mRNA decay in the immune response.
Since November 2020	Laura Guiguettaz (IE) **Project title :** Role of translation-dependent mRNA decay in the immune response.
Nov 2017 – Nov 2018	Emilie Laurent (IE) **Project title :** CRISPR-Cas9 delivery through Mu rine Leukemia Virus-Like Particles. 1 publication as co-author.

Postdoctoral Fellows

Since March 2017	Emmanuel Labaronne, PhD **Project title :** Characterization of the kinetics of expression and translation of viral and cellular RNAs during HIV-1 infection.
Since October 2019	Ronaldo De Carvalho, PhD **Project title :** Cross-talk between cytosolic and mitochondrial translation during macrophage activation.

Graduate Students

2011-2014	Erin Heyer (Melissa Moore laboratory) **Project title :** Development of a protocol to prepare stranded cDNA libraries for high-throughput sequencing of RNA (2 joint publica tions).

Since September 2016	Juliana Blin **Project title :** Dynamics of 80S monosome and polysome translation during macrophage activa tion. 3 publications as co-author. 1 review article as first author.
Since September 2017	Thibault Sohier **Project title :** Ribosome heterogeneity during Sindbis virus infection. 2 publications as co-author.

Master and bachelor students

Thibault Sohier (M1; February/August 2015)

Juliana Blin (M2; September 2015/May 2016)

Thierry Cottineau (M1; January/March 2018)

David Delphin (M1; January/March 2019)

Sarah Lepage (M1; March/August 2019)

Samir Ouabou (M2; February/July 2019)

Johanna Hirel (L2; June/July 2015)

Laura Raguénès (L2 IUT; April/July 2016)

Florian Provost (L2 IUT; April/July 2017)

Erwan Eriau (L3; June/July 2017)

Gabriel Laghlali (L3; June/July 2017)

Oriane Landrein (L2 IUT; April/July 2019)

Chloé Selliez (L3; April/July 2020)

Tiphanie Le Blanc (M1; May/July 2020)

Robin Gineyts (L3; June/July 2020)

Fanny Le Blanc (L3; June/July 2020)

Previous work and main achievements

Throughout my scientific carrier, RNA has been at the heart of my research interests and activities. RNA is a key player in many different cellular processes. Therefore, keeping it as a central hub has allowed me to explore several fields such as molecular virology, innate immunity, fundamental gene expression regulation mechanisms and even trans-generational inheritance of acquired traits. Furthermore, I had the chance to explore a large variety of experimental approaches ranging from *in vitro* cell-free translation extracts to cellular and animal models and more recently high-throughput sequencing methods.

Since 2006, I have worked on the regulation of mRNA translation by small RNAs, translational control of viral infections, the role of double-stranded RNA binding proteins in regulating gene expression and in the development of viral vectors for protein delivery. These projects were carried out in the laboratories of Dr. Theophile Ohlmann (CIRI, ENS de Lyon) and Prof. Melissa Moore (University of Massachusetts Medical School, USA).

I. Graduate work

(September 2006 – September 2010)
Unité de Virologie U758 under direction of Dr. Théophile Ohlmann

I initially joined Théophile Ohlmann's laboratory in September 2005 as a Master 2 student with the goal to dissect the molecular determinants of translational control of lentiviruses using *in vitro* translation extracts. This project continued during the first year of my PhD and led to the publication of a first author manuscript in the beginning of 2008 [1].
At the same time, microRNAs were emerging in the literature as important regulators of mRNA translation but their precise mechanism was still elusive. I soon became very interested in the microRNA field and, thanks to the incredible scientific freedom that Théophile granted to all the members of his laboratory, I was able to change my main PhD project at the end of 2007 in order to study microRNAs and try to characterize their mechanism of action. Indeed, Théophile's laboratory being specialized in the use and development of cell-free translation extracts to dissect the molecular mechanisms of mRNA translation, I thought that I could use this expertise to decipher the mechanism of action of microRNAs.

In parallel of these projects, a colleague from Evelyne Manet and Henri Gruffat research group (Dr. Fabrice Mure) had preliminary results suggesting that a protein from Epstein-Barr virus involved in nuclear-export of viral mRNAs also appeared to modulate their translation. We therefore began a collaboration in order to characterize this observation. Below you will find a more detailed description of the different projects from my graduate work.

1. Translational control of the genomic RNA from Human Immunodeficiency Virus Type 2 (HIV-2):

HIV-2 is a member of the lentivirus group of retroviruses and is, together with HIV-1, the etiological agent of acquired immunodeficiency syndrome (AIDS) in humans. Retroviruses are enveloped positive-sense single-stranded RNA viruses. Upon infection, the genomic RNA of HIV-2 is reverse-transcribed and the resulting double stranded viral DNA is inte-

grated within the host cell genome. Upon integration, the proviral DNA is transcribed by RNA Polymerase II into a single ~9kb transcript, which is capped and polyadenylated (Figure 1a). At early stages of the infection cycle, the full-length genomic RNA is alternatively spliced to give rise to fully spliced and partially spliced mRNAs coding for essential proteins (Tat, Rev, Env) and accessory proteins (Vpr, Vif, Nef and Vpx). At late stages of the infection cycle, the full-length unspliced genomic RNA is exported to the cytoplasm thanks to the action of the viral nuclear export factor Rev (Figure 1a). This genomic RNA plays a dual functional role as it is used both as a template for translation of the structural and enzymatic viral poly-proteins (Gag and Gag/Pol) and also as the genomic RNA that is incorporated within viral particles. Encapsidation of the genomic RNA is initiated by the dimerization of two genomic RNAs and the recruitment of the Gag protein at specific RNA structures located in the 5' untranslated region of the RNA dimers, also known as the "packaging signals" $(\psi)^2$. This initial nucleation event is followed by Gag multimerization and binding throughout the rest of the genomic RNA which is then packaged within the capsid structure formed by Gag.

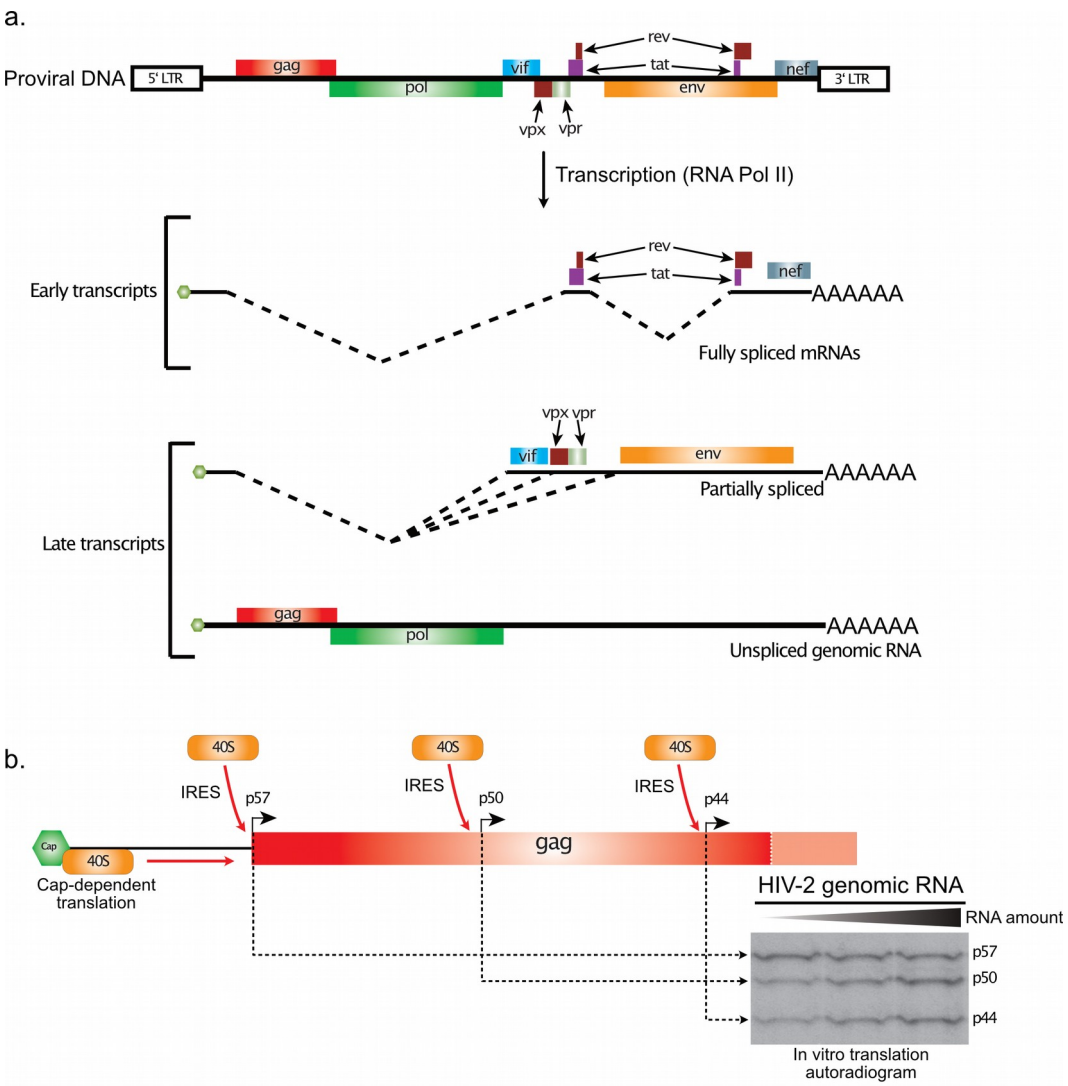

Figure 1. a. Schematic representation of early and late viral transcript produced during HIV-2 infection. **b.** In vitro translation of the HIV-2 genomic RNA leads to the expression of three Gag isoforms (p57, p50 and p44) from three in-frame AUG codons driven by independent ribosome entry sites.

In this context, the main aim of my project was to understand how the genomic RNA of HIV-2 could conciliate these two mutually exclusive processes and regulate the transition from translation to encapsidation. Interestingly, previous work from Théophile Ohlmann's

laboratory had shown the presence of an Internal Ribosome Entry Site (IRES) within the coding sequence of Gag. This IRES is responsible for the expression of the full-length Gag polyprotein (57kDa in size) as well as two N-terminally truncated shorter isoforms (50 and 44kDa respectively) produced from two in-frame downstream AUG codons [3](Figure 1b).

During my PhD I further characterized this IRES sequence using *in vitro* translation extract and cultured cells. These approaches allowed me to demonstrate that the IRES consisted in three independent ribosome entry sites which are capable of recruiting 40S ribosomes directly at each of the three AUG codons [1](Figure 1b). I then tested whether the activity of each IRES element could be modulated by viral encoded proteins such as the Gag protein itself and the viral protease. Indeed, Gag is directly responsible for encapsidation of the genomic RNA and the viral protease had previously been shown to cleave translation initiation factors eIF4G and PABP in order to shutdown cellular translation [4]. Using *in vitro* translation extracts, I was able to show that Gag binding to its own mRNA lead to a dose-dependent inhibition of translation. Interestingly, each IRES was inhibited at a different Gag concentration, the most proximal to the packaging signal (leading to production of the full length 57kDa Gag isoform) being the most sensitive to Gag binding while the most distal (leading to production of the 44kDa Gag isoform) was the most resistant. Moreover, the viral protease was also able to shutdown Gag translation in a dose-dependent manner. Our results therefore suggested that these two proteins could allow the switch from translation to encapsidation of the HIV-2 genomic RNA.

2. Dissecting the mechanism of action of microRNAs in repressing mRNA translation:

microRNAs (miRNAs) are small non-coding RNAs (18-25 nucleotides long) that are encoded by the cell genome. miRNAs associate with Argonaute proteins and act as a guides to interact with target mRNAs through partial base-pairing. Binding of miRNAs generally occurs at the 3' untranslated region (3'UTR) of target mRNAs and leads to translational repression and/or mRNA decay. In 2007, despite strong efforts carried out to dissect the mechanisms responsible for translational repression by miRNAs, the latter still remained largely uncharacterized. We therefore decided to develop a cell-free *in vitro* translation extract to recapitulate a microRNA response that was similar in many points to that observed *in vivo* and in cultured cells [5].

This system is based on rabbit reticulocyte lysate, which is commercially available and has been used to study the molecular details of mRNA translation for more than 50 years. Rabbit reticulocyte lysate is obtained through a simple preparation protocol that involves the recovery of reticulocyte cells (enucleated cells corresponding the last progenitor upstream of mature red blood cells) and their lysis by addition of water. As a consequence, untreated rabbit reticulocyte lysate contains endogenous messenger RNAs as well as tRNAs and all the translation machinery. However, these endogenous mRNAs were traditionally removed from the system by the addition of micrococcal nuclease in order to obtain a system were the translation of exogenous mRNAs could be studied on a per gene basis. I therefore decided to work with untreated rabbit reticulocyte lysate (which contains endogenous mRNAs) and found that it is highly enriched in endogenous microRNAs as well as in Argonaute proteins and other protein factors involved in microRNA biosynthesis and effector functions (Figure 2a and b). By using a set of reporter constructs (Figure 2c) containing target sites for the most abundant miRNAs in the lysate, that were either perfectly complementary (mimicking the siRNA/mRNA duplex) or partially complementary (mimicking the miRNA/mRNA duplex), I further showed that endogenous

microRNAs were active in repressing translation and also directing cleavage of target mRNAs that display full base-pairing (Figure 2d). Interestingly, translational repression was not linked to deadenylation of target mRNAs and occurred very rapidly, as soon as 10 minutes after translation was triggered[5].

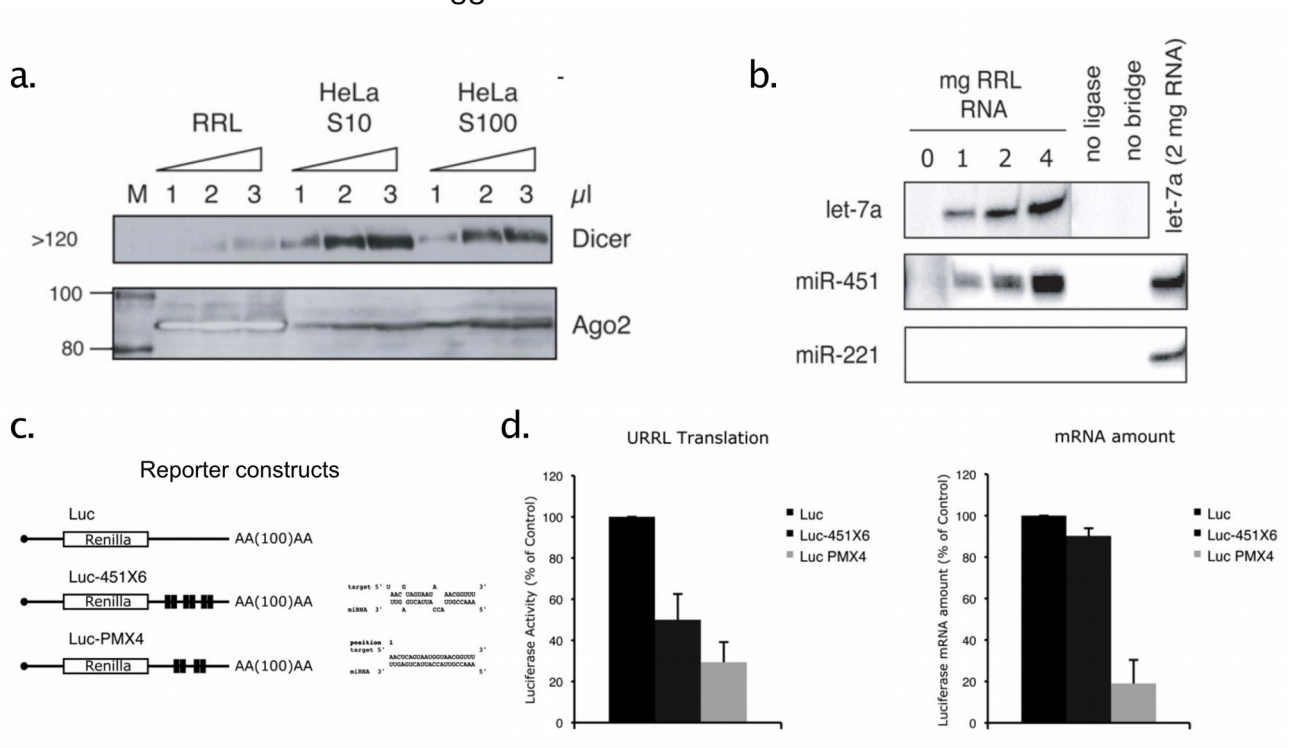

Figure 2. Untreated rabbit reticulocyte lysate recapitulates miRNA activity *in vitro*. a. Western-blot of rabbit reticulocyte lysate (RRL) or HeLa S10 and S100 extracts against Dicer and Argonaute-2 proteins. **b.** Splinted ligation assays against let-7, miR-451 and miR-221 carried out using increasing amounts of total RNA from untreated rabbit reticulocyte lysate. **c.** Schematic representation of luciferase coding reporter RNAs driven by the human β-globin 5′UTR in which six miRNA bulged target sites for miR-451 (Luc-451X6) or four perfectly complementary target sites for miR-451 (Luc PMX4) were inserted in the 3′UTR. **d.** In vitro translation of reporter RNAs in rabbit reticulocyte (left panel) and quantitation of their abundance upon translation by qPCR (right panel).

Using this system, I then attempted to characterize the precise mechanism by which miRNAs regulate mRNA translation [6]. To this aim, I designed an experimental approach that was based on chemical and viral-derived translation inhibitors that targeted each major step of the mRNA translation process. I sequentially inhibited, the recognition of the mRNA 5' cap structure, scanning of the 40S ribosomal subunit to reach the AUG start codon, recruitment of the 60S ribosomal subunit and translation elongation and found that miRNAs appeared to target 40S ribosome scanning. I then used a series of viral Internal Ribosome Entry Sites (IRES) that have different translation initiation mechanisms and display differential requirement for translation initiation factors. This strategy allowed me to show that miRNAs regulate ribosome scanning and suggested a mechanism involving the RNA helicase eIF4A [6]. These results were later confirmed by an independent study, showing that miRNAs regulate eIF4A2 (a paralog of eIF4A) to repress translation[7].

3. Translation stimulation of unspliced mRNAs by the Epstein-Barr virus nuclear-export factor protein EB2:

In eukaryotes, gene expression is regulated at multiple levels ranging from transcription, pre-mRNA splicing and transcript maturation, nuclear-export of the mature mRNA, translation and degradation of both the mRNA and the corresponding protein. Although these processes occur in a sequential and compartmentalized manner, they are strongly inter-

connected and factors involved in early stages of the gene expression pathway can have an impact at later steps. As an example, splicing of pre-mRNAs in the cell nucleus leads to the deposition of a protein complex at each exon-exon junction, known as the exon junction complex or EJC[8]. This complex favors nuclear-export of spliced mRNAs and their translation once in the cytoplasm [8,9]. Unspliced mRNAs and transcripts produced from intronless genes are therefore usually poorly exported to the cytoplasm and do not recruit ribosomes efficiently.

Epstein-Barr virus (EBS) belongs to the Herpesvirus family. It is an enveloped double-stranded DNA virus with a genome size of 192kb coding for close to 80 different proteins. Is it estimated that about 90% of human population is infected with the virus [10] and infection with EBV is linked to several malignancies such as infectious mononucleosis and Burkitt's and Hodgkin's lymphomas [11].

The viral protein EB2 is an essential factor that is expressed during the early steps of EBV replication cycle. EB2 share characteristics of cellular nuclear export factors, it shuttles from the nucleus to the cytoplasm and it interacts with the TAP/NXF1 complex in order to export unspliced viral mRNAs (Figure 3b) [12,13]. Preliminary experiments carried out by Fabrice Mure and Henri Gruffat in 2007 suggested that in addition to stimulating nuclear export of unspliced mRNAs, EB2 could also stimulate their translation.

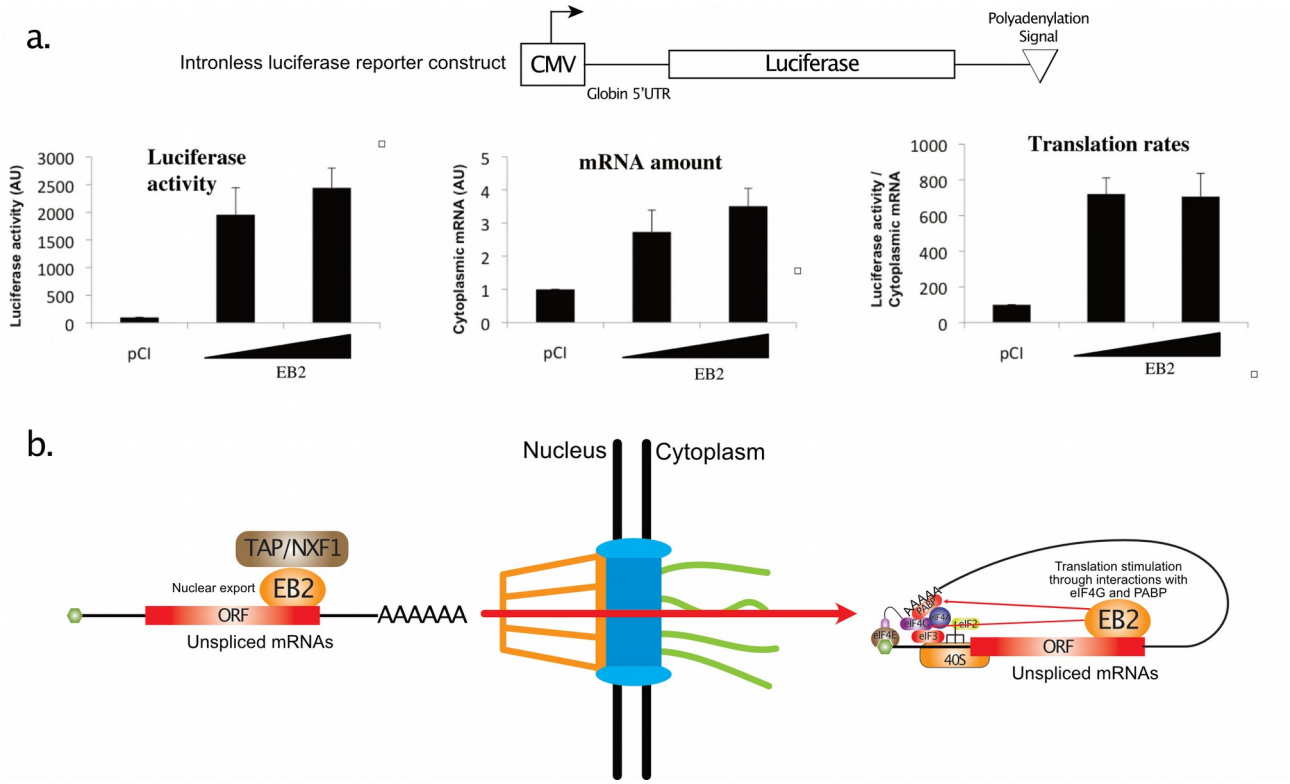

Figure 3. EB2 stimulates nuclear export and translation of intronless mRNAs. a. Schematic representation of the luciferase intronless coding vector used in the study presenting positions of the CMV promoter and BGH polyadenylation signal (top panel). Measure of luciferase activity and quantification of cytoplasmic luciferase-encoding mRNAs by quantitative RT-PCR. Translational efficiency was calculated by normalizing the total luciferase activity to the amount of cytoplasmic luciferase mRNA. AU: arbitrary units. **b.** Scheme describing the role of EB2 is exporting unspliced mRNAs from the nucleus and stimulating their translation in the cytoplasm through interactions with PABP and eIF4G.

To further characterize the role of EB2, we designed a set of intronless or intron containing luciferase reporter genes for which we could precisely measure cytoplasmic RNA levels and their associated luciferase activity to obtain a proxy of their translation efficiency (Figure 3a). Our results indicated that EB2 could efficiently export intronless mRNA (4 fold increase compared to control) and strongly stimulate their translation (7 fold increase

compared to control) without affecting expression of endogenous cellular spliced mRNAs (Figure 3a). Interestingly, EB2 does not seem to have any sequence specificity as any intronless reporter devoid of viral-derived elements responds to EB2 expression. On the contrary, addition of an intron (even in the 3'UTR of the pre-mRNA which results in nonsense-mediated mRNA decay) is sufficient to abolish the effect of EB2 in nuclear export and translation stimulation. Finally, we also showed that EB2 is associated to actively translating mRNAs in the cytoplasm and improves association of unspliced mRNAs with heavy polysomes. Together, our results indicated that EB2 is able to functionally replace introns and their role in stimulating nuclear-export and translation of mRNAs. Moreover, we were able to show that this feature is conserved across EB2-related proteins from other herpesviruses such as cytomegalovirus (CMV).

This work was continued by the laboratory of Henri Gruffat and Théophile Ohlmann, which recently showed that EB2 binds to eIF4G and PABP to stabilize the cap-binding complex and stimulate translation (Figure 3b) [14].

II. Postdoctoral work

(October 2010 – October 2014)
University of Massachusetts Medical School under direction of Prof. Melissa Moore

1. Characterizing the role of the double-stranded RNA-binding protein Staufen1 in regulating gene expression:

Double-stranded RNA binding proteins are involved in diverse biological roles such as RNA interference (Dicer, TRBP), viral sensing (PKR, PACT), RNA transport (Staufen1 and 2) and RNA editing (ADAR1 and 2). However, in 2011, little was known about the specificity of these proteins in recognizing their target RNAs and their exact binding sites within cells. To answer these questions, we decided to map the RNA-binding sites of the dsRBP Staufen1 using an approach combining RNA-immunoprecipitation coupled to high-throughput sequencing (Figure 4a). Staufen1 was previously shown to be involved in regulating RNA transport in neurons, assembly of stress granules and in regulating viral RNA translations [15–18]. Staufen1 recognizes dsRNA through interactions with the RNA sugar-phosphate backbone, without making significant contacts with the bases [19]. Consequently, it does not cross-link efficiently to dsRNA when exposed to ultra-violet light and therefore traditional cross-linking immunoprecipitation approaches such as CLIP-seq were not possible [20,21]. I therefore adapted a protocol that was being developed in Melissa Moore's laboratory (RNA:Protein immunopurification in Tandem or RIPiT [22]) to the study of dsRBPs (Figure 4a). Briefly, the protein of interest, bearing a Flag-tag, is expressed at near endogenous levels in cells. Crosslinking is then performed using formaldehyde, which efficiently crosslinks dsRBPs to target RNA and the protein is immunoprecipitated under denaturing conditions with anti-Flag beads. After immunoprecipitation, the protein is eluted from beads using recombinant Flag peptide and a second immunoprecipitation is performed against the protein of interest or one of its known interacting partners. The purified complex is treated with RNase in order to obtain an RNA footprint of the protein of interest. Protected RNA is finally recovered and submitted for high-throughput sequencing. Applying RIPiT to Staufen1 revealed that the protein binds dsRNA stretches longer than 9 base-pairs independently of their sequence [23]. Staufen1 binding sites occurs at the coding sequence and the 3'UTR of all cellular RNAs (Figure 4b). Interestingly, Staufen1 recruitment to mRNAs is correlated to the amount of dsRNA in the latter. We also found that Staufen1 interacts with ribosomes in an RNA-independent manner suggesting that it could use the ribosome to "scan" mRNAs and bind to dsRNA-structures.

Finally, by measuring mRNA translation levels in cells depleted of Staufen1 through ribosome profiling, we showed that Staufen1 binding to the coding sequence of mRNAs leads to upregulation of their translation. We therefore concluded that Staufen1 acts as a dsRNA sensor which probes for the amount of dsRNA in all expressed transcripts and regulates their translation through its interaction with ribosomes (see Figure 4c for our working model).
Staufen1 and other dsRBPs do not appear to have a strong sequence specificity in their target sites. Therefore, our results suggest that these proteins could be in competition for binding to dsRNA and that their relative expression level or subcellular localization could play an important role in defining their impact on regulating gene expression.

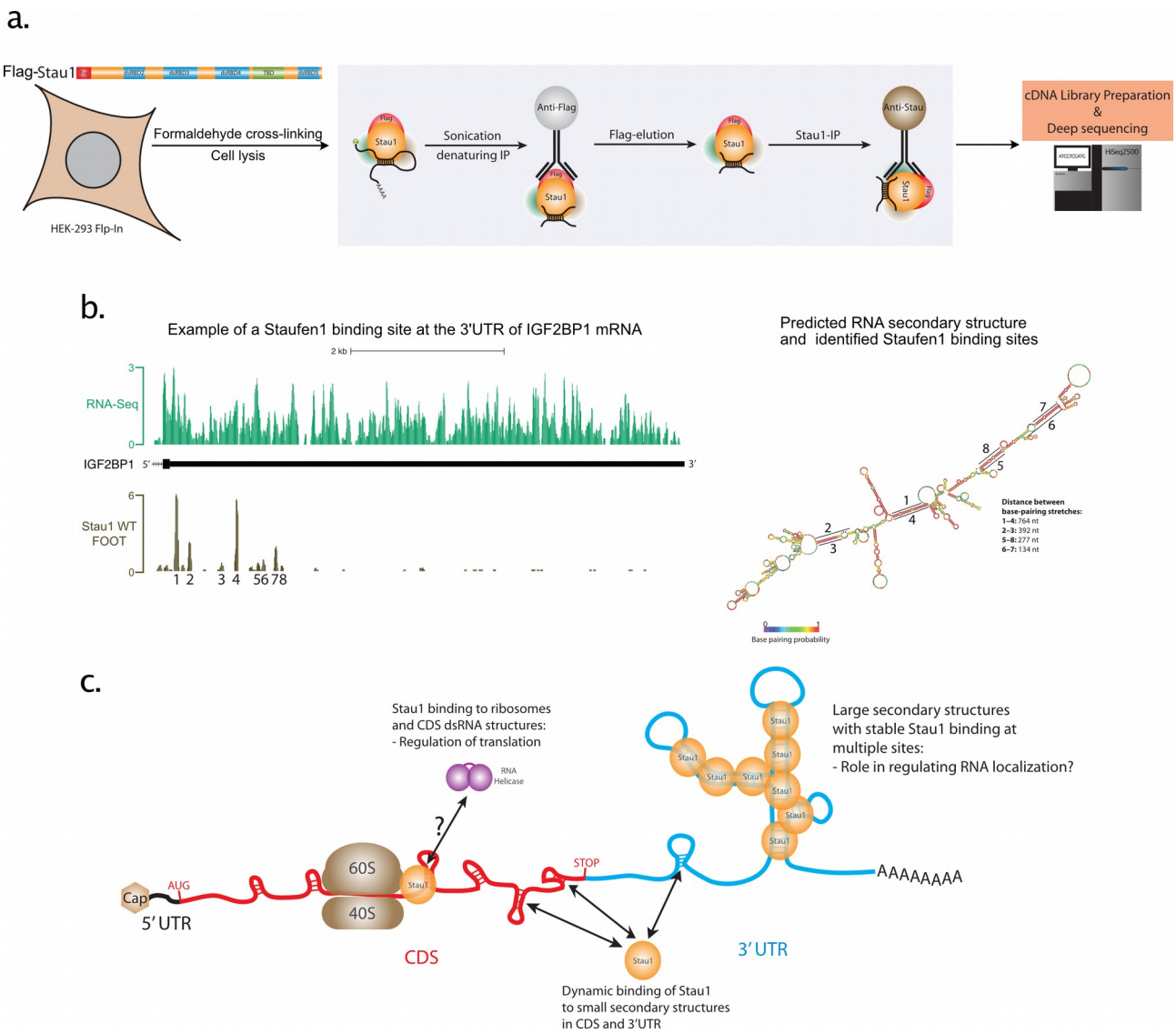

Figure 4. Staufen1 senses overall mRNA secondary structure to regulate translation. a. Scheme of the RNA-Immunoprecipitation in Tandem protocol (RIPiT) implemented to map Staufen1 RNA-binding sites**. b.** Sequencing read distribution for RNA-seq (green) and Staufen1 RIPiT (brown) cDNA libraries in the 3'UTR of the Igf2bp1 coding transcript (left panel) and the corresponding predicted secondary structure colored for base-pairing probability (Identified Staufen1 binding sites are annotated on the predicted structure). **c.** Model of Stau1 RNA binding and its functional role in translation. Stau1 interacts with both actively translating ribosomes and secondary structures in CDS and 3′UTR regions. Some 3′UTRs contain highly complex secondary structures (for example, inverted Alu pairs) that serve as kinetically stable Stau1-binding sites. However, Stau1 also makes transient interactions with smaller secondary structures throughout CDS and 3′UTR regions. Formation of these structures is a function of overall CDS and 3′UTR GC content. Whereas interaction of Stau1 with 3′UTR Alu pairs has a small positive effect on cytoplasmic mRNA levels, high Stau1 CDS occupancy both increases ribosome density and slightly decreases cytoplasmic mRNA levels.

2. Role of long non-coding RNAs in regulating the innate immune response:

While working at the University of Massachusetts Medical School, I actively collaborated with the laboratory of Professor Katerine Fitzgerald (University of Massachusetts Medical School) whose main focus is to study the role of long non-coding RNAs in regulating innate immunity. In this context, I first implemented a sucrose gradient approach combined with the use of translation inhibitors to confirm whether specific long non-coding RNAs were indeed "non-coding" and did not associate with the translation machinery [24]. I also adapted a protocol derived from the RNA antisense purification technique [25] to purify the endogenous long non-coding RNA EPS from cells and identify its DNA interacting partners. This protocol consists first in fixing cells to crosslink RNA to DNA and proteins and then to capture a specific endogenous long non-coding RNA using antisense biotinilated RNA probes produced in vitro. Probes are generated through T7 RNA polymerase *in vitro* transcription reactions programmed with biotinilated nucleotides to generate a long antisense biotinilated transcript. This transcript is fragmented through alkaline hydrolysis and gel purified to obtain probes ranging from 50~70 nucleotides in length. Probes anneal to the target RNA and are then captured using streptavidin beads. Purified RNA together with its interacting DNA and proteins can then be used for high-throughput sequencing and mass spectrometry. Using this protocol, we were able to show that the long non-coding RNA EPS interacts with the promoter region of several genes involved in inflammation to repress their transcription [26].

This collaboration familiarized me with cells of the immune system and made me realize that they are excellent models to study post-transcriptional control mechanisms of gene expression. This was further reinforced by an invitation from Kate Fitzgerald to write a review about the topic [27].

Current Research and projects

I obtained a permanent position in December 2014 at Centre International de Recherche en Infectiologie (CIRI U1111, ENS Lyon) within Théophile Ohlmann's group. Since then, my main research projects have been related to the study of post-transcriptional regulation of gene expression with a particular emphasis on mRNA translation and its cross-talks with other cellular processes. We use viral infections and cells of the immune system as working models as they represent dynamic systems where mRNA translation and other post-transcriptional control mechanisms have been shown to play a critical role in regulating gene expression.

In addition to these main research projects, we are also involved in developing innovative tools for the delivery of proteins and ribonucleoprotein complexes (RNPs) into cells using retroviral Virus-Like particles (VLPs). This technically oriented project allowed us to create Nanoblades [28], a CRISPR-Cas9 delivery vector that allows efficient genome editing in many primary cells, which will be essential for our main projects.

Most of our projects currently rely on high-throughput technical approaches such as next-generation sequencing and quantitative mass-spectrometry which generate large datasets and require specific skills (bioinformatics and statistics) for their analysis. That is why, in 2017, I applied to a junior group leader call from "Laboratoire de Biologie et modélisation de la Cellule (LBMC – ENS Lyon)" which gathers research groups interested in all aspects of quantitative biology and in biocomputing approaches to study and model cellular processes. Thus I joined the LBMC in February 2018 together with one postdoctoral fellow (Emmanuel Labaronne) and two graduate students (Juliana Blin and Thibault Sohier). Although this change had a significant impact in our research activities, it has been beneficial to most of our projects as we now have access to a biocomputing core facility led by Dr. Laurent Modolo (an expert in bioinformatics and biostatistics) that assist all research groups from LBMC. We also enjoy from a research environment more focused toward fundamental mechanisms of gene expression, while at the same time being in close proximity to CIRI and benefit from collaborations with experts in infectious diseases and immunology. Finally, since January 2020, David Cluet (Ingénieur de Recherche de 1ère Classe, CNRS) has joined our research group. David has a dual wet/dry laboratory expertise which perfectly suits our research activities.

Project #1
A viral-derived protein delivery system to mediated efficient genome-editing in primary cells

Persons involved: Philippe Mangeot (Co-PI), Emilie Laurent, Thibault Sohier and Juliana Blin.

Targeted genome editing tools such as Meganucleases (MGN), Zinc-finger nucleases (ZFN), Transcription activator-like effector nucleases (TALENs) and more recently the Clustered Regularly Interspaced Short Palindromic Repeats (CRISPR) have revolutionized most biomedical research fields. Indeed, such tools have the power to precisely edit the genome of eukaryotic cells by inducing double-stranded DNA (dsDNA) breaks at specific loci. Relying on the cell endogenous repair pathways, such dsDNA breaks can be repaired by Non-Homologous End-Joining (NHEJ) and Homology-Directed Repair (HDR) allowing the removal or insertion of new genetic information at a desired locus. Consistent with the great promises of such technologies in gene therapy, several studies have shown that mutations associated with human diseases could be "repaired" *ex-vivo* (in cultured cell lines) and in the mice germline using MGN, TALENs and CRISPRs either by transfection of plasmids coding for the nucleases, transduction with viral-derived vectors coding for the nucleases or by injecting the protein complexes directly into the cell. Among the above mentioned tools, CRISPR/Cas9 is the most simple to implement and the most versatile. Indeed, it consists on the expression of a bacterial derived nuclease, known as Cas9 (for CRISPR-associated protein 9) together with a guideRNA (gRNA) that is complementary to the DNA locus to target. Through its association with the gRNA, Cas9 is targeted to the genomic DNA locus where it will induce a dsDNA break. Therefore, by simply modifying the sequence of the gRNA, the user can specify the region of the genome to cleave. All of the above-mentioned approaches (including CRISPR) suffer from the poor transfectability of primary cells or live tissues when using plasmid transfection. Moreover, the impossibility to target all cells in a tissue in the case of DNA or protein microinjection and risk of genomic integration within cellular genes for viral-delivery vectors are severe limitations too. To solve these issues, together with Philippe Mangeot (research engineer within Théophile Ohlmann's group and expert in viral vectors), we designed a new viral vector that allows an efficient delivery of the CRISPR ribonucleoprotein (RNP) machinery into cells [28]. To achieve this, we hijacked the natural ability of the Gag polyprotein from Murine Leukemia Virus (MLV) to generate "empty" virus-like particles (VLPs) that are released in the supernatant of producer cells. We fused the Cas9 protein to the C-terminal end of the Gag polyprotein (Figure 5a) and expressed this construct together with a plasmid coding for an sgRNA and a viral envelope in HEK293T cells (Figure 5b). This results in the release of large amounts of VLPs loaded with the Cas9 protein bound to its sgRNA and pseudotyped with two engineered viral envelopes which allow transduction of a wide spectrum of eukaryotic cells (Figure 5b). We call this technology Nanoblades since it can deliver a cleaving agent to a large spectrum of cells without requiring a DNA plasmid to code for CRISPR components.

We have used Nanoblades to efficiently mediate genome-editing in primary cells such as human fibroblasts (Figure 5c), mouse bone-marrow cells, human CD34+ cells and human induced pluripotent stem cells (hiPS). Nanoblades can also be used in vivo to mediate genome editing in mouse oocytes without requiring direct microinjection and also in the liver of adult individuals upon retro-orbital injection. Moreover, Nanoblades can be complexed with donor DNA to perform knock-in experiments without requiring any transfection agent. Importantly, Nanoblades deliver the Cas9 protein in a rapid and dose-

dependent manner with no requirements for transcription or translation of the Cas9 gene and sgRNAs in target cells thus allowing to perform kinetics experiments in a controlled manner (Figure 5c). This particular features have been used by our collaborators, Aline Marnef and Gaëlle Legube (LBCMCP, Centre de Biologie Intégrative (CBI), CNRS, Université de Toulouse) to study double-strand break repair [29,30]. Nanoblades production protocol is rapid, inexpensive and accessible to any laboratory equipped for cell culture.

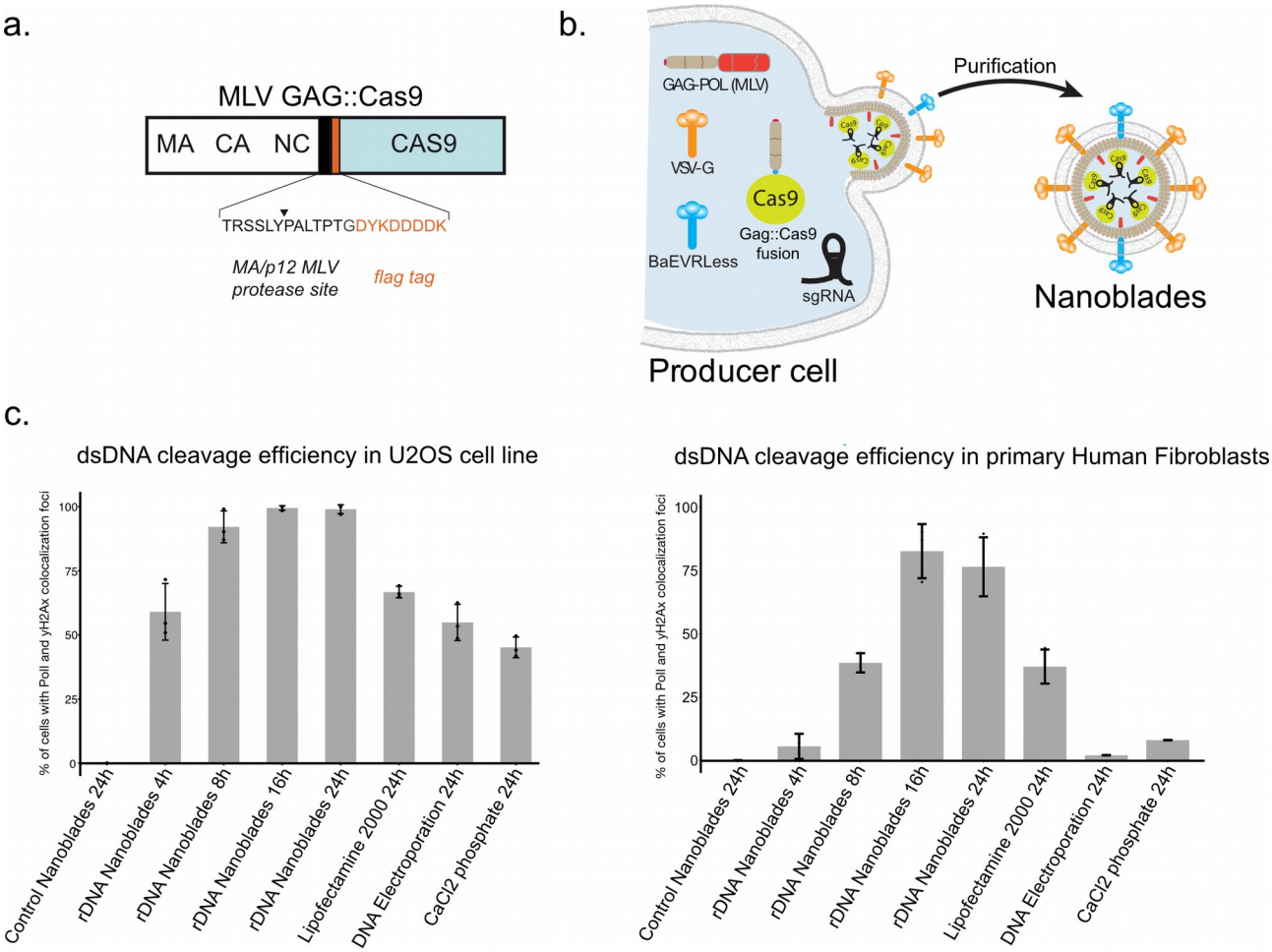

Figure 5. Genome-editing through Cas9/sgRNA loaded Murine Leukemia Virus-like particles. a. Scheme describing the MLV Gag::Cas9 fusion and **b.** the Nanoblade production protocol based on the transfection of HEK-293T cells by plasmids coding for Gag-Pol, Gag::Cas9, VSV-G, BaEVRLess, and the sgRNA. **c.** dsDNA cleavage efficiency at ribosomal-RNA coding loci in USOS and primary Human fibroblasts as assessed by measuring the percentage of cells with PolI and γH2Ax Histone co-localization foci.

Future directions:

We published the manuscript describing the Nanoblades technology in January 2019. Since then, we have slowed the pace of its development. Nevertheless, we are trying to improve the technology for its use with other Cas9 related proteins with different PAM requirements in order to expand the genome targeting possibilities. We are also trying to improve Cas9 loading and delivery. Indeed, we have noticed that the efficiency of protein cargo loading within virus-like particles is affected by the molecular size of the protein that is fused to Gag. We are therefore currently trying to split the Cas9 protein into two independent segments that could be loaded separately within Nanoblades and fused within target cells to recreate a functional Cas9 protein in target cells. For this, we will explore the protein splicing approach that allows the seamless fusion of two proteins bearing specific sequences (called inteins) at their N- and C-termini [31]. We expect from these experiments to improve the efficiency of genome-editing and allow the efficient loading of large Cas9 variants within VLPs.

Project #2
Assessing the role of ribosomes and mRNA translation in shaping the immune response

The immune response protects the host against microbes and foreign substances that can enter the body. This is allowed by an orchestrated sequence of events that can be divided into two types of responses, innate and adaptive immunity.
The innate response is a rapid and highly regulated process triggered by “pattern recognition receptors (PRRs)” that are present in distinct cellular compartments and recognize different conserved microbial components known as “pathogen-associated molecular patterns (PAMPs)” [32]. PRRs can also recognize endogenous or exogenous non-microbial components that are released during tissue injury and are known as “alarmins” or “danger-associated molecular patterns (DAMPs)”[33]. The innate response also involves the local recruitment of blood components such as plasma proteins and leukocytes (white blood cells) to the affected site, leading to inflammation.
Macrophages are central players of the inflammatory process[34] as they mediate initial recognition of infection, mainly through PRRs such as Toll-like receptors (TLRs), nucleotide-binding oligomerization domain (NOD)-like receptors (NLRs), C-type lectin receptors (CLRs) and retinoic acid inducible gene-I (RIG-I)-like receptors (RLRs)[32]. This initial recognition leads to the production and release of inflammatory mediators, such as chemokines and cytokines that promote inflammation by altering the local vascular system, increasing vascular permeability and attracting effector cells (mainly neutrophils) to the site of infection[35]. Activated neutrophils create a cytotoxic environment by releasing highly reactive oxygen and nitrogen species (ROS and RNS) that kill microbes and host cells without discrimination thus causing collateral tissue damage[35]. This results in the classic signs of inflammation, pain, heat, redness, swelling and loss of function. Upon clearance of the infectious agent, the acute inflammatory response is followed by the resolution phase, which again is mainly orchestrated by resident and recruited macrophages with anti-inflammatory functions[36,37]. Neutrophil infiltration is then blocked and enhanced recruitment of monocytes participates in removal of dead cells and regulate tissue remodeling[38].
Although a robust inflammatory response is required as a first line of defense against pathogen infections, uncontrolled or prolonged inflammation can lead to inflammatory disorders such as septic shocks[39] or atherosclerosis[40] as well as autoimmune diseases such as arthritis or lupus[41]. It is therefore important to understand the molecular pathways that finely tune activation and effector functions of cells involved in the inflammatory response such as macrophages.
At the molecular level, stimulation of macrophages by PRR ligands triggers signaling cascades that converge on well-defined transcription factors, including NF-κB and interferon-regulatory factors (IRFs) among others, that are constitutively expressed under an inactive form[42]. Post-translational modification of these transcription factors induces their translocation to the nucleus where they regulate transcription of specific genes, also known as primary response genes[42]. This results in the activation of a complex, coordinated and highly dynamic gene expression program that is temporally regulated by transcriptional on and off switches[42]. This program varies depending on the cell lineage and the specific triggering signals and involves multiple layers of regulation including histone modification as well as DNA and chromatin changes. Although less studied, post-transcriptional control pathways also participate in shaping the inflammatory gene expression program[43]. They include regulation of pre-messenger RNA (pre-mRNA) splicing, mRNA stability and translation. These post-transcriptional mechanisms play a

crucial role in modulating the strength of the inflammatory response as well as its temporal regulation[43].

The innate immune response acts as a first barrier to limit pathogen proliferation and is essential to activate the antigen-specific adaptive immune response. Activated dendritic cells presenting pathogen-derived antigens in association with major histocompatibility complex class II (MHCII), migrate from the infected tissues into the lymph nodes where they interact with naïve CD4+ T lymphocytes. Only the T lymphocytes able to recognize specifically the MHCII/antigen complex through their T cell receptor (TCR) will undergo activation. This leads to their clonal proliferation and cell differentiation into effector or memory T cells. Effector T cells orchestrate the pathogen clearance, while memory T cells will persist in the organism and respond more rapidly upon a second infection with the same pathogen. CD4+ T lymphocyte activation and proliferation are associated to a profound remodeling of the transcriptional and metabolic landscape, as well as drastic changes in overall and transcript-specific translation efficiency.

Translational control plays an essential role in regulating gene expression. Because it acts on pre-existing mRNAs, its effects are reversible thus allowing for a rapid and dynamic response[44]. Translation can also be regulated in space in order to produce proteins locally at specific sub-cellular sites[45]. Furthermore, translational control can occur both globally (i.e through the regulation of canonical factors required for translation of most mRNAs) or in a transcript-specific fashion (i.e through cis-acting regulatory elements embedded within transcripts themselves)[44]. Finally, when translation is coupled to mRNA degradation pathways in what is known as translation-dependent mRNA decay, it allows for the fine tuning of gene-expression and for mRNA quality control by restricting protein-output to only a few proteins produced from a single transcript[46].

mRNA translation is a sophisticated process that involves one of the largest macromolecular complex in the cell, the ribosome, and a large number of cellular factors that assist ribosomes at each stage of the translation process. Translation can be divided into four main steps[44]: **1.** Initiation, where the small subunit of the ribosome (40S subunit) binds to the 5'end of the mRNA, scans the 5' untranslated region until it reaches the AUG start codon and the large ribosomal subunit (60S subunit) is recruited to form the 80S ribosome. **2.** Elongation, where the 80S ribosome translates the coding sequence of the mRNA by translocating from codon to codon catalyzing the peptide bond between the nascent peptide chain and newly incorporated amino-acid. **3.** Termination, where the newly synthesized protein is released and the two ribosomal subunits split. **4.** Recycling, where the ribosomal subunits are prepared for a new round of translation.

Translation initiation involves at least 34 core initiation factors[47] that assist the small subunit in recognizing the 5' cap structure of mRNAs, scanning the 5' untranslated region and selecting a start codon located in a good kozak context. In addition to the core initiation factors, a multitude of auxiliary factors and transcript cis-acting features participate in regulating the initiation process[47]. Translation initiation is often considered as the limiting step of the overall translation process[47]. Consistent with this, most of the regulatory pathways described in the literature target translation initiation through the activity of the canonical initiation or through auxiliary factors[44,47]. However, the advent of high-throughput sequencing methods (such as ribosome profiling) to measure ribosome density and the position of ribosomes on the coding-sequence of cellular mRNAs in a transcriptome-wide manner has recently revealed new unexpected mechanisms of translational control[48]. For example, pausing or stalling of ribosomes during translation elongation can have an impact on protein output, transcript stability and even on the correct folding of the translated protein[49,50]. Interestingly, these findings have been accompanied by the discovery that ribosomes themselves can also play an important role in regulating the translation process[51,52]. Indeed, ribosomes have been historically

perceived as homogenous machines composed of a defined set of ribosomal proteins and ribosomal RNA with no other role than translating mRNAs into proteins and participating in mRNA quality control pathways such as non-sense mediated decay. However, this vision has recently been challenged by findings indicating that ribosomal proteins can actively participate in regulating translation of specific mRNAs [52]. Moreover, the composition in core ribosomal proteins can differ between ribosomes from different tissues[53]. These findings are consistent with experiments showing that mutation or inactivation of different core ribosomal proteins in mice and other organisms can have no significant impact on viability or overall mRNA translation rates, but rather affect expression of a specific subset of genes [53]. From these studies, the notion of "specialized ribosomes" has emerged, where a subset of ribosomes with a unique composition preferentially translate specific transcripts[54]. In this control pathway, a cross-talk between ribosomes and *cis*-acting features present in mRNAs regulates their protein-output. This vision has become even more complex as a recent analysis of ribosome-associated proteins obtained from mouse embryonic stem cells, revealed an incredible diversity of extra-ribosomal proteins that contact ribosomes, including proteins involved in RNA metabolism, proteins that mediate post-translational modifications and even metabolic enzymes[55].

Being at the heart of the translation process, ribosomes are in close contact with both the mRNA and the nascent protein. They could therefore function as structural hubs for a wide diversity of proteins to mediate post-translational modifications of proteins as they are being translated, to induce degradation or remodeling of the translated mRNA or to read specific sequences or chemical modifications of the mRNA and modulate translation or mRNA decay as a consequence.

Translation is tightly regulated in cells of the innate and adaptive immune system. For example, stimulation of dendritic cells with lipopolysaccharide (LPS), a component of the outer membrane of Gram-negative bacteria that is recognized by the Toll-like receptor 4 (TLR4), triggers an immediate and massive increase in global protein synthesis within the first 60 minutes[56]. Consistent with this, signaling pathways activated through some PRRs have been shown to regulate global mRNA translation by modulating the activity of canonical translation initiation factors such as eIF2 and eIF4E[43]. Moreover, gene-specific translational control has been shown for transcripts bearing particular *cis*-acting features such as AU-rich elements or the GAIT motif (IFN-**γ**-**a**ctivated **i**nhibitor of **t**ranslation/GAIT) that temporally restrict translation of many mRNAs coding for cytokines and other proteins involved in the regulation of the inflammatory response [43,57]. Similarly, mRNA translation is dynamically regulated in CD4+ T Cells upon activation and this regulation is essential in the switch from quiescence to the effector phenotype [58].

In this context, our project aims at studying how ribosomes and their cross-talk with other transcriptional and post-transcriptional cellular processes play a role in finely tuning gene expression and modulating the outcome of innate and adaptive immune cell activation.

The main objectives of our project are to characterize the impact of mRNA translation and "specialized ribosomes" in shaping the immune response by:

1. Characterizing the atlas of ribosome-associated proteins in the course of macrophage stimulation and their impact on the inflammatory response.

2. Studying the cross-talks between ribosomes and mRNA translation with mRNA decay pathways and their importance for macrophage stimulation.

3. Exploring the potential coordination between cytosolic and mitochondrial translation that could participate in modulating the metabolic activity of cells undergoing activation.

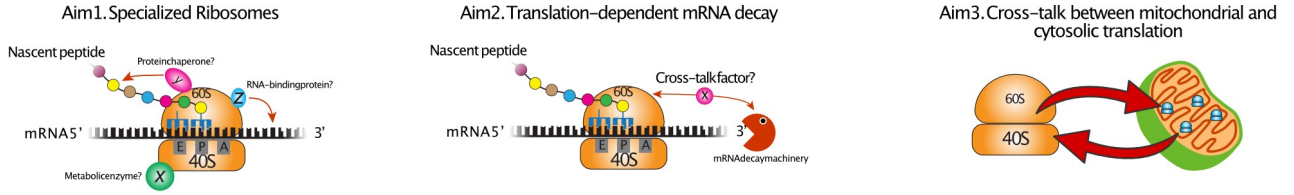

-Identify ribosome associated factors
-Characterize their role during inflammation
-Specialized ribosomes translate specific mRNAs?

-Identify transcripts degraded upon translation
-Characterize the cis-and trans-acting factors responsible
-Importance of translation-dependent decay in inflammation

-Identify mitoribosome-associated proteins
-Monitor mitoribosomal translation efficiency
-Are cytosolic and mitochondrial translation synchronized?

Aim 1. The atlas of ribosome-associated proteins in the course of macrophage stimulation and its impact on the inflammatory response:

Persons involved: Thibault Sohier and Ronaldo De Carvalho.

Protein synthesis is one of the major tasks performed by the cell and ribosomes are among the largest cellular macromolecular machines described. With a size of 4.3MDa and composed of at least 80 core ribosomal proteins and 4 different ribosomal RNAs[59], ribosomes catalyze the synthesis of proteins but also play important regulatory roles. Being in close contact with the translated mRNA and the nascent poly-peptide, ribosomes can serve as docks for accessory proteins involved in protein post-translational modifications, protein folding and degradation, but also in RNA metabolism and sub-cellular compartmentalization.
Because the inflammatory response requires a rapid and dramatic modulation of the cell gene expression program, we hypothesize that it is accompanied by significant changes in the association and dissociation of ribosomal core and accessory proteins. We therefore plan to identify for the first time and in an unbiased manner, the complete set of ribosome associated proteins (RAPs) and their dynamics of association during the activation of mouse bone marrow derived macrophages (BMDMs). For this, we will immunopurify endogenous ribosomes bearing Flag-tagged ribosomal proteins and analyse their associated proteins by quantitative mass-spectrometry. The identified factors will be further validated for their interaction with ribosomes in live cells by confocal microscopy and by co-immunoprecipitation assays. The most interesting factors, that is to say RAPs that play unexpected roles or involved in gene expression regulatory pathways, will be selected and their ribosome-associated roles will be characterized. In particular, the subsets of “specialized ribosomes” that are decorated with our proteins of interest will be purified to further assess their protein composition and their exact position on translated mRNAs. Finally, to study their role of selected RAPs in regulating gene expression and macrophage activation, we will perform site-directed mutagenesis to inactivate their expression or abolish their ribosome association.
Taken together, we expect in this aim to identify new and uncharacterized post-transcriptional regulatory mechanisms involving ribosomes and their cross-talk with other cellular processes during the inflammatory response. We expect that our strategy will uncover new cellular factors that were not previously linked to inflammation and that could represent new targets for drugs aiming to modulate the inflammatory response. We also expect that our results will pave the way for the study of specialized ribosomes in various infectious contexts and particularly during viral infection. Indeed, all known viruses depend entirely on the host cellular translation apparatus for synthesis of viral proteins and several viral proteins have been shown to interact with ribosomes. It would therefore be of great interest to study how viral infections can modify the protein composition of ribosomes as well as the consequences on viral and cellular outcomes.

Aim 2. Cross-talks between ribosomes and translation with mRNA decay pathways:

Persons involved: Laura Guiguettaz, Emmanuel Labaronne, David Cluet.

Translation-dependent mRNA decay (TDD) pathways involve various cis-acting regulatory elements that recruit the mRNA degradation machinery as a consequence of translation[60]. TDD includes mRNA surveillance mechanisms such as nonsense mediated decay (NMD), no-go decay (NGD) or non-stop mediated decay (NSD) that allow cells to rapidly degrade aberrant mRNAs[46]. Translation-dependent decay of transcripts containing binding sites for the double-stranded RNA binding protein Staufen, are other known TDD mechanisms that regulate expression of normal mRNAs under various physiological conditions[61,62].
NMD was initially thought to only trigger degradation of aberrant mRNAs. However, recent studies have shown that alternative splicing, long 3'UTRs and the presence of upstream ORFs (uORFs) can also trigger NMD[63,64]. Furthermore, evidence of constitutive NMD was found in neurons where the immediate early gene Arc, expressed upon synaptic stimulation, was shown to contain a spliced intron in its 3'UTR, causing it to self-destruct upon translation by NMD[65]. When combined with a strong stimulation of transcription upon synaptic stimulation, TDD of the Arc mRNA leads to a rapid degradation upon its translation thus allowing for a strong protein expression that is restricted to a very short time frame[65].
Similarly to neurons, cells of the immune system have to respond rapidly to a stimulus and organize a complex program of differentiation that involves sequential expression of particular sets of genes in a time-constrained manner. Regulation of gene expression through TDD could therefore play an important role in finely tuning the inflammatory response by allowing the rapid clearance of transcripts upon transcriptional shut-off and thus restricting expression in time. Most studies found in the literature have specifically focused on one TDD pathway, NMD, in different cellular contexts. However, no study so far has addressed the global impact of TDD pathways in regulating gene expression.
Using a combination of transcription and translation inhibitors, we aim at identifying all transcripts that are regulated by TDD during the inflammatory response and in cells of the adaptive immune system using high-throughput sequencing approaches. In addition, we plan to monitor mRNA translation rates as well as the structure of all cellular transcripts expressed (including the position of their 5’ and 3’ end) to assemble a transcriptome with corresponding translation rates for all expressed transcripts. The obtained data will then be analyzed to extract quantitative and qualitative information (such as transcript length, GC content, presence of spliced introns in the 3’UTR, presence of AREs, codon usage, presence of upstream ORFs, binding sites for proteins involved in mRNA decay) to identify possible *cis*- and *trans*-acting features responsible for triggering TDD using machine learning approaches. Finally, we will assess for the importance of TDD in regulating macrophage activation and effector functions by removing the previously identified *cis*-acting features or *trans*-acting factors responsible for triggering TDD.
Based on the results obtained from this Aim, we expect to uncover the extent of TDD in regulating gene expression as well as describing new molecular actors involved in mediating TDD. We further expect to reveal the importance of TDD in orchestrating the inflammatory gene program during macrophage activation.

Aim 3. Coordination between cytosolic and mitochondrial translation during immune cell activation:

Persons involved: Ronaldo De Carvalho

Mitochondria are dynamic metabolic organelles implicated in many cellular processes such as ATP generation through respiration, regulation of apoptosis, production of reactive oxygen species (mtROS), calcium homeostasis, amino-acid metabolism and in various signaling pathways including some implicated in innate immunity[66,67]. The mammalian mitochondrial genome is a circular double-stranded DNA molecule coding for two ribosomal RNA, 22 tRNA and 13 proteins[66]. Interestingly, all of the 13 mitochondrial-encoded proteins are core subunits of the oxidative phosphorylation (OXPHOS) complexes that are required for ATP generation. The remaining ~1500 proteins of the mitochondrial proteome (including mitochondrial ribosomal proteins and proteins of the OXPHOS complex) are nuclear encoded. As a consequence, coordination between the mitochondrial and nuclear genome is important for mitochondrial homeostasis. Recent evidence from yeast, C.elegans and mice further indicates cross-talks between cytosolic and mitochondrial translation programs in order to synchronize synthesis of OXPHOS complexes and avoid mitonuclear protein imbalance[68,69]. Although mitochondria probably have an eubacterial origin, mitoribosomes differs significantly from bacterial ribosomes. They have a reversed protein/RNA ratio (69% protein and 31% RNA for mitoribosomes compared to 33% protein and 67% for bacterial ribosomes) and almost half of the mitoribosomal proteins are specific to mitoribosomes and do not have bacterial homologs [70]. The roles of mitoribosomal specific proteins are not fully understood but some have been implicated in translational control [71].
Upon stimulation, cells of the immune system undergo a transition from a quiescent state into a metabolic active state in which mitochondria play an essential regulatory role [67,72]. For example, proinflammatory M1 macrophages activated by IFN-γ undergo a decrease in oxidative phosphorylation and a corresponding increase in aerobic glycolysis. On the contrary, anti-inflammatory M2 macrophages maintain high rates of oxidative phosphorylation upon activation [72]. Similarly, naïve T cells depend mainly on oxidative phosphorylation as their primary method of respiration while activated T cells display higher glycolysis levels[73].
Based on these observations, we hypothesize that mitochondrial and cytosolic translation could undergo a coordinated remodeling during immune cell activation. We therefore plan on monitoring mitochondrial and cytosolic translation as well as mitoribosome composition to test whether they are modulated during the immune response and identify potential factors involved in this regulation.

Methodology and preliminary results

Aim1. The atlas of ribosome-associated proteins in the course of macrophage stimulation and its impact on the inflammatory response:

In this aim, we propose to characterize accessory proteins that interact with ribosomes during the course of macrophage activation and to further dissect the functional consequences of such interactions.

1.1. Flag-tagging of endogenous ribosomal proteins:

Adding a flag tag to endogenous ribosomal proteins will allow us to specifically purify ribosomes using commercial magnetic beads coupled with anti-flag antibodies that are

highly specific and efficient. Transgenic mice expressing tagged ribosomal proteins have been previously generated in the literature [74,75]. However, the ribosomal proteins that were tagged in these mice (RPL22 and RPL10A) were later shown not to be incorporated into all assembled ribosomes[51,55]. We therefore decided to target other ribosomal protein coding genes both from the small and the large ribosomal subunit. Based on the cryo-EM structure of the human ribosome[76], we have selected four mouse core ribosomal proteins (RPS5, RPS12, RPL7a, RPL11) that bear accessible N-terminal or C-terminal ends to introduce the Flag-tag through homology-directed recombination (Figure 6a). This procedure was successfully performed first in HEK293T cells using our patented method "Nanoblades"[77] that efficiently deliver the CRISPR/Cas9 technology together with single-stranded DNA oligos bearing the Flag-tag sequence flanked by homology arms homologous to the targeted region. Clonal cell lines expressing Flag-tagged ribosomal proteins from all alleles were obtained for Rps5 and Rpl7a and are viable. Heterozygous cell lines were also obtained for Rps12 and Rpl11. In these cell-lines, we validated expression and incorporation of the Flag-tagged proteins into translating ribosomes by sucrose gradient sedimentation (see Figure 1b for an example).

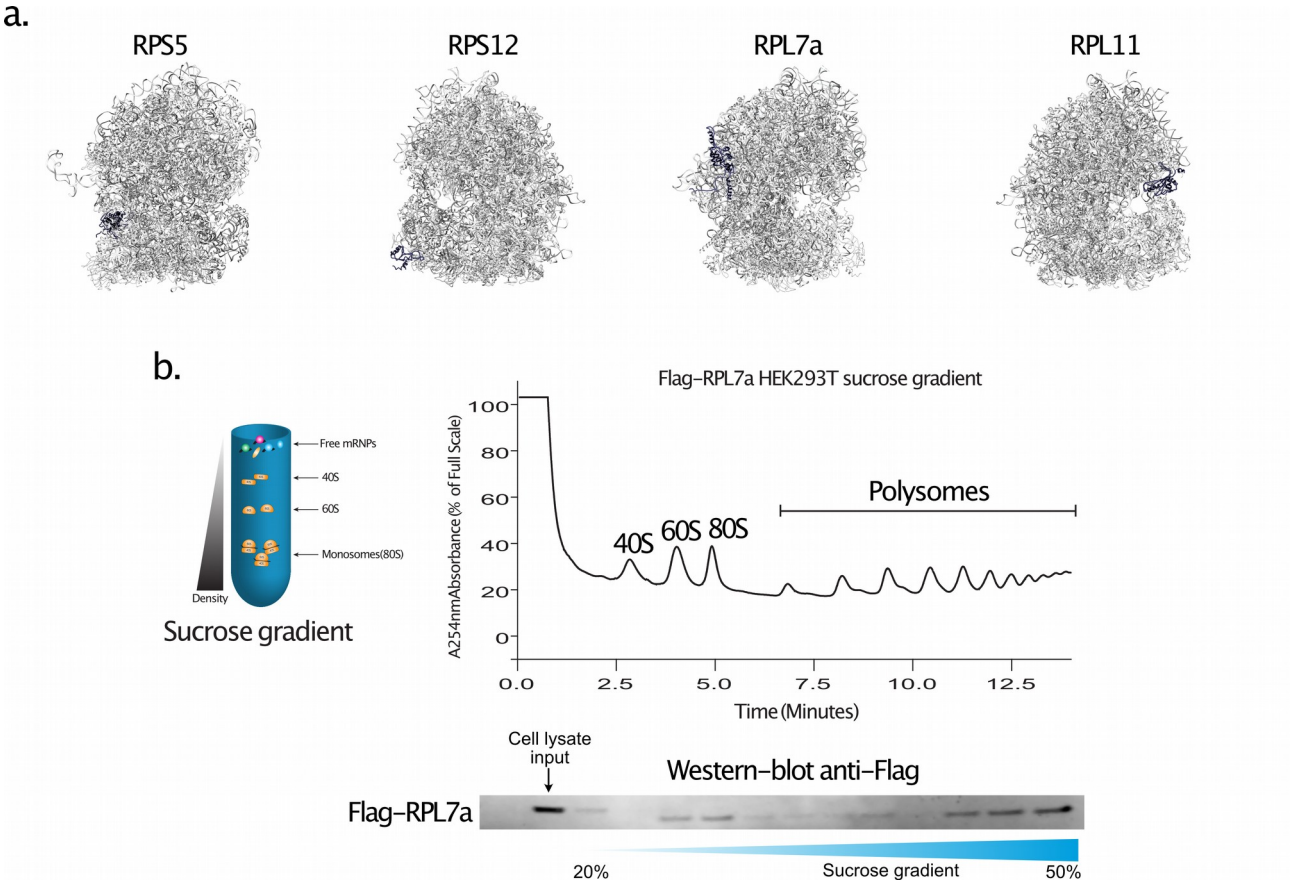

Figure 6. Flag-tagging of endogenous ribosomal proteins in HEK293T cells. a. Position (highlighted in purple) of selected candidate ribosomal proteins to flag in the crystal structure of the mammalian ribosome. **b.** Sucrose sedimentation of cytoplasmic extracts obtained from Flag-RPL7a cells and western-blotting of collected fractions using anti-Flag antibodies.

For the past year, we have tried to generate transgenic mice expressing Flag-tagged ribosomal proteins through electroporation of the Cas9 protein [78] together with the sgRNA and the DNA donor bearing the Flag-tag sequence with homology arms for Rps5 and Rpl11. However, despite many attempts, we have been unable to generate viable mice. We do not think this viability issues are linked to the presence of the Flag-tag but rather because of the possible inactivation of the ribosomal protein coding gene when the Cas9 protein cleaves the targeted locus but recombination does not occur. To overcome this

problem, we are currently trying the Prime-editing approach recently published by the Liu laboratory [79] in order to introduce the Flag-tag sequence at the Rps5 and Rpl11 loci without inducing dsDNA breaks at the targeted sites and thus avoiding inactivation of their expression. In parallel, we are also testing the use of biotinilated puromycin to purify ribosomes through the previously described RiboLace protocol [80] without requiring the expression of a Flag-tagged ribosomes. In this case, the biotinilated puromycin incorporates within actively translating ribosomes, samples are then treated with Rnase A+T1 and ribosomes precipitated using Streptavidin-beads and eluted from beads using EDTA to induce disassembly of the two ribosomal subunits.

1.2. Purification of flag-tagged ribosomes and analysis of their protein composition:
Once the transgenic mice expressing Flag-tagged ribosomal proteins will be generated, bone-marrow derived macrophages (BMDMs) will be cultured and ribosomes purified to characterize their composition during the time-course of activation. Particular attention will be given to the stimulatory signals used to activate cells in order to identify factors that specifically associate with ribosomes in a given activation pathway. For this, BMDMs will be stimulated either with ultra pure lypopolysaccharide to activate the TLR4 pathway, or with Pam3CSK4 to activate the TLR2/TLR1, or with cGAMP to activate the cytosolic DNA-sensing stimulator of IFN genes (STING) pathway to induce pro-inflammatory responses. Conversely, BMDMs will also be incubated with IL4 or IL13 to induce anti-inflammatory responses[81]. Upon activation, cells will be lysed to obtain the cytoplasmic fraction, which will then be treated with RNases to collapse polysomes into 80S ribosomes and their mRNA footprint (Figure 7a and b). Ribosomes will then be immunopurified using anti-flag magnetic beads (Figure 2c). After washing the purified complexes on beads, ribosomes will be specifically eluted using saturating amounts of a Flag-peptide. This protocol offers high specificity because both immunoprecipitation and elution from beads depend on the Flag epitope. Furthermore, for the past year, we have used our HEK-293T cell lines expressing Flag-tagged RPS12, RPS5, RPL7a and RPL11 to optimize the immunoprecipitation protocol. We currently have a protocol that minimizes background noise and allows enrichment of ribosomal proteins up to 1000 fold compared to the negative control (untagged cells) when performing mass spectrometry (Figure 8d). Furthermore, we have set up an alternative protocol combining formaldehyde crosslinking, RNase treatment and Flag-immunoprecipitation of ribosomes which allows to capture more transient interactions also with a high signal-to-noise ratio (average of 250 fold enrichment of ribosomal proteins in Flag-ribosome samples compared to the untagged negative control). Preliminary analysis of our Mass spectrometry data suggests that RPS5, RPL7a and RPL11 are good candidates to identify RAPs in a unbiased manner. On the contrary, RPS12 displayed a strong bias towards 80S and light monosomes upon Flag-immunoprecipitation thus suggesting that the Flag-tag might not be accessible within heavy and dense polysomes (data not shown).
Proteins samples obtained from purified ribosomes at different times following activation will be specifically labeled using tandem mass tags. This strategy will allow us to mix all the samples corresponding to each time-point for a given stimulation pathway and subject them to liquid chromatography tandem-mass spectrometry (LC-MS/MS) analysis together. Sample preparation for LC-MS/MS and data analysis will be done in collaboration with Prof. Alfredo Castello-Palomares and Prof. Shabaz Mohammed (University of Oxford, UK) who are experts in this technique. Upon mass-spectrometry, identified proteins will be classified into different categories based on their functional role and relevant candidates will be validated for their interaction with ribosomes in live cells by immunofluorescence and co-immunoprecipitation experiments. If possible, we will focus on relevant candidates spanning different cellular functions (RNA metabolism,

enzymes, related to inflammation, uncharacterized function…) and also those showing differential association to ribosomes during the course of macrophage activation.

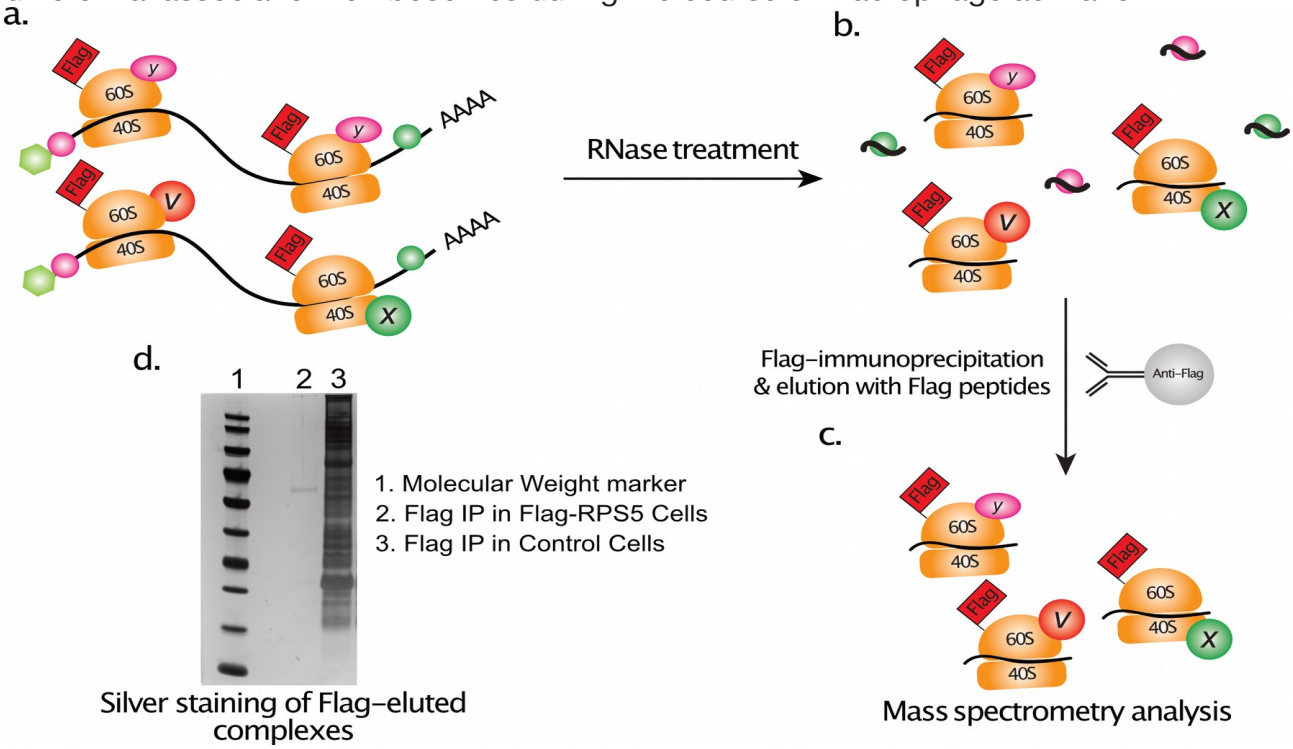

Figure 7. Ribosome immunopurification protocol. a and b. Cytoplasmic lysates from Flag-expressing cells are treated with RNase to collapse polysomes into 80S monosomes and their associated mRNA footprints. **c.** Following Flag-IP and elution from beads using Flag peptides, samples are sent for Mass spectrometry analysis. **d.** Silver-staining of Flag-tagged ribosomes purified using Flag-affinity agarose beads from wildtype HEK293T cells ("Flag IP in Control Cells" lane) and in Flag-RPS5 expressing cells ("Flag IP in Flag-RPS5 Cells" lane).

Preliminary mass spectrometry data from HEK293T cells has lead to the identification of close to 130 proteins that associate with ribosomes under native conditions and close to 280 upon formaldehyde-crosslinking (data not shown). We are therefore confident that the protocol is ready to be tested on primary BMDMs once the transgenic mice will be available.

1.3. Functional characterization of specialized ribosomes:

Because ribosomes are amongst the most abundant components within cells, we expect most of the identified accessory proteins to be present in substoichiometric amounts. Hence, we anticipate that only a fraction of all cellular ribosomes will be decorated with our candidate proteins. Based on this assumption, it will be of interest to further study the particular subsets of ribosomes that associate with our selected candidate proteins and could qualify as "specialized ribosomes". For this, we plan to adapt the RNA-Immunopurification in Tandem (RIPiT) protocol[22,23] that I developed during my postdoctoral training to purify subsets of ribosomes that are associated with a particular non-ribosomal protein. Briefly, cell lysates will be treated with RNases to collaps polysomes into 80S ribosomes associated to their mRNA footprint. Ribosomes will be purified using Anti-Flag beads and eluted from beads using saturating amounts of Flag-peptide. A second immunoprecipitation against the ribosome-associated factor of interest is then performed to recover the specific subset of ribosomes bound to our protein of interest. After this, samples will be analyzed by LC-MS/MS to identify other proteins that co-associate with ribosomes together with our protein of interest. In parallel, we will collect the RNA footprints of the purified ribosomes and perform high-throughput sequencing to identify their exact position on the translated mRNAs. From this experiments, we expect to characterize the exact composition and mRNA targets of

different pools of “specialized ribosomes”.
To further understand the functional consequences of the interaction of our proteins of interest with ribosomes we will perform mutagenesis experiments in order to map the domains that are responsible for ribosome binding. Following this, we will perform genome-editing experiments in order to either inactivate the candidate factors or mutate their ribosome binding sites in mouse BMDMs or transgenic mice. Then we will monitor the consequences of the loss in ribosome-association or the complete absence of the factor on the stimulation of macrophages by performing RNA-seq, ribosome-profiling experiments, FACS analysis and elisa tests to measure multiple parameters of the inflammatory such as cytokine production.

Aim2. Cross-talks between ribosomes and translation with mRNA decay pathways:

In this aim, we propose to assess the impact of mRNA translation in inducing decay of translated transcripts, to identify new cis- and trans-acting features involved in this regulatory pathway and to reveal the importance of translation-dependent decay in regulating macrophage and T CD4+ cell activation.

2.1. Monitoring translation-dependent mRNA decay during macrophage and T CD4+ cell activation:

To monitor translation-dependent mRNA decay (TDD) and address its impact in regulating gene expression during immune cell activation, we have established and optimized a protocol that allows to measure mRNA decay rates in the presence and absence of translation (Figure 8a). This approach relies in the use of transcription and translation inhibitors coupled to high-throughput sequencing to measure mRNA levels. Briefly, this protocol (Figure 8a) consists in activating (or not) primary mouse CD4+ T Cells or BMDMs for a given amount of time and then blocking transcription during 3 hours in the absence or presence of a translation inhibitor. During these 3 hours, we recover three aliquots of the cells (at the 0, 1h and 3h time points after blocking transcription) add synthetic RNA spike-in as an external control to allow for gene expression normalization before preparing samples for RNA-seq to measure mRNA levels. Doing so, we are able to obtain a decay rate for each cellular mRNA during the time-course. Then, by comparing these half-lives to those obtained in the presence of translation inhibitors, we are able to precisely quantify the impact of translation on decay rates. Based on this measure, TDD substrates are defined as transcripts for which degradation is significantly delayed upon incubation with translation inhibitors (Figure 8b). From this data, a TDD index can be calculated, corresponding to the extent of observed mRNA decay that is dependent on translation (Figure 8b, red formula). For any given transcript, the TDDindex can range from 0 (no observed translation-dependent mRNA decay) to 1 (unstable transcript which degradation is entirely translation-dependent). In addition to the TDDindex, we can calculate a translation-independent decay Index (TIDindex) corresponding to the extent of observed decay that is not dependent on translation(Figure 8b, blue formula). The sum of the TDD and TID indexes corresponds to the overall observed decay at the 1h or 3h time point in the presence of the transcription inhibitor.

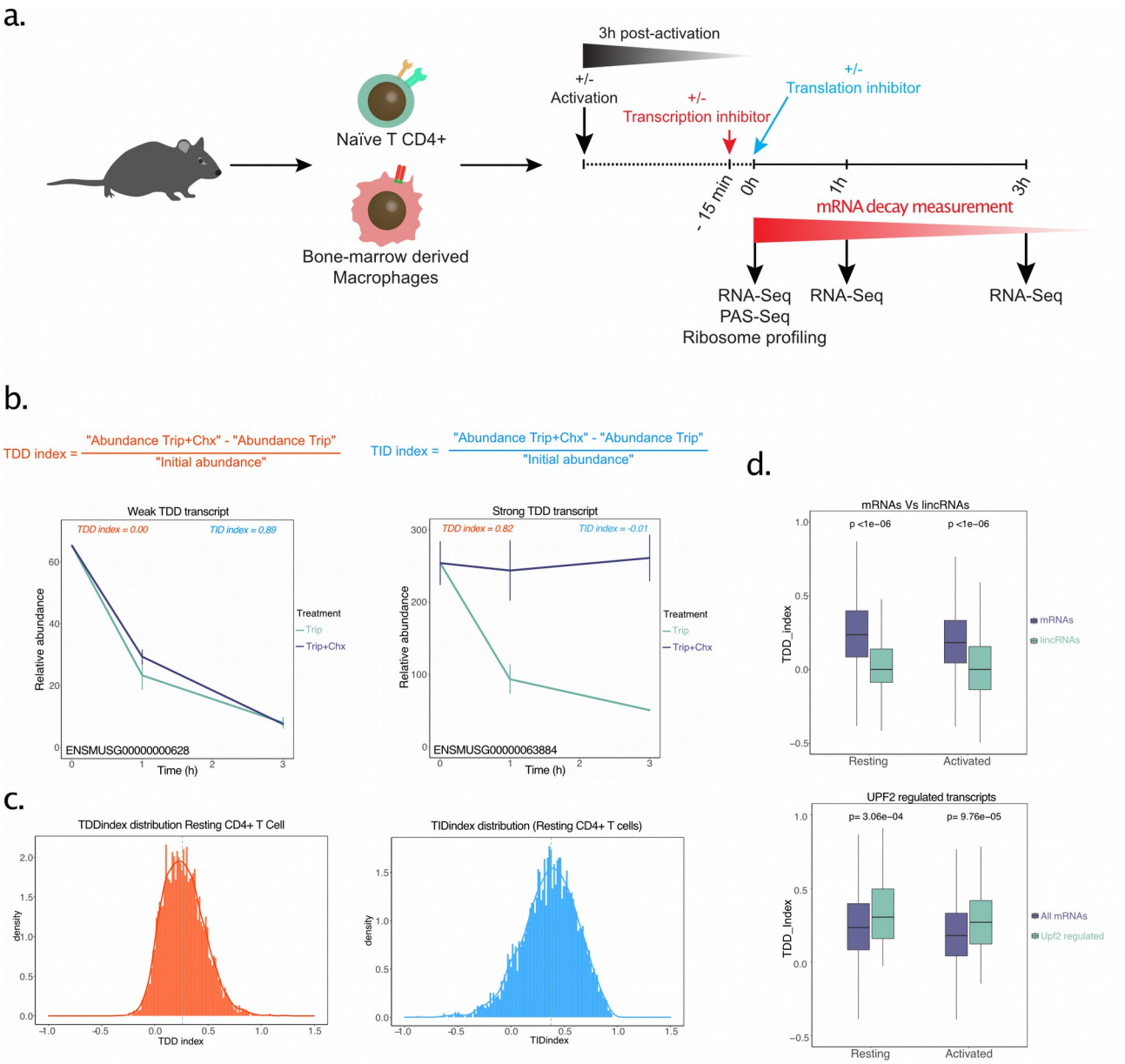

Figure 8. Monitoring TDD in primary CD4+ T cells BMDMs. a. Protocol for monitoring TDD. **b.** Measurement of mRNA decay rates in the presence and absence of translation for, a non-TDD transcript (left panel), a strong TDD transcript (Right panel). **c.** Distribution of TDDindex and TIDindex amon all expressed transcripts in resting CD4+ T cells. **d.** Distribution of TDD index in protein coding mRNAs Vs lincRNAs (Top-panel) and in all expressed mRNAs Vs known UPF2 regulated transcripts (bottom panel).

To avoid experimental biases introduced by transcription and translation inhibitors, all experiments were performed in three independent replicates using two different transcription inhibitors (DRB and Triptolide) and two different translation inhibitors (Cycloheximide and Harringtonine) in all possible combinations (DRB alone, DRB + Cycloheximide, DRB + Harringtonine, Triptolide alone, Triptolide + Cycloheximide and Triptolide + Harringtonine).

In parallel of these experiments, we also performed ribosome profiling and poly(A)-site sequencing (PAS-seq) in resting and activated cells in order to calculate the ribosome density of all expressed transcripts as well as to map their precise 3' end. Combined with regular RNA-seq, this data allowed us to obtain a global view of transcript structure, abundance and a proxy for translation efficiency in a genome-wide manner.

Preliminary results:

Surprisingly, our results indicate that most cellular transcripts appear to undergo TDD to some extent (Figure 8c). This unexpected result does not appear to be a technical artifact

induced by the drugs used to block translation and transcription since long-non coding RNAs (which are capped and polyadenylated like mRNAs but are not translated) are not significantly regulated by TDD (Figure 8d, top panel). On the contrary, transcripts previously described to be regulated by Upf2 (an essential factor in nonsense-mediated decay) do display higher than average TDDindexes (Figure 8d, bottom panel) thus validating our approach to monitor translation-dependent mRNA decay.

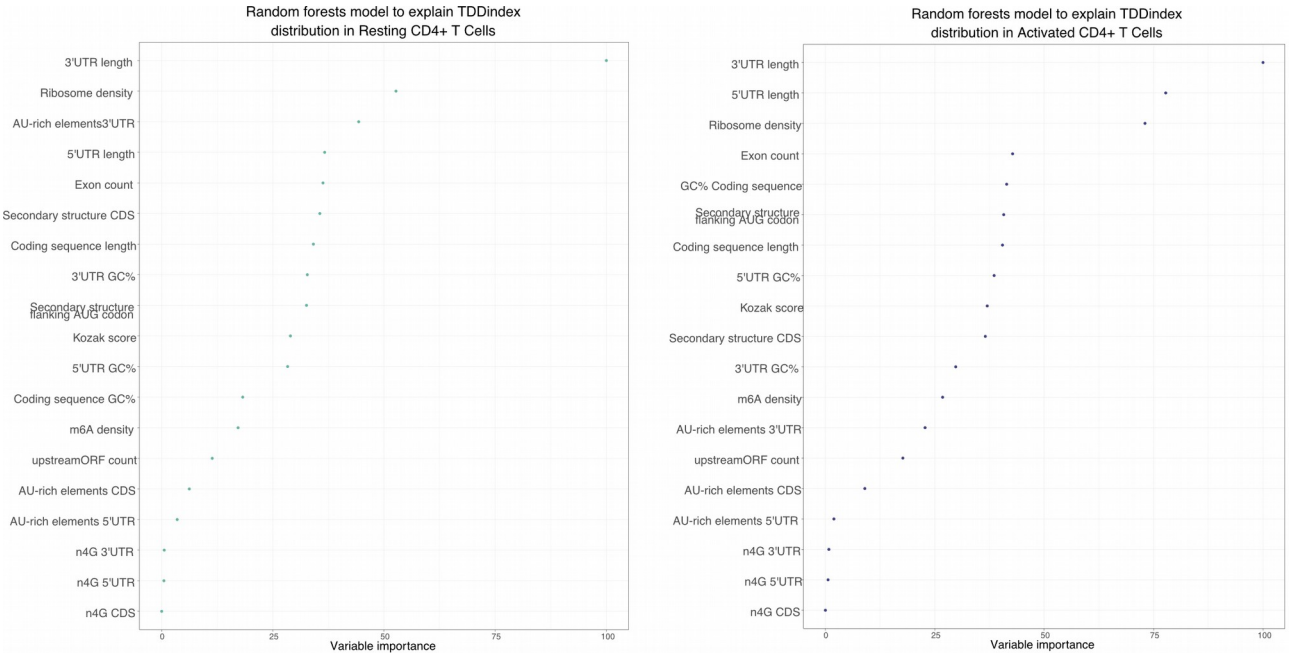

Figure 9. Random forests analysis identifies cis- and trans-acting features explaining TDDindex. Explicative variables used as input to build random forests decision trees are listed with their corresponding importance in predicting the TDDindex. Left panel corresponds to results in resting CD4+ T cells while the right panel corresponds to results obtained in activated CD4+ T cells.

2.2. Identification of mRNA *cis*- and *trans*-acting features responsible for TDD:

Because our approach identifies all TDD targets independently of the mechanism that triggers it (NMD, uORFs, AREs), we plan on characterizing the *cis*- and *trans*-acting features responsible for inducing TDD in our identified transcripts.

For each cellular transcript in each tested cell type and time point, we used our assembled transcriptome to collect information such as total transcript length, length of the 5'UTR, coding sequence (CDS) and 3'UTR, GC content, Kozak context surrounding the AUG start codon and codon usage among others. In order to identify features that might explain the observed TDDindex values, we performed exploratory data analysis using a random decision forests approach, a machine learning algorithm that allows data mining to identify explicative factors that can predict an observed variable (in this case the TDDindex). For simplicity reasons, all results presented herein correspond to resting and activated CD4+ T cells, but similar findings were also obtained in BMDMs (Figure 9).

A role for untranslated regions and ribosome density in defining TDD

Random forests analysis indicated that ribosome density together with 3'UTR and 5'UTR length are major factors responsible for explaining the extent of TDD in the overall transcript population (Figure 9). Interestingly, we observe a negative correlation between 5' and 3'UTR length and the extent of TDD (Figure 10, middle and bottom panels). These results appear in contradiction with previous findings related to long 3'UTR being degraded in a UPF1-dependent manner but are in agreement with results obtained in zebrafish showing that long 3'UTRs can protect mRNA from mRNA decay induced by

poor codon usage [82]. Contrary to UTR length, ribosome density shows a bimodal relationship with TDD, being positively correlated to the TDDindex for low to medium values of ribosome density and then reaching a plateau (Figure 10, top panel).

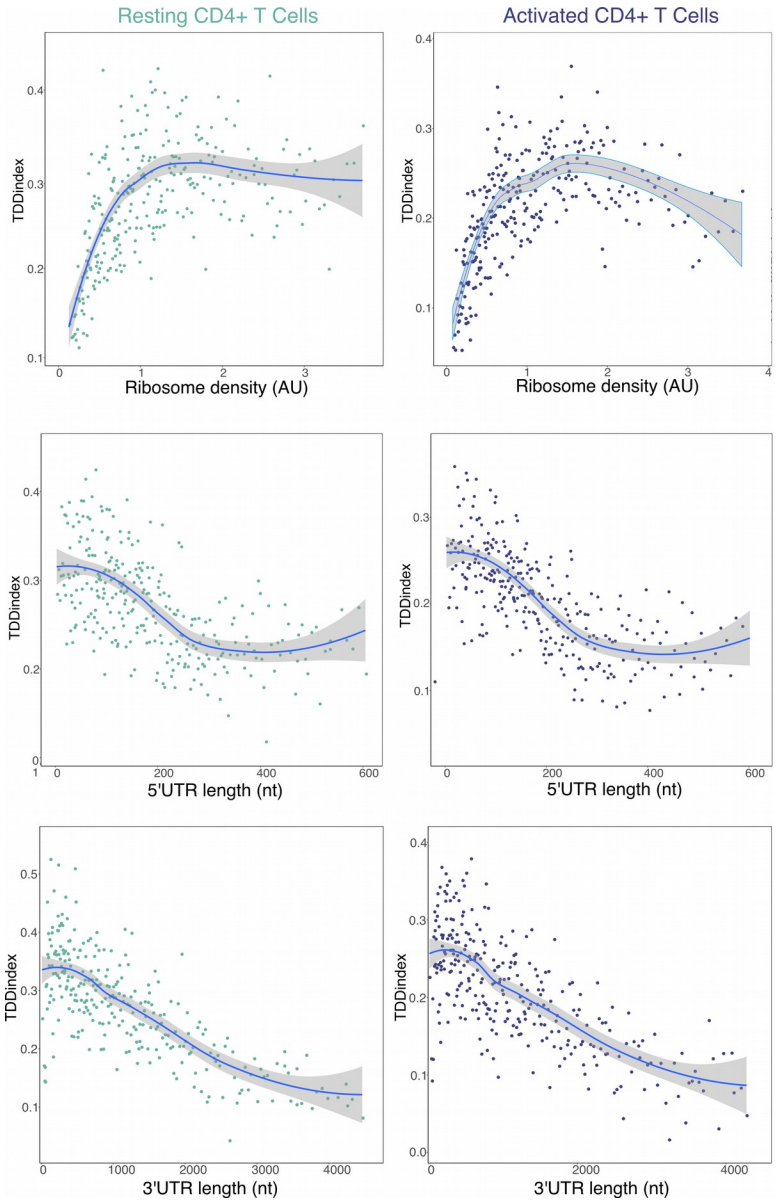

Figure 10. Ribosome density and UTR length are linked to the TDDindex. Relationship between ribosome density (Top panel), 5'UTR length (Middle panel) and 3'UTR length (Bottom panel) with the TDDindex in resting (left) and activated (right) CD4+ T cells. In all plots, transcript were first sorted either by their ribosome density, 5'UTR length or 3'UTR length, then they were binned in groups of 30 transcripts and the average TDDindex was calculated and plotted. This was done to obtain a clearer view of the trend.

Codon usage and GC3 content are linked to TDD

Codon usage and GC content at the wobble position (GC3) have been recently shown to modulate mRNA decay in human cells [83–86]. Particularly, one of these studies indicated that mRNAs with GC3 rich codons are more efficiently translated and overall more stable than those with GC3 poor codons [84]. In resting CD4+ T cells, our findings validate those previously published when looking at overall mRNA decay (Figure 11a). However, when looking at the extent of TDD and GC3 content we observe the exact opposite results (Figure 11b). Transcripts with GC3 rich codons have higher TDDindexes than those with GC3 poor codons. On the contrary, translation-independent mRNA decay appears to follow the same distribution than overall mRNA degradation with respect to GC3 content (Figure11c). These result suggest that the observed effect of GC3 content in mediating mRNA decay are largely driven by a translation-independent degradation pathway and

not through an active translation-dependent mechanisms.

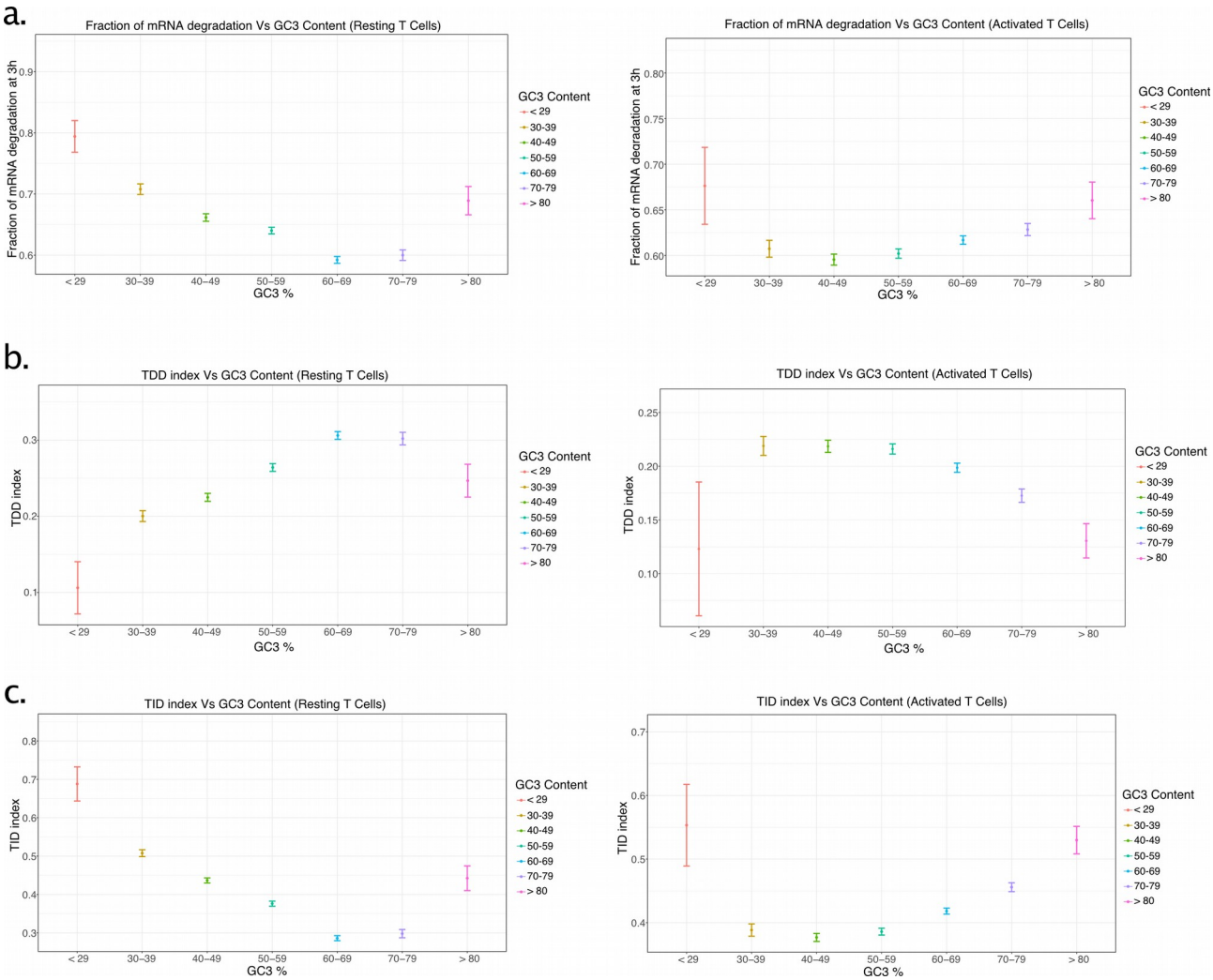

Figure 11. RNA decay, TDDindex and TIDindex are related to GC% at the wobble position of codons (GC3%). Transcripts were sorted with respect to their GC3 content and binned in seven groups (from low to high GC3 content). Then, fraction of mRNA degradation (Top panel) or the TDDindex (Middle panel) or the TIDindex (Bottom panel) were plotted for each group in resting (left panels) or activated CD4+ T cells (right panels).

Interestingly, upon CD4+ T Cell activation, the relationship between GC3 content and mRNA decay is strongly reshuffled and does not appear to follow the same trend as in resting CD4+ T cells (Figure 11, right panels). Nevertheless, even in this scenario, the relationship between overall mRNA decay and GC3 content is again driven mainly through a translation-independent mRNA degradation pathway.

These results suggest that the relationship between GC3 content and TDD is not solely dependent on transcript *cis*-acting elements but could be driven by *trans*-acting factors which availability or activity could be modulated during T cell activation.

Changes in ribosome-density upon T cell activation modulate the extent of TDD, TID and overall mRNA decay

Our results suggest that ribosome density is an important factor in defining the extent of TDD. To validate this finding and test whether ribosome density is directly involved in TDD decay, we tested whether changes in ribosome density upon CD4+ T Cell activation were also linked to the expected changes in their TDDindex. For this, we computed the fold change of ribosome density between resting and activated CD4+ T Cells that we plotted against the observed changes in the TDDindex between these two conditions (Figure 12 a). Interestingly, we observe an overall positive correlation between the fold change in

ribosome density and the observed change in TDDindexes (i.e. transcript with decreased ribosome density upon T cell activation show a decrease in their TDDindex while transcripts with increased ribosome density have a tendency to show higher TDDindexes. Surprisingly, we observed the opposite relationship when plotting changes in the TIDindex against changes in ribosome density again suggesting that translation-independent mRNA decay is also affect by ribosome density (Figure 12b). This finding is better observed when plotting changes in TDDindex against changes in the TIDindex while coloring the fold change in ribosome density between resting and activated CD4+ T Cells (Figure 12d). Here we observe that changes in TDD and TIDindexes are negatively correlated between each other and clearly explained by changes in ribosome density (Figure 12d).

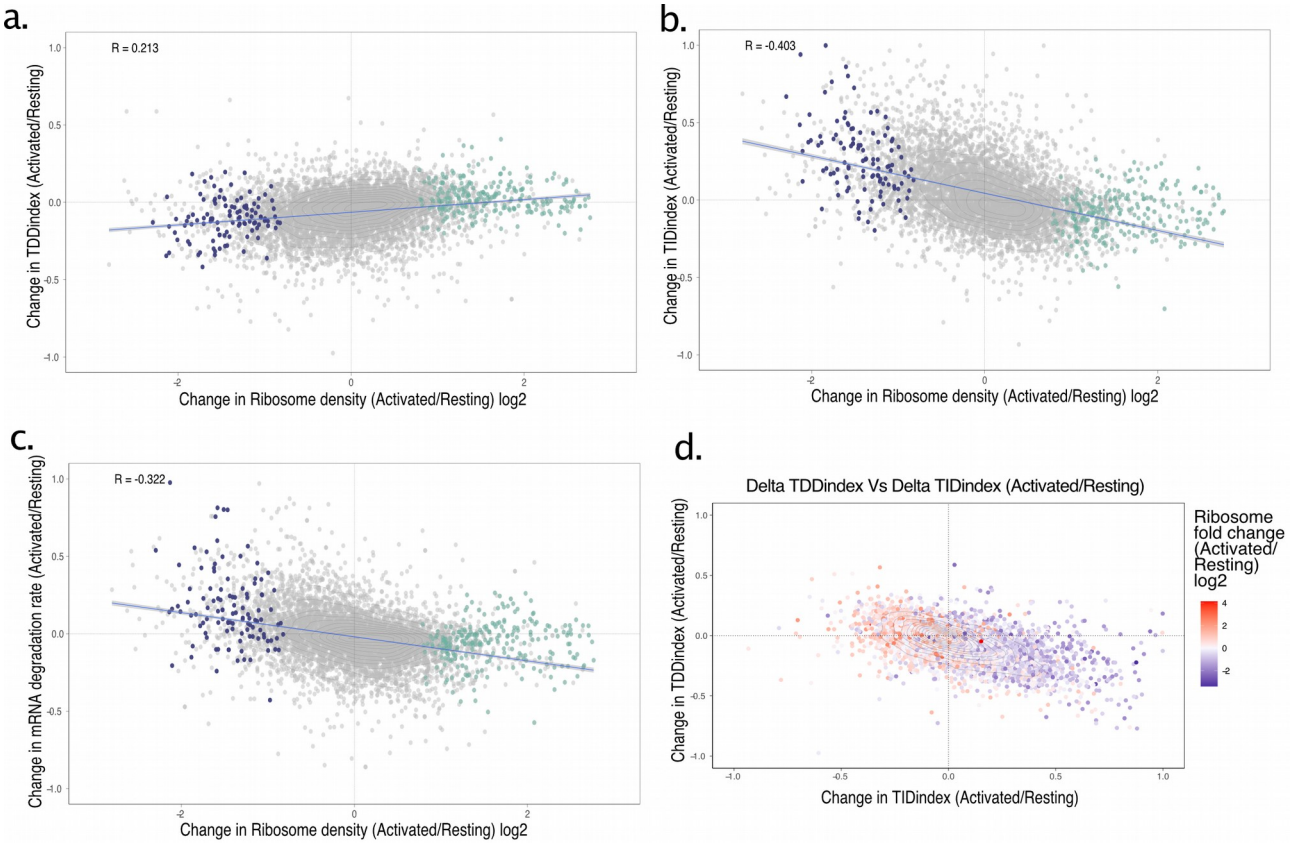

Figure 12. Changes in ribosome density are associated to corresponding changes in TDD and TID indexes. a. The fold change in ribosome density (log2 fold scale) between resting and activated CD4+ T cells is plotted against the observed changes in the TDDindex. **b.** The fold change in ribosome density (log2 fold scale) between resting and activated CD4+ T cells is plotted against the observed changes in the TIDindex. **c.** The fold change in ribosome density (log2 fold scale) between resting and activated CD4+ T cells is plotted against the observed changes in mRNA degradation rates.

Interestingly, as previously observed with GC3 content, overall mRNA decay shows a similar trend as translation-independent decay with respect to changes in ribosome density. That is to say, an increase in ribosome density upon T cell activation is associated with a decrease in mRNA decay while a decrease in ribosome density is associated to an increase in mRNA decay (Figure 12c).

Taken together, our results suggest that translation-dependent and independent degradation pathways are mutually exclusive pathways that are defined (at least partially) by ribosome density. Overall, translation-independent mRNA decay appears more efficient than translation-dependent decay. This findings could be linked to recent results from Dominique Weill's laboratory indicating GC content as an important determinant of recruitment of mRNAs into p-bodies [83]. We believe that ribosome density could be responsible for determining mRNA recruitment within p-bodies, mRNAs poorly associated

with ribosomes being more efficiently recruited in the latter contrary to mRNAs highly associated with ribosomes. Nevertheless, more experiments are required to validate these findings.

2.3. Mechanism of action of TDD and TID pathways:

In order to dissect the molecular mechanisms of TDD and TID, we plan on working in BMDMs which we can efficiently modify genetically using Nanoblades [28]. Recent studies have pointed to different factors that could associate to ribosomes in order to trigger translation-dependent mRNA decay such as ZNF598, Xrn1 and the Ccr4-Not complex [87–90]. We therefore plan a strategy to perform RIPiT-seq against ribosomes associated to those proteins in order to map their position along translated mRNAs and test whether transcripts prone to TDD are indeed enriched in ribosomes bound to those factors. In parallel, we will also use our Mass-spectrometry data from Aim 1 to identify potential mRNA decay factors that associate with translating ribosomes. Expression of these factors will also be impaired in BMDMs using Nanoblades to test the consequences on mRNA decay rates as well as the fraction of TDD and TID using our transcription/translation inhibitor protocol.

In addition to these experiments, we plan on testing the role of UTR length in modulating TDD and if possible to characterize its mechanism of action. Previous results from Yukihide Tomari's laboratory indicate that long 3'UTRs could protect mRNAs with poor codons from Ccr4-Not recruitment but the exact mechanism is still largely unknown [82]. For this, we plan on constructing reporter genes with different 5'UTR, CDS GC content and 3'UTR lengths allowing different ribosome loading capacities and containing a streptavidin RNA motif to purify them using streptavidin magnetic beads. We will then use these reporter constructs to monitor the extent of translation-dependent and independent mRNA decay and if possible to study the recruitment of mRNA decay factors by western-blotting or mass spectrometry. We expect from this experiments to obtain clues for the molecular mechanism of TDD and independent mRNA decay pathways as well as the role of cis-acting transcript features in modulating recruitment of mRNA decay factors.

Aim3. Testing the potential coordination between cytosolic and mitochondrial translation during immune cell activation:

In order to study mitochondrial translation we rely again on introducing a Flag-tag epitope within nuclear genes coding for mitoribosomal proteins. For this, selected several genes that had accessible Cas9 target sites near their Stop-codon to induce a double-strand break and introduce the Flag-tag sequence through homology-directed recombination at the 3'end of the coding sequence to express a C-terminal flag-tagged protein (Figure 13a). Using this approach in cultured HEK293T cells, we have been able to tag different proteins from the small and large mitoribosomal subunits without affecting cell viability. Similarly to the cytosolic ribosome, the flag-tagged mitoribosomal proteins are well incorporated within mitoribosomes (Figure 13b) and efficiently pulled-down using the same protocol as that optimized for the cytosolic ribosome. Preliminary mass-spectrometry results, indicate an efficient purification of mitoribosomes and similar signal-to-noise ratios as those obtained with cytosolic ribosomes when comparing to the control IP condition. This approach in HEK293T has already led to the identification of many mitoribosome associated proteins (data not shown) that could be involved in the regulation of translation and other related processes within mitochondria.

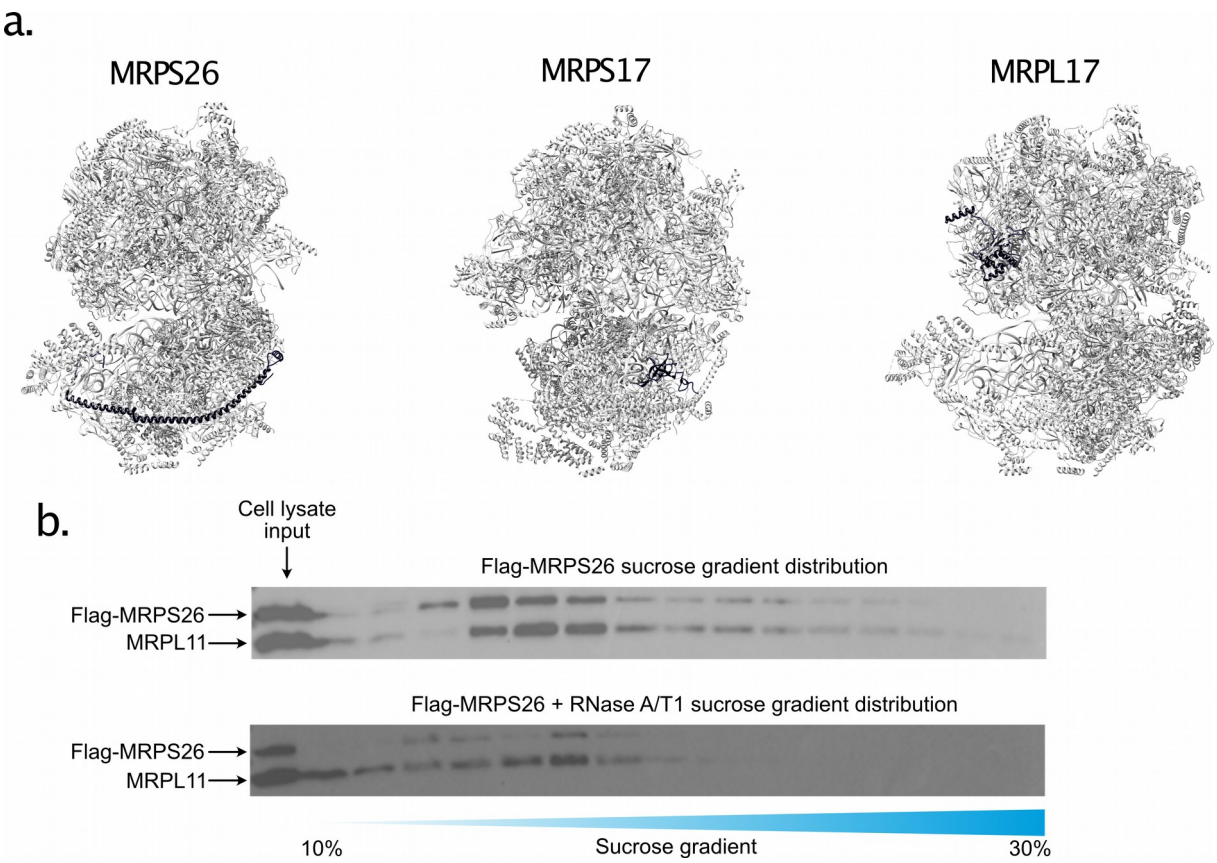

Figure 13. Flag-tagging of endogenous mitoribosomal proteins in HEK293T cells. a. Position (highlighted in purple) of selected candidate mitoribosomal proteins to flag in the crystal structure of the mammalian mitoribosome. **b.** Sucrose sedimentation of cytoplasmic extracts obtained from Flag-MRPS26 cells and western-blotting of collected fractions using anti-Flag antibodies and anti-MRPL11 antibodies.

In parallel of these experiments we have generated transgenic mice expressing a Flag-tagged MRPS17 protein through CRISPR/Cas9 electroporation together with a donor DNA bearing the Flag-tag sequence with homology arms flanking the mrps17 targeted locus. In this case, upon optimization of the Cas9 electroporation conditions, we were able to generate transgenic mice bearing the Flag-tag at the mrps17 locus. Homozygous mice are viable thus indicating that the presence of the Flag-tag does not affect mitoribosome function. We are performing backcrosses to eliminate potential mutations at Cas9 off-target sites and will soon be able to perform experiments using these mice.

Cytoribosome and mitoribosome profiling during immune cell activation

To monitor cytosolic and mitochondrial translation we plan on performing Flag-immunoprecipitation of mitoribosomes from resting and activated CD4+ T Cells and BMDMs following a protocol previously published in yeast to purify Flag-tagged mitoribosomes and perform mitoribosome profiling [68]. From the same cell extracts, we will also perform cytosolic ribosome profiling using classical approach relying on sucrose gradient sedimentation. Performing these experiments at different times upon cell activation, we will test whether translation of nuclear and mitochondrial encoded OXPHOS subunits is differentially affected and whether there is any evidence of synchronization between the two compartments. If we find evidence for differential translation regulation among the different transcripts coding for OXPHOS subunits we will use Mass-spectrometry data from mitoribosome-associated proteins in order to try to identify protein factors that could mediate such regulation.

General conclusion and perspectives

Overall, our projects focus on ribosomes and their role in serving as hubs for non-ribosomal proteins to regulate translation and possibly other related processes such as mRNA decay or post-translational modification of nascent proteins. We are mainly interested in cells of the immune system as they undergo a profound and dynamic modification of their gene expression program that could involve changes in the set of ribosome associated proteins. However, as we develop the technical tools required to study ribosome composition, we also plan to apply them to other cellular contexts such as viral infections. Indeed, mRNA translation is the only step of the viral replication cycle for which all known viruses are entirely dependent on the host cellular machinery. Modification of ribosome composition upon viral infection could therefore be an important regulatory layer to hijack this essential cellular component. We expect from this work to characterize a new layer of gene expression regulation that would involve cross-talks between different processes related to translation during immune cell activation.

In addition to using ribosome immuno-purification and mass spectrometry to characterize the pool of ribosome-associated proteins in cells, we plan in the near future to develop alternative approaches that could allow us to map the position of such interactions on the ribosome and if possible yield information on the dynamics of the association. To this aim, we will establish a quantitative yeast two-hybrid protocol that was recently published by David Cluet [91] (Research engineer that joined our laboratory in January 2020) to test direct interactions of ribosomal proteins against a library of cellular ORFs and obtain affinity values for the positive interactions. A similar approach will also be tested within the context of assembled ribosomes in mammalian cells using a split fluorescent protein protocol to screen for protein interactors of specific ribosomal proteins[92].

Our results about the impact of ribosome density on mRNA stability raise several questions regarding how elongating ribosomes mediate decay of the mRNA they translate. Recent studies point towards ribosome collisions as important determinants of mRNA decay and some of the molecular aspects of this phenomenon are starting to be elucidated [88,93,94]. However, how cis-acting features such as UTR length and codon usage affect translation-dependent mRNA are yet to be fully understood. Furthermore, how translation-dependent and independent pathways compete against each other will be an important focus of our research efforts in the next years.

Finally, the study of mitoribosomal translation is an exploratory and more risky project that I think could lead to the characterization of new factors involved in finely tuning and synchronizing cytosolic and mitochondrial translational programs. Since mitochondria play a multitude of essential roles during immune cell activation, I think it is one of the most relevant context to study this question.

References

1. Ricci, E. P. *et al.* In vitro expression of the HIV-2 genomic RNA is controlled by three distinct internal ribosome entry segments that are regulated by the HIV protease and the Gag polyprotein. **14**, 1443–1455 (2008).
2. Rein, A. RNA Packaging in HIV. *Trends in Microbiology* **27**, 715–723 (2019).
3. Herbreteau, C. H. *et al.* HIV-2 genomic RNA contains a novel type of IRES located downstream of its initiation codon. *Nature structural & molecular biology* **12**, 1001–1007 (2005).
4. Prévôt, D. *et al.* Characterization of a novel RNA-binding region of eIF4GI critical for ribosomal scanning. *The EMBO journal* **22**, 1909–1921 (2003).
5. Ricci, E. P. *et al.* Activation of a microRNA response in trans reveals a new role for poly(A) in translational repression. **39**, 5231 (2011).
6. Ricci, E. P. *et al.* miRNA repression of translation in vitro takes place during 43S ribosomal scanning. **41**, 586–598 (2012).
7. Meijer, H. A. *et al.* Translational Repression and eIF4A2 Activity Are Critical for MicroRNA-Mediated Gene Regulation. *Science* **340**, 82–85 (2013).
8. Le Hir, H., Moore, M. J. & Maquat, L. E. Pre-mRNA splicing alters mRNP composition: evidence for stable association of proteins at exon-exon junctions. *Genes & development* **14**, 1098–1108 (2000).
9. Nott, A., Le Hir, H. & Moore, M. J. Splicing enhances translation in mammalian cells: an additional function of the exon junction complex. *Genes & development* **18**, 210–222 (2004).
10. Smatti, M. K. *et al.* Epstein–Barr Virus Epidemiology, Serology, and Genetic Variability of LMP-1 Oncogene Among Healthy Population: An Update. *Frontiers in Oncology* **8**, (2018).
11. Baumforth, K. R., Young, L. S., Flavell, K. J., Constandinou, C. & Murray, P. G. The Epstein-Barr virus and its association with human cancers. *Molecular Pathology* **52**, 307–322 (1999).
12. Hiriart, E. *et al.* A Novel Nuclear Export Signal and a REF Interaction Domain Both Promote mRNA Export by the Epstein-Barr Virus EB2 Protein.
13. Juillard, F. *et al.* Epstein-Barr Virus Protein EB2 Contains an N-Terminal Transferable Nuclear Export Signal That Promotes Nucleocytoplasmic Export by Directly Binding TAP/NXF1. *The Journal of Virology* **83**, 12759–12768 (2009).
14. Mure, F. *et al.* Epstein-Barr Virus Protein EB2 Stimulates Translation Initiation of mRNAs through Direct Interactions with both Poly(A)-Binding Protein and Eukaryotic Initiation Factor 4G. *Journal of Virology* **92**, (2017).
15. Duchaine, T. F. *et al.* Staufen2 isoforms localize to the somatodendritic domain of neurons and interact with different organelles. *Journal of Cell Science* **115**, 3285–3295 (2002).
16. de Lucas, S., Peredo, J., Marión, R. M., Sanchez, C. & Ortín, J. Human Staufen1 Protein Interacts with Influenza Virus Ribonucleoproteins and Is Required for Efficient Virus Multiplication. *The Journal of Virology* **84**, 7603–7612 (2010).
17. Dugré-Brisson, S. *et al.* Interaction of Staufen1 with the 5' end of mRNA facilitates translation of these RNAs. **33**, 4797–4812 (2004).
18. Thomas, M. G., Martinez Tosar, L. J., Desbats, M. A., Leishman, C. C. & Boccaccio, G. L. Mammalian Staufen 1 is recruited to stress granules and impairs their assembly. *Journal of Cell Science* **122**, 563–573 (2009).
19. Ramos, A. *et al.* RNA recognition by a Staufen double-stranded RNA-binding domain. *The EMBO journal* **19**, 997–1009 (2000).
20. Liu, Z. R., Wilkie, A. M., Clemens, M. J. & Smith, C. W. Detection of double-stranded

RNA-protein interactions by methylene blue-mediated photo-crosslinking. **2**, 611–621 (1996).
21. Liu, Z. R., Sargueil, B. & Smith, C. W. Methylene blue-mediated cross-linking of proteins to double-stranded RNA. *Methods in enzymology* **318**, 22–33 (2000).
22. Singh, G., Ricci, E. P. & Moore, M. J. RIPiT-Seq: a high-throughput approach for footprinting RNA:protein complexes. *Methods (San Diego, Calif)* **65**, 320–332 (2014).
23. Ricci, E. P. *et al.* Staufen1 senses overall transcript secondary structure to regulate translation. *Nature structural & molecular biology* **21**, 26–35 (2014).
24. Carpenter, S. *et al.* A long noncoding RNA mediates both activation and repression of immune response genes. *Science (New York, NY)* **341**, 789–792 (2013).
25. Engreitz, J., Lander, E. S. & Guttman, M. RNA Antisense Purification (RAP) for Mapping RNA Interactions with Chromatin. in *Nuclear Bodies and Noncoding RNAs* (eds. Nakagawa, S. & Hirose, T.) vol. 1262 183–197 (Springer New York, 2015).
26. Atianand, M. K. *et al.* A Long Noncoding RNA lincRNA-EPS Acts as a Transcriptional Brake to Restrain Inflammation. *Cell* **165**, 1672–1685 (2016).
27. Carpenter, S., Ricci, E. P., Mercier, B. C., Moore, M. J. & Fitzgerald, K. A. Post-transcriptional regulation of gene expression in innate immunity. *Nature Reviews Immunology* **14**, 361–376 (2014).
28. Mangeot, P. E. *et al.* Genome editing in primary cells and in vivo using viral-derived Nanoblades loaded with Cas9-sgRNA ribonucleoproteins. *Nature Communications* **10**, (2019).
29. Marnef, A. *et al.* A cohesin/HUSH- and LINC-dependent pathway controls ribosomal DNA double-strand break repair. *Genes Dev.* **33**, 1175–1190 (2019).
30. Arnould, C. *et al. Loop extrusion as a mechanism for DNA Double-Strand Breaks repair foci formation*. http://biorxiv.org/lookup/doi/10.1101/2020.02.12.945311 (2020) doi:10.1101/2020.02.12.945311.
31. Vila-Perelló, M. & Muir, T. W. Biological Applications of Protein Splicing. *Cell* **143**, 191–200 (2010).
32. Kawai, T. & Akira, S. The roles of TLRs, RLRs and NLRs in pathogen recognition. *Int Immunol* **21**, 317–337 (2009).
33. Bianchi, M. E. DAMPs, PAMPs and alarmins: all we need to know about danger. *J Leukoc Biol* **81**, 1–5 (2007).
34. Dunster, J. L. The macrophage and its role in inflammation and tissue repair: mathematical and systems biology approaches. *WIREs Syst Biol Med* **8**, 87–99 (2016).
35. Kolaczkowska, E. & Kubes, P. Neutrophil recruitment and function in health and inflammation. *Nature Reviews Immunology* **13**, 159–175 (2013).
36. Serhan, C. N. & Savill, J. Resolution of inflammation: the beginning programs the end. *Nature Immunology* **6**, 1191–1197 (2005).
37. Medzhitov, R. Origin and physiological roles of inflammation. *Nature* **454**, 428–435 (2008).
38. Ashley, N. T., Weil, Z. M. & Nelson, R. J. Inflammation: Mechanisms, Costs, and Natural Variation. *Annual Review of Ecology, Evolution, and Systematics* **43**, 385–406 (2012).
39. Bosmann, M. & Ward, P. A. The inflammatory response in sepsis. *Trends in Immunology* **34**, 129–136 (2013).
40. Moore, K. J., Sheedy, F. J. & Fisher, E. A. Macrophages in atherosclerosis: a dynamic balance. *Nature Reviews Immunology* **13**, 709–721 (2013).
41. Aringer, M., Günther, C. & Lee-Kirsch, M. A. Innate immune processes in lupus erythematosus. *Clinical Immunology* **147**, 216–222 (2013).
42. Medzhitov, R. & Horng, T. Transcriptional control of the inflammatory response. *Nature Reviews Immunology* **9**, 692–703 (2009).

43. Carpenter, S., Ricci, E. P., Mercier, B. C. & Moore, M. J. Post-transcriptional regulation of gene expression in innate immunity. *Nature Reviews \dots* **14**, 361–376 (2014).
44. Hershey, J. W. B., Sonenberg, N. & Mathews, M. B. Principles of Translational Control: An Overview. *Cold Spring Harb Perspect Biol* **4**, (2012).
45. Jung, H., Gkogkas, C. G., Sonenberg, N. & Holt, C. E. Remote Control of Gene Function by Local Translation. *Cell* **157**, 26–40 (2014).
46. Lykke-Andersen, J. & Bennett, E. J. Protecting the proteome: Eukaryotic cotranslational quality control pathways. *J Cell Biol* **204**, 467–476 (2014).
47. Jackson, R. J., Hellen, C. U. T. & Pestova, T. V. The mechanism of eukaryotic translation initiation and principles of its regulation. *Nature reviews Molecular cell biology* **11**, 113–127 (2010).
48. Ingolia, N. T., Ghaemmaghami, S., Newman, J. R. S. & Weissman, J. S. Genome-wide analysis in vivo of translation with nucleotide resolution using ribosome profiling. *Science (New York, NY)* **324**, 218–223 (2009).
49. Richter, J. D. & Coller, J. Pausing on Polyribosomes: Make Way for Elongation in Translational Control. *Cell* **163**, 292–300 (2015).
50. Radhakrishnan, A. *et al.* The DEAD-Box Protein Dhh1p Couples mRNA Decay and Translation by Monitoring Codon Optimality. *Cell* **167**, 122–132.e9 (2016).
51. Shi, Z. *et al.* Heterogeneous Ribosomes Preferentially Translate Distinct Subpools of mRNAs Genome-wide. *Molecular Cell* **67**, 71-83.e7 (2017).
52. Kondrashov, N. *et al.* Ribosome-Mediated Specificity in Hox mRNA Translation and Vertebrate Tissue Patterning. *Cell* **145**, 383–397 (2011).
53. Shi, Z. & Barna, M. Translating the Genome in Time and Space: Specialized Ribosomes, RNA Regulons, and RNA-Binding Proteins. *Annual Review of Cell and Developmental Biology* **31**, 31–54 (2015).
54. Xue, S. & Barna, M. Specialized ribosomes: a new frontier in gene regulation and organismal biology. *Nature Reviews Molecular Cell Biology* **13**, 355–369 (2012).
55. Simsek, D. *et al.* The Mammalian Ribo-interactome Reveals Ribosome Functional Diversity and Heterogeneity. *Cell* **169**, 1051-1065.e18 (2017).
56. Lelouard, H. *et al.* Regulation of translation is required for dendritic cell function and survival during activation. *The Journal of Cell Biology* **179**, 1427–1439 (2007).
57. Sampath, P. *et al.* Noncanonical function of glutamyl-prolyl-tRNA synthetase: gene-specific silencing of translation. *Cell* **119**, 195–208 (2004).
58. Ricciardi, S. *et al.* The Translational Machinery of Human CD4+ T Cells Is Poised for Activation and Controls the Switch from Quiescence to Metabolic Remodeling. *Cell Metabolism* (2018) doi:10.1016/j.cmet.2018.08.009.
59. Wilson, D. N. & Doudna Cate, J. H. The Structure and Function of the Eukaryotic Ribosome. *Cold Spring Harb Perspect Biol* **4**, (2012).
60. Giorgi, C. & Moore, M. J. The nuclear nurture and cytoplasmic nature of localized mRNPs. *Seminars in cell & developmental biology* **18**, 186–193 (2007).
61. Winstall, E., Gamache, M. & Raymond, V. Rapid mRNA degradation mediated by the c-fos 3' AU-rich element and that mediated by the granulocyte-macrophage colony-stimulating factor 3' AU-rich element occur through similar polysome-associated mechanisms. *Molecular and cellular biology* **15**, 3796–3804 (1995).
62. Kim, Y. K., Furic, L., Desgroseillers, L. & Maquat, L. E. Mammalian Staufen1 Recruits Upf1 to Specific mRNA 3′UTRs so as to Elicit mRNA Decay. *Cell* **120**, 195–208 (2005).
63. Yepiskoposyan, H., Aeschimann, F., Nilsson, D., Okoniewski, M. & Mühlemann, O. Autoregulation of the nonsense-mediated mRNA decay pathway in human cells. **17**, 2108–2118 (2011).
64. Saltzman, A. L. *et al.* Regulation of multiple core spliceosomal proteins by alternative splicing-coupled nonsense-mediated mRNA decay. *Molecular and cellular biology* **28**,

4320–4330 (2008).
65. Giorgi, C. *et al.* The EJC factor eIF4AIII modulates synaptic strength and neuronal protein expression. *Cell* **130**, 179–191 (2007).
66. Friedman, J. R. & Nunnari, J. Mitochondrial form and function. *Nature* **505**, 335–343 (2014).
67. West, A. P., Shadel, G. S. & Ghosh, S. Mitochondria in innate immune responses. *Nature Reviews Immunology* **11**, 389–402 (2011).
68. Couvillion, M. T., Soto, I. C., Shipkovenska, G. & Churchman, L. S. Synchronized mitochondrial and cytosolic translation programs. *Nature* **533**, 499–503 (2016).
69. Molenaars, M. *et al.* A Conserved Mito-Cytosolic Translational Balance Links Two Longevity Pathways. *Cell Metabolism* **31**, 549-563.e7 (2020).
70. Sharma, M. R. *et al.* Structure of the Mammalian Mitochondrial Ribosome Reveals an Expanded Functional Role for Its Component Proteins. *Cell* **115**, 97–108 (2003).
71. Mays, J.-N. *et al.* The mitoribosome-specific protein mS38 is preferentially required for synthesis of cytochrome c oxidase subunits. *Nucleic Acids Research* **47**, 5746–5760 (2019).
72. Angajala, A. *et al.* Diverse Roles of Mitochondria in Immune Responses: Novel Insights Into Immuno-Metabolism. *Frontiers in Immunology* **9**, (2018).
73. Wahl, D. R., Byersdorfer, C. A., Ferrara, J. L. M., Opipari, A. W. & Glick, G. D. Distinct metabolic programs in activated T cells: opportunities for selective immunomodulation. *Immunological Reviews* **249**, 104–115 (2012).
74. Lesiak, A. J., Brodsky, M. & Neumaier, J. F. RiboTag is a flexible tool for measuring the translational state of targeted cells in heterogeneous cell cultures. *BioTechniques* **58**, 308–317 (2015).
75. Sanz, E. *et al.* Cell-type-specific isolation of ribosome-associated mRNA from complex tissues. *Proceedings of the National Academy of Sciences* **106**, 13939–13944 (2009).
76. Khatter, H., Myasnikov, A. G., Natchiar, S. K. & Klaholz, B. P. Structure of the human 80S ribosome. *Nature* **520**, 640–645 (2015).
77. Mangeot, P. E. *et al.* Efficient genome editing in primary cells and in vivo using viral-derived 'Nanoblades' loaded with Cas9/sgRNA ribonucleoproteins. *bioRxiv* 202010 (2017) doi:10.1101/202010.
78. Teixeira, M. *et al.* Electroporation of mice zygotes with dual guide RNA/Cas9 complexes for simple and efficient cloning-free genome editing. *Scientific Reports* **8**, (2018).
79. Anzalone, A. V. *et al.* Search-and-replace genome editing without double-strand breaks or donor DNA. *Nature* **576**, 149–157 (2019).
80. Clamer, M. *et al.* Active Ribosome Profiling with RiboLace. *Cell Reports* **25**, 1097-1108.e5 (2018).
81. Mosser, D. M. & Zhang, X. Activation of murine macrophages. *Current protocols in immunology / edited by John E. Coligan ... [et al.]* **Chapter 14**, Unit 14.2 (2008).
82. Mishima, Y. & Tomari, Y. Codon Usage and 3′ UTR Length Determine Maternal mRNA Stability in Zebrafish. *Molecular Cell* **61**, 874–885 (2016).
83. Courel, M. *et al.* GC content shapes mRNA storage and decay in human cells. *eLife* **8**, (2019).
84. Hia, F. *et al.* Codon bias confers stability to human mRNA s. *EMBO reports* **20**, (2019).
85. Narula, A., Ellis, J., Taliaferro, J. M. & Rissland, O. S. Coding regions affect mRNA stability in human cells. *RNA* **25**, 1751–1764 (2019).
86. Wu, Q. *et al.* Translation affects mRNA stability in a codon dependent manner in human cells. *eLife* **8**, e45396 (2019).
87. Garzia, A. *et al.* The E3 ubiquitin ligase and RNA-binding protein ZNF598 orchestrates

ribosome quality control of premature polyadenylated mRNAs. *Nature Communications* **8**, (2017).
88. Juszkiewicz, S. *et al.* ZNF598 Is a Quality Control Sensor of Collided Ribosomes. *Molecular Cell* **72**, 469-481.e7 (2018).
89. Tesina, P. *et al.* Structure of the 80S ribosome–Xrn1 nuclease complex. *Nature Structural & Molecular Biology* **26**, 275–280 (2019).
90. Buschauer, R. *et al.* The Ccr4-Not complex monitors the translating ribosome for codon optimality. *Science* **368**, eaay6912 (2020).
91. Cluet, D. *et al.* A quantitative tri-fluorescent yeast two-hybrid system: from flow cytometry to in-cellula affinities. 49.
92. Bischof, J. *et al.* Generation of a versatile BiFC ORFeome library for analyzing protein–protein interactions in live Drosophila. *ELife* **7**, (2018).
93. Sundaramoorthy, E. *et al.* ZNF598 and RACK1 Regulate Mammalian Ribosome-Associated Quality Control Function by Mediating Regulatory 40S Ribosomal Ubiquitylation. *Molecular Cell* **65**, 751-760.e4 (2017).
94. Tuck, A. C. *et al.* Mammalian RNA Decay Pathways Are Highly Specialized and Widely Linked to Translation. *Molecular Cell* (2020) doi:10.1016/j.molcel.2020.01.007.

Selected Publications

Downloaded from rnajournal.cshlp.org on May 8, 2020 - Published by Cold Spring Harbor Laboratory Press

In vitro expression of the HIV-2 genomic RNA is controlled by three distinct internal ribosome entry segments that are regulated by the HIV protease and the Gag polyprotein

EMILIANO P. RICCI,[1,2,4] CÉCILE H. HERBRETEAU,[1,2,4] DIDIER DECIMO,[1,2] ANDREAS SCHAUPP,[1,2] SIDDHARTHA A.K. DATTA,[3] ALAN REIN,[3] JEAN-LUC DARLIX,[1,2] and THÉOPHILE OHLMANN[1,2]

[1]Ecole Normale Supérieure de Lyon, Unité de Virologie Humaine, IFR 128, Lyon F-69364, France
[2]Inserm, U758, Lyon F-69364, France
[3]HIV Drug Resistant Program, National Cancer Institute, Frederick, Maryland 21702-1201, USA

ABSTRACT

The HIV-2 genomic RNA serves both as a messenger for protein synthesis and as a genome for viral assembly and particle production. Our previous work has shown that the HIV-2 genomic RNA encodes two additional Gag proteins that are N-terminal truncated isoforms of the p57 Gag polyprotein. In this study, by the use of mono- and bicistronic RNAs we show that translation at the three AUGs is driven by three distinct and independent internal ribosome entry segments both in vitro and ex vivo. Furthermore we used the recombinant Gag and HIV-2 protease to show that, in vitro, translation is tightly regulated by these two viral proteins. This regulation is exerted both at the level of protein production and also on the selection of the AUG initiation site which changes the ratio at which the three different Gag isoforms are produced.

Keywords: HIV; translation initiation; Gag; IRES; HIV protease

INTRODUCTION

In eukaryotic cells, gene expression is controlled from the early stage of RNA synthesis up to translation in the cytoplasm (Gale et al. 2000). For the majority of eukaryotic mRNAs, translation begins by the attachment of the 40 S ribosomal subunit to the 5′-capped end of the transcript followed by linear scanning until it reaches an initiation codon in a good nucleotide context (Kozak 1989). This process is mediated by a number of proteins called initiation factors that allow both efficient binding of the ribosome to the mRNA and migration to the initiation codon. Among them, the eIF4F complex composed of eIF4E, eIF4A, and eIF4G plays a critical role both in promoting ribosomal entry onto the mRNA and scanning of the preinitiation complex (Gingras et al. 1999). eIF4E is a 26 kDa phosphoprotein whose function is to bind to the 5′-end cap structure of the eukaryotic mRNA in order to direct the assembly of the preinitiation complex; eIF4A is an RNA helicase that has the ability to unwind short RNA duplexes in an ATP dependent manner. Finally, the eIF4G initiation factor is the scaffold protein for eIF4E, eIF4A, and the poly(A) binding protein (PABP) (Prevot et al. 2003a).

In 1988, the study of picornaviral RNA translation led to the characterization of an alternative mechanism of translation initiation by direct ribosome binding to the 5′-UTR (Jang et al. 1988; Pelletier and Sonenberg 1988). This is rendered possible by an RNA domain called the internal ribosome entry segment (IRES), which enables efficient translation independently from the 5′-capped end of the mRNA (Jackson et al. 1994). During this process, the 40 S ribosomal subunit associated with initiation factors in the form of a 43 S preinitiation complex binds to the IRES located upstream of the AUG initiation site (Vagner et al. 2001; Stoneley and Willis 2004). In many instances, this mechanism was shown to be mediated by the IRES three-dimensional (3D) structure (Yaman et al. 2003; Otto and Puglisi 2004; Spahn et al. 2004).

Although a large number of IRES sequences of viral and cellular origins have now been identified, a structural model for IRES activity has not yet emerged suggesting that there is not one but several RNA motifs that enable ribosomal

[4]These authors contributed equally to this work.

Reprint requests to: Théophile Ohlmann, Ecole Normale Supérieure de Lyon, Unité de Virologie Humaine, IFR 128, Lyon F-69364, France; e-mail: tohlmann@ens-lyon.fr; fax: (33) 472-728-137.

Article published online ahead of print. Article and publication date are at http://www.rnajournal.org/cgi/doi/10.1261/rna.813608.

Downloaded from rnajournal.cshlp.org on May 8, 2020 - Published by Cold Spring Harbor Laboratory Press

entry (Bonnal et al. 2003). In agreement with this idea, there is a broad diversity of nonrelated genes that use internal ribosome entry (Vagner et al. 2001).

IRES elements have now been identified within the simian immunodeficiency virus (SIV) and the human immunodeficiency virus type I (HIV-1) (Ohlmann et al. 2000; Buck et al. 2001; Waysbort et al. 2001; Brasey et al. 2003), HIV-2 (Herbreteau et al. 2005), and more recently, feline immunodeficiency virus (FIV) (Camerini et al. 2008) members of the lentivirus family, suggesting that translation of the retroviral genomic RNA is tightly controlled (Balvay et al. 2007). The human immunodeficiency virus type 2 is a member of the lentivirus group of retroviruses and is, with HIV-1, the etiological agent of AIDS in humans (Bock and Markovitz 2001). Although HIV-2 and HIV-1 share a common genetic organization, HIV-2 is more closely related to simian immunodeficiency viruses (Lemey et al. 2003).

The full-length genomic RNA of HIV-2 serves both as genome for the production of new virions and as messenger RNA for the synthesis of Gag and Gag-Pol precursors during the late step of viral replication (Butsch and Boris-Lawrie 2002). The HIV-2 genomic RNA has a 548-nucleotide (nt)-long 5′-UTR, which harbors several RNA motifs necessary for genome dimerization and packaging (Reeves and Doms 2002). These motifs are the preferential binding sites for the neo-synthesized Gag proteins thus forming an RNA–Gag complex that creates a scaffold for multimerization of additional Gag molecules. Building such a complex ultimately results in selection of the genomic RNA for encapsidation and viral assembly.

Our previous work has shown that the HIV-2 genomic RNA codes for the wild-type (WT) p57 Gag protein and two additional N truncated Gag isoforms that are produced by internal entry of the ribosomes from the coding region. However, the translational mechanism by which ribosomes can be displayed to three distinct initiation sites was not further investigated.

By using mono- and bicistronic constructs together with antisense 2′-*O*-methyloligoribonucleotides, we now show that three independent IRES are located within the HIV-2 gag coding region. These sequences have the ability to drive translation initiation at each of the three AUG initiation codons. Further investigation into this complex mechanism of ribosomal entry reveals that selection of the initiation site is mainly influenced by two virally encoded proteins, namely, the protease and the Gag polyprotein.

RESULTS

Gag translation is driven by three IRES located within the coding region

We have previously shown that translation of the HIV-2 genomic RNA from the authentic AUG1 site (producing p57) occurs by internal entry of the ribosomes on an IRES sequence which has the unique ability to load ribosomes upstream of its core sequence (Herbreteau et al. 2005). This is rendered possible by a region of 50 nucleotides located just downstream from the first AUG (position +548) that forms a long range RNA interaction and was shown to be critical for initiation at the authentic initiation site (Herbreteau et al. 2005). However, the mechanism by which initiating ribosomes are able to access the two other downstream AUG sites (positions +746 and +899) remained to be determined as well as the role of the 5′-UTR in the overall translation mechanism of the wild type genomic RNA.

Thus, we have constructed a series of bicistronic RNAs that is depicted in Figure 1A, and which contains the neomycin gene as the first cap-dependent cistron and harbors the LacZ gene as the second cistron. Various regions of the HIV-2 genomic RNA including the 5′-UTR, the coding region encompassing AUG1 to AUG3, or a series of deletions, were inserted in the bicistronic RNA and translated in the rabbit reticulocyte lysate. As shown previously (Herbreteau et al. 2005), the 5′-UTR alone led to poor expression of the LacZ gene (Fig. 1B, lane 1) whereas

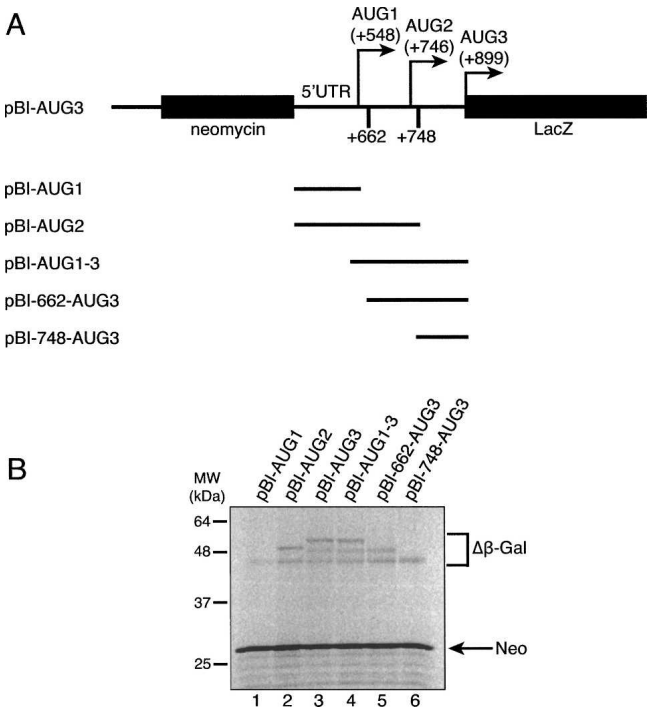

FIGURE 1. Mapping HIV-2 IRES activity. (*A*) Schematic representation of the bicistronic constructs (pBi) used in this study. Different regions of the HIV-2 genomic RNA were inserted in the intercistronic spacer of the Neomycin-LacZ bicistronic vector. (*B*) In vitro translation in the rabbit reticulocyte lysate of the uncapped bicistronic RNA constructs (200 ng/10 μL) as indicated on *top* of the figure. Translation products were then resolved on a 15% SDS-PAGE and subjected to autoradiography. Results are representative of at least three independent experiments.

Downloaded from rnajournal.cshlp.org on May 8, 2020 - Published by Cold Spring Harbor Laboratory Press

efficient translation of the three β-Gal isoforms was observed when the 5′-UTR was followed by segments of the gag coding region spanning from AUG1 to AUG3 (Fig. 1B, lanes 2,3). Moreover, complete removal of the 5′-UTR did not affect IRES activity in agreement with our previous findings (Fig. 1B, lane 4; Herbreteau et al. 2005). Internal deletions within the *gag* coding region were then generated in the context of the bicistronic construct. Interestingly, 5′ deletions starting some 114 nucleotides downstream from the AUG1 site did not impair translation initiation at AUG2 and AUG3 (Fig. 1B, lane 5). Moreover, a further 5′ deletion starting downstream from AUG2 did not affect translation at the third AUG site (Fig. 1B, lane 6).

In order to confirm the in vitro results, capped and polyadenylated bicistronics RNAs containing either the entire Gag coding region from AUG1 to AUG3 or a series of 5′deletions between the Firefly and the Renilla luciferase coding region (Fig. 2A) were transfected in HeLa cells. As expected, the empty vector was poorly translated (Fig. 2C, "pFR-NoIRES"). Activity of bicistronics RNAs containing the entire Gag coding region or 5′ deletions (Fig. 2C) was also quite low but was still twofold to fourfold above the negative control. It should be noted that luciferase activity driven by monocistronic capped and polyadenylated RNAs containing the HIV-2 coding region was also very low (data not shown). We have expressed the 2A protease from poliovirus in HeLa cells to cleave eIF4G. Proteolysis of eIF4G by this protease inhibits cap-dependent translation whereas IRES-driven translation is maintained or stimulated (Ziegler et al. 1995; Ohlmann et al. 1997). Upon eIF4G cleavage by the virally encoded protease 2A (Fig. 2B), translation of the Renilla luciferase driven by the HIV-2 Gag coding region, or segments of it, was highly stimulated compared to the negative control (Fig. 2C). Interestingly, as observed in vitro, 5′ deletions of the Gag coding region starting downstream from AUG1 (pFR-662-AUG3) or downstream from AUG2 (pFR-748-AUG3) showed translational activities comparable to that of the entire Gag coding region (pFR-AUG1-3) (Fig. 2C). These data indicate that translation initiation occurs independently at each of the three AUG initiation sites both in vitro and ex vivo suggesting the presence of three distinct and independent IRES elements.

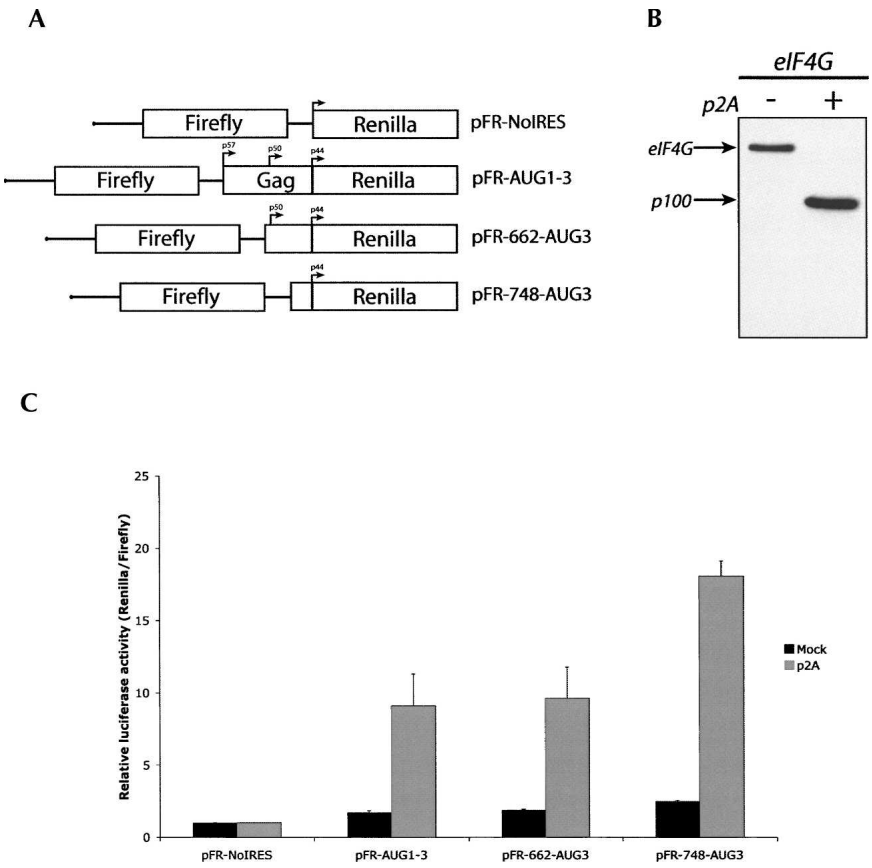

FIGURE 2. IRES activity in HeLa cells. (*A*) Schematic representation of the dual luciferase bicistronic constructs (pFR) used in this study. Different regions of the HIV-2 genomic RNA were inserted in the intercistronic spacer of the firefly-Renilla bicistronic vector (see Materials and Methods). (*B*) Western blot analysis of eIF4G from HeLa cells transfected with an RNA coding for the 2A protease from poliovirus. (*C*) Transfection of capped and polyadenylated bicistronic RNA constructs (0.156 pmol) in HeLa cells previously transfected (p2A) or not (Mock) with an RNA coding for the p2A protease. Luciferase activities were measured 3 h post-transfection. R/F ratios were calculated and normalized to the value of the pFR-NoIRES construct. Error bars represent the standard deviation obtained from three independent experiments.

In order to confirm that internal initiation takes place at each of the three AUG initiation sites from monocistronic RNAs in vitro, we have used the L-protease from foot-and-mouth disease virus (FMDV) that also cleaves eIF4G. Thus, the RRL was pre-incubated for 10 min with increasing concentrations of in vitro generated L-protease in order to cleave eIF4G (see Supplemental Fig. 1). Then, the RRL was programmed with a set of different control RNAs in which the LacZ coding region is driven by the capped 5′-UTR of globin (Fig. 3, lanes 1–3) or the uncapped IRES of EMCV (Fig. 3, lanes 4–6). Capped and uncapped wild-type HIV-2 genomic RNA (Fig. 3, T7-WT HIV-2, lanes 7–12) and the HIV-2 genomic RNA devoided of its 5′-UTR and commencing directly at AUG1 (Fig. 3, T7-AUG1 HIV-2, lanes 13–18) were also translated in the RRL treated by the L-protease. As expected, cap-dependent Globin-LacZ translation was strongly inhibited by addition

Downloaded from rnajournal.cshlp.org on May 8, 2020 - Published by Cold Spring Harbor Laboratory Press

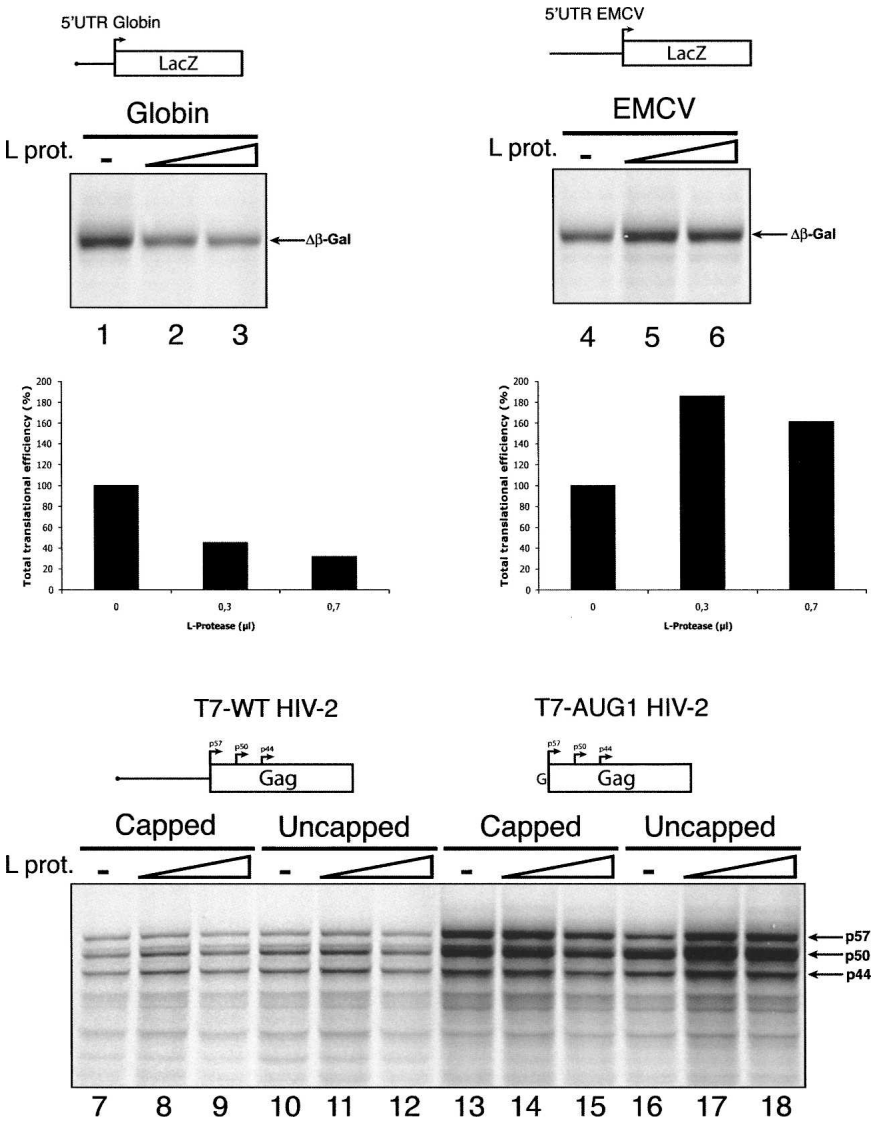

FIGURE 3. Cleavage of eIF4G stimulates HIV-2 translation. A RRL under full translation conditions was preincubated for 10 min without (lanes *1,4,7,10,13,16*) or with 0.3 µL (lanes *2,5,8,11,14,17*) or 0.7 µL (lanes *3,6,9,12,15,18*) of in vitro produced FMDV L-protease. Globin-LacZ (15 ng/10 µL), EMCV-LacZ (184 ng/10 µL), T7-WT (200 ng/10 µL), and T7-AUG1 (35 ng/10 µL) were translated as indicated on the figure and the resulting products resolved on a 13% SDS-PAGE and submitted to autoradiography. The relative intensities of the bands were quantified using a storm 850 phosphoimager and expressed as arbitrary units presented at the *bottom* of each panel. T7-WT and T7-AUG1 overall translation was quantified by the addition of the activities of each of the Gag isoforms. Results are representative of at least three independent experiments.

of the protease in a dose-dependent manner (Fig. 3, lanes 2,3) whereas EMCV IRES-driven translation was stimulated (Fig. 3, lanes 4–6). Interestingly, production of the three Gag isoforms p57, p50, and p44 from the wild-type RNA was not diminished by the addition of the L-protease whether this mRNA was capped or uncapped (Fig. 3, lanes 7–12). Translation of the leaderless HIV-2 RNA, which is more efficient than that from the wild-type RNA, was poorly affected by eIF4G cleavage showing a small inhibition only at high doses of L-protease (Fig. 3, lanes 13–18). Interestingly, the relative ratio of expression of the three gag isoforms was not affected by this proteolytic event.

To further confirm these results and to evaluate any contribution of the cap from the wild-type HIV-2 RNA, we carried out translation assays using a competitive untreated rabbit reticulocyte lysate (Fig. 4). We have recently shown that this system faithfully recapitulates the synergistic effect of the cap and the poly(A) tail and the selective advantage of IRES dependent translation (Soto Rifo et al. 2007). Therefore, the untreated RRL was programmed with increasing amounts of the polyadenylated capped and uncapped HIV-2 polyadenylated RNAs (Fig. 4, lanes 1–6). As observed in the nuclease treated lysate, translation of the uncapped and polyadenylated T7-WT was as efficient, if not more, as the capped version of the RNA, suggesting a poor contribution of the cap to overall Gag translation (Fig. 4, lanes 1–6). Furthermore, addition of the L protease also led to translation stimulation of the capped and polyadenylated T7-WT RNA, whereas endogenous globin and lipoxygenase translation was inhibited (Fig. 4, lanes 7–10). These experiments show that the synergy between the poly(A) tail and the cap exerts only a mild effect on overall translation from the HIV-2 wild-type genomic RNA, confirming the use of an internal initiation mechanism to produce the Gag polyproteins.

The three IRES are functionally independent

The next step was to determine whether each of the three AUGs could be used for initiation independently from each other. Therefore, the experimental approach consisted of the hybridization of short 2′-*O*-methyloligoribonucleotides that were annealed to different regions of the HIV-2 mRNA molecule. Annealing of the oligos to the RNAs was tested by electrophoresis of RNA–oligo duplexes on agarose gels (see Supplemental Fig. 2). As a control experiment to evaluate the effect of oligo hybridization on ribosomal scanning, a 2′-*O*-methyloligoribonucleotide complementary to the globin 5′-UTR was used and the resulting oligo–mRNA duplex was translated

Downloaded from rnajournal.cshlp.org on May 8, 2020 - Published by Cold Spring Harbor Laboratory Press

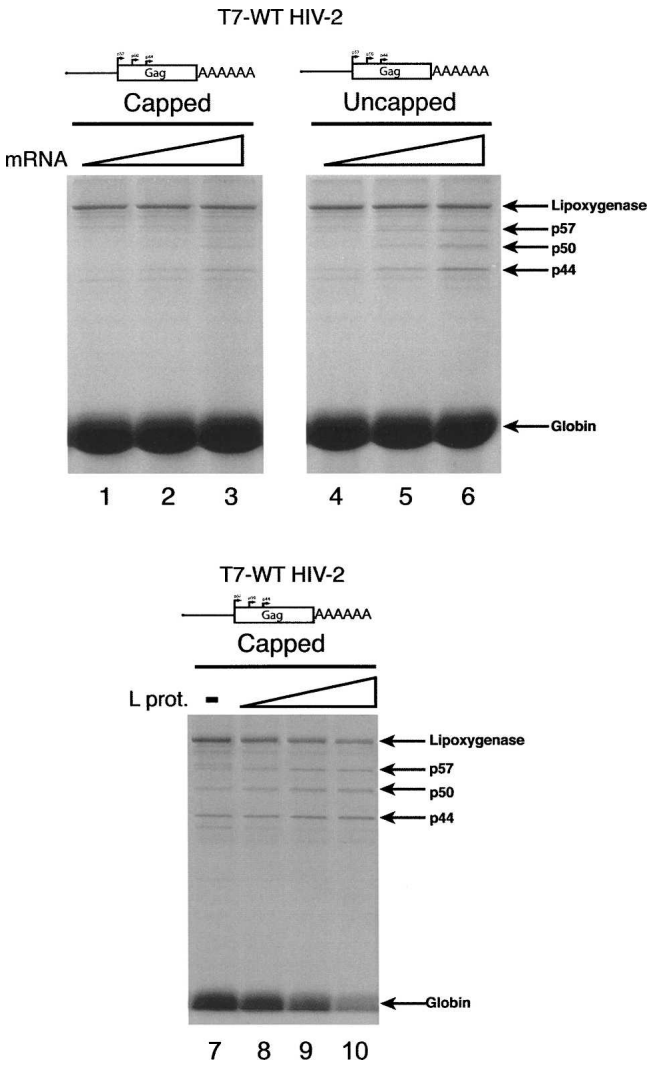

FIGURE 4. Translation of the HIV-2 T7-WT RNA in a competitive cap and poly-A dependent RRL. Translation of increasing amounts (50, 100, and 200 ng) of capped (lanes *1–3*) and uncapped (lanes *4–6*) poly-adenylated T7-WT RNA in the untreated RRL containing endogenous Globin and lipoxygenase mRNAs as indicated on the figure. Translation of 200 ng of capped and poly-adenylated T7-WT RNA following preincubation of the untreated RRL for 10 min without (lane *7*) or with 0.3 μL (lane *8*), or 0.7 μL (lane *9*), or with 1 μL (lane *10*) of in vitro produced FMDV L-protease. Translation products were resolved on a 13% SDS-PAGE and submitted to autoradiography. Results are representative of at least three independent experiments.

in the RRL (Fig. 5, lanes 1–4). This resulted in a drastic inhibition of translation of the globin–LacZ RNA showing that the oligo–mRNA duplex was stable enough to arrest most of the scanning 40 S ribosomes. Interestingly, when a 2′-*O*-methyloligoribonucleotide was annealed to the primary binding site (PBS), which lies in the middle of the HIV-2 5′-UTR, we could only observe a marginal decrease in translation from the first AUG site with no effect on the downstream AUGs (Fig. 5, lanes 5–8). Hybridization of an oligo targeting the RNA region including the AUG1 initiation site resulted in the pronounced inhibition of translation at the proximal site but with virtually no effect on the expression of p50 and p44 which are synthesized from initiation at AUG2 and AUG3, respectively (Fig. 5, lanes 9–12). In a similar manner, hybridization of a 2′-*O*-methyloligoribonucleotide at the second AUG site (AUG2) yielded some unexpected results (Fig. 5, lanes 13–16). First of all, it did not impair expression of p44 from the third AUG initiation site, suggesting that translation at AUG3 does not result from leaky scanning or read through from AUG2. Second, it can be clearly seen on the autoradiography that initiation occurred upstream of the AUG2 as judged by the slightly larger translation product made (Fig. 5, cf. lane 9 and lanes 10–12). This product (named p52) might result from translation initiation at a non-AUG codon since no AUG triplets (either in frame or out of frame) are located between AUG 1 and AUG2 and may correspond to an in-frame CUG codon that is present some 19 codons upstream of AUG2.

Taken together, these results indicate that there are three distinct and functionally independent internal entry sites located entirely in the gag coding region: IRES 1 lies downstream from its AUG entry site as described previously, the second IRES is located between AUG1 and AUG2, and the third IRES spans between AUG2 to AUG3. Interestingly, each of these three IRES has its own initiation site.

The HIV-2 protease regulates the pattern of expression of Gag isoforms

We next went on to investigate the molecular determinants that could control HIV-2 translation. In particular, it was of interest to study the effects of the viral HIV-2 protease on the translation of its cognate mRNA. This protease was previously shown to play a role in translation by cleaving the initiation factor eIF4G (Ventoso et al. 2001; Ohlmann et al. 2002). Such a proteolytic event yields an N-terminal fragment which contains the eIF4E binding site and a carboxy-terminal domain identical to the L-protease generated eIF4G fragment except that it lacks a small 40 aa RNA binding domain previously described as being critical for ribosomal scanning (Prevot et al. 2003a). As a result, this C-terminal eIF4G fragment resulting from HIV-2 protease cleavage, which harbors the eIF4A and eIF3 binding site, is not competent to support ribosomal scanning. Thus, the RRL was pretreated with increasing amounts of the HIV-2 protease and then programmed with Globin-LacZ, EMCV-LacZ, capped and uncapped wild-type HIV-2 (T7-WT HIV-2), or the capped and uncapped leaderless HIV-2 (T7-AUG1 HIV-2) together with the Hepatitis C virus (HCV) mRNAs whose translation is not dependent on the integrity of eIF4G (Fig. 6). The cleavage of eIF4G was monitored by Western blot (see Supplemental Fig. 3). Addition of the recombinant HIV-2 protease did not affect HCV IRES translation (Fig. 6, lanes 8,9), indicating that no damage to the general

Downloaded from rnajournal.cshlp.org on May 8, 2020 - Published by Cold Spring Harbor Laboratory Press

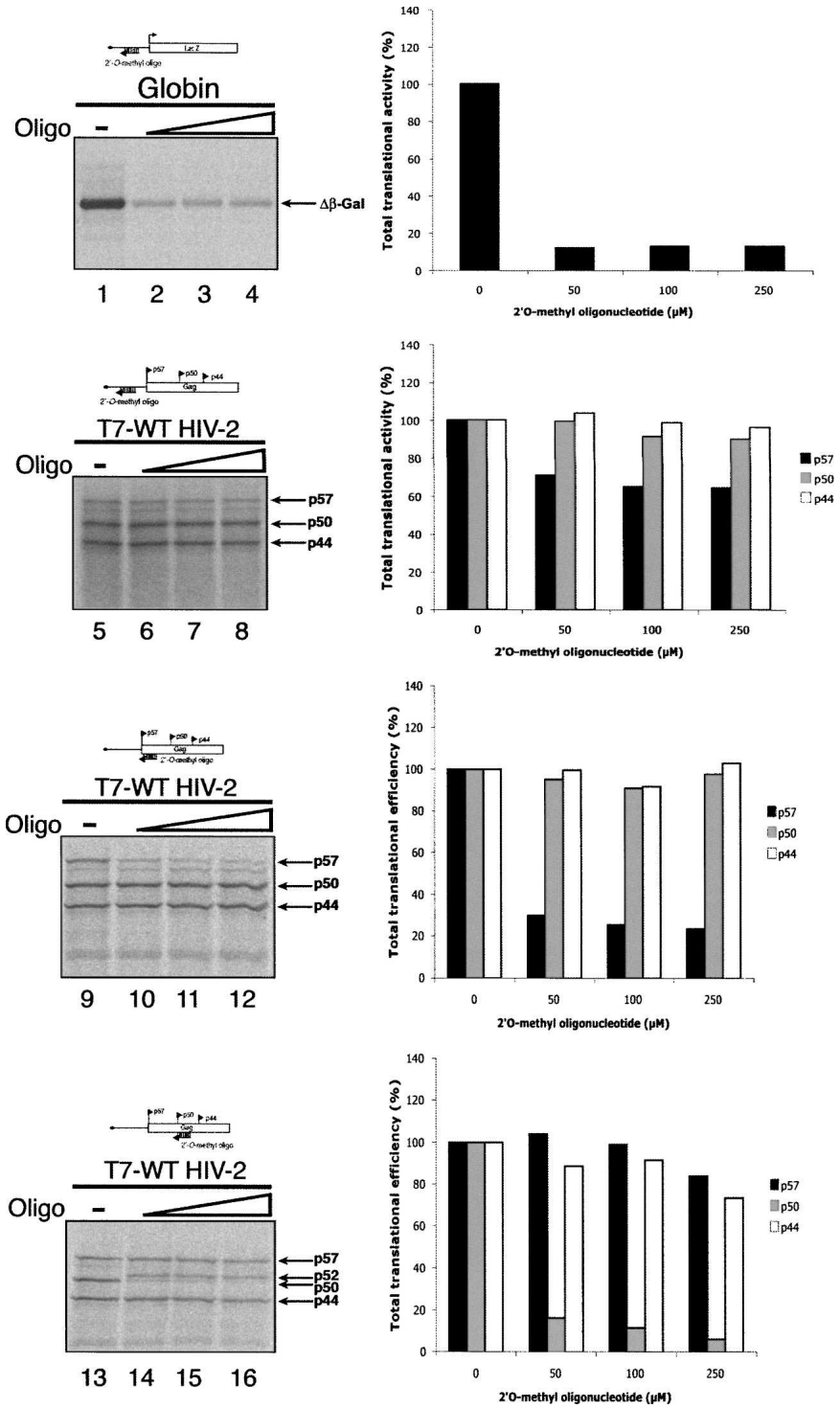

FIGURE 5. Three independent IRES control p57, p50, and p44 protein expression. Increasing concentrations (lane *1*: 0 μM, lane *2*: 50 μM, lane *3*: 100 μM, and lane *4*: 250 μM) of antisense 2′-*O*-methyloligoribonucleotides directed against the 5′-UTR of globin-LacZ (lanes *1–4*), the primary binding site (PBS) of HIV-2 (lanes *5–8*), the region encompassing AUG1 (*9–12*), or the region encompassing AUG2 (lanes *13–16*) were hybridized to capped T7-WT RNA (200 ng/10 μL) and the resulting oligo–RNA complex was translated in the RRL. Translation products were resolved on a 13% SDS-PAGE and submitted to autoradiography. The relative intensities of the bands were quantified using a storm 850 phosphoimager and expressed as arbitrary units presented on the *right-hand* side of each panel. The position of translation products is indicated on the figure. Results are representative of at least three independent experiments.

translational machinery was caused by addition of the retroviral enzyme. As expected, expression of Globin-LacZ was virtually abolished (Fig. 6, lane 3) whereas translation of EMCV-IRES containing mRNA was affected to a lesser extent (Fig. 6, lane 6).

In contrast, production of p57, p50, and p44 Gag resulting from translation of T7-WT at the three AUG sites was only marginally impaired by addition of the HIV-2 enzyme (Fig. 6, lanes 11,12,14,15) whereas expression of the leaderless construct was inhibited by about 60% (Fig. 6, lanes 17,18,20,21). It is interesting to note that capping of the mRNAs (either T7-WT or the leaderless) did not change the pattern of protein expression. More importantly, and unlike the situation with the L-protease (see Figs. 3, 4), the pattern of expression of p57, p50, and p44 from the wild-type or the leaderless constructs was modified by addition of the HIV-2 protease. For instance, synthesis of p57 was inhibited from the WT RNA whereas production of p50 and p44 remained virtually similar to the control (Fig. 6, cf. lane 10 and lanes 11,12). In contrast, initiation at the third AUG site was almost abolished from the leaderless construct (Fig. 6, cf. lane 13 and lanes 14,15).

Taken together, these results show that expression of the HIV-2 protease has quantitative and qualitative impacts on the translation of its cognate mRNA and these effects are affected by the presence or absence of the 5′-UTR. This suggests that the level of expression of p57, p50, and p44 can vary according to changes in the physiological conditions used and that the 5′-UTR can affect the mechanism by which the ribosomes are recruited to the Gag coding region, thus explaining the different results obtained from the wild-type and the leaderless RNAs.

The Gag polyprotein controls its own translation

During the early steps of virus assembly, the Gag polyprotein plays a critical role in HIV-2 RNA packaging by binding to the mRNA, which allows the resulting

Downloaded from rnajournal.cshlp.org on May 8, 2020 - Published by Cold Spring Harbor Laboratory Press

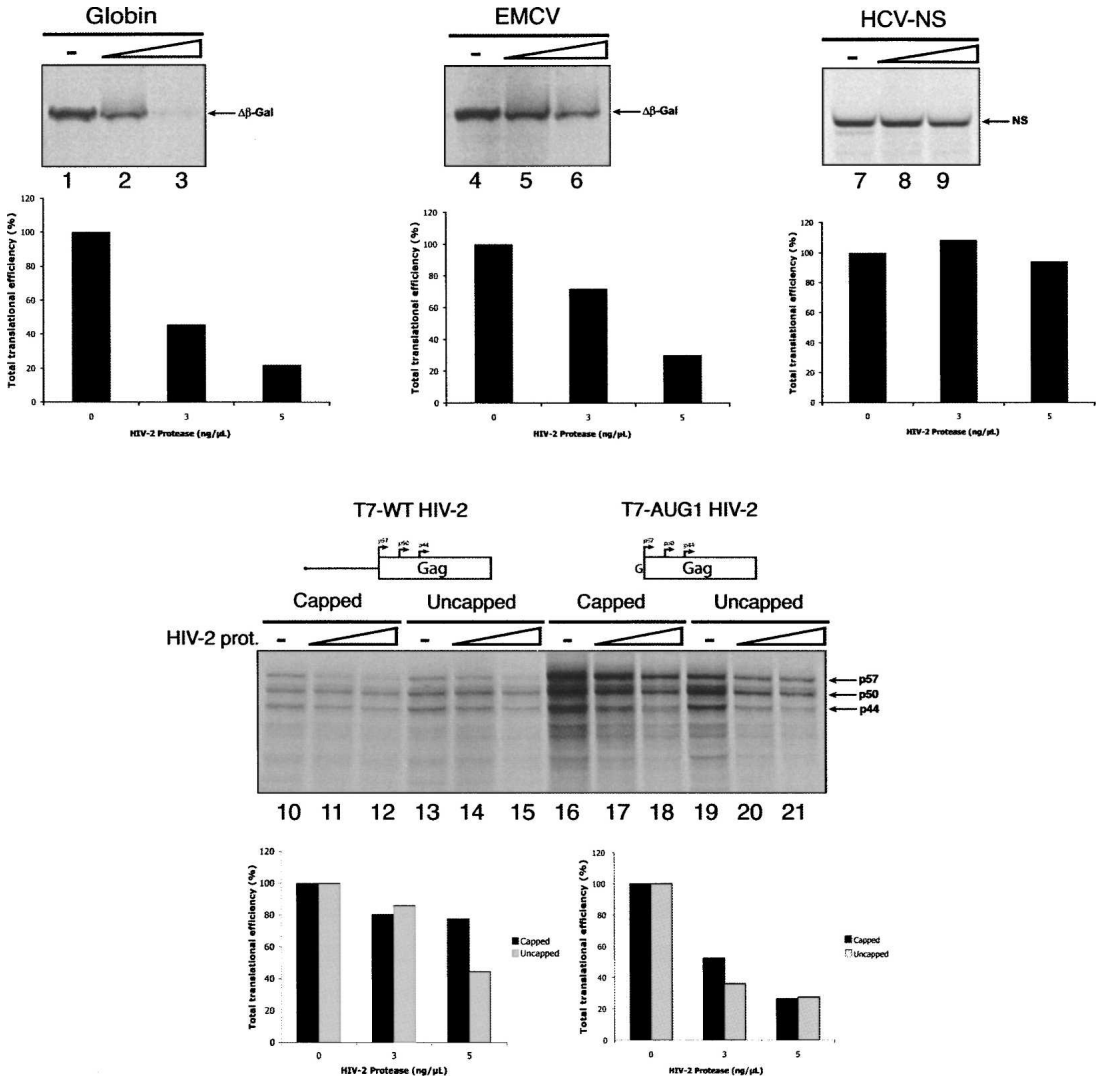

FIGURE 6. Addition of the recombinant HIV-2 protease modifies AUG codon selection. A RRL under full translation conditions was preincubated for 1 h without (lanes *1*,*4*,*7*,*10*,*13*,*16*,*19*) or with 3 ng/μL (lanes *2*,*5*,*8*,*11*,*14*,*17*,*20*), or 5 ng/μL (lanes *3*,*6*,*9*,*12*,*15*,*18*,*21*) of recombinant HIV-2 protease prior to addition of Palinavir (10 μM). The following transcripts: Globin-LacZ (15 ng/10 μL), EMCV-LacZ (184 ng/10 μL), HCV NS (100 ng/10 μL), T7-WT (200 ng/10 μL), and T7-AUG1 (35 ng/10 μL) were then translated as indicated on the figure and the resulting products resolved on a 10% SDS-PAGE and submitted to autoradiography. The relative intensities of the bands were quantified using a storm 850 phosphoimager and expressed as arbitrary units presented at the *bottom* of each panel. T7-WT and T7-AUG1 overall translation was quantified by the addition of the activities of each of the Gag isoforms. Results are representative of at least three independent experiments.

ribonucleoprotein complex to be addressed to the plasma membrane (Kaye and Lever 1999). Interestingly, this process occurs at times when the genomic viral RNA is translated and, thus, most probably interferes with the process of protein synthesis. Curiously, the effect of the Gag polyprotein on translation has rarely been directly investigated by using in vitro translational assays. Thus, we have used recombinant HIV-1 Gag polyprotein that was added to translation assays programmed with different constructs including mRNAs in which LacZ production was driven by the Globin 5′-UTR or the EMCV IRES. The capped HIV-2 T7-WT and T7-AUG1 HIV-2 RNAs were also translated in the presence of increasing concentration of recombinant Gag polyprotein. It should be noted that the HIV-1 Gag protein was shown to be able to bind to the HIV-2 RNA packaging signals with a similar affinity to the HIV-1 RNA signals (Kaye and Lever 1998); however this was confirmed in our experiment setting by Far Western and dot blot (data not shown). The relative molar ratio of Gag recombinant protein to RNA used ranged from 0 to 82 and the resulting Gag–RNA ribonucleoprotein complex was translated in the RRL under the conditions described in Materials and Methods. Results presented in Figure 5 show that, at low concentration, Globin-LacZ expression was only partly affected by the addition of Gag (Fig. 7, lanes 1–9). Translation driven by the EMCV IRES seemed to

Downloaded from rnajournal.cshlp.org on May 8, 2020 - Published by Cold Spring Harbor Laboratory Press

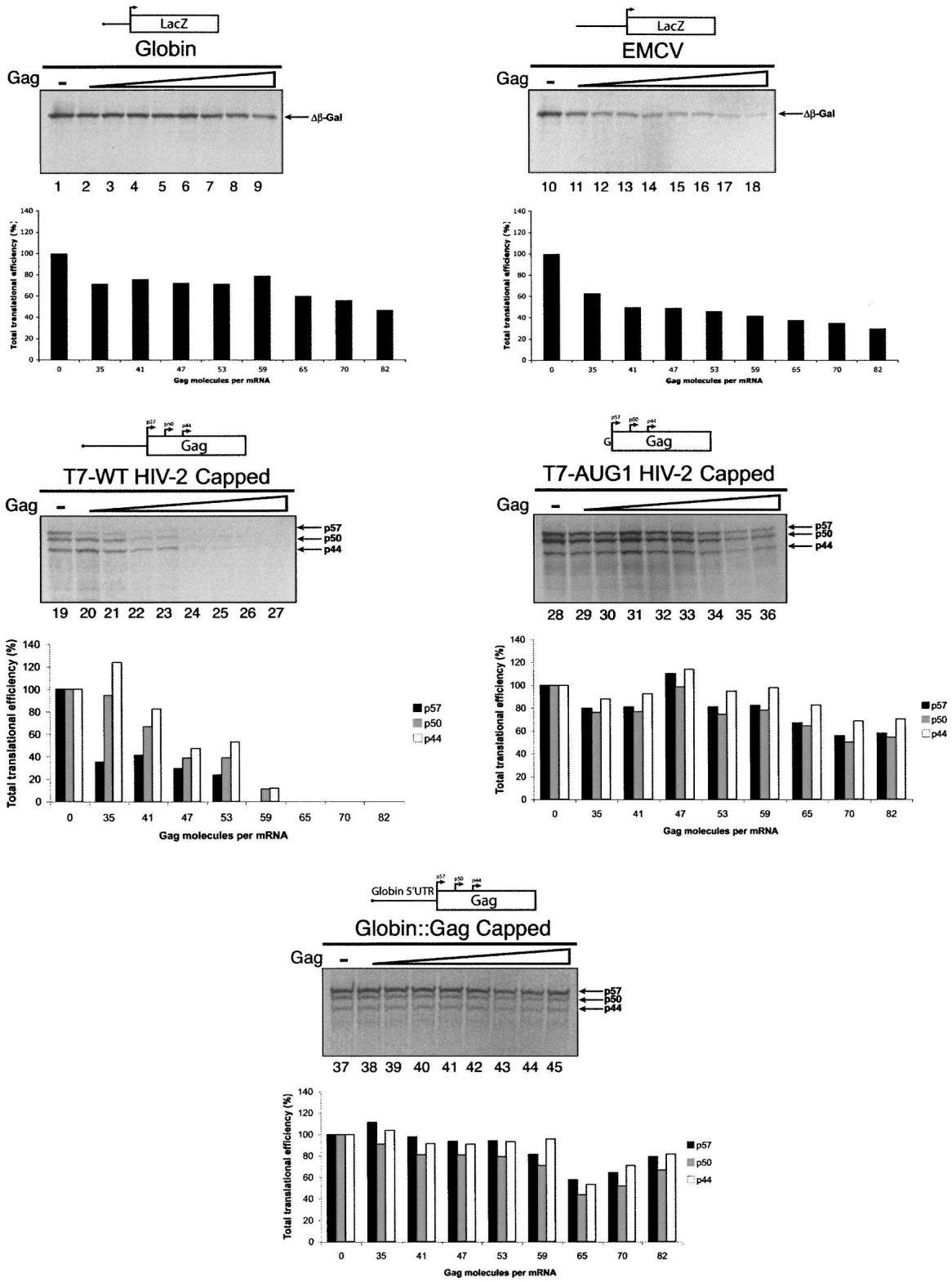

FIGURE 7. The Gag recombinant protein exerts a regulatory effect on the translation of the HIV-2 genomic RNA. Capped globin-LacZ (15 ng/10 μL, lanes *1–9*), capped EMCV-LacZ (184 ng/10 μL, lanes *10–18*), capped T7-WT (200 ng/10 μL, lanes *19–27*), capped T7-AUG1 (35 ng/10 μL, lanes *28–36*), and capped Globin::Gag (35 ng/10 μL, lanes *37–45*) RNAs were preincubated for 10 min at 30°C in the presence of increasing amounts of recombinant HIV-1 Gag protein ranging from 0 to 82 Gag molecules per RNA as indicated on the figure. The resulting Gag-RNAs complexes were then translated in the RRL for 45 min and the resulting products were resolved on a 13% SDS-PAGE and submitted to autoradiography. The relative intensities of the bands were quantified using a storm 850 phosphoimager and presented at the *bottom* of each panel.

Downloaded from rnajournal.cshlp.org on May 8, 2020 - Published by Cold Spring Harbor Laboratory Press

be more sensitive to the addition of the Gag polyprotein as production of β-Gal was gradually diminished in a dose dependent manner (Fig. 7, lanes 10–18).

However, in sharp contrast, translation of HIV-2 WT construct was markedly inhibited by preincubation of the mRNA even at low concentration of the recombinant Gag protein (Fig. 7, lanes 22,23) and translation was actually abolished at higher concentrations (Fig. 7, lanes 24 and above). Moreover, a significant change in the pattern of expression of the different Gag isoforms could also be observed at low concentrations of Gag added with expression of the longest p57 Gag isoform being more affected (Fig. 7, cf. lane 19 and lanes 20,21, and see the quantification panel). Interestingly, translation of the leaderless HIV-2 RNA (T7-AUG1) was also inhibited by recombinant Gag addition (Fig. 7, lanes 28–36), but this was not accompanied by drastic changes in the pattern of expression of the three Gag isoforms. Overall, translation from this construct was more resistant to Gag addition than the 5′-UTR containing wild type HIV-2 genomic RNA. It is noteworthy that the addition of a recombinant RNA binding protein such as the Lupus autoantigen (La) failed to induce any quantitative or qualitative variation on the expression of Gag isoforms ruling out any nonspecific effect (data not shown). Furthermore, translation of a chimeric RNA which contains the 5′-UTR of human β-globin driving the synthesis of the HIV-2 Gag coding region was also monitored (Globin::Gag). Interestingly this showed a translational profile which was similar to that of the globin-LacZ RNA and the leaderless HIV-2 RNA (Fig. 7, lanes 37–45). In fact, translation from this RNA was not really sensitive to addition of the recombinant Gag protein and no significant change in the use of initiation codons could be observed. These experiments suggest that Gag polyprotein plays a regulatory role in the translation of its cognate mRNA and this regulation appears to be exerted via an interaction with the viral 5′-UTR.

This work and previous data have shown that translation of the HIV-2 genomic RNA can take place in the complete absence of 5′-UTR from a leaderless construct (Herbreteau et al. 2005). However, results presented herein suggest that the 5′-UTR may exert an inhibitory role in the presence of the Gag polyprotein by acting as a dock for Gag recruitment near the AUG1 codon, thus inhibiting p57 translation. Indeed, the 5′-UTR of lentiviruses harbors RNA signals that are the preferential Gag binding site for RNA packaging in the course of viral assembly. To investigate the role of the 5′-UTR–Gag interactions in the process of translation initiation, two different RNA competitors were independently preincubated with the Gag protein at a high protein to RNA ratio (83:1). These RNA competitors correspond to the whole 546-nt-long HIV-2 5′-UTR (from +1 to nucleotide 546) or a 546-nt-long unspecific RNA sequence taken from the unrelated β-Galactosidase (β-Gal) gene. These RNA competitors were added in a 1:1 molar ratio with the T7-WT and T7-AUG1 RNAs.

The results presented in Figure 8 show that translation of T7-WT and T7-AUG1 drive the synthesis of Gag p57, p50, and p44 together with another intermediate isoform that was observed previously (Fig. 5; data not shown) and which might result from alternative translation initiation at a non-AUG codon located between AUG1 and AUG2. Addition of an excess amount of recombinant Gag protein (83 molar excess over the RNA concentration) results in the complete inhibition of protein synthesis from both the wild type (T7-WT) and the leaderless (T7-AUG1) RNAs (Fig. 8, lanes 2,8). Interestingly, in the case of the wild-type construct, addition of the β-Gal unspecific RNA competitor was able to rescue translation of the p50 and p44 isoforms but not that of the p57 longest protein (Fig. 8, lane 4). The expression of the longest Gag isoforms was only completely restored when the HIV-2 5′-UTR was used as a competitor RNA (Fig. 8, lane 6). Interestingly, addition of the 5′-UTR or the unspecific RNA competitor was of similar efficiency to fully restore translation from the leaderless construct (Fig. 8, T7-AUG1

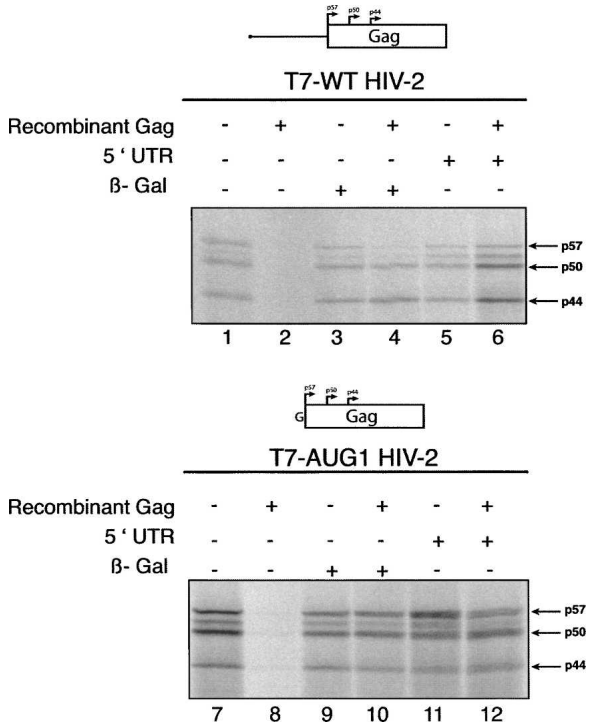

FIGURE 8. The 5′-UTR of the HIV-2 genomic RNA act as a dock for the Gag polyprotein thus having an inhibitory effect on its own translation. RRL under full translational conditions was incubated in the absence (lanes *1,7*) or presence of a large excess of recombinant Gag protein (all other lanes, 82:1 protein to RNA ratio). Uncapped T7-WT (15 ng/μL) and T7-AUG1 (5 ng/μL) RNAs were translated in the absence (lanes *2,8*) or presence of the HIV-2 5′-UTR added in *trans* (lanes *5,6,11,12*) or an unspecific β-Gal RNA (lanes *3,4,9,10*). Samples were processed on a 12% SDS-PAGE and submitted to autoradiography.

Downloaded from rnajournal.cshlp.org on May 8, 2020 - Published by Cold Spring Harbor Laboratory Press

HIV-2, lanes 10,12). Taken together, these data suggest that the Gag polyprotein regulates translation of its cognate RNA by binding to its 5′-UTR. This results in the overall modulation of translation efficiency together with changes in the selection of the AUG initiation site.

DISCUSSION

We have recently demonstrated that translation of the HIV-2 genomic RNA drives the synthesis of Gag p57 and two isoforms named Gag p50 and Gag p44 that are initiated at three distinct AUG codons. This mechanism is rendered possible by the use of an IRES in the coding region which has the unique ability to recruit ribosome upstream of its core domain (Herbreteau et al. 2005). As a result, translation of the HIV-2 genomic RNA can occur in the complete absence of 5′-UTR from an RNA that commences directly at the AUG initiation codon.

In this article, we extend this study further and show that the three distinct Gag isoforms are produced by three independent IRES both in vitro and ex vivo. The first IRES is located downstream from the authentic AUG1 initiation site as previously shown (Herbreteau et al. 2005). The second IRES element is located between the first and the second AUG, between positions nucleotides 662 and 746. The last and third IRES element maps between positions nucleotides 748 and 899, which corresponds to the RNA region located between AUG2 and AUG3 (Figs. 1, 2).

To ensure that translation at the three distinct AUG sites was the result of internal initiation and not due to leaky ribosomal scanning from the first AUG codon, the L-protease from FMDV was utilized to inhibit cap-dependent translation. Upon addition of the viral enzyme, expression from the three AUG sites was enhanced indicating the use of a cap-independent mechanism (Fig. 3). Interestingly, this could be observed whether the mRNAs were capped or not, showing that the cap structure plays only little role in this process. This result was further confirmed by the use of a synergistic competitive reticulocyte lysate (Soto Rifo et al. 2007) in which the addition of a cap structure to the polyadenylated wild-type RNA showed no effect on overall Gag translation (Fig. 4). The use of antisense 2′-*O*-methyloligoribonucleotides that block ribosomal scanning also yielded some interesting results (Fig. 5). First of all, it showed that annealing of an antisense oligo to the PBS in the middle of the HIV-2 5′-untranslated region only had a mild effect on protein production, confirming that the presence of the gag coding region is both necessary and sufficient for translation (Fig. 5, lanes 5–8). Second, hybridization of the oligos at different positions within the gag coding region suggests that access at each of the AUG initiation sites occurs in an independent manner (Fig. 5, lanes 9–16).

We then went on to investigate the viral molecular determinants that can control HIV-2 IRES-driven translation. A first candidate was the HIV-2 protease as the latter was shown to play a role in the control of translation by cleaving the initiation factor eIF4G (Prevot et al. 2003b). This cleavage was shown to inhibit ribosomal scanning without affecting 43 S binding to the mRNA (Prevot et al. 2003b). Treatment of the rabbit reticulocyte lysate with the HIV-2 protease ultimately resulted in the shutoff of Globin-LacZ mRNA translation, inhibition of both EMCV and the leaderless HIV-2 constructs, but had virtually no effect on the wild-type HIV-2 genomic RNA (Fig. 6). More importantly, changes in the relative utilization of the AUG initiation codons could be observed. Initiation at the proximal site on the wild-type HIV-2 RNA was inhibited without affecting expression from the two downstream AUG codons. This result strongly suggests that initiation at AUG1 could involve some ribosomal scanning whereas initiation from AUG2 and AUG3 would occur by direct ribosomal binding to these sites. These results suggest that the pattern of expression of the HIV-2 Gag isoforms can be affected independently from each other and that the presence or absence of the 5′-UTR plays a role in this process. These differences observed in the absence of the 5′-UTR could be explained by the fact that leaderless mRNAs have been shown to be able to recruit 80S ribosomes directly to the start codon (Andreev et al. 2006). Interestingly, the cleavage of eIF4G by the FMDV–L-protease did not modify the relative ratio of Gag isoform synthesis arguing for a very specific influence of the enzyme on its cognate genomic RNA (Fig. 3).

In view of these data, it was of interest to investigate whether other viral proteins could modulate translation of the HIV-2 genomic RNA. An obvious candidate was the Gag polyprotein itself, since the latter is involved in the packaging of the HIV-2 genomic RNA by binding structured RNA stem-loops that lie within the 5′-UTR (Kaye and Lever 1998; Griffin et al. 2001) and could interfere with translation. Addition of increasing concentrations of recombinant Gag did not seriously affect translation driven by the globin 5′-UTR (Fig. 7). However, it had a very strong impact on the WT HIV-2 construct by sharply inhibiting protein synthesis at a relatively low Gag concentration and influencing the relative ratio of utilization of the AUG start sites (Fig. 7). In fact, initiation at the AUG1 proximal site was drastically impaired whereas translation at the second and third AUG codons remained unaffected until a high concentration of Gag was used. Interestingly, inhibition of WT HIV-2 translation was sudden and drastic when a certain concentration of Gag was added to the RRL (Fig. 7, lanes 23,24). In contrast, expression of p57, p50, and p44 from the HIV-2 leaderless construct was gradually inhibited. Such a situation also occurred when the EMCV IRES was used (Fig. 7, lanes 10–18) with a

Downloaded from rnajournal.cshlp.org on May 8, 2020 - Published by Cold Spring Harbor Laboratory Press

gradual impairment of protein production. However, translation of Gag isoforms from the chimeric RNA (Globin::Gag) showed no significant inhibition upon recombinant Gag addition, suggesting that the HIV-2 5′-UTR plays an important role in this inhibition process.

Thus, we postulated that the different behavior of these constructs to Gag addition may reveal cooperative binding of the polyprotein to the packaging signals located within the 5′-UTR. This was investigated by adding in *trans* the HIV-2 5′-UTR or an unrelated β-Gal RNA sequence to the RRL supplemented with a relatively large excess of Gag polyprotein (Fig. 8). *Trans*-addition of either the viral leader or an unrelated β-Gal sequence resulted in the rescue of expression of p50 and p44 isoforms from both the WT and leaderless HIV-2 constructs. However, translation at the proximal AUG site (AUG1) could only be restored by the *trans*-addition of the viral leader on its cognate genomic RNA.

In summary, data presented herein show that both the HIV-2 protease and the viral polyprotein can modulate translation of the genomic RNA in such a way that initiation at the AUG1 proximal site becomes rapidly inhibited (Figs. 6, 7) upon slight increase in protein concentration whereas production of p50 and p44 continues until a relatively high amount of Gag is added. Since the presence of IRES elements driving synthesis of truncated Gag isoforms has become a conserved feature of the lentiviral family as it has now been characterized within the HIV-1 (Buck et al. 2001), SIV (Nicholson et al. 2006), and HIV-2 (Herbreteau et al. 2005) genomic RNAs, this suggests that initiation from the coding region may be a way to increase the production of the CA, NC, and p6 proteins. Based on these data, we propose a model for HIV-2 translation in which the ribosomes initially reach the proximal AUG1 site to produce the full-length polyprotein. While the latter is being synthesized, it binds preferentially to its cognate 5′-UTR creating a scaffold of RNA–Gag complex which progressively occludes the accessibility of the 5′-UTR for ribosomes by steric hindrance (our results; see also (Kaye and Lever 1998; Griffin et al. 2001). At this stage, preferential production of the Gag truncated isoforms is taking place from ribosomal entry at the internal AUG codons, ensuring that viral protein production continues during the initial steps of viral assembly. It is noteworthy that these Nt-truncated Gag isoforms have the ability to interact with the full length p57 Gag polyprotein to assemble in the form of virus-like particles at the plasma membrane (Herbreteau et al. 2005). At a later stage, when full length Gag and the truncated isoforms have been produced in a sufficient amount, translation of the HIV-2 genomic RNA is stopped by the binding and accumulation of these proteins on its cognate messenger. Such a mechanism could discriminate between the end of viral protein synthesis and the beginning of viral packaging and assembly.

MATERIALS AND METHODS

Protease, antibodies, recombinant Gag protein, and other reagents

The L-protease from FMDV was generated by in vitro translation as described previously (Prevot et al. 2003a). The recombinant HIV-1 Gag protein was prepared as described (Datta et al. 2007) and solubilized in a buffer containing 20 mM Tris HCl pH 7.4, 0.5 M NaCl, 5 mM DTT, 1 mM PMSF, and a protease inhibitors cocktail (Roche Inc.). These conditions are taken in consideration for translation experiments performed in the presence of this protein to maintain equivalent levels of salt, pH, DTT, and anti-protease in each reaction tube.

Hybridization of 2′-*O*-methyloligoribonucleotides

Antisense 2′-*O*-methyloligoribonucleotides spanning positions nucleotides 306–327 (antisense to the PBS), nucleotides 548–566 (antisense to AUG1), nucleotides 747–765 (antisense to AUG2) of the HIV-2 RNA were annealed to RNA in 20 mM Hepes/KCl (pH 7.6) and 100 mM KCl for 3 min at 65°C followed by 20 min incubation at room temperature.

An antisense 2′-*O*-methyloligoribonucleotide spanning positions nucleotides 22–42 (antisense to Globin 5′-UTR) was annealed to Globin-LacZ as described above and used as a control for measuring ribosomal scanning inhibition.

Plasmid construction

Standard procedures were used for plasmid DNA construction, purification, and linearization. Details of the constructs used in this study are given below.

pBi-AUG1, pBi-AUG2, pBi-AUG3, pBi-AUG1-3, pBi 662-AUG3, and pBi 748-AUG3

Sequences of the HIV-2 from the +1 transcription start site (R) up to the AUG start codon at position 548 (pBi-AUG1), or from the +1 up to the AUG at position 746 (pBi-AUG2), or from the +1 up to the AUG at position 899 (pBi-AUG3), or from position 546 to position 899 (pBi-AUG1-3), or from position 662 to position 899 (pBi-662-AUG3), or from position 748 to position 899 (pBi-748-AUG3) were amplified by PCR, digested by NheI (PCR added restriction site) and inserted into pBi-NL (described in Ronfort et al. 2004) previously digested by NheI. pEMCV-LacZ and pHCV-NS have been previously described (Prevot et al. 2003b). pGlobin-LacZ contains the 5′-UTR of rabbit β Globin (52 nt in length) which drives translation of the *LacZ* gene (kindly donated by Dr. B. Sargueil, CNRS, Gif sur Yvette, France). For Globin::Gag, the sequence of T7 promoter followed by the globin 5′-UTR was amplified by PCR and digested by XbaI and NcoI (PCR added restriction site). The digested sequence was then inserted into the pcDNA3.1 (Invitrogene) vector previously digested by XbaI and NcoI. The sequence of the Gag coding region was amplified by PCR and digested by NcoI and AflII (PCR added restriction site). The digested sequence was then inserted into the pcDNA3.1 vector, containing the 5′-UTR of globin, previously digested by NcoI and AflII.

Downloaded from rnajournal.cshlp.org on May 8, 2020 - Published by Cold Spring Harbor Laboratory Press

pFR vector

The firefly luciferase coding region (amplified by PCR) containing the restriction site for BamHI (at the 5′ end) and a 50-nt polylinker (at the 3′ end, containing restriction sites for AflII, AflIII, AccI, KpnI, PstI, PmlI, SpeI, and SalI) followed by a BglII restriction site, was inserted into the pRenilla vector (described in Soto Rifo et al. 2007) previously digested with BamHI. EcoRI and EcoRV restriction sites located within the firefly luciferase coding region were then mutated using the QuickChange site-directed mutagenesis kit (Stratagene).

pFR-NoIRES, pFR-AUG3, pFR-AUG1-3, pFR-662-AUG3, and pFR-748-AUG3

Sequences of the HIV-2 from position 546 to position 899 (pFR-AUG1-3), or from position 662 to position 899 (pFR-662-AUG3), or from position 748 to position 899 (pFR-748-AUG3) were amplified by PCR, digested by SalI and BamHI (PCR added restriction site) and inserted into the pFR vector previously digested by SalI and BamHI.

In vitro transcription and translation

The Neo-Lac Z plasmid DNAs were linearized at the SspI site thus producing a 46 kDa truncated version of β-Galactosidase. The Globine::Gag pcDNA3.1 plasmid DNA was linearized at the EcoRI site. The pFR plasmid was linearized at the EcoRI just after the synthetic poly(A) tail. RNAs were synthesized in vitro as previously described (Prevot et al. 2003b). The integrity of the RNAs was checked by electrophoresis on nondenaturing agarose gels and their concentration was quantified by spectrophotometry at 260 nm using a Nanodrop (Nanodrop Technologies).

In vitro transcribed RNAs were translated in 10 μL of either the Flexi Rabbit Reticulocyte System (Promega Co.) or the supplemented untreated RRL 50% (v/v) each (as described in Soto Rifo et al. 2007) in the presence of 75 mM KCl, 2.5 mM $MgCl_2$, 20 μM of each amino acid (minus methionine), and 0.6 mCi/mL of [^{35}S]-methionine (GE Healthcare Life Sciences). Translation was carried out for 30 min at 30°C and stopped by the addition of 2× SDS-loading buffer. Translation products were resolved by 15%SDS-PAGE, gels were dried and subjected to autoradiography using Biomax films (Eastman Kodak Co.). Densitometric analyses were performed by phosphorimaging with a Storm 850 PhosphorImager.

T7 RNA polymerase transcription of PCR DNA fragments

The DNA sequence corresponding to the coding region of HIV-2 *gag* (pROD10), were amplified by PCR using a 3′ oligonucleotide starting at the end of the HIV-2 *gag*, and a 5′ to 3′ sense oligonucleotide starting with the T7 promoter sequence and complementary to the +1 region of the 5′-UTR, or to the AUG1 start codon, to generate T7-WT and T7-AUG1, respectively. Following purification of the PCR fragments, in vitro transcription using the T7 bacteriophage polymerase was conducted as described above. It should be noted that due to the much higher translational efficiency of the leaderless construct as shown previously (Herbreteau et al. 2005), the latter was utilized at a lower RNA concentration than the wild-type HIV-2 construct.

RNA transfection

HeLa cells were transfected using the TransIT RNA transfection kit (Mirus Bio Corporation) as described (Dieterich et al. 2007).

Measure of luciferase activities from HeLa cells transfected with bicistronics RNAs

HeLa cells were plated at a density of 150,000 cells per well (24 well plate) and transfected with 100 ng of the p2A RNA coding for the protease from poliovirus (Ronfort et al. 2004). After 2 h, the cells were transfected again with 0.156 pmol of the corresponding capped and polyadenylated bicistronic RNA. Three hours post transfection, cells were lysed and luciferase activities were measured using the dual reporter luciferase assay (Promega) on a Veritas luminometer (Turner Biosystems) following the manufacturer's protocol.

SUPPLEMENTAL DATA

Supplemental material can be found at http://www.rnajournal.org.

ACKNOWLEDGMENTS

The following reagents were obtained through the AIDS Research and Reference Reagent Program, NIAID, NIH: HIV-2 PR. from Bret Shirley and Mr. Michael Cappola, Boehringer Ingelheim Pharmaceuticals, Inc. We thank Dr. Bruno Sargueil (CNRS, Gif sur Yvette, France) for kindly donating the pglobin plasmid, Dr. S. J. Morley for donating eIF4G antibodies. The research of S.A.K.D and A.R. was supported in part by the intramural research program of the NIH, National Cancer Institute. A.S. was funded by the Friedrich-Naumann-Stiftung. C.H.H. was funded by MENRT and FRM grants; E.P.R. is funded by a MENRT grant and work in our laboratory is supported by grants from ANR, ANRS, INSERM, ACI, and TRIOH from EC sixth PCRD.

Received September 5, 2007; accepted March 11, 2008.

REFERENCES

Andreev, D.E., Terenin, I.M., Dunaevsky, Y.E., Dmitriev, S.E., and Shatsky, I.N. 2006. A leaderless mRNA can bind to mammalian 80S ribosomes and direct polypeptide synthesis in the absence of translation initiation factors. *Mol. Cell. Biol.* **26:** 3164–3169.

Balvay, L., Lastra, M.L., Sargueil, B., Darlix, J.L., and Ohlmann, T. 2007. Translational control of retroviruses. *Nat. Rev. Microbiol.* **5:** 128–140.

Bock, P.J. and Markovitz, D.M. 2001. Infection with HIV-2. *AIDS* (Suppl 5) **15:** S35–S45.

Bonnal, S., Boutonnet, C., Prado-Lourenco, L., and Vagner, S. 2003. IRESdb: The internal ribosome entry site database. *Nucleic Acids Res.* **31:** 427–428.

Brasey, A., Lopez-Lastra, M., Ohlmann, T., Beerens, N., Berkhout, B., Darlix, J.L., and Sonenberg, N. 2003. The leader of human immunodeficiency virus type 1 genomic RNA harbors an internal

Downloaded from rnajournal.cshlp.org on May 8, 2020 - Published by Cold Spring Harbor Laboratory Press

ribosome entry segment that is active during the G2/M phase of the cell cycle. *J. Virol.* **77:** 3939–3949.

Buck, C.B., Shen, X., Egan, M.A., Pierson, T.C., Walker, C.M., and Siliciano, R.F. 2001. The human immunodeficiency virus type 1 gag gene encodes an internal ribosome entry site. *J. Virol.* **75:** 181–191.

Butsch, M. and Boris-Lawrie, K. 2002. Destiny of unspliced retroviral RNA: Ribosome and/or virion? *J. Virol.* **76:** 3089–3094.

Camerini, V., Decimo, D., Balvay, L., Pistello, M., Bendinelli, M., Darlix, J.L., and Ohlmann, T. 2008. A "dormant" IRES controls translation of the feline immunodeficiency virus (FIV). *J. Virol.* **82:** 3574–3883.

Datta, S.A., Curtis, J.E., Ratcliff, W., Clark, P.K., Crist, R.M., Lebowitz, J., Krueger, S., and Rein, A. 2007. Conformation of the HIV-1 Gag protein in solution. *J. Mol. Biol.* **365:** 812–824.

Dieterich, K., Soto Rifo, R., Faure, A.K., Hennebicq, S., Ben Amar, B., Zahi, M., Perrin, J., Martinez, D., Sele, B., Jouk, P.S., et al. 2007. Homozygous mutation of AURKC yields large-headed polyploid spermatozoa and causes male infertility. *Nat. Genet.* **39:** 661–665.

Gale Jr., M., Tan, S.L., and Katze, M.G. 2000. Translational control of viral gene expression in eukaryotes. *Microbiol. Mol. Biol. Rev.* **64:** 239–280.

Gingras, A.C., Raught, B., and Sonenberg, N. 1999. eIF4 initiation factors: Effectors of mRNA recruitment to ribosomes and regulators of translation. *Annu. Rev. Biochem.* **68:** 913–963.

Griffin, S.D., Allen, J.F., and Lever, A.M. 2001. The major human immunodeficiency virus type 2 (HIV-2) packaging signal is present on all HIV-2 RNA species: Cotranslational RNA encapsidation and limitation of Gag protein confer specificity. *J. Virol.* **75:** 12058–12069.

Herbreteau, C.H., Weill, L., Decimo, D., Prevot, D., Darlix, J.L., Sargueil, B., and Ohlmann, T. 2005. HIV-2 genomic RNA contains a novel type of IRES located downstream of its initiation codon. *Nat. Struct. Mol. Biol.* **12:** 1001–1007.

Jackson, R.J., Hunt, S.L., Gibbs, C.L., and Kaminski, A. 1994. Internal initiation of translation of picornavirus RNAs. *Mol. Biol. Rep.* **19:** 147–159.

Jang, S.K., Krausslich, H.G., Nicklin, M.J., Duke, G.M., Palmenberg, A.C., and Wimmer, E. 1988. A segment of the 5′ nontranslated region of encephalomyocarditis virus RNA directs internal entry of ribosomes during in vitro translation. *J. Virol.* **62:** 2636–2643.

Kaye, J.F. and Lever, A.M. 1998. Nonreciprocal packaging of human immunodeficiency virus type 1 and type 2 RNA: A possible role for the p2 domain of Gag in RNA encapsidation. *J. Virol.* **72:** 5877–5885.

Kaye, J.F. and Lever, A.M. 1999. Human immunodeficiency virus types 1 and 2 differ in the predominant mechanism used for selection of genomic RNA for encapsidation. *J. Virol.* **73:** 3023–3031.

Kozak, M. 1989. The scanning model for translation: An update. *J. Cell Biol.* **108:** 229–241.

Lemey, P., Pybus, O.G., Wang, B., Saksena, N.K., Salemi, M., and Vandamme, A.M. 2003. Tracing the origin and history of the HIV-2 epidemic. *Proc. Natl. Acad. Sci.* **100:** 6588–6592.

Nicholson, M.G., Rue, S.M., Clements, J.E., and Barber, S.A. 2006. An internal ribosome entry site promotes translation of a novel SIV Pr55(Gag) isoform. *Virology* **349:** 325–334.

Ohlmann, T., Pain, V.M., Wood, W., Rau, M., and Morley, S.J. 1997. The proteolytic cleavage of eukaryotic initiation factor (eIF) 4G is prevented by eIF4E binding protein (PHAS-I; 4E-BP1) in the reticulocyte lysate. *EMBO J.* **16:** 844–855.

Ohlmann, T., Lopez-Lastra, M., and Darlix, J.L. 2000. An internal ribosome entry segment promotes translation of the simian immunodeficiency virus genomic RNA. *J. Biol. Chem.* **275:** 11899–11906.

Ohlmann, T., Prevot, D., Decimo, D., Roux, F., Garin, J., Morley, S.J., and Darlix, J.L. 2002. In vitro cleavage of eIF4GI but not eIF4GII by HIV-1 protease and its effects on translation in the rabbit reticulocyte lysate system. *J. Mol. Biol.* **318:** 9–20.

Otto, G.A. and Puglisi, J.D. 2004. The pathway of HCV IRES-mediated translation initiation. *Cell* **119:** 369–380.

Pelletier, J. and Sonenberg, N. 1988. Internal initiation of translation of eukaryotic mRNA directed by a sequence derived from poliovirus RNA. *Nature* **334:** 320–325.

Prevot, D., Darlix, J.L., and Ohlmann, T. 2003a. Conducting the initiation of protein synthesis: The role of eIF4G. *Biol. Cell.* **95:** 141–156.

Prevot, D., Decimo, D., Herbreteau, C.H., Roux, F., Garin, J., Darlix, J.L., and Ohlmann, T. 2003b. Characterization of a novel RNA-binding region of eIF4GI critical for ribosomal scanning. *EMBO J.* **22:** 1909–1921.

Reeves, J.D. and Doms, R.W. 2002. Human immunodeficiency virus type 2. *J. Gen. Virol.* **83:** 1253–1265.

Ronfort, C., De Breyne, S., Sandrin, V., Darlix, J.L., and Ohlmann, T. 2004. Characterization of two distinct RNA domains that regulate translation of the *Drosophila* gypsy retroelement. *RNA* **10:** 504–515.

Soto Rifo, R., Ricci, E.P., Decimo, D., Moncorge, O., and Ohlmann, T. 2007. Back to basics: The untreated rabbit reticulocyte lysate as a competitive system to recapitulate cap/poly(A) synergy and the selective advantage of IRES-driven translation. *Nucleic Acids Res.* **35:** e121.

Spahn, C.M., Jan, E., Mulder, A., Grassucci, R.A., Sarnow, P., and Frank, J. 2004. Cryo-EM visualization of a viral internal ribosome entry site bound to human ribosomes: The IRES functions as an RNA-based translation factor. *Cell* **118:** 465–475.

Stoneley, M. and Willis, A.E. 2004. Cellular internal ribosome entry segments: Structures, *trans*-acting factors and regulation of gene expression. *Oncogene* **23:** 3200–3207.

Vagner, S., Galy, B., and Pyronnet, S. 2001. Irresistible IRES. Attracting the translation machinery to internal ribosome entry sites. *EMBO Rep.* **2:** 893–898.

Ventoso, I., Blanco, R., Perales, C., and Carrasco, L. 2001. HIV-1 protease cleaves eukaryotic initiation factor 4G and inhibits cap-dependent translation. *Proc. Natl. Acad. Sci.* **23:** 23.

Waysbort, A., Bonnal, S., Audigier, S., Esteve, J., and Prats, A. 2001. Pyrimidine tract binding protein and La autoantigen interact differently with the 5′ untranslated regions of lentiviruses and oncoretrovirus mRNAs. *FEBS Lett.* **490:** 54–58.

Yaman, I., Fernandez, J., Liu, H., Caprara, M., Komar, A.A., Koromilas, A.E., Zhou, L., Snider, M.D., Scheuner, D., Kaufman, R.J., et al. 2003. The zipper model of translational control: A small upstream ORF is the switch that controls structural remodeling of an mRNA leader. *Cell* **113:** 519–531.

Ziegler, E., Borman, A.M., Deliat, F.G., Liebig, H.D., Jugovic, D., Kean, K.M., Skern, T., and Kuechler, E. 1995. Picornavirus 2A proteinase-mediated stimulation of internal initiation of translation is dependent on enzymatic activity and the cleavage products of cellular proteins. *Virology* **213:** 549–557.

Published online 8 March 2011 *Nucleic Acids Research, 2011, Vol. 39, No. 12* ***5215–5231***
doi:10.1093/nar/gkr086

Activation of a microRNA response in *trans* reveals a new role for poly(A) in translational repression

Emiliano P. Ricci[1,2,3], Taran Limousin[1,2,3], Ricardo Soto-Rifo[1,2,3], Rachel Allison[4], Tuija Pöyry[4], Didier Decimo[1,2,3], Richard J. Jackson[4] and Théophile Ohlmann[1,2,3,*]

[1]Ecole Normale Supérieure de Lyon, Unité de Virologie Humaine, IFR 128, [2]Inserm, U758, Lyon, F-69364 France, [3]Université de Lyon, Lyon, France and [4]Department of Biochemistry, University of Cambridge, 80 Tennis Court Rd., Cambridge CB2 1GA, UK

Received September 8, 2010; Revised January 26, 2011; Accepted February 2, 2011

Downloaded from https://academic.oup.com/nar/article-abstract/39/12/5215/2411295 by guest on 08 May 2020

ABSTRACT

Here, we report that the untreated rabbit reticulocyte lysate contains over 300 different endogenous microRNAs together with the major components of the RNA-induced silencing complex and thus can be used as a model *in vitro* system to study the effects of microRNAs on gene expression. By using this system, we were able to show that microRNA hybridization to its target resulted in a very rapid and strong inhibition of expression that was exerted exclusively at the level of translation initiation with no involvement of transcript degradation or deadenylation. Moreover, we demonstrate that the magnitude of microRNA-induced repression can only be recapitulated in the context of a competitive translating environment. By using a wide spectrum of competitor cellular and viral RNAs, we could further show that competition was not exerted at the level of general components of the translational machinery, but relied exclusively on the presence of the poly(A) tail with virtually no involvement of the cap structure.

INTRODUCTION

microRNAs (miRNAs) are small non-coding RNAs (18–25 nt long) that are encoded by the cell genome. Once associated with the RNAi-induced silencing complex (RISC), they can regulate gene expression by interacting, in most cases, with the 3′ untranslated region (3′-UTR) of the messenger RNA (mRNA) to affect its translation and/or stability. miRNAs have been found in plants, animals and viruses, some of which are very well conserved during evolution, thus suggesting an important role (1,2). Interestingly, miRNAs were shown to be implicated in most of the biological processes studied so far (i.e. development, cell growth, cell division, etc.) (3,4). This is also reflected by the fact that about 60% of human coding genes possess conserved target-sites for miRNAs (5,6) showing the extent of miRNA-dependent regulation of gene expression.

Interaction between miRNAs and target mRNAs generally involves a full-match base pairing at the seed region (nucleotides 2–8 at the miRNA 5′-end), followed by a bulge region (a few nucleotides long) and partial complementarity to the 3′-end of the miRNA (7–9). Interestingly, full pairing between the miRNA and an mRNA leads to degradation of the latter by an small interfering RNA (siRNA) response that first cleaves the target transcript at the site of interaction and then provokes the complete degradation by the cell (10–12). Nevertheless, very few cases of natural full matching interactions have been reported in animals (12,13). In contrast, for the predominant bulged target-sites, repression of protein synthesis mediated by miRNAs depends on the RISC complex, which essentially consists of Argonaute, and GW182 proteins (common to the siRNA pathway) (14,15). However, the actual mechanisms by which miRNAs regulate gene expression are not yet fully understood. Several proposed mechanisms involve translational repression at the initiation (16–21) or post-initiation steps (22–24), and also mRNA deadenylation and mRNA target degradation (25–28). Furthermore, even though the RISC machinery is required for repression, it is not fully clear whether it plays a direct role or if it allows the recruitment of other cellular factors that could account for this repression (29–34).

Cell-free extracts have been instrumental in understanding the molecular mechanism of translation, and thus it would be of great interest to develop an *in vitro* system that would be able to recapitulate translational repression mediated by miRNAs. Most existing *in vitro* systems that

*To whom correspondence should be addressed. Tel: (33) 472 728 953; Fax: (33) 472 728 137; Email: tohlmann@ens-lyon.fr

© The Author(s) 2011. Published by Oxford University Press.
This is an Open Access article distributed under the terms of the Creative Commons Attribution Non-Commercial License (http://creativecommons.org/licenses/by-nc/2.5), which permits unrestricted non-commercial use, distribution, and reproduction in any medium, provided the original work is properly cited.

allow an miRNA response rely on 'home-made' cell-free extracts that are technically difficult to produce and yield a low-level of translational activity (17,19,26,27). Recently, an *in vitro* system based on the rabbit reticulocyte lysate (RRL) has been proposed (20,21), but it relies exclusively on exogenous artificial miRNAs that need to be pre-annealed to the target mRNA before translation and more importantly it was developed in the nuclease-treated RRL, a system which does not recapitulate the cap/poly(A) dependence (35–37).

This is a drawback as the cap and poly(A) tail of mRNAs were recently shown to be critical players in miRNA-dependent translational repression (16–19), thus their synergy must be recapitulated *in vitro*, in order to reproduce all aspects of miRNA regulation of translation. Here, we have exploited the properties of the untreated RRL that was previously described to be both cap and poly-A dependent for translation (38), to faithfully reproduce translational repression driven by endogenous miRNAs. Biochemical analysis showed that the RISC machinery, as well as high amount of endogenous miRNAs, is present in RRL. Moreover, functional assays using an exogenous mRNA bearing target sites for endogenous miRNAs showed that endogenous RISC components were able to recapitulate all major aspects of translational repression observed *in vivo* with no evident deadenylation or degradation of target transcripts. Finally yet importantly, we also show that no miRNA response can be observed in the nuclease-treated RRL despite the fact that the latter also contains endogenous miRNAs in similar quantities. However, addition of competitor mRNAs to the nuclease-treated RRL restored a potent miRNA response. Interestingly, only polyadenylated competitor mRNAs were able to restore an miRNA response in the nuclease-treated RRL independently of the presence of a cap in the 5′ end. This was further investigated by showing that addition of free poly(A) was sufficient to restore a potent miRNA response *in trans*. Taken together, our results suggest a role for poly(A)-binding protein (PABP) in translational repression independent of its role in deadenylation which has recently been demonstrated (39–41). Finally, we propose the use of the untreated RRL as a standard *in vitro* system, available to any user, that recapitulates many previously described features of the miRNA response: pre-miRNA processing, miRNA hybridization to their target site and their effects on translation (in the case of bulged target sites) and mRNA cleavage (in the case of a full match pairing between the miRNA and the target mRNA).

MATERIALS AND METHODS

DNA constructs and *in vitro* transcription

Plasmids containing target sites for miR451 (Luc-451X6, Luc PMX4 and Luc-451MutX6) and let7 (Luc-let7X6) were derived from the pGlobin-Renilla, pEMCV-Renilla and pHCV-Renilla vectors recently described (38). Target sites were constructed by hybridizing two synthetic oligodeoxyribonucleotides (Eurogentec) that contained the target motifs separated by the natural let-7a spacer from the lin41 gene and cloned into the 3′UTR of the digested (HindIII) vector. These target sites were amplified by polymerase chain reaction (PCR) and sequentially cloned in the EcoRV and XbaI restriction sites to produce a construct containing six target sites in the 3′UTR of the renilla luciferase gene. Plasmids were linearized at the EcoRI site to produce polyadenylated RNAs, and at the XbaI site for producing non-polyadenylated RNAs. The firefly coding plasmid was constructed by cloning the firefly luciferase coding region into the pGlobin-Renilla vector digested by BamHI and EcoRV (thus releasing the renilla luciferase coding region). pHCV-NS, pCrPV-LacZ vectors were linearized respectively at the MluI and SspI, as described in ref. 42. Uncapped RNAs were transcribed following the protocol described in ref. 38, and treated with RQ1 DNAse (Promega Co., Madison, WI, USA). *In vitro* synthesized transcripts were capped using the ScriptCap kit (Epicentre), which allows full capping of RNAs in the 5′–5′ orientation.

Radiolabeled RNAs were transcribed as described above but UTP and GTP were replaced by [α-^{32}P]UTP (800 Ci/mmol, 10 mCi/ml) and [α-^{32}P]GTP (800 Ci/mmol, 10 mCi/ml). Prior to translation, mRNAs were heat denatured at 65°C for 5 min and then immediately placed on ice.

Polyadenylation of mRNAs by the poly(A) polymerase was performed using the Poly(A) Tailing Kit, following the manufacturer's protocol (Ambion).

Western blotting of RISC components

RRL volumes of 1, 2 and 3 µl, or HeLa cell S10 and S100 lysates (prepared as described in (43) were resolved by 10% sodium dodecyl sulfate–polyacrylamide gel electrophoresis (SDS–PAGE). Proteins were then transferred to a nitrocellulose membrane by electroblotting and incubated with antibodies specific for Dicer, Ago2 and PABP. Western blotting against TNRC6 was performed following the protocol described in ref. (44). For this, 100 µl of untreated RRL were used to immunoprecipitate TNRC6 using 5 µl of anti-TNRC6 antibodies (Santacruz Technology) and 15 µl of protein A magnetic beads (Millipore). Beads together with antibodies were incubated with untreated RRL for 2 h, then washed three times with radioimmunoprecipitation assay (RIPA) buffer and loaded on 7.5% SDS–PAGE. Proteins were transferred to a polyvinylidene fluoride (PVDF) membrane by electroblotting and incubated with antibodies specific for TNRC6 described in ref. (45).

Microarray assay

Microarray assay was performed by LC Science Company. Five micrograms of total RNA sample isolated from untreated RRL (Promega) were size-fractionated using a YM-100 Microcon centrifugal filter (Millipore) and the small RNAs (<300 nt) isolated were 3′-extended with a poly(A) tail using poly(A) polymerase. An oligonucleotide tag was then ligated to the poly(A) tail for subsequent fluorescent dye staining. Hybridization was performed overnight on a µParaflo microfluidic chip using a micro-circulation pump (Atactic Technologies).

Downloaded from https://academic.oup.com/nar/article-abstract/39/12/5215/2411295 by guest on 08 May 2020

On the microfluidic chip, each detection probe consisted of a chemically modified nucleotide coding segment complementary to target microRNA (from miRBase, http://microrna.sanger.ac.uk/sequences/) and a spacer segment of polyethylene glycol to extend the coding segment away from the substrate. The detection probes were made by *in situ* synthesis using photogenerated reagent (PGR) chemistry. The hybridization melting temperatures were balanced by chemical modifications of the detection probes. Hybridization used 100 µl 6 × SSPE buffer [0.90 M NaCl, 60 mM Na_2HPO_4, 6 mM ethylenediaminetetraacetic acid (EDTA), pH 6.8] containing 25% formamide at 34°C. After hybridization, detection was carried out by fluorescence labeling using tag-specific Cy3 and Cy5 dyes. Hybridization images were collected using a laser scanner (GenePix 4000B, Molecular Device) and digitized using Array-Pro image analysis software (Media Cybernetics). Data were analyzed by first subtracting the background and then normalizing the signals using a LOWESS filter[10] (Locally-weighted Regression) and *P*-values of the *t*-test were calculated; differentially detected signals were those with <0.01 *P*-values.

Splinted ligation assays of selected miRNAs

Total reticulocyte lysate RNA was prepared using the *mir*Vana kit (Ambion), and specific miRNAs assayed by the splinted ligation method (46). In all cases, the ligation oligodeoxynucleotide was 5′-CGCTTATGACATTC/reversed-dC/-3′, and was 5′-end-labeled using T4 polynucleotide kinase (NEB) according to the supplier's recommendation.

Bridge oligodeoxynucleotides (Eurofins-MWG-Operon) had three-carbon spacers at each end, and the following sequences:

for let7a, 5′-GAATGTCATAAGCGAACTATACAACC TACTACCTCA-3′;
miR-451, 5′-GAATGTCATAAGCGAACTCAGTAAT GGTAACGGTTT-3′;
and miR-221, 5′-GAATGTCATAAGCGGAAACCCAG CAGACAATGTAGCT-3′.

The splinted ligation was performed in a 15-µl volume as described in ref. 46: 100 fmol bridge oligonucleotide, 100 fmol ^{32}P-labeled ligation oligonucleotide and 1, 2 or 4 µg reticulocyte RNA were denatured at 95°C for 1 min in 75 mM KCl and 20 mM Tris–HCl, pH 8.0. After annealing at 65°C for 2 min and then at 37°C for 10 min, 400 U T4 DNA ligase (NEB) and ligase buffer [to a final of 50 mM Tris–HCl, pH 7.5, 10 mM $MgCl_2$, 10 mM DTT, 1 mM adenosine triphosphate (ATP)] was added to the reaction mixture, which was incubated at 30°C for 1 h. Reaction was terminated by heat inactivation at 75°C for 15 min followed by addition of 10 U of calf intestinal alkaline phosphatase (NEB) and incubation at 37°C for 15 min. Then 15 µl formamide dye was added and the material was fractionated on a 15% urea–polyacrylamide gel, which was dried and the bands quantified using a PhosphorImager.

Preparation of untreated RRL and *in vitro* translation assays

Untreated RRL was prepared essentially as previously described (38,47). Briefly, 1 ml of untreated RRL (Promega Co., Madison, WI, USA) was supplemented, before thawing, with 25 µM haemin (Fluka) and 25 µg/ml creatine phosphokinase (Rabbit Skeletal Muscle, Calbiochem). After thawing, RRL was further supplemented with 5 mg/ml creatine phosphate (Disodium Salt, Calbiochem), 50 µg/ml bovine liver tRNAs (Sigma–Aldrich) and 3 mM D-glucose (Sigma–Aldrich).

Translation reactions were performed in a final volume of 30 µl consisting of 20 µl of untreated RRL, 0.46 fmol of heat-denatured mRNAs, in the presence of KCl (100 mM), $MgCl_2$ (0.5 mM) and amino acids mixture (20 µM each). When indicated, 2′-*O*-Me oligonucleotides complementary to miR-451 or let-7a were added to a final concentration of 35 nM. RRL under full translational condition was incubated together with the heat denatured mRNA for 1 h at 10°C, followed by 2 min at 20°C, 2 min at 25°C and 30 or 60 min at 30°C. The reaction was then stopped by the addition of 50 µl of luciferase lysis buffer to 10 µl of the translation reaction. When indicated, 5 pmol of competitor RNAs, or 1.2 pmol of free poly(A) RNA (400-nt average length, GE Healthcare), or 27 µM (final concentration) of free cap-analog (New England Bioloabs), were added to the extracts before translation.

Translation in wheat germ extract (Promega Co., Madison, WI, USA) was carried out using 0.46 fmol of mRNA following the manufacturer's protocol. Translation reactions were stopped by the addition of 50 µl of lysis buffer.

Renilla luciferase activity was measured in a Veritas™ luminometer (Turner Biosystems), using the Renilla Luciferase Assay System (Promega Co., Madison, WI, USA).

mRNA integrity assay

Radiolabeled mRNAs (0.46 fmol) were translated as described above. At the end of translation, RNAs were extracted using TRIzol (Invitrogen) and loaded on a 4% polyacrylamide 7 M urea gel. The gel was dried and submitted to autoradiography using X-ray films (Fuji).

Quantitative PCR assays

miRNA quantification was carried out using the Ncode miRNA kit (Invitrogen) according to the manufacturer's protocol using 1 µg of total RNA extracted from untreated RRL.

mRNA stability after translation was performed by extracting total RNA from 20 µl of the translation reaction using TRIzol (Invitrogen). Reverse transcription of 500 ng of total RNA was performed using qScript kit (Quanta). Quantitative PCR was then performed as described (48) using endogenous glyceraldehyde 3-phosphate dehydrogenase (GAPDH) mRNA as an internal control.

Downloaded from https://academic.oup.com/nar/article-abstract/39/12/5215/2411295 by guest on 08 May 2020

Poly(A) tail length assay

Monitoring of the poly(A) tail length was carried out using the Ncode miRNA kit (Invitrogen) with the following modifications: Total RNA extracted from RRL (after translation of the target mRNA) and the capped and polyadenylated Luc or Luc-451X6 mRNAs (after transcription) were polyadenylated following the manufacturer's protocol (using 1 μg of total RNA or 0.1 ng of pure target mRNA). Reverse transcription of the polyadenylated RNAs was carried out using the universal RT primer provided with the kit, that anneals at the 3′end of the mRNA poly(A) tail. The resulting cDNAs were then used as template for PCR using a universal antisense primer (complementary of the specific sequence of the RT oligo used to reverse transcribe the target mRNA) and a specific sense primer complementary to the 3′ end of the renilla coding region. PCR products were then resolved on a 2% agarose gel.

Processing of miRNA precursors

Two-hundred femtomoles of 5′ end-labeled pre-miR-122 (Dharmacon) were incubated in 70% RRL (with 10 mM creatine phosphate, 100 mM KCl, 0.5 mM $MgCl_2$, 0.1 mM each amino acid) at 30°C. At 10-min intervals, 10-μl samples were taken up to 1 h, then a final sample was taken at 90 min. Samples were denatured in 10 μl formamide dye and then separated on a 15 % urea–polyacrylamide gel. The intensity of the bands was quantified by phosphorimager analysis.

Statistical analysis

Data were tested for normality using the one-sample Kolmogorov–Smirnov test ($N = 45$ for each group of samples). Having verified the normal distribution (P-value of 0.25), statistical significances were calculated on the normally distributed data sets using a paired Student's t-test.

RESULTS

A functional RISC machinery as well as endogenous miRNAs are present in the untreated RRL

The RRL has been used for some time to study the control of protein synthesis as it presents a high metabolic activity and contains all cytoplasmic components that are needed for efficient translation. Most workers use the nuclease-treated RRL in which endogenous mRNAs have been destroyed by the use of the calcium-dependent micrococcal nuclease (47). Although this system has been widely used over the last 30 years, it has also been criticized, as it does not faithfully reproduce physiological conditions pertaining in the cytoplasm of cells (35–37). Thus, we have recently designed an *in vitro* system based on the untreated reticulocyte lysate (which contains endogenous mRNAs, mainly globin and lipoxygenase) that faithfully recapitulates the cap and poly-A synergy (38).

As this lysate has not been treated with nucleases, it was of interest to test for the presence of endogenous miRNAs and RISC components. For this, western blotting of RRL proteins was carried out using antibodies specific for Dicer, Argonaute2 (Ago2) and TNRC6A (the mammalian homolog of GW-182), as they all play a role in the maturation of miRNA precursors (Dicer, Ago2) or directly in the repression of targeted mRNAs (Ago2 and TNRC6). As a control, western blotting was also carried out on HeLa cell S10 and S100 lysates that were previously shown to contain RISC proteins (14) (Figure 1A). As shown, RRL contains endogenous Dicer in detectable amounts, although its expression level appears to be lower than that observed in S10 and S100 HeLa extracts (Figure 1A). TNRC6A was also detected both in HeLa and RRL (Figure 1A, right). However, Ago2 was much more abundant in the RRL than in S10 and S100 HeLa extracts, which is consistent with previous reports (49,50) (it should be noted that the bands corresponding to Ago2 in the RRL appear white as its concentration is saturating). The presence of most of the components of the RISC machinery in the RRL prompted us to test whether processing of a precursor miRNA (pre-miRNA) could take place. For this, a radiolabeled (5′-end label) miR-122 precursor was chosen, as it is not expressed in the rabbit reticulocyte lysate; this precursor was incubated in the RRL for different periods of times and the results are presented (Supplementary Figure S1). Interestingly, the pre-miR-122 was rapidly processed into two different intermediates molecules (Supplementary Figure S1, see intermed 1 and 2) and mature miR-122 molecules were observed as early as 10 min after the beginning of the incubation (Supplementary Figure 1, see miR-122) to reach 15% of the input pre-miR-122 after 90 min. It is noteworthy that the appearance of two putative processing intermediates is almost immediate (Supplementary Figure S1) and then seems to decrease with time.

The next step was to look for the presence of endogenous miRNAs. For this, total RNA was purified from untreated RRL and hybridized on a microarray (LC Sciences) with probes against most known mammalian miRNAs (Figure 1B). Surprisingly, more than 300 different miRNAs could be detected in the untreated RRL (Figure 1B and Supplementary Table S1). Among them, some could be found at very high concentration and were those corresponding to miRNAs that are known to be upregulated during erythroid differentiation such as miR-451 (51,52) (which literally saturated the reading). On the other hand, miRNAs that were shown to be downregulated during erythroid cell differentiation process such as miR-155 and miR-221 (51,52) could hardly be detected on the microarray and were expressed about much less than miR-451 (Figure 1B, see table). Interestingly, ubiquitous members of the let-7 family of miRNAs (comprising let-7a to let-7i) were present at high concentration with the let-7a member being the most abundant.

In order to confirm these results, a splinted ligation assay (46) was performed against both miR-451 and let-7a (highly expressed) and miR-221 (virtually absent from the RRL) (Figure 1C, additional miRNAs were also tested and the results are presented in Supplementary Figure S2). As observed, both let-7a and especially miR-451 gave a strong band in a yield

Downloaded from https://academic.oup.com/nar/article-abstract/39/12/5215/2411295 by guest on 08 May 2020

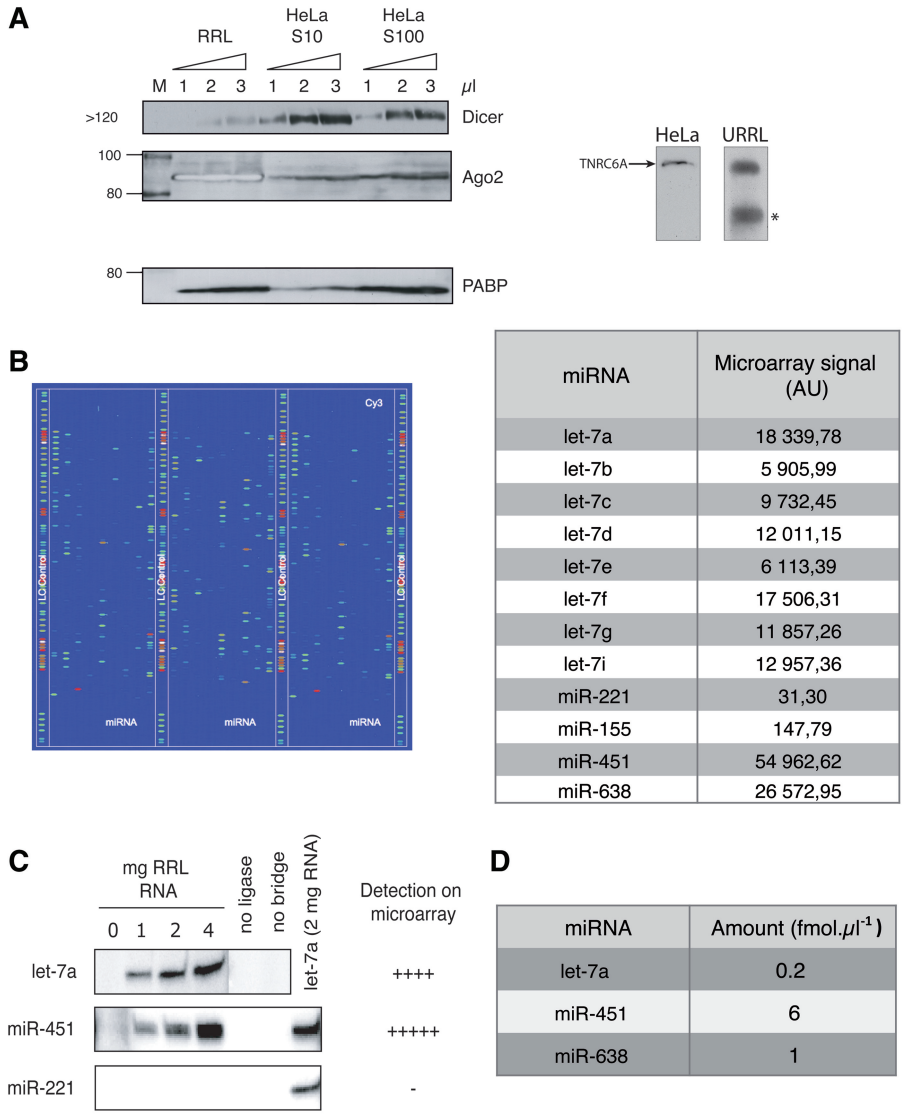

miRNA	Microarray signal (AU)
let-7a	18 339,78
let-7b	5 905,99
let-7c	9 732,45
let-7d	12 011,15
let-7e	6 113,39
let-7f	17 506,31
let-7g	11 857,26
let-7i	12 957,36
miR-221	31,30
miR-155	147,79
miR-451	54 962,62
miR-638	26 572,95

miRNA	Amount (fmol.μl^{-1})
let-7a	0.2
miR-451	6
miR-638	1

Figure 1. Rabbit reticulocyte lysate contains RISC components as well as endogenous miRNAs. (**A**) RISC proteins are present in the RRL. 1, 2 or 3 µl of RRL, HeLa cell S10 and S100 lysates were analyzed by western blotting with antibodies specific for Dicer, Ago2 and PABP as a loading control. TNRC6 was immunoprecipitated and analyzed by western blotting using specific antibodies. An asterisk corresponds to a non-specific band observed for TNRC6 in untreated RRL. (**B**) Endogenous miRNAs can be detected in untreated RRL. Total RNAs extracted from untreated RRL were hybridized to a microarray containing probes for most known mammalian miRNAs (LC Sciences). Each colored spot corresponds to an miRNA that is present in RRL; a total of more than 300 different miRNAs were detected. Microarray raw data signal is presented for let7, miR-221, miR-155, miR-451 and miR-638 (full data can be found in Supplementary Table S1). (**C**) Splinted ligation assays against let-7, miR-451 and miR-221 were carried out using increasing amounts of total RNA to validate microarray results. miRNAs not identified by microarray, such as miR-221, were not detected by splinted ligation. (**D**) Quantification of miRNAs present in untreated RRL. Quantitative PCR was carried out using specific primers against let-7, miR-451 and miR-638.

proportional to the amount of RRL RNA analyzed, whereas no endogenous miR-221 could be detected (Figure 1C).

Finally, by using quantitative PCR, the amounts of endogenous miR-451, let-7a and miR-638 were quantified and the results are summarized in Figure 1D. This gave an estimated concentration of 0.2, 6 and 1 fmol per microliter of lysate for let-7a, miR-451 and miR-638, respectively. Interestingly, these concentrations of endogenous miRNAs remained essentially similar between different batches of lysate obtained from different rabbits (data not shown).

Taken together, these results show that the untreated RRL contains all the components required to recapitulate a miRNA response.

Endogenous miRNAs are functional and can trigger both a mi- and si- RNA response on target mRNAs

In order to test the effects of endogenous miRNAs on gene expression, different reporter constructs containing the beta globin 5′UTR driving translation of the Renilla luciferase open reading frame (ORF) and followed by four to six (depending on the construct) target sites for miR-451 in their 3′UTR were designed (Figure 2A).

Downloaded from https://academic.oup.com/nar/article-abstract/39/12/5215/2411295 by guest on 08 May 2020

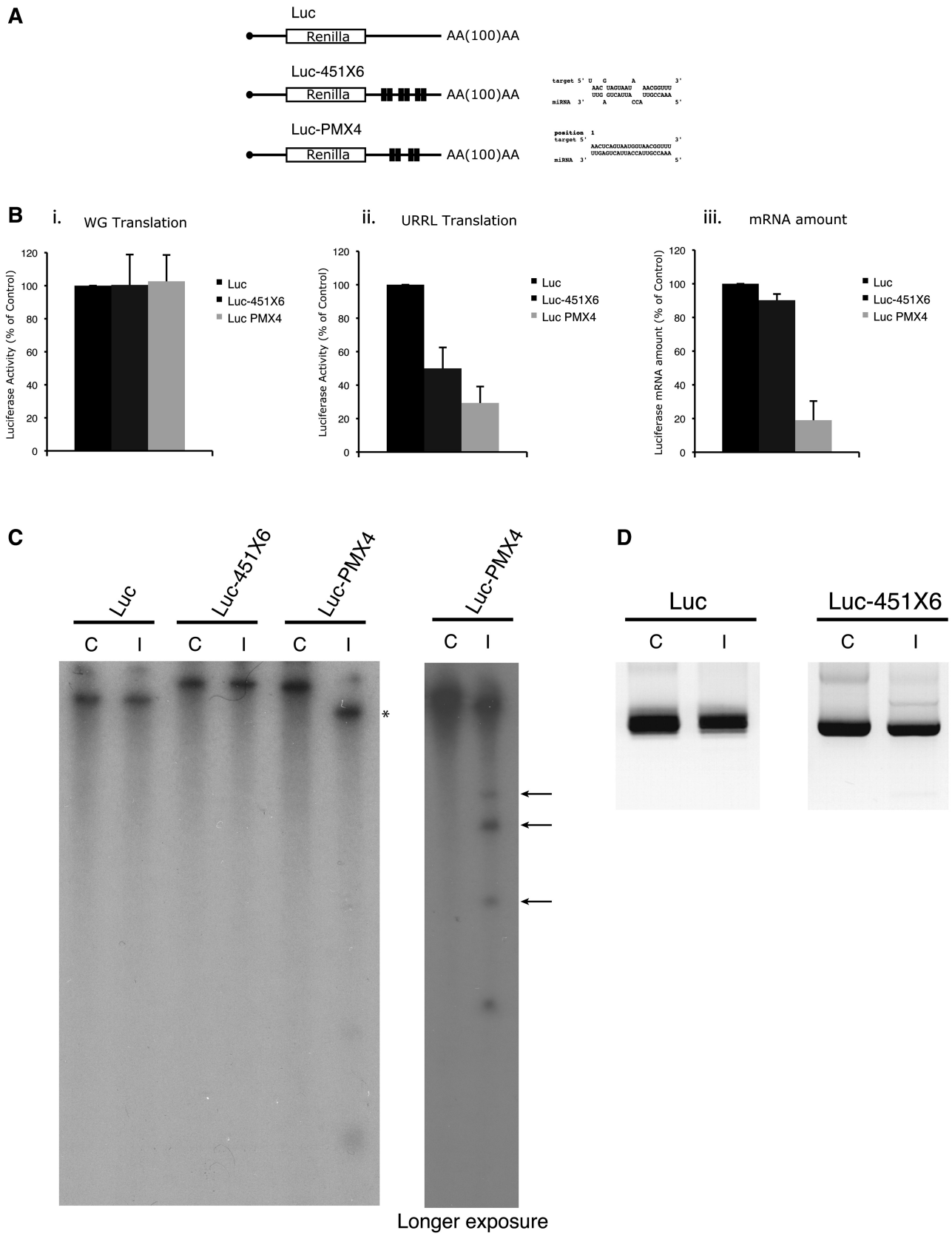

Figure 2. Endogenous miRNAs are fully functional for si- and miRNA regulation of gene expression. (**A**) Schematic representation of the reporter RNAs used in this study. The renilla luciferase reporter gene (designated Luc) is driven by the human β-globin 5′UTR in which six miRNA bulged target sites for miR-451 (Luc-451X6) or four perfectly complementary target sites for miR-451 (Luc PMX4) were designed in the 3′UTR of the reporter gene as indicated in the figure. Target mRNA/miRNA interaction schemes were obtained using the RNA hybrid software (72). (**B**) Endogenous miRNAs are able to

(continued)

Downloaded from https://academic.oup.com/nar/article-abstract/39/12/5215/2411295 by guest on 08 May 2020

Two types of target site were created: (i) the first corresponds to a miRNA target with full complementarity to the seed in the 5′ end of the miRNA followed by a bulge and partial complementarity to the target RNA in the 3′end (named Luc-451X6 in Figure 2A) and (ii) the second is an siRNA target with full complementarity between the miRNA and the target RNA (named Luc PMX4 in Figure 2A). As a control, a luciferase construct containing no target site was used (Luc) (Figure 2A). The ability of miR-451 to bind to the target sites was first verified by annealing mature miR-451 to each of the three RNAs described above; a band shift can be observed when both the miR-451 sites together with the miR-451 oligos were added (Supplementary Figure S3). Capped and polyadenylated RNAs were produced by *in vitro* transcription and then translated in the untreated RRL. Prior to translation, RNAs were heat-denatured at 65°C for 5 min. This was followed by a 1-h incubation at 10°C in the RRL to allow annealing of endogenous miR-451 and finally the reactions were incubated at 30°C for 30 min so that translation could occur. As a control, the RNAs were translated under the same experimental conditions in wheat germ extract as this system does not contain endogenous miR-451 (53). As shown in Figure 2B (panel i), translation efficiency in the wheat germ extract was virtually the same for the three mRNAs, indicating that the presence of target sites on the 3′ UTR does not affect translation in the absence of complementary endogenous miR-451. However, protein synthesis in untreated rabbit reticulocyte lysate (panel ii) resulted in a 2-fold inhibition of luciferase expression from the Luc-451X6 RNA and a 3-fold inhibition for Luc PMX4 compared to the control RNA containing no target sites (Luc). To avoid any non-specific effect the binding of the endogenous miRNAs to target mRNAs could have on overall translation, we also tested the levels of phosphorylated-eIF2α after translation of both Luc and Luc-451X6 mRNAs. It is important to note that we did not detect any difference of phosphorylated-eIF2α levels between Luc and Luc-451X6 samples after translation (data not shown), strongly suggesting that translational inhibition of Luc-451X6 did not depend on activation of the PKR pathway. Interestingly, when RNA levels were measured by quantitative-PCR after translation, we could not detect any significant difference between Luc and Luc-451X6 (Figure 2B, panel iii), whereas the amount of Luc PMX4 RNA (containing the siRNA target sites) was significantly lower, showing that RNA degradation had taken place. These data suggest that both an siRNA- and miRNA-mediated response can be observed in the RRL from endogenous miRNAs. Furthermore, similar results were also obtained using mRNAs containing target sites for let-7a (Supplementary Figure S4), thus indicating that multiple endogenous miRNAs are functional in the untreated RRL.

Recent data have indicated that miRNA hybridization could cause specific deadenylation of the transcript and this could be partly responsible for translation repression (28). Thus, we have monitored the integrity of target mRNAs after translation in the RRL. For this, radiolabeled Luc, Luc-451X6 and Luc PMX4 RNAs were extracted at the end of the translation reaction and subjected to PAGE on a 4% UREA-denaturing gel. It is important to note that such an approach allowed us to differentiate between the polyadenylated and non-polyadenylated forms of the target mRNAs as presented in Supplementary Figure S5. As shown on Figure 2C, no size difference could be observed for Luc and Luc-451X6 mRNAs before, and after translation (Figure 2C, Luc-451X6 lanes C and I), suggesting that no deadenylation had occurred during the period of incubation. This result was further confirmed by using a higher resolution PCR-based approach (see 'Materials and Methods' section) to specifically analyze the length of the poly(A) tail. Once again, this showed no difference whatsoever in poly(A) tail length before and after translation for Luc and Luc-451X6 mRNAs (Figure 2D). Interestingly, this was clearly not the case for Luc PMX4 RNA (containing siRNA target sites) which migrated at a lower molecular size following incubation in the RRL, suggesting that RNA degradation had taken place (Figure 2C, Luc PMX4 lanes C and I). It is noteworthy that hybridization of the miR-451 to the target PMX4 yielded a discrete band rather than a smear, suggesting that the RNA was cleaved at the sites of interaction with the miRNA (Figure 2C, see asterisks). This was confirmed by running the samples for a shorter time and exposing the film for longer to reveal the presence of three radiolabeled RNA fragments of smaller size (Figure 2C, see longer exposure; see arrows) that might correspond to the 3′ end of the target RNA cleaved at each of the four miR-451 target sites.

Taken together, these data indicate that endogenous rabbit reticulocyte miRNAs are functional and can control gene expression at the level of translation (miRNA response) or RNA degradation (siRNA response). Moreover, under our experimental conditions, translation inhibition observed upon miRNA association is not due to the deadenylation of the RNA target transcript.

Figure 2. Continued
downregulate translation and stability of targeted mRNAs. Translation of 0.46 fmol of Luc (black bars), Luc-451X6 (dark gray bars) and Luc PMX4 (light gray bars) was carried out for 30 min in wheat germ extract (panel i) and untreated RRL (panel ii) showing a downregulation of Luc-451X6 and Luc PMX4 expression only in untreated RRL in which miR-451 is present. Stability of mRNAs in untreated RRL was monitored after translation by quantitative PCR (panel iii). Error bars correspond to the standard deviation calculated from three independent experiments. (**C**) Integrity of targeted mRNAs after translation in untreated RRL. Radiolabeled Luc, Luc-451X6 and Luc PMX4 mRNAs were analyzed on a denaturing polyacrylamide gel (left) before (Control lane: C) or after translation (Incubated lane: I). The right panel corresponds to the same samples from the left panel, ran for a shorter time and exposed for a longer period; asterisks indicate the 5′ cleavage product of the Luc PMX4 mRNA; arrows indicate potential Luc PMX4 target site fragments obtained after RISC-mediated cleavage of the mRNA. (**D**) Determination of the variations in the length of the poly(A) tail for Luc and Luc-451X6 constructs before and after translation by using a PCR-based approach (see 'Materials and Methods' section).

Downloaded from https://academic.oup.com/nar/article-abstract/39/12/5215/2411295 by guest on 08 May 2020

Translation inhibition occurs rapidly and can be inhibited by addition of anti miR-451 oligonucleotides

Kinetic studies of miRNA-mediated repression were then carried out in the RRL to monitor the translation rates at different time points from 0 to 90 min. As shown in Figure 3A, a 30% decrease in translational efficiency was observed as early as 20 min after the start of incubation. Interestingly, translation repression increased with time to reach a maximum of 55% after 90 min of incubation with no significant degradation of Luc-451X6 transcripts (data not shown). This indicates that assembly of the RISC complex and the resulting miRNA-mediated translation inhibition takes place rapidly in the RRL system.

In order to test the specificity of endogenous miR-451 to mediate translational repression, 2′-*O*-methyl modified antisense oligoribonucleotides were used (Figure 3B). These oligonucleotides can specifically interact with endogenous miR-451 to preclude it from being incorporated into the RISC complex and/or to interact with its mRNA target sequence (54). The modified oligonucleotides were added before the pre-incubation of the mRNAs in the RRL and translation was monitored at 30, 60, 90 and 120 min. As a control, an antisense oligonucleotide complementary to let-7a was also used in a parallel incubation. As observed in Figure 3B, translation of the RNA construct containing the miR451 sites (Luc-451X6) was inhibited compared to the control Luc mRNA. However, addition of the antisense oligonucleotide directed against endogenous miR-451 abolished this inhibition and restored Luc-451X6 translation to levels similar to that of the control RNA. This was observed at early and later times, even when translation was strongly repressed in the absence of the antisense oligonucleotide (Figure 3B, see 90 and 120 min). The specificity of this effect was demonstrated by the fact that an antisense oligonucleotide not specific to miR451 (directed against let-7a) could not relieve translation repression of Luc-451X6 mRNA (Figure 3B).

Finally, in order to test for the specificity of the interaction between miR-451 and its target site, a new target motif was designed (Luc-451MutX6) which has several mutations in the seed region (Figure 3C). The corresponding *in vitro* synthesized capped and polyadenylated Luc, Luc-451X6 and Luc-451MutX6 RNAs were translated in wheat germ extract and the RRL. As shown previously (Figure 2), no difference could be observed in the translation efficiency of these three constructs in the wheat germ extract (Figure 3C, panel i). However, the RNA containing mutations in the seed region was no longer repressed in the RRL system (Figure 3C, panel ii, compare Luc-451MutX6 with Luc-451X6) confirming the importance of the seed match in the miRNA response. Analysis of the RNA level by quantitative real time (RT)-PCR did not show any significant difference between the three constructs indicating that the effect was not due to RNA degradation (Figure 3C, panel iii).

Translational repression shows a target site additive effect and can be saturated by high amounts of RNA

Target site cooperation was shown to improve miRNA translational repression in various cultured cell lines (55–57). Therefore, luciferase RNAs containing two, four or six target sites for miR-451 in their 3′UTR were designed, transcribed and translated in the untreated RRL. As seen in Figure 4A, translation of an RNA bearing only two target sites for miR-451 was reduced by only 20% compared to the control RNA. However, translation of the same RNA in which four target motifs have been inserted was inhibited by 40% compared to the control RNA, but the addition of two additional miR-451 sites did not further repress translation. These data show that instead of cooperation, increasing the number of target sites exerts an additive repressive effect on the target mRNA up to a certain level after which the miRNA response cannot be improved.

To further investigate this issue, we have varied the concentration of exogenous mRNA added to the RRL. The standard experimental conditions that have been tested so far correspond to a ratio of 260 molecules of endogenous miRNA per one molecule of luciferase Luc-451X6 mRNA (corresponding to 0.46 fmol of target mRNA); thus the final ratio is 43 miRNA molecules per target site. This was made variable by changing the concentration of exogenous target Luc-451X6 mRNA (Figure 4B). At a 30 to 1 ratio (corresponding to 4.6 fmol of target mRNA), which corresponds to five miRNA molecules per target site, translational repression dropped to 30% compared to the control RNA with no target sites (Figure 4B, see 4.6 fmol). Interestingly, at a ratio of <1 miRNA per target site (corresponding to 46 fmol of target mRNA), no repression at all could be observed (Figure 4B, see 46 fmol). This result suggests that the RISC machinery can be saturated by high amounts of target mRNA.

Internal ribosome entry site-mediated translation is insensitive to miRNAs

Translation initiation mediated by some internal ribosome entry sites (IRES) has been reported to be refractory to miRNA regulation (17,18). Therefore, we tested whether IRES-driven translation could be affected by miRNAs in our system. For this, target sites for miR-451 were inserted in the 3′UTR of constructs coding for the renilla luciferase driven by the encephalomyocarditis (EMCV) and hepatitis C virus (HCV) IRESes. EMCV and HCV IRES were chosen because of their different requirement for initiation factors; EMCV requires the entire set of initiation factors with the exception of eIF4E (58), whereas HCV can bypass the need for all eIF4 initiation factors (59). These constructs were used to produce uncapped and polyadenylated EMCV RNAs (–/+), and uncapped non-polyadenylated HCV RNAs (–/–) as found in native virions. Untreated RRL was then programmed with these constructs together with a capped and polyadenylated β-Globin RNA control (Figure 5A).

As observed (Figure 5B), translation driven by the HCV IRESes in the untreated RRL was not inhibited at all by the binding of miR-451. Interestingly, translation of the

Downloaded from https://academic.oup.com/nar/article-abstract/39/12/5215/2411295 by guest on 08 May 2020

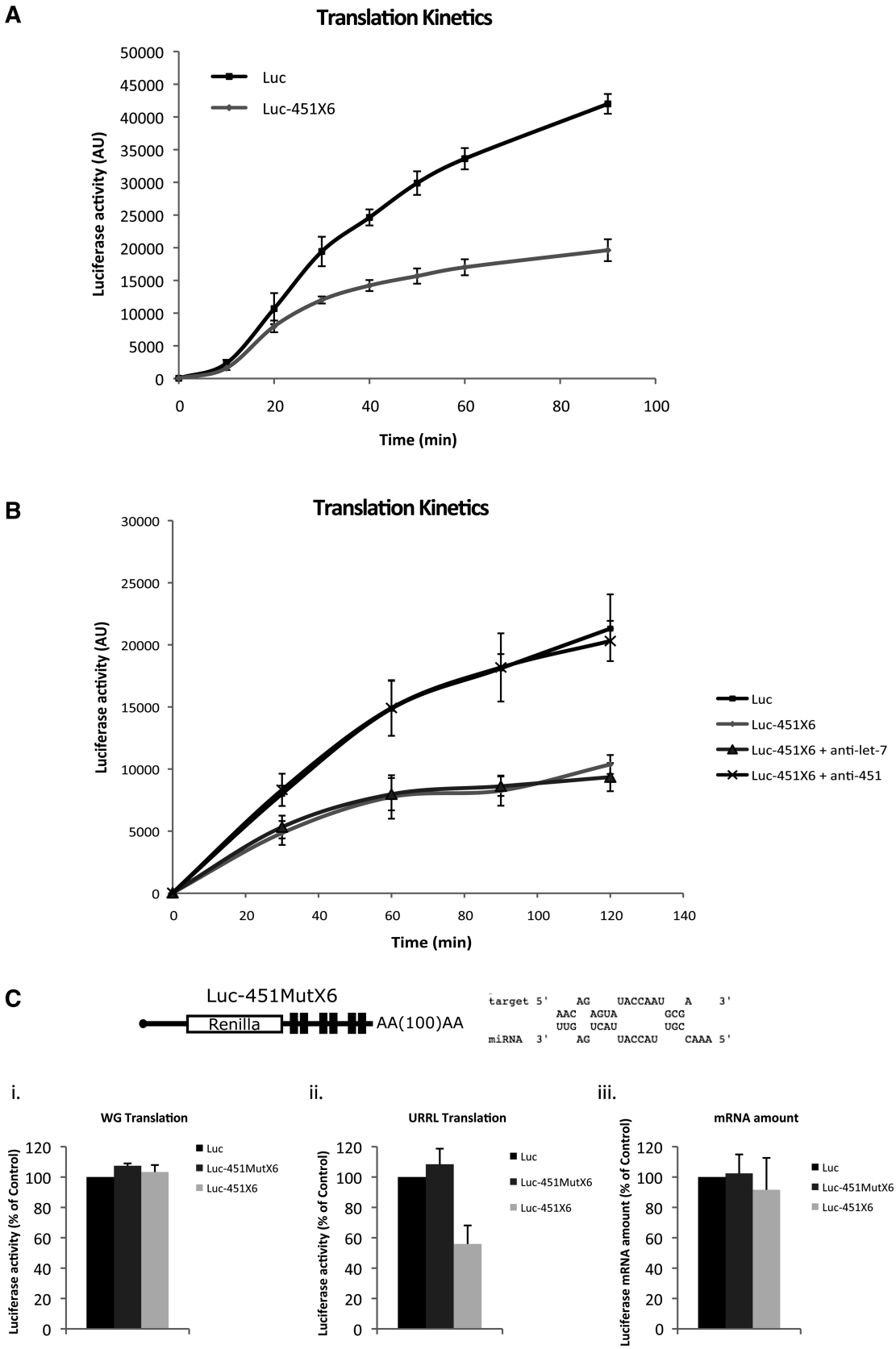

Figure 3. Translational repression mediated by endogenous miRNAs occurs rapidly and is specific to both the target site and the miRNA. (**A**) Translation kinetics of Luc and Luc-451X6 mRNAs was performed at different time points: 0, 10, 20, 30, 40, 50, 60 and 90 min after the beginning of translation in the untreated RRL. Error bars correspond to the standard deviation calculated from three independent experiments. (**B**) Translational repression mediated by miR-451 was counteracted by the addition of a specific antisense oligonucleotide. Translation of Luc and

(continued)

Downloaded from https://academic.oup.com/nar/article-abstract/39/12/5215/2411295 by guest on 08 May 2020

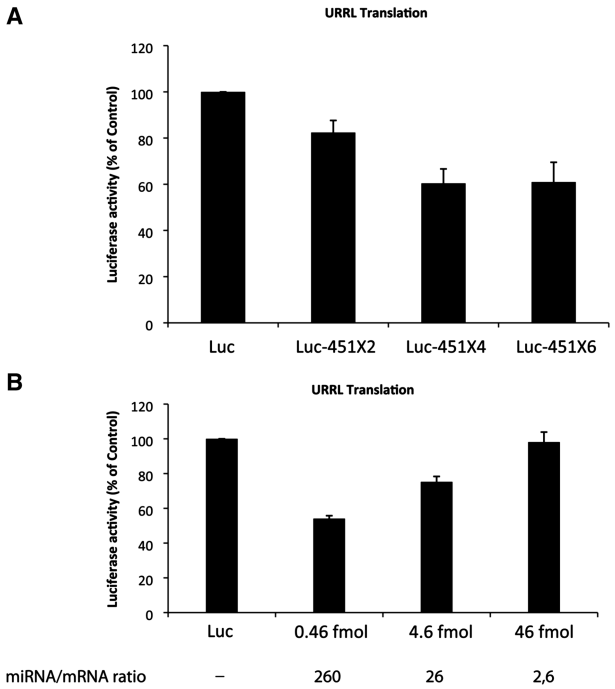

Figure 4. Translational repression mediated by miR-451 can be saturated by high amounts of mRNAs and shows target site additive repression. (**A**) Target site additive effect improves translational repression. Untreated RRL was programmed with Luc and Luc-451 bearing 2, 4 or 6 target sites mRNAs (designated, Luc-451X2, X4 and X6) and luciferase activity was measured 30 min after the beginning of translation. Error bars correspond to the standard deviation calculated from three independent experiments. (**B**) Untreated RRL was programmed with 0.46, 4.6 or 46 fmol of Luc and Luc-451X6 mRNAs and luciferase activity with Luc-451X6 was measured as a percentage of that observed with the same concentration of Luc mRNA after 30 min of translation. The molar ratio of miR-451 to the target mRNA is indicated on the bottom of the figure. Error bars correspond to the standard deviation calculated from three independent experiments.

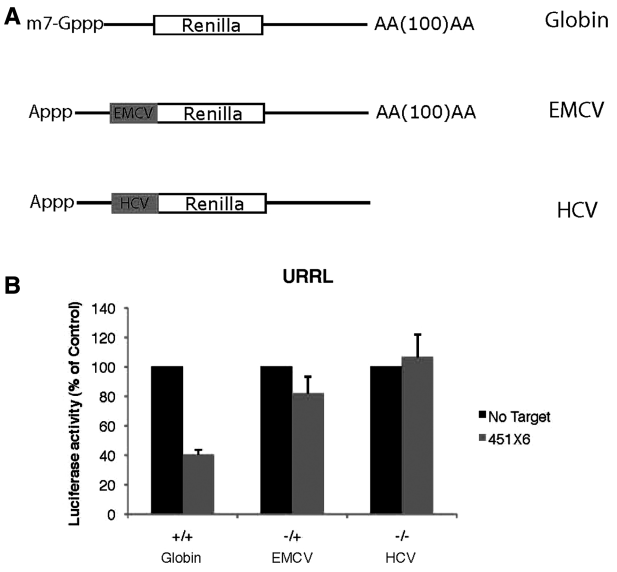

Figure 5. Translation mediated by internal ribosome entry sites is refractory to miRNA-mediated regulation. (**A**) Schematic representation of target RNAs used in this experiment: 'Globin' corresponds to a capped and polyadenylated luciferase coding RNA driven by the human β-Globin 5′UTR, 'EMCV' corresponds to an uncapped (A-capped) and polyadenylated RNA driven by the EMCV IRES, 'HCV' corresponds to an uncapped and non-polyadenylated RNA driven by the HCV IRES. (**B**) Translation of 0.46 fmol of Globin, EMCV and HCV RNAs bearing no target sites (No Target, black bars) or 6 target-sites for miR-451 (451X6, gray bars), was carried out in untreated RRL for 60 min. Error bars correspond to the standard deviation calculated from three independent experiments.

EMCV RNA showed only a slight inhibition (18% of the control) (Figure 5B).

This suggests that translation initiation mediated by IRES elements is resistant to miRNA repression and, above all, strongly argues that translational repression mediated by miRNAs occurs at the level of translation initiation.

Specific siRNA activity, but not translational repression, occurs in the nuclease-treated RRL

RRL is generally treated with micrococcal nuclease in order to degrade endogenous mRNAs and to allow the study of translation of a single exogenous mRNA species. Since endogenous miRNAs are thought to be incorporated into RISC, they should be protected against the micrococcal nuclease treatment. To verify this, we performed quantitative PCR against different miRNAs previously described in the untreated RRL. Interestingly, the amounts of endogenous miRNAs were almost identical between untreated and nuclease-treated RRL (compare Figure 6A with Figure 1D), indicating that either mature miRNAs are too small to be degraded by the micrococcal nuclease or that they are protected by the RISC proteins. As nuclease-treated RRL contains endogenous miRNAs at levels similar to those of the untreated RRL (Figure 6A), it was of interest to compare their activity. For this, nuclease-treated RRL as well as wheat germ extract were programmed with 0.46 fmol of Luc, Luc-451X6 and Luc PMX4 mRNAs (Figure 6B). As expected, translation in the wheat germ extract yielded no significant differences between translation rates of each mRNA (Figure 6B, left). Surprisingly, in the nuclease-treated RRL, which does not contain any endogenous mRNA, we only detected a weak inhibition (15% compared to Control) of

Figure 3. Continued
Luc-451X6 mRNAs was programmed in the untreated RRL after addition of oligonucleotides complementary to either let-7 or miR-451. Luciferase activity was measured at different time points: 0, 30, 60, 90 and 120 min after the beginning of translation. Error bars correspond to the standard deviation calculated from three independent experiments. (**C**) Translational repression mediated by miR-451 is specific for the target site. Six target sites for miR-451 with a mutated seed region were inserted in the 3′UTR of the Luc construct (Luc-451X6Mut, dark gray bars) and translation of this mRNA was compared to that of Luc (black bars) and Luc-451X6 (light gray bars) in wheat germ extract (panel i) and untreated RRL (panel ii). The relative stability of mRNAs in untreated RRL was monitored after translation by quantitative PCR and are represented as 'mRNA amount' (panel iii). Error bars correspond to the standard deviation calculated from three independent experiments.

Downloaded from https://academic.oup.com/nar/article-abstract/39/12/5215/2411295 by guest on 08 May 2020

A

miRNA	Amount (fmol.μl^{-1})
let-7a	0.2
miR-451	4.5
miR-638	1.2

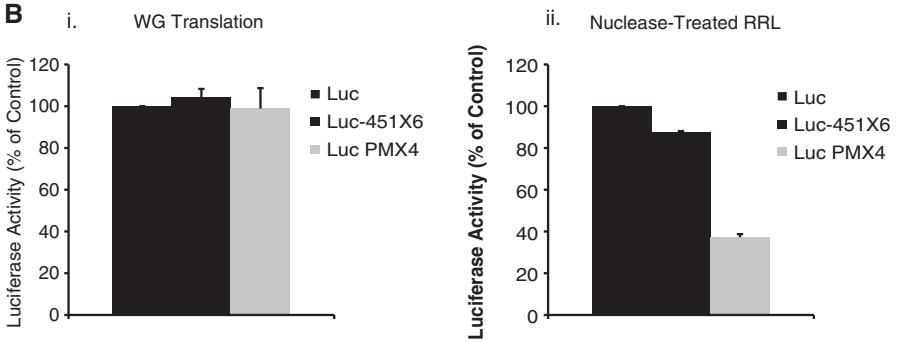

Figure 6. Specific siRNA activity, but not translational repression, occurs in the nuclease-treated RRL. (**A**) Quantification of miRNAs present in nuclease-treated RRL. Quantitative PCR was carried out using specific primers against let-7, miR-451 and miR-638. (**B**) Translation of 0.46 fmol of Luc (black bars), Luc-451X6 (dark gray bars) and Luc PMX4 (light gray bars) was carried out for 30 min in wheat germ extract and nuclease-treated RRL. Error bars correspond to the standard deviation calculated from three independent experiments.

Luc-451X6 mRNA (Figure 6B, right). However, Luc PMX4 expression was still strongly impaired to a level of inhibition similar to that previously observed in the untreated RRL (70% compared to Control, Figure 6B, right). These results indicate that endogenous miRNAs contained in the nuclease treated RRL can still recapitulate an siRNA response but are unable to mediate inhibition of translation by an miRNA mechanism.

The miRNA response in nuclease-treated RRL can be restored by poly(A) tail containing RNAs

Nuclease-treated RRL has been shown to be poorly cap and poly(A) dependent for translation as opposed to crude RRL (38). One of the reasons for this lack of cap/poly(A) synergy could be the lack of competition with endogenous mRNAs. This could also be responsible for the absence of an miRNA response in the nuclease-treated RRL. To test this hypothesis, we have monitored translation of Luc and Luc-451X6 mRNAs in the presence of a 10^4-fold excess of competitor mRNAs. For this, 5 pmol of *in vitro* transcribed capped and polyadenylated competitor (+/+), capped/non-polyadenylated (+/–), uncapped/polyadenylated (–/+) and uncapped/non-polyadenylated (–/–), mRNAs (containing the β-globin 5′UTR followed by the firefly luciferase coding sequence) were added to each translation reaction before the addition of Luc or Luc-451X6 mRNAs. As shown in Figure 7, addition of these competitor RNAs led to an inhibition of both Luc and Luc-451X6 translation, with the capped and polyadenylated (+/+) having the biggest effect (Figure 7, top panel see lane +/+). Interestingly, an efficient miRNA response could only be restored upon addition of competitor mRNAs that contained a poly(A) tail whereas addition of non-polyadenylated mRNAs only had a marginal effect on miRNA activity (Figure 7, compare +/– and –/– lanes with the non-competitor lane). Interestingly, a potent miRNA activity in nuclease-treated RRL could be restored by the addition of poly(A) containing transcripts independently of the presence of a cap structure at their 5′end (Figure 7, bottom panel compare +/+ and –/+ and +/– lanes with no competitor lane). This suggests that only the presence of the poly(A) tail is required to restore miRNA-mediated translational repression in the nuclease-treated lysate. However, it could be argued that the presence of the poly(A) tail could restore a miRNA activity because of the fact that poly(A) containing transcripts are better translated than non-poly(A) containing RNAs. Thus, the effects observed would only be the consequence of an increased competition for ribosomes.

Free poly(A) RNA is sufficient to restore a microRNA response in nuclease-treated RRL

In order to investigate this effect further, we have added uncapped and non-polyadenylated mRNAs driven by the HCV and cricket paralysis virus (CrPV) IRES to nuclease-treated lysates prior to translation. Indeed, these two viral RNAs are able to recruit ribosomes very efficiently on their IRES sequence with no need for a cap structure and a poly(A) tail (see Supplementary Figure S6A for relative translational efficiencies of each competitor RNA tested). As observed, addition of 5 pmol of HCV and CrPV competing mRNAs failed to restore a potent miRNA activity (Figure 8A, compare RRL to HCV and CrPV lanes). These results indicate that the competition for ribosomes is not the major cause of inhibition

Downloaded from https://academic.oup.com/nar/article-abstract/39/12/5215/2411295 by guest on 08 May 2020

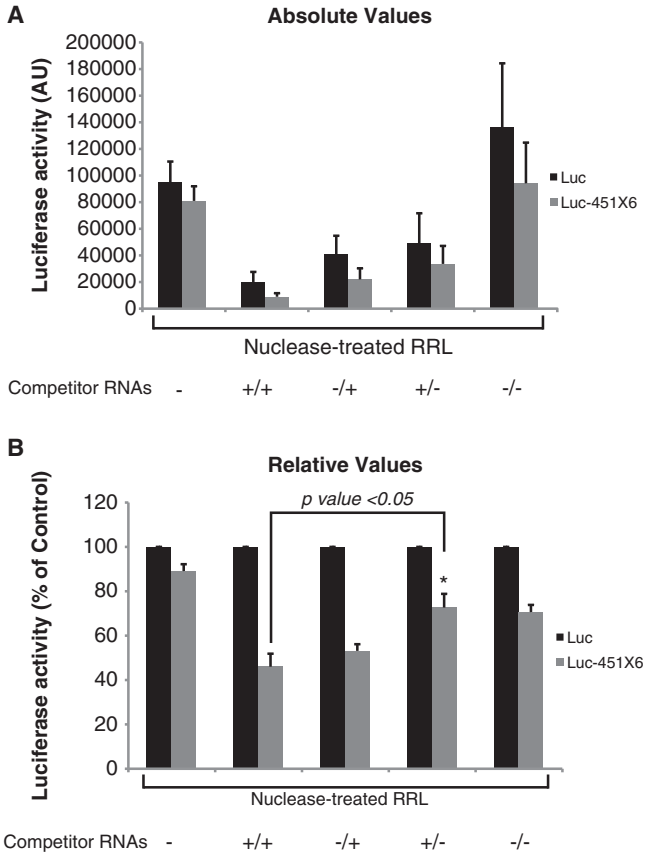

Figure 7. Polyadenylated competitor mRNAs restore a strong miRNA activity in the nuclease-treated RRL. Translation of 0.46 fmol of Luc (black bars), and Luc-451X6 (gray bars) was carried out for 60 min in untreated RRL (URRL) or nuclease-treated RRL alone (RRL) or in the presence of 5 pmol of capped/polyadenylated firefly luciferase competitor mRNAs (+/+), uncapped/polyadenylated (–/+), capped/non-polyadenylated (+/–) and uncapped/non-polyadenylated mRNAs (–/–). Total renilla luciferase activity (**A**) as well as luciferase activity normalized against Luc expression (**B**) are presented. Statistical significance [Luc-451X6 (+/+) versus Luc-451X6 (+/–)] was calculated using the paired Student's *t*-test; $*P < 0.05$. Error bars corresponds to three independent experiments.

mediated by miRNAs, therefore suggesting a specific role for the poly(A) tail.

In order to investigate this further, we performed similar experiments using free cap analog or free poly(A) as competitors (Figure 8B). As free poly(A) was shown to stimulate PABP activity both in plants and mammals (60,61), we tested whether free poly(A) could also modulate miRNA activity. For this, exogenous free poly(A) (400 nt in average length) was added to the translation reaction in the same molar amount to that of the previous experiments using competitor mRNAs. As observed, addition of free poly(A) to the nuclease-treated RRL restored miRNA activity (by 60%) to a level of magnitude close to that observed in crude RRL (Figure 8B compare the URRL and poly(A) lanes). To rule out any effect of the 5′ cap, we also added free cap-analog alone or in the presence of free poly(A) (Figure 8B, see Cap analog lane). As observed, addition of free cap analog to the nuclease-treated RRL, could not restore the miRNA activity in the nuclease-treated RRL even though the overall level of global translation efficiency was significantly affected (Figure 8B, see lane Cap analog). Furthermore, the addition of both free cap analog and free poly(A), although leading to a strong translational inhibition of both Luc and Luc-451X6 mRNAs, did not further increase miRNA activity compared to free poly(A) alone [Figure 8B, compare the poly(A) lane to Cap analog + poly(A)]. Interestingly, we could observe a dose-dependent effect of the addition of free poly(A) RNA in restoring a miRNA repression in nuclease-treated RRL (Supplementary Figure S6B). However, this dose-dependent effect was observed within a narrow range (<2-fold increase) of poly(A) RNA (Supplementary Figure S6B).

Because IRES-mediated translation appeared to be refractory to translational repression mediated by miRNAs in untreated RRL, we tested whether this was also the case in RRL upon addition of free poly(A) RNA. For this, capped and polyadenylated Globin RNAs, uncapped and polyadenylated EMCV RNAs (–/+), and uncapped non-polyadenylated HCV RNAs (–/–), containing miR-451 target-sites (451X6) or not (No target), were programmed in RRL (Figure 8C, left). As expected, translation of all these RNAs (including Globin) was not regulated by endogenous miR-451 (Figure 8C, left). However, upon addition of free poly(A) RNA, translation of Globin-451X6 RNA was downregulated by 2-fold compared to the Globin RNA bearing no miRNA target sites (Figure 8C, right). Interestingly, translation of EMCV and HCV RNAs was still insensitive to miRNA-mediated repression even in the presence of free poly(A) RNA. This result suggests that the effect of free-poly(A) in stimulating miRNA activity is only exerted on cap-dependent translation.

Free poly(A) restores translational repression on a non-polyadenylated target RNA in a *trans* fashion

Due to the effect of the poly(A) RNA addition for efficient miRNA repression, we next wondered whether poly(A) tail removal from target RNAs could also affect repression. For this, untreated RRL was programmed with capped and polyadenylated (+/+) and capped and non-polyadenylated (+/–) Luc and Luc-451X6 mRNAs (Figure 9A). As observed, removal of the poly(A) tail from the target mRNA resulted in an attenuated miRNA-mediated repression, which dropped to 25% of the control RNA (i.e. bearing no target sites) (Figure 9B). Interestingly, translation of non-polyadenylated Luc-451X6 RNAs in the nuclease treated RRL was not inhibited but rather moderately stimulated (40%) by miR-451 (Figure 9C, left). However, upon addition of free poly(A) RNA to nuclease-treated RRL, translational repression was restored both for capped and polyadenylated Luc-451X6 RNAs (65% compared to the control) and also for capped and non-polyadenylated Luc-451X6 RNAs (51% compared to the control) (Figure 9C, right).

Downloaded from https://academic.oup.com/nar/article-abstract/39/12/5215/2411295 by guest on 08 May 2020

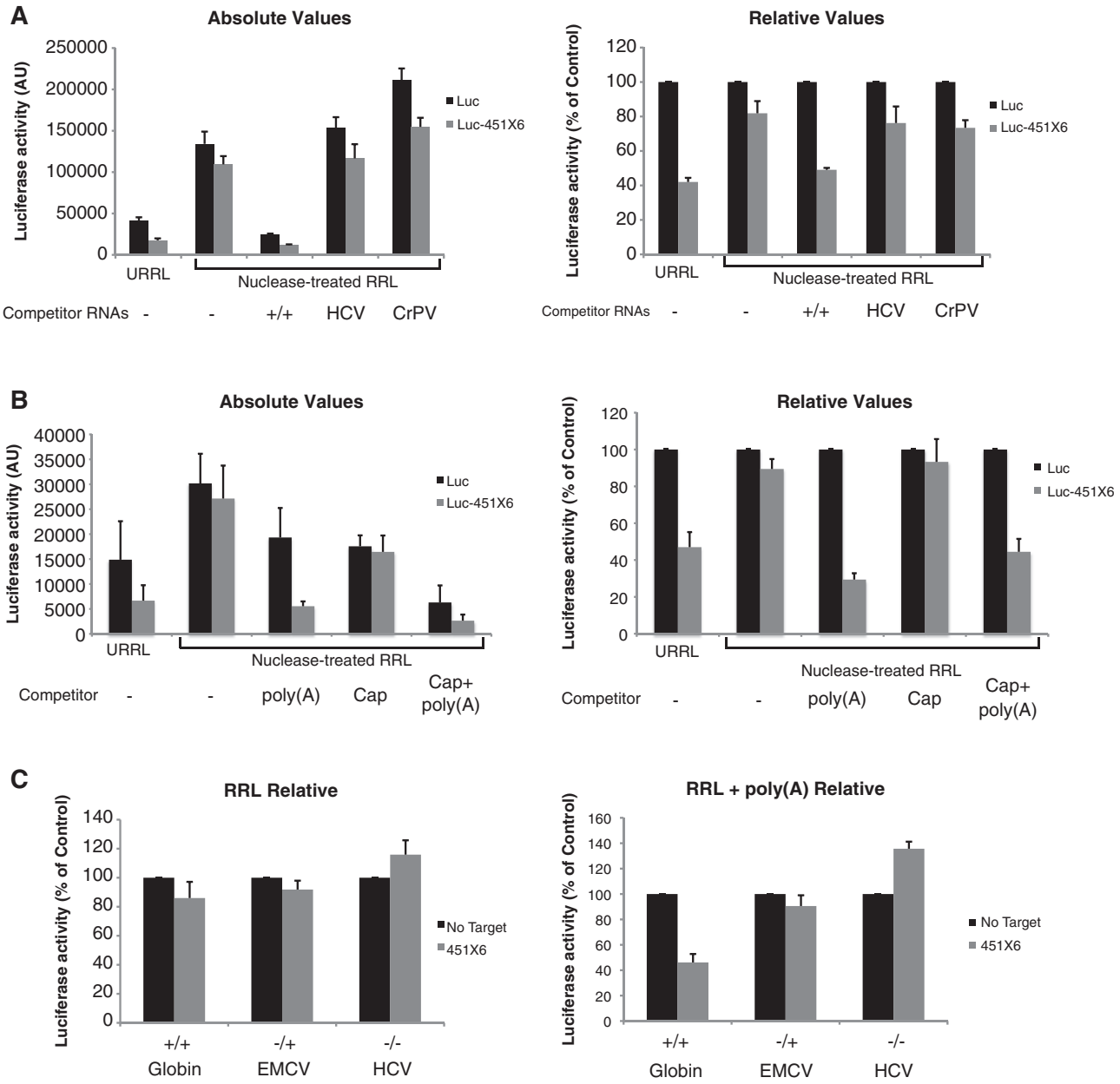

Figure 8. Free poly(A) RNA is sufficient to restore a microRNA response in nuclease-treated RRL. (**A**) Translation of 0.46 fmol of Luc (black bars), and Luc-451X6 (gray bars) was carried out for 60 min in untreated RRL (URRL) or nuclease-treated RRL alone (RRL) or in the presence of 5 pmol of capped/polyadenylated Firefly-coding competitor mRNAs under control of the β-globin 5′UTR (+/+) or uncapped/non-polyadenylated mRNAs under the control of the HCV and CrPV IRESes. (**B**) Translation of 0.46 fmol of Luc (black bars), and Luc-451X6 (gray bars) was carried out for 1 h in untreated RRL (URRL) or nuclease-treated RRL alone (RRL) or in the presence of 1.2 pmol of free poly(A) [poly(A)] (GE Healthcare), 27 μM of free cap analog (Cap analog) (New England Biolabs) or 1.2 pmol of free poly(A) together with 27 μM of cap analog [Cap analog + poly(A)]. Total luciferase activity (left panel) as well as luciferase activity normalized against Luc expression (right panel) are presented. (**C**) Translation of 0.46 fmol of Globin, EMCV and HCV RNAs bearing no target sites (No Target, black bars) or 6 target-sites for miR-451 (451X6, gray bars), was carried out in RRL (left panel) and RRL in the presence of free poly(A) RNA (right panel) for 60 min. Error bars correspond to three independent experiments.

Taken together, these results suggest that the poly(A) tail is required whether in *cis* or in *trans* to achieve efficient repression mediated by miRNAs.

DISCUSSION

Despite an extensive amount of work, the molecular mechanism by which miRNAs control translation remains elusive. Based on experiments and results obtained using different systems, some reports describe translational repression at the initiation and post-initiation steps, linked in some cases to the deadenylation of the target mRNA which contributes to translational repression, while others reports a rapid degradation of the target mRNAs or even co-translational proteolysis of the nascent polypeptide (9,16–34). *In vitro* translation

Downloaded from https://academic.oup.com/nar/article-abstract/39/12/5215/2411295 by guest on 08 May 2020

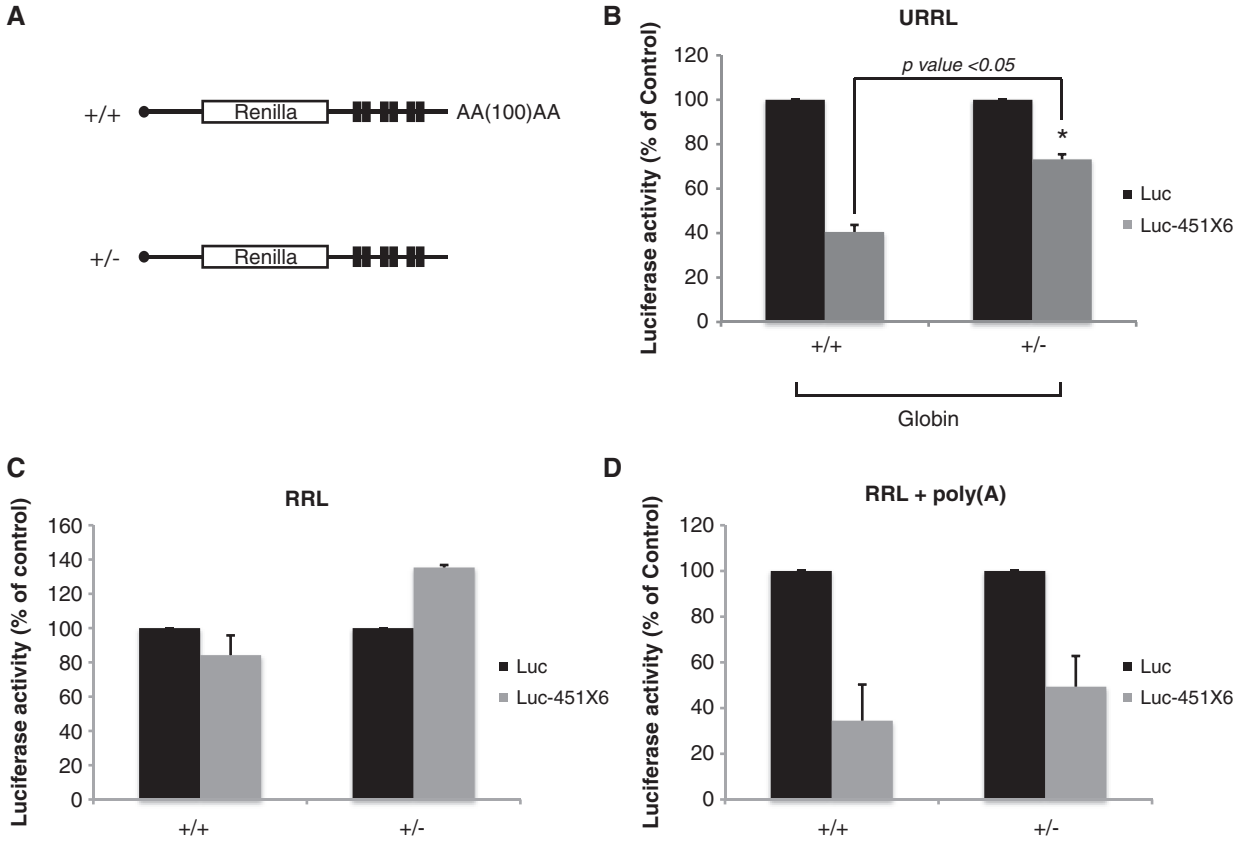

Figure 9. Free poly(A) restores translational repression of a non-polyadenylated target RNA *in trans*. (**A**) Schematic representation of the RNAs used in this experiment corresponding to the Luc and Luc-451X6 RNAs that are capped and polyadenylated (+/+) or capped and non-polyadenylated (+/–). (**B**) Translation of 0.46 fmol of capped/ polyadenylated and capped/non-polyadenylated Luc (black bars), and Luc-451X6 (gray bars) RNAs in untreated RRL for 60 min. Statistical significance (Luc-451X6 +/+ versus Luc-451X6 +/–) was calculated using the paired Student's *t*-test; $*P < 0.05$. (**C**) Translation of the same RNAs was carried out in nuclease-treated RRL (left panel) and in nuclease-treated RRL in the presence of 1.2 pmol of free poly(A) RNA (right panel). Error bars correspond to three independent experiments.

systems have been instrumental for the study of translational regulation as they allow the control of many parameters that are important in protein synthesis such as mRNA amount, salt conditions, initiation factor concentrations, time of incubation and mRNA degradation. The most commonly used *in vitro* system is the RRL, which was conceived and developed about 30 years ago and has been widely used since (47). Recently, Novina and colleagues (20,21) have developed an interesting approach to study miRNAs in the nuclease-treated RRL. However a major drawback comes from the fact that the nuclease-treated RRL does not recapitulate the cap and poly(A) synergy (35–37), which seems to be a major determinant in the miRNA response. In addition, Novina and colleagues have been using exogenous artificial miRNAs and so this approach does not allow investigation of all aspects of miRNA repression such as pre-miRNA processing, miRNA binding and nucleation of the RISC complex.

Here, we report that the non-nuclease-treated RRL (38) is capable of faithfully recapitulating translational control of gene expression mediated by miRNAs. Importantly, our system exploits the presence of endogenous miRNAs that are found in the rabbit reticulocyte lysate, namely miR-451 that has been recently shown to be implicated in the maturation of erythroid cells (51,52,62,63).

We first showed that the RISC protein components are present in the RRL (Figure 1) and are fully active to process miRNA precursors (Supplementary Figure S1). By western blotting, we detected low levels of Dicer, while Ago2 was highly abundant. Interestingly, processing of pre-miR-451 has been recently shown to occur through a dicer-independent (but Ago2 dependent) pathway (64). This could possibly explain the relatively low abundance of dicer compared to Ago2 (Figure 1A). Finally, we also detected TNR6CA (also known as GW182), which is an important player of the miRNA repression pathway.

We could then show that translational repression of mRNAs targeted by endogenous miRNAs recapitulated all major aspects of miRNA-dependent regulation. Indeed, translation is repressed by about 2-fold (Figure 2) as has been observed not only for natural targets in cultured cells (1,65–69) but also in other *in vitro* cell-free extracts based on insect embryos (26). Importantly, this effect on gene expression is specific to the binding of the miRNA to its target and can be reversed by addition of complementary oligonucleotides and saturating amounts of target mRNAs (Figures 3 and 4). Moreover, regulation of

Downloaded from https://academic.oup.com/nar/article-abstract/39/12/5215/2411295 by guest on 08 May 2020

translation was particularly sensitive to modifications impairing complementarity within the seed region of the miRNA, and showed target site cooperation (Figures 3 and 4). Most importantly, target mRNAs were neither deadenylated nor degraded by the action of the miRNA (Figure 2), and this lack of deadenylation could be explained by the fact that our *in vitro* system allowed us to measure translational activity after only 30 min of incubation. This is particularly interesting as it allows the effects that miRNAs can have on translation to be uncoupled from those on deadenylation and transcript degradation. However, transcript degradation can be reproduced by having full pairing between the miRNA and the mRNA target, which triggers a siRNA response (Figure 2). Interestingly, in a recent report by Fabian and coworkers (39), miRNA-dependent deadenylation was shown to occur 1 h after the beginning of the translation reaction. This could therefore explain our lack of visible deadenylation as we monitor mRNA integrity between 30 and 60 min after the start of translation. Finally, we also show that repression occurs at the level of translation initiation as RNAs under control of the EMCV and HCV IRESes were not repressed by the action of miR-451 (Figure 5).

We have also shown that the nuclease-treated RRL contained the same concentration of endogenous miRNAs as the untreated RRL; yet, we were surprised to find out that these miRNAs were unable to repress translation of a reporter gene in the case of bulged target sites (Figure 6). However, in the case of a perfect match target site, the same endogenous miRNAs fully recapitulated an siRNA effect with the same magnitude as that observed with untreated RRL. In order to understand the reasons of such a discrepancy between the mi- and siRNA mechanisms, we tested several different conditions. Because nuclease-treated RRL lacks endogenous mRNAs, we first reasoned that addition of competitor mRNAs, in similar amount to that of crude RRL, could restore a functional miRNA activity (Figure 7). Interestingly, this showed that only capped/polyadenylated and uncapped/polyadenylated RNAs were able to restore an effective repression mediated by miRNAs in nuclease-treated RRL, with virtually no effect of addition of non-polyadenylated RNAs (Figure 7). This suggested either a role of the poly(A) tail in this effect, or the need for competing RNAs that are efficiently translated.

In order to discriminate between these two possibilities, we have used viral IRESes from HCV and CrPV that are either naturally uncapped and non-polyadenylated (in the case of HCV) or that can function with no need for initiation factors (nor initiator tRNA in the case of CrPV). Interestingly, addition of competitor RNAs containing either the HCV or the CrPV IRESes failed to restore miRNA repression in the nuclease treated system (Figure 8A), suggesting that competition for general components of the translational machinery was not critical for the efficiency of the miRNA response; however, it rather points out to a specific role for some initiation factors that bind either the cap or the poly(A) tail. Thus, we next designed an experiment in which the nuclease treated lysate was supplemented by addition of cap analogue and free poly(A) prior to translation (Figure 8B). Interestingly, overall translational efficiency of Luciferase was affected to a similar extent by the addition of either the cap analog or the free poly(A) with addition of both having an additive effect (Figure 8B, black bars). However, and to our surprise, addition of free poly(A) alone was both necessary and sufficient to restore an miRNA response in the nuclease treated lysate, whereas addition of free cap analog failed to do so (Figure 8B). Interestingly, addition of free poly(A) could also restore efficient repression on non-polyadenylated RNAs which were not effectively repressed in crude RRL (Figure 9C). On the contrary, translation driven by the EMCV and HCV IRESes could not be repressed by miRNAs even upon addition of free poly(A) RNA, suggesting that only cap-dependent translation would be sensitive to miRNA-mediated translational inhibition.

While this work was in progress, several reports have addressed the critical role of PABP in the miRNA response at the level of transcript deadenylation (39–41) and also on translation where GW182 was proposed to compete with PABP for eIF4G binding (41). Our results nicely confirm and extend these data by showing that the poly(A) tail can also play a role in *trans* for the efficient repression of target mRNAs. But how is the poly(A) able to modulate the miRNA response in *trans*? Interestingly, several studies carried out using wheat germ cell-free extracts have shown that addition of free poly(A) can improve PABP binding to the eIF4F complex and stimulate its activity (60,70). Moreover, free poly(A) has been shown to stimulate translation of non polyadenylated mRNAs in *trans* in the nuclease-treated RRL by improving the interaction between PABP and eIF4G (61). However, a mechanism where GW182 and PABP compete for eIF4G binding, although possible, is nevertheless unlikely in our system as translation driven by the EMCV [which under normal conditions depends on the PABP/eIF4G interaction (71)] is not repressed by miRNAs. However, it could be possible that miRNAs regulate the activity of the eIF4F complex. Thus, it would be conceivable that free poly(A) as well as polyadenylated competitor mRNAs could improve PABP binding to the eIF4F complex, thus allowing miRNAs to effectively regulate eIF4F activity and inhibit translation of the target mRNA. This would be also in agreement with the fact that the HCV IRES, which is independent of the eIF4F complex for translation remains unaffected by miRNAs.

Taken together, we describe here a new *in vitro* cell-free extract that faithfully reproduces the regulation of translation mediated by miRNAs, which is commercially available, easy to use and yielding highly reproducible results. Interestingly, our system allows translation repression to be studied at very early times when deadenylation has not yet taken place.

SUPPLEMENTARY DATA

Supplementary Data are available at NAR Online.

Downloaded from https://academic.oup.com/nar/article-abstract/39/12/5215/2411295 by guest on 08 May 2020

ACKNOWLEDGEMENTS

We thank W. Filipowicz for Ago2 and TNRC6 antibodies, D. Scadden for Tudor-SN antibody and S. Morley for PABP antibody. We thank B. Blanquier and IFR128 for qPCR facilities. We also thank Dr. Marie Sémon for statistical analysis of our data.

FUNDING

ANRS and ANR; E.P.R. was a recipient of "Ministère de la Recherche et de la Technologie" and "Fondation pour la Recherche Medicale (FRM)" fellowships. Funding for open access charge: INSERM.

Conflict of interest statement. None declared.

REFERENCES

1. Bartel,D.P. (2009) MicroRNAs: target recognition and regulatory functions. *Cell*, **136**, 215–233.
2. Umbach,J.L. and Cullen,B.R. (2009) The role of RNAi and microRNAs in animal virus replication and antiviral immunity. *Genes Dev.*, **23**, 1151–1164.
3. He,L. and Hannon,G.J. (2004) MicroRNAs: small RNAs with a big role in gene regulation. *Nat. Rev. Genet.*, **5**, 522–531.
4. Zhang,R. and Su,B. (2009) Small but influential: the role of microRNAs on gene regulatory network and 3′UTR evolution. *J. Genet. Genomics*, **36**, 1–6.
5. Friedman,R.C., Farh,K.K.-H., Burge,C.B. and Bartel,D.P. (2009) Most mammalian mRNAs are conserved targets of microRNAs. *Genome Res.*, **19**, 92–105.
6. Lewis,B.P., Burge,C.B. and Bartel,D.P. (2005) Conserved seed pairing, often flanked by adenosines, indicates that thousands of human genes are microRNA targets. *Cell*, **120**, 15–20.
7. Brennecke,J., Stark,A., Russell,R.B. and Cohen,S.M. (2005) Principles of microRNA-target recognition. *PLoS Biol.*, **3**, e85.
8. Brodersen,P. and Voinnet,O. (2009) Revisiting the principles of microRNA target recognition and mode of action. *Nat. Rev. Mol. Cell Biol.*, **10**, 141–148.
9. Jackson,R.J. and Standart,N. (2007) How do microRNAs regulate gene expression? *Sci. STKE*, **2007**, re1.
10. Hutvagner,G. and Zamore,P.D. (2002) A microRNA in a multiple-turnover RNAi enzyme complex. *Science*, **297**, 2056–2060.
11. Song,J.-J., Smith,S.K., Hannon,G.J. and Joshua-Tor,L. (2004) Crystal structure of Argonaute and its implications for RISC slicer activity. *Science*, **305**, 1434–1437.
12. Yekta,S., Shih,I.-H. and Bartel,D.P. (2004) MicroRNA-directed cleavage of HOXB8 mRNA. *Science*, **304**, 594–596.
13. Davis,E., Caiment,F., Tordoir,X., Cavaille,J., Ferguson-Smith,A., Cockett,N., Georges,M. and Charlier,C. (2005) RNAi-mediated allelic trans-interaction at the imprinted Rtl1/Peg11 locus. *Curr. Biol.*, **15**, 743–749.
14. Chendrimada,T.P., Gregory,R.I., Kumaraswamy,E., Norman,J., Cooch,N., Nishikura,K. and Shiekhattar,R. (2005) TRBP recruits the Dicer complex to Ago2 for microRNA processing and gene silencing. *Nature*, **436**, 740–744.
15. Gregory,R.I., Chendrimada,T.P., Cooch,N. and Shiekhattar,R. (2005) Human RISC couples microRNA biogenesis and posttranscriptional gene silencing. *Cell*, **123**, 631–640.
16. Humphreys,D.T., Westman,B.J., Martin,D.I.K. and Preiss,T. (2005) MicroRNAs control translation initiation by inhibiting eukaryotic initiation factor 4 E/cap and poly(A) tail function. *Proc. Natl Acad. Sci. USA*, **102**, 16961–16966.
17. Mathonnet,G., Fabian,M.R., Svitkin,Y.V., Parsyan,A., Huck,L., Murata,T., Biffo,S., Merrick,W.C., Darzynkiewicz,E., Pillai,R.S. *et al.* (2007) MicroRNA inhibition of translation initiation in vitro by targeting the cap-binding complex eIF4F. *Science*, **317**, 1764–1767.
18. Pillai,R.S., Bhattacharyya,S.N., Artus,C.G., Zoller,T., Cougot,N., Basyuk,E., Bertrand,E. and Filipowicz,W. (2005) Inhibition of translational initiation by Let-7 MicroRNA in human cells. *Science*, **309**, 1573–1576.
19. Thermann,R. and Hentze,M.W. (2007) Drosophila miR2 induces pseudo-polysomes and inhibits translation initiation. *Nature*, **447**, 875–878.
20. Wang,B., Love,T.M., Call,M.E., Doench,J.G. and Novina,C.D. (2006) Recapitulation of short RNA-directed translational gene silencing *in vitro*. *Mol. Cell*, **22**, 553–560.
21. Wang,B., Yanez,A. and Novina,C.D. (2008) MicroRNA-repressed mRNAs contain 40 S but not 60 S components. *Proc. Natl Acad. Sci. USA*, **105**, 5343–5348.
22. Maroney,P.A., Yu,Y., Fisher,J. and Nilsen,T.W. (2006) Evidence that microRNAs are associated with translating messenger RNAs in human cells. *Nat. Struct. Mol. Biol.*, **13**, 1102–1107.
23. Nottrott,S., Simard,M.J. and Richter,J.D. (2006) Human let-7a miRNA blocks protein production on actively translating polyribosomes. *Nat. Struct. Mol. Biol.*, **13**, 1108–1114.
24. Petersen,C.P., Bordeleau,M.-E., Pelletier,J. and Sharp,P.A. (2006) Short RNAs repress translation after initiation in mammalian cells. *Mol. Cell*, **21**, 533–542.
25. Eulalio,A., Huntzinger,E., Nishihara,T., Rehwinkel,J., Fauser,M. and Izaurralde,E. (2009) Deadenylation is a widespread effect of miRNA regulation. *RNA*, **15**, 21–32.
26. Iwasaki,S., Kawamata,T. and Tomari,Y. (2009) Drosophila argonaute1 and argonaute2 employ distinct mechanisms for translational repression. *Mol. Cell*, **34**, 58–67.
27. Wakiyama,M., Takimoto,K., Ohara,O. and Yokoyama,S. (2007) Let-7 microRNA-mediated mRNA deadenylation and translational repression in a mammalian cell-free system. *Genes Dev.*, **21**, 1857–1862.
28. Wu,L., Fan,J. and Belasco,J.G. (2006) MicroRNAs direct rapid deadenylation of mRNA. *Proc. Natl Acad. Sci. USA*, **103**, 4034–4039.
29. Behm-Ansmant,I., Rehwinkel,J., Doerks,T., Stark,A., Bork,P. and Izaurralde,E. (2006) mRNA degradation by miRNAs and GW182 requires both CCR4:NOT deadenylase and DCP1:DCP2 decapping complexes. *Genes Dev.*, **20**, 1885–1898.
30. Chu,C.Y. and Rana,T.M. (2006) Translation repression in human cells by microRNA-induced gene silencing requires RCK/p54. *PLoS Biol.*, **4**, e210.
31. Eulalio,A., Behm-Ansmant,I., Schweizer,D. and Izaurralde,E. (2007) P-body formation is a consequence, not the cause, of RNA-mediated gene silencing. *Mol. Cell. Biol.*, **27**, 3970–3981.
32. Jakymiw,A., Lian,S., Eystathioy,T., Li,S., Satoh,M., Hamel,J.C., Fritzler,M.J. and Chan,E.K. (2005) Disruption of GW bodies impairs mammalian RNA interference. *Nat. Cell. Biol.*, **7**, 1267–1274.
33. Liu,J., Rivas,F.V., Wohlschlegel,J., Yates,J.R. III, Parker,R. and Hannon,G.J. (2005) A role for the P-body component GW182 in microRNA function. *Nat. Cell. Biol.*, **7**, 1261–1266.
34. Pauley,K.M., Eystathioy,T., Jakymiw,A., Hamel,J.C., Fritzler,M.J. and Chan,E.K. (2006) Formation of GW bodies is a consequence of microRNA genesis. *EMBO Rep.*, **7**, 904–910.
35. Borman,A.M., Michel,Y.M. and Kean,K.M. (2000) Biochemical characterisation of cap-poly(A) synergy in rabbit reticulocyte lysates: the eIF4G-PABP interaction increases the functional affinity of eIF4E for the capped mRNA 5′-end. *Nucleic Acids Res.*, **28**, 4068–4075.
36. Michel,Y.M., Poncet,D., Piron,M., Kean,K.M. and Borman,A.M. (2000) Cap-Poly(A) synergy in mammalian cell-free extracts. Investigation of the requirements for poly(A)-mediated stimulation of translation initiation. *J. Biol. Chem.*, **275**, 32268–32276.
37. Svitkin,Y.V., Evdokimova,V.M., Brasey,A., Pestova,T.V., Fantus,D., Yanagiya,A., Imataka,H., Skabkin,M.A., Ovchinnikov,L.P., Merrick,W.C. *et al.* (2009) General RNA-binding proteins have a function in poly(A)-binding protein-dependent translation. *EMBO J.*, **28**, 58–68.
38. Soto Rifo,R., Ricci,E.P., Décimo,D., Moncorgé,O. and Ohlmann,T. (2007) Back to basics: the untreated rabbit reticulocyte lysate as a competitive system to recapitulate cap/

Downloaded from https://academic.oup.com/nar/article-abstract/39/12/5215/2411295 by guest on 08 May 2020

poly(A) synergy and the selective advantage of IRES-driven translation. *Nucleic Acids Res.*, **35**, e121.
39. Fabian,M.R., Mathonnet,G., Sundermeier,T., Mathys,H., Zipprich,J.T., Svitkin,Y.V., Rivas,F., Jinek,M., Wohlschlegel,J., Doudna,J.A. *et al.* (2009) Mammalian miRNA RISC recruits CAF1 and PABP to affect PABP-dependent deadenylation. *Mol. Cell*, **35**, 868–880.
40. Piao,X., Zhang,X., Wu,L. and Belasco,J.G. (2010) CCR4-NOT deadenylates RISC-associated mRNA in human cells. *Mol. Cell. Biol.*, **30**, 1486–1494.
41. Zekri,L., Huntzinger,E., Heimstadt,S. and Izaurralde,E. (2009) The silencing domain of GW182 interacts with PABPC1 to promote translational repression and degradation of microRNA targets and is required for target release. *Mol. Cell. Biol.*, **29**, 6220–6231.
42. Ricci,E.P., Herbreteau,C.H., Decimo,D., Schaupp,A., Datta,S.A.K., Rein,A., Darlix,J.-L. and Ohlmann,T. (2008) In vitro expression of the HIV-2 genomic RNA is controlled by three distinct internal ribosome entry segments that are regulated by the HIV protease and the Gag polyprotein. *RNA*, **14**, 1443–1455.
43. Hunt,S.L. and Jackson,R.J. (1999) Polypyrimidine-tract binding protein (PTB) is necessary, but not sufficient, for efficient internal initiation of translation of human rhinovirus-2 RNA. *RNA*, **5**, 344–359.
44. Moser,J.J., Chan,E.K. and Fritzler,M.J. (2009) Optimization of immunoprecipitation-western blot analysis in detecting GW182-associated components of GW/P bodies. *Nat. Protoc.*, **4**, 674–685.
45. Zipprich,J.T., Bhattacharyya,S., Mathys,H. and Filipowicz,W. (2009) Importance of the C-terminal domain of the human GW182 protein TNRC6C for translational repression. *RNA*, **15**, 781–793.
46. Maroney,P.A., Chamnongpol,S., Souret,F. and Nilsen,T.W. (2007) A rapid, quantitative assay for direct detection of microRNAs and other small RNAs using splinted ligation. *RNA*, **13**, 930–936.
47. Pelham,H.R. and Jackson,R.J. (1976) An efficient mRNA-dependent translation system from reticulocyte lysates. *Eur. J. Biochem.*, **67**, 247–256.
48. Ricci,E.P., Mure,F., Gruffat,H., Decimo,D., Medina-Palazon,C., Ohlmann,T. and Manet,E. (2009) *Nucleic Acids Res.*, **37**, 4932–4943.
49. Chakravarty,I., Bagchi,M.K., Roy,R., Banerjee,A.C. and Gupta,N.K. (1985) Protein synthesis in rabbit reticulocytes. Purification and properties of an Mr 80,000 polypeptide (Co-eIF-2A80) with Co-eIF-2 A activity. *J. Biol. Chem.*, **260**, 6945–6949.
50. Zou,C., Zhang,Z., Wu,S. and Osterman,J.C. (1998) Molecular cloning and characterization of a rabbit eIF2C protein. *Gene*, **211**, 187–194.
51. Masaki,S., Ohtsuka,R., Abe,Y., Muta,K. and Umemura,T. (2007) Expression patterns of microRNAs 155 and 451 during normal human erythropoiesis. *Biochem. Biophys. Res. Commun.*, **364**, 509–514.
52. Merkerova,M., Belickova,M. and Bruchova,H. (2008) Differential expression of microRNAs in hematopoietic cell lineages. *Eur. J. Haematol.*, **81**, 304–310.
53. Heimberg,A.M., Sempere,L.F., Moy,V.N., Donoghue,P.C.J. and Peterson,K.J. (2008) MicroRNAs and the advent of vertebrate morphological complexity. *Proc. Natl Acad. Sci. USA*, **105**, 2946–2950.
54. Meister,G., Landthaler,M., Dorsett,Y. and Tuschl,T. (2004) Sequence-specific inhibition of microRNA- and siRNA-induced RNA silencing. *RNA*, **10**, 544–550.
55. Hon,L.S. and Zhang,Z. (2007) The roles of binding site arrangement and combinatorial targeting in microRNA repression of gene expression. *Genome Biol.*, **8**, R166.
56. Doench,J.G., Petersen,C.P. and Sharp,P.A. (2003) siRNAs can function as miRNAs. *Genes Dev.*, **17**, 438–442.
57. Pillai,R.S., Artus,C.G. and Filipowicz,W. (2004) Tethering of human Ago proteins to mRNA mimics the miRNA-mediated repression of protein synthesis. *RNA*, **10**, 1518–1525.
58. Pestova,T.V., Hellen,C.U. and Shatsky,I.N. (1996) Canonical eukaryotic initiation factors determine initiation of translation by internal ribosomal entry. *Mol. Cell. Biol.*, **16**, 6859–6869.
59. Pestova,T.V., Shatsky,I.N., Fletcher,S.P., Jackson,R.J. and Hellen,C.U. (1998) A prokaryotic-like mode of cytoplasmic eukaryotic ribosome binding to the initiation codon during internal translation initiation of hepatitis C and classical swine fever virus RNAs. *Genes Dev.*, **12**, 67–83.
60. Bi,X. and Goss,D.J. (2000) Wheat germ poly(A)-binding protein increases the ATPase and the RNA helicase activity of translation initiation factors eIF4A, eIF4B, and eIF-iso4F. *J. Biol. Chem.*, **275**, 17740–17746.
61. Borman,A.M., Michel,Y.M., Malnou,C.E. and Kean,K.M. (2002) Free poly(A) stimulates capped mRNA translation in vitro through the eIF4G-poly(A)-binding protein interaction. *J. Biol. Chem.*, **277**, 36818–36824.
62. Dore,L.C., Amigo,J.D., Dos Santos,C.O., Zhang,Z., Gai,X., Tobias,J.W., Yu,D., Klein,A.M., Dorman,C., Wu,W. *et al.* (2008) A GATA-1-regulated microRNA locus essential for erythropoiesis. *Proc. Natl Acad. Sci. USA*, **105**, 3333–3338.
63. Pase,L., Layton,J.E., Kloosterman,W.P., Carradice,D., Waterhouse,P.M. and Lieschke,G.J. (2009) miR-451 regulates zebrafish erythroid maturation in vivo via its target gata2. *Blood*, **113**, 1794–1804.
64. Cheloufi,S., Dos Santos,C.O., Chong,M.M. and Hannon,G.J. (2010) A dicer-independent miRNA biogenesis pathway that requires Ago catalysis. *Nature*, **465**, 584–589.
65. Johnnidis,J.B., Harris,M.H., Wheeler,R.T., Stehling-Sun,S., Lam,M.H., Kirak,O., Brummelkamp,T.R., Fleming,M.D. and Camargo,F.D. (2008) Regulation of progenitor cell proliferation and granulocyte function by microRNA-223. *Nature*, **451**, 1125–1129.
66. Baek,D., Villén,J., Shin,C., Camargo,F.D., Gygi,S.P. and Bartel,D.P. (2008) The impact of microRNAs on protein output. *Nature*, **455**, 64–71.
67. Mencia,A., Modamio-Hoybjor,S., Redshaw,N., Morin,M., Mayo-Merino,F., Olavarrieta,L., Aguirre,L.A., del Castillo,I., Steel,K.P., Dalmay,T. *et al.* (2009) Mutations in the seed region of human miR-96 are responsible for nonsyndromic progressive hearing loss. *Nat. Genet.*, **41**, 609–613.
68. Seitz,H. (2009) Redefining microRNA targets. *Curr. Biol.*, **19**, 870–873.
69. Selbach,M., Schwanhäusser,B., Thierfelder,N., Fang,Z., Khanin,R. and Rajewsky,N. (2008) Widespread changes in protein synthesis induced by microRNAs. *Nature*, **455**, 58–63.
70. Khan,M.A. and Goss,D.J. (2005) Translation initiation factor (eIF) 4B affects the rates of binding of the mRNA m7G cap analogue to wheat germ eIFiso4F and eIFiso4F.PABP. *Biochemistry*, **44**, 4510–4516.
71. Svitkin,Y.V., Imataka,H., Khaleghpour,K., Kahvejian,A., Liebig,H.D. and Sonenberg,N. (2001) Poly(A)-binding protein interaction with elF4G stimulates picornavirus IRES-dependent translation. *RNA*, **7**, 1743–1752.
72. Rehmsmeier,M., Steffen,P., Hochsmann,M. and Giegerich,R. (2004) Fast and effective prediction of microRNA/target duplexes. *RNA*, **10**, 1507–1517.

Downloaded from https://academic.oup.com/nar/article-abstract/39/12/5215/2411295 by guest on 08 May 2020

586–598 Nucleic Acids Research, 2013, Vol. 41, No. 1 Published online 17 November 2012
doi:10.1093/nar/gks1076

miRNA repression of translation *in vitro* takes place during 43S ribosomal scanning

Emiliano P. Ricci[1,2,3], Taran Limousin[1,2,3,*], Ricardo Soto-Rifo[1,2,3], Paulina S. Rubilar[1,2,3], Didier Decimo[1,2,3] and Théophile Ohlmann[1,2,3,*]

[1]Ecole Normale Supérieure de Lyon, Unité de Virologie Humaine, [2]Inserm U758, Lyon, F-69364 and [3]Université de Lyon, France

Received June 13, 2012; Revised and Accepted October 15, 2012

Downloaded from https://academic.oup.com/nar/article-abstract/41/1/586/1159551 by guest on 08 May 2020

ABSTRACT

microRNAs (miRNAs) regulate gene expression at multiple levels by repressing translation, stimulating deadenylation and inducing the premature decay of target messenger RNAs (mRNAs). Although the mechanism by which miRNAs repress translation has been widely studied, the precise step targeted and the molecular insights of such repression are still evasive. Here, we have used our newly designed *in vitro* system, which allows to study miRNA effect on translation independently of deadenylation. By using specific inhibitors of various stages of protein synthesis, we first show that miRNAs target exclusively the early steps of translation with no effect on 60S ribosomal subunit joining, elongation or termination. Then, by using viral proteases and IRES-driven mRNA constructs, we found that translational inhibition takes place during 43S ribosomal scanning and requires both the poly(A) binding protein and eIF4G independently from their physical interaction.

INTRODUCTION

microRNAs (miRNAs) are small non-coding RNAs that participate in many cellular processes as essential gene regulators. miRNAs act as guides for the RNA-induced silencing complex (RISC) to bind messenger RNAs (mRNAs) and to repress their translation and/or decrease their stability. Usually, miRNAs bind to their target mRNAs at the 3′-untranslated region (3′-UTR) through partial base pairing (1). As a consequence, miRNAs can potentially interact with numerous target mRNAs. In agreement with this, 60% of all mammalian mRNAs have been reported to contain conserved miRNA target sequences (2).

Many mechanisms have been proposed to explain how miRNAs could regulate gene expression including translational repression, mRNA deadenylation and accelerated decay, which are non exclusive but rather sequential. In fact, recent data suggest that translational repression is the first mechanism of miRNA-induced gene repression, followed by mRNA deadenylation and eventually its degradation (3–7). Concerning translational repression, miRNAs were first reported to regulate translation at post-initiation steps (8–12), but recent data strongly suggest that repression takes place at the initiation stage (7,13–20).

However, there is still some controversy about the stage at which translation initiation could be repressed. Although many reports point to the 5′ cap structure as an essential factor necessary for translational repression (7,14,16–19), the need for other *cis*-acting factors such as the poly(A) tail is less clear with some data indicating an essential role for the poly(A) tail (14,19,21,22), while others report that its removal or replacement by the 3′ stem-loop tail of histone transcripts does not affect miRNA activity (17,23,24). In addition, PABP has been recently implicated in miRNA effect by interacting with the C-terminal domain of GW182 to promote translational repression and deadenylation (6,25–28).

Moreover, studies have failed to converge regarding the actual stage of translation initiation regulated by miRNAs. Some reports state that miRNAs act by targeting cap recognition and recruitment of the 43S complex (16,17,29), while others describe repression at the level of 60S ribosomal subunit joining (13,20). Thus, the precise molecular mechanisms by which miRNAs mediate translational repression remain a matter of debate.

Recent data strongly suggest that translational repression occurs prior to transcript deadenylation and degradation (3,5,30,31). This fits well with the rabbit reticulocyte lysate (RRL) model that we have previously described, which contains endogenous miRNAs that are fully

*To whom correspondence should be addressed. Tel: +33 472 728 953; Fax: +33 472 728 137; Email: tohlmann@ens-lyon.fr
Correspondence may also be addressed to Taran Limousin. Tel: +33 472 728 953; Fax: +33 472 728 137; Email: taran.limousin@ens-lyon.org

The authors wish it to be known that, in their opinion, the first three authors should be regarded as joint First Authors.

© The Author(s) 2012. Published by Oxford University Press.
This is an Open Access article distributed under the terms of the Creative Commons Attribution License (http://creativecommons.org/licenses/by-nc/3.0/), which permits non-commercial reuse, distribution, and reproduction in any medium, provided the original work is properly cited. For commercial re-use, please contact journals.permissions@oup.com.

functional to repress translation and to induce an siRNA response (22). One of the main advantages of this system is that repression occurs only at the level of translation with no effect on transcript degradation or deadenylation (22). Thus, it allows to focus only on the molecular mechanism used by miRNAs to interfere with protein synthesis. We have exploited the advantage of the RRL to assess the impact of miRNA repression on each individual step of protein synthesis (e.g. initiation, ribosomal subunit joining, elongation, termination and peptide release). Our results first show that miRNAs interfere only with translation initiation. Using a combination of viral proteases together with reporter genes containing cellular 5′-UTR with different structure or IRESes from different viral families, we could show that repression takes place at the level of 43S ribosomal scanning. Moreover, we show evidence that both PABP and eIF4G are necessary for miRNA-mediated translation inhibition, but this requirement is independent from the physical interaction between these two proteins.

MATERIALS AND METHODS

DNA constructs and *in vitro* transcription

Plasmids containing target sites for miR-451 (Luc, Luc-451X6, Luc-451mut) were already described (22). 5′-UTRs were obtained by PCR on cDNA obtained from Hela-cells total RNAs (BCL3, GAPDH, Cyclin D2, Line-1 and Hsp70-1), pEMCV-renilla and pHCV-renilla plasmids (32), pXLPV and pEMCV-PV plasmids (33), pXLCSFV 1–423.NS plasmid (34) avian encephalomyocarditis viruses (AEVs) plasmid (35), and Seneca Valley virus (SVV)+55 construct (36) using specific primers containing EcoRV restriction site and T7 promoter (for sense primers) and BamHI restriction site (for antisense primers). PCR products were digested and cloned in Luc and Luc-451X6 vectors previously digested by PvuII and BamHI restriction enzymes.

Plasmids were digested using EcoRI (polyadenylated RNAs), NaeI [internalized poly(A)] or XbaI (non polyadenylated RNAs) restriction enzymes. RNAs were obtained by using 1 mg linearized plasmid, 10 U T7 RNA polymerase (Promega Co., Madison, WI, USA), 20 U of RNAsin (Promega Co, Madison, WI, USA), 10 mM of rATP, rUTP and rCTP, 0.48 mM rGTP, 3 mM DTT and 1.3 mM m7GpppG (capped RNAs) or ApppG (uncapped RNAs) cap analog (New England Biolabs) in transcription buffer [40 mM Tris–HCl (pH 7.9), 6 mM $MgCl_2$, 2 mM spermidine and 10 mM NaCl]. The transcription reaction was carried out at 37°C for 2 h, and the RNAs were treated with RQ1 DNAse (Promega Co., Madison, WI, USA) and precipitated with Ammonium Acetate at 2.5 M final concentration. The integrity of the RNAs was checked by electrophoresis on non-denaturating agarose gels and their concentration was quantified by spectrophotometry at 260 nm using Nanodrop (NanoDropTechnologies, Wilmington, DE, USA). For radiolabeled RNAs the same protocol was used except that rUTP was omitted and replaced by 20 mCi of aP^{32} rUTP.

Western blotting

To test for initiation factor integrity, 3 µl of each reaction was recovered after translation and resolved on a 10% SDS–PAGE. Proteins were then transferred to a PVDF membrane by electroblotting and incubated with antibodies against PABP or eIF4G (kind gifts from Dr Morley).

Preparation of untreated RRL and *in vitro* translation assays

Untreated RRL was prepared essentially as previously described (32). Translation reactions were performed in a final volume of 30 µl consisting of 20 µl of untreated RRL, 0.46 fmol of heat denatured mRNAs, in the presence of KCl (100 mM), $MgCl_2$ (0.5 mM) and amino acids mixture (20 µM each). RRL under full translational condition was incubated together with the heat denatured mRNA for 1 h at 10°C, followed by 2 min at 20°C, 2 min at 25°C and 30 or 60 min at 30°C. The reaction was then stopped by the addition of 50 µl of luciferase lysis buffer to 10 µl of the translation reaction.

Renilla activity was measured and normalized to an internal Firefly luciferase mRNA for all experiments that do not involve the addition of a translational inhibitor (Figures 1, 2, 4 and 5).

For all the experiments, we express translation efficiency as the percentage of luciferase activity compared to the control Luc mRNA (set at 100%); for miRNA effect, in each condition, the luciferase activity from the Luc-451X6 mRNA is expressed as a percentage of its control Luc mRNA (set to 100%).

For analysis of radiolabeled RNA integrity, RNA were translated as described and extracted at indicated times with Tris-reagent following manufacturer conditions. Total RNAs were run on a 2% agarose gel and analyzed by autoradiography on a phosphorimager.

Preparation of viral proteases

Commercial 3C protease from human rhinovirus (HRV) was obtained from Novagen (Madison, WI, USA). The L-protease from the foot-and-mouth disease virus (FMDV) was produced by *in vitro* translation using nuclease-treated RRL as previously described (32) and 2 µl were added prior to translation. The human immunodeficiency virus type-2 (HIV-2) protease was obtained from the NIH and 2 µl were added prior to translation. For rescue experiment, translation reactions were treated 10 min with 2 µl HIV-2 protease, cleavage was then blocked with 10 µM palinavir and translation were carried during 1 h in presence of dialysis buffer or recombinant PABP or eIF4G (kind gift of C.S. Fraser).

Preparation of PABP recombinant protein

Escherichia coli BL21 cells expressing the pET15b-PABP vector (kindly provided by Martin Bushell) were grown until A600 reached 0.6–0.8 and then, induced overnight at 30°C with IPTG 0.5 mM. Bacterial pellets were

Downloaded from https://academic.oup.com/nar/article-abstract/41/1/586/1159551 by guest on 08 May 2020

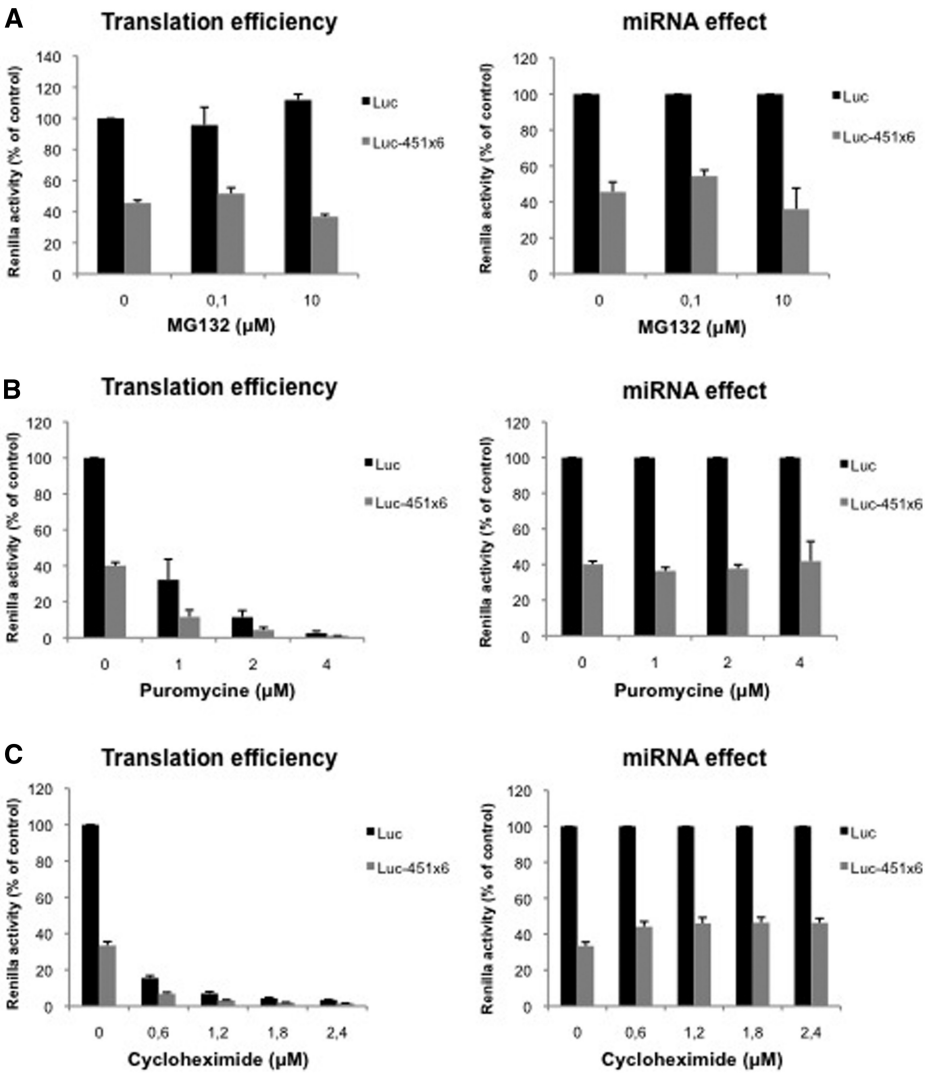

Figure 1. miRNAs do not target translation elongation nor degradation of nascent peptides through the proteasome. (**A**) Translation of Luc and Luc-451X6 RNAs was carried out in untreated RRL in presence of indicated concentration of MG132. (**B**) Translation of Luc and Luc-451X6 RNAs was carried out in untreated RRL in presence of indicated concentration of puromycine. (**C**) Translation of Luc and Luc-451X6 RNAs was carried out in untreated RRL in presence of indicated concentration of cycloheximide. Results are shown as translation efficiency (left panels) and miRNA effect (right panels), as described in 'Materials and Methods' section. Error bars correspond to SD obtained from three independent experiments.

resuspended in native lysis buffer (50 mM NaH_2PO_4 [pH 8.0]; 300 mM NaCl and 10 mM imidazole) supplemented with 1 mg/ml lysozyme (Sigma) and cells were lysed by sonication. Supernatant was recovered and incubated with Ni-NTA resin (Qiagen) (previously equilibrated in lysis buffer) at 4°C for 2 h under gentle shaking. The resin was then washed three times with five volumes of washing buffer [50 mM NaH_2PO_4 [pH 8.0]; 300 mM NaCl and 20 mM imidazole and protease inhibitor cocktail (Roche)] and protein was then eluted with elution buffer (50 mM NaH_2PO_4 [pH 8.0]; 300 mM NaCl; 500 mM Imidazole and protease inhibitor cocktail). The eluted protein was desalted and concentrated with dialysis buffer (20 mM HEPES [pH 7.5], 100 mM KCl, 2 mM DTT and protease inhibitor cocktail) using Spin-X UF Concentrators (Corning).

RESULTS

miRNAs repress mRNA translation independently of deadenylation and decay of target mRNAs

In this study, we have used the untreated RRL as a model *in vitro* system to study the effects of endogenous miRNAs on translation of exogenous reporter transcripts. For this, we used a Renilla luciferase reporter construct that harbors, unless specified, a globin 5′-UTR and are followed by a 3′-UTR containing either six target-sites for miR-451 (namely 'Luc-451X6') or lacking miRNA target sites (namely 'Luc'). We deliberately chose to use miR-451 as a model miRNA for this study as we previously showed that it is highly expressed in the reticulocyte lysate and recapitulates all aspects of the miRNA response (22). Protein synthesis was quantified by measuring

Downloaded from https://academic.oup.com/nar/article-abstract/41/1/586/1159551 by guest on 08 May 2020

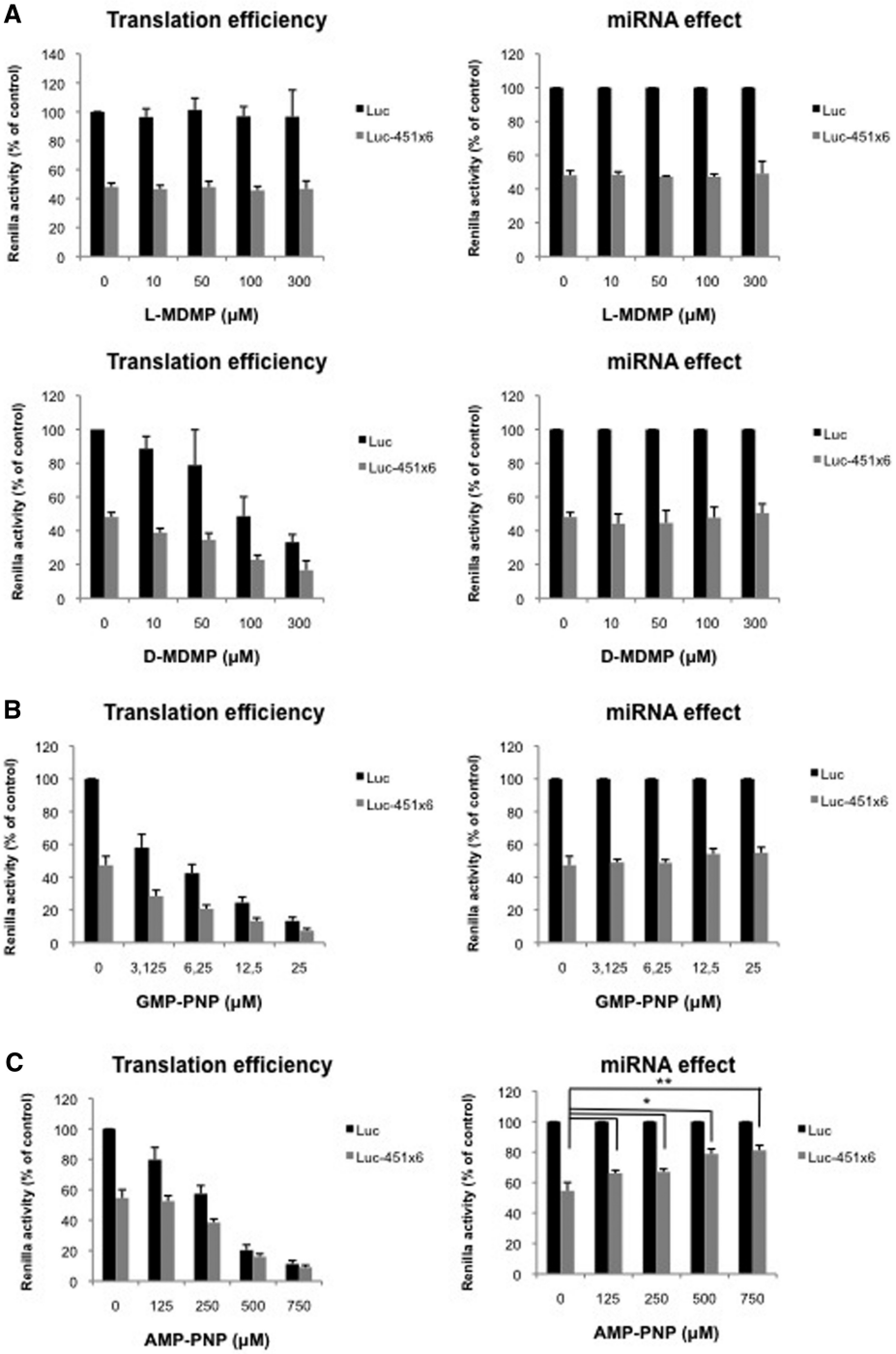

Figure 2. 60S ribosomal joining is not regulated by miRNAs. (**A**) Translation of Luc and Luc-451X6 RNAs was carried out in untreated RRL in presence of indicated concentration of L-MDMP (top panels) or D-MDMP (bottom panels). (**B**) Translation of Luc and Luc-451X6 RNAs was carried out in untreated RRL in presence of indicated concentration of GMP-PNP. (**C**) Translation of Luc and Luc-451X6 RNAs was carried out in untreated RRL in presence of indicated concentration of AMP-PNP. Results are shown as translation efficiency (left panels) and miRNA effect (right panels), as described in 'Materials and Methods' section. Error bars correspond to SD obtained from three independent experiments. * corresponds to a *P*-value <0.05; ** corresponds to a *P*-value <0.01; (non directional t-test).

luciferase activity and both translation efficiency and miRNA effect are quantified and plotted on individual bar graphs (see 'Materials and Methods' section).

In our previous published work, we had shown that translational repression occurred in the absence of any deadenylation of the target mRNA. This was demonstrated by checking the integrity of radiolabeled RNAs after translation and by real-time quantitative PCR (22). However, because the extent of deadenylation could be difficult to assess, we have used another

Downloaded from https://academic.oup.com/nar/article-abstract/41/1/586/1159551 by guest on 08 May 2020

experimental strategy to show evidence that inhibition of gene expression in our system was not due to shortening of the poly(A) tail. In order to do this, we have adapted the method recently described by Tomari and colleagues (37) which consists of internalizing the poly(A) tail by adding a stretch of non specific residues at the 3′ end of the poly(A) tail (Supplementary Figure S1A). In the present case, 280 nt were added and the integrity of the radiolabeled transcripts that contain 6 miR-451 target sites or 6 mutated sequences was checked on agarose gel (Supplementary Figure S1B). We did not observe any deadenylation or degradation of the mRNAs at the early time points (0, 0.5, 1 and 2 h). However, at 3 h, we detected a decrease in the amount of both control and targeted mRNA, which suggests that some decay has occurred (Supplementary Figure S1B). We then tested the effect of poly(A) tail internalization on miRNA-mediated repression. Interestingly, RNAs with normal and internalized poly(A) were inhibited by miR-451 to a similar level (50%), even after 6 h of incubation (Supplementary Figure S1C). As an additional control, we have also investigated whether mutations in the seed region of the target gene could reverse the effects of miR-451. Supplementary Figure 1D shows the translational efficiency and the miR-451 effects over a 6 hours period of time.

Altogether, these data confirm the results that we had obtained in our previous published work and further validates that inhibition of gene expression takes place at the level of translation in the RRL.

miRNAs do not target translation elongation nor degradation of nascent peptides through the proteasome

Taking advantage of our system that allows translational repression in the absence of deadenylation and mRNA decay, we have assessed the impact of miRNA repression in the presence of a large spectrum of effectors that are known to block translation at each of the various steps of protein synthesis (initiation, ribosomal subunit joining, elongation, termination and peptide release).

We initially started with the proteasome inhibitor MG132 as miRNAs have been suggested to regulate translation elongation through the proteolytic cleavage of nascent peptides (11) and was already used to study miRNA activity in living cells (17). As observed (Figure 1A, left panel), addition of MG132 did not significantly affect luciferase production from both Luc and Luc-451X6 mRNAs. Furthermore, translational repression mediated by miR-451 was not affected thus suggesting that miRNAs do not target the proteolytic degradation of nascent peptides, at least not through a proteasome-induced process (Figure 1A, right panel).

We then tested whether miR-451 could cause the premature drop-off of elongating ribosomes as previously suggested for the artificial miRNA CXCR4 (12). For this, we added increasing amounts of puromycin to our translation reactions and then monitored translation of Luc and Luc-451X6 mRNAs (Figure 1B). Puromycin causes the premature termination of elongating ribosomes thus inducing ribosome drop-off. As observed (Figure 1B, left panel), addition of puromycin to translation extracts led to a dose-dependent inhibition of luciferase expression from both RNAs reaching a 60-fold inhibition at the highest concentration. Strikingly, the relative level of miRNA-mediated repression remained constant to ~60% of the control in all conditions tested (Figure 1B, right panel). Interestingly, similar results were obtained when translation elongation was inhibited by the addition of cycloheximide, which stalls elongating 80S ribosomes on the mRNA without inducing their drop-off (Figure 1C). Indeed, as observed for puromycin, addition of increasing amounts of cycloheximide strongly inhibited luciferase expression without inducing further effects on miRNA-451 repression (Figure 1C, right panel).

Taken together, these results suggest that miRNAs do not interfere with translation elongation or proteosomal degradation of nascent peptides.

60S ribosomal joining is not regulated by miRNAs

We next tested whether the ribosomal subunits joining step could be affected by miR-451. This was suggested by a report showing that let-7 miRNAs could regulate this stage of translation with RISC being able to associate with 60S ribosomes through eIF6 to interfere with the formation of the 80S ribosome on targeted mRNAs (13); such an hypothesis has also been challenged by other researchers (38). A similar mechanism was also proposed in the nuclease-treated RRL using the artificial CXR4 miRNA system showing poor association of the 60S subunit to the 40S ribosomal subunit (20).

In an attempt to reduce formation of 80S ribosomes, we took advantage of MDMP, a chemical compound that specifically impairs the association of 60S and 40S ribosomal subunits (39,40). As observed, addition of increasing amounts of D-MDMP (the biologically active stereoisomer) led to a dose-dependent inhibition of both Luc and Luc-451X6 mRNAs translation (Figure 2A, bottom left panel) whereas addition of the inactive L-stereoisomer did not affect translation (Figure 2A, top left panel). Interestingly, despite the inhibition of translational rates, miRNA-mediated repression was not changed upon addition of D-MDMP (Figure 2A, bottom right panel) suggesting that miRNAs did not interfere with the joining of the 60S ribosomal subunit.

Ribosomal subunit joining is also regulated by the release of initiation factors from the 40S ribosome upon recognition of the AUG initiation codon. This stage is mediated by hydrolysis of the GTP molecule associated to eIF2 and eIF5B (41). Interestingly, since Argonaute 2 was first characterized to be a protein that regulates eIF2 recycling both in RRL and wheat germ extracts (42), it was of interest to test whether it could affect 60S ribosome joining by inhibiting eIF2 release. For this, we used GMP-PNP, a non-hydrolysable GTP analog that stalls the 48S complex at the AUG start codon and prevents 60S ribosome binding. As observed (Figure 2B, left panel), addition of GMP-PNP led to a dose-dependent inhibition of Luc and Luc-451X6 mRNAs translation reaching a 7-fold inhibition at the highest concentration. However, as observed for MDMP, translational repression Luc-451X6 mRNA was not affected therefore

Downloaded from https://academic.oup.com/nar/article-abstract/41/1/586/1159551 by guest on 08 May 2020

suggesting that RISC did not interfere with the hydrolysis of eIF2-bound GTP (Figure 2B, right panel).

As discussed earlier, translation initiation requires two molecules of GTP to proceed but is also dependent on ATP hydrolysis through the use of various DEAD-Box RNA helicases that are required for translation initiation, among which is eIF4A (43). The latter is an ATP dependent RNA helicase which is required both for initial ribosome binding to the mRNA and linear scanning of the ribosome from the binding site to the AUG initiation codon (44). In fact, eIF4A was shown to 'prepare' a landing pad for ribosomes on the mRNA and then unwinds the RNA secondary structures encountered during ribosomal scanning (44). In order to test whether ATP hydrolysis can be targeted by miRNA repression, we used AMP-PNP, a non-hydrolysable analogue of ATP. As observed (Figure 2C, left panel), addition of AMP-PNP to translation extracts led to a dose-dependent inhibition of Luc translation reaching up to 10-fold repression. Interestingly, Luc-451X6 translation appeared to be relatively more resistant to AMP-PNP than Luc translation, especially at low amounts of AMP-PNP (Figure 2C, left panel). This is particularly striking when Luc-451X6 translation was normalized against that of Luc RNA (Figure 2C, right panel) and we could observe a derepression of miRNA activity following the addition of AMP-PNP suggesting that miR-451 interferes with ATP hydrolysis. However, although they are indicative of a link between ATP hydrolysis and miRNA repression, these data must be interpreted with care due to the involvement of ATP in many biological processes including tRNA aminoacylation or even formation of the RISC complex (45).

Taken together, data obtained with various inhibitors suggest that miRNA repression does not take place at the level of 60S subunit joining, nor elongation, nor termination thus suggesting a potential role at the level of initiation.

PABP and eIF4G are required for miRNA-mediated repression independently from their physical interaction

miRNA-mediated repression at the level of translation initiation has been suggested by other studies in cell free system to primarily depend on the involvement of PABP and eIF4F (6,16). This prompted us to further assess the role of these factors in our *in vitro* system. For this, we used a combination of different viral proteases that are able to cleave PABP, eIF4G or both.

The protease 3C from Human Rhinovirus is known to inhibit translation initiation through cleavage of PABP without affecting the composition of the eIF4F complex (46). We thus used this enzyme to block PABP function prior to translation of Luc or Luc-451X6 mRNAs. As shown on western blotting, PABP was efficiently cleaved at the highest concentration of the protease added (Supplementary Figure S2A) and this resulted in translation inhibition (Figure 3A, left panel). However, the relative effect of miRNA-mediated translation inhibition was significantly relieved, from 50% to 20% (Figure 3A, right panel) suggesting that PABP is required for the miRNA response in the RRL.

We then used the L-protease of FMDV which destabilizes the eIF4F complex by processing eIF4G in a N-terminus fragment that contains binding sites for eIF4E and PABP and a C-terminus domain which harbors the binding sites for eIF3 and eIF4A (47). Thus, *in vitro* translated L-protease was added to the untreated RRL prior to translation of Luc and Luc-451X6 RNAs. As visualized by western blot, eIF4G was cleaved upon addition of L-protease (Supplementary Figure S2B) and this resulted in translation inhibition (Figure 3B, left panel, compare Control and L-protease lanes). Addition of the protease inhibitor E64 restored wild-type levels of translation indicating that translational repression was merely the result of the cleavage of eIF4G. Interestingly, miRNA-mediated repression was not affected and, if anything, rather slightly stimulated by the addition of L-protease (Figure 3B, right panel). This indicates that neither the integrity of eIF4F nor the N-terminal domain of eIF4G is necessary for miRNA function and suggests that RISC does not target the eIF4G-PABP physical interaction.

Finally, we have used the viral protease from the HIV-2 to measure its effect on translation of Luc and Luc-451X6 mRNAs. This enzyme has been shown to cleave eIF4G at two different sites yielding three different fragments (48,49). Interestingly, it also hydrolyses PABP at two different sites and proteolysis of both factors contributes to translation inhibition (50). Cleavage of eIF4G was shown to be complete upon addition of the HIV-2 protease in the RRL as visualized by western blotting (Supplementary Figure S2C). Remarkably, the consequence of this cleavage resulted in the complete loss of miR-451 effect. This was dependent on proteolytic activity since addition of specific inhibitors was sufficient to restore the miRNA response (Figure 3C, right panel). To test whether the specific loss of PABP and eIF4G cleavage was responsible for the effect on the miRNA-mediated inhibition, we have supplemented the HIV-2 protease treated lysate with the intact proteins (Figure 3D). Interestingly, both proteins were able to restore the miRNA effect to a partial, but significant, level. Addition of both in the same reaction did not significantly increase the rescue (data not shown). This nicely confirms the role for PABP in translation inhibition caused by miRNAs. However, the effect of eIF4G proteolysis seems to be, a priori, not in agreement with our data obtained with the L protease (see above) and showing no change upon eIF4G cleavage. But it is important to remember that those two virally encoded enzymes do not cleave the eIF4G molecule at the same sites. As a result, the consequences of the proteolytic action of these two virally encoded proteases are very different on translation initiation (49). We have previously shown that the HIV-2 protease removes a short region of 40 amino acids from the central domain of eIF4G that was shown to exhibit a strong RNA binding activity and this event results in the specific inhibition of ribosomal scanning by a, yet, unknown mechanism (48,49).

Taken together, these data suggest that both PABP and the carboxy-terminal domain of eIF4G are required for efficient miRNA repression and this effect seems to be linked to ribosomal scanning.

Downloaded from https://academic.oup.com/nar/article-abstract/41/1/586/1159551 by guest on 08 May 2020

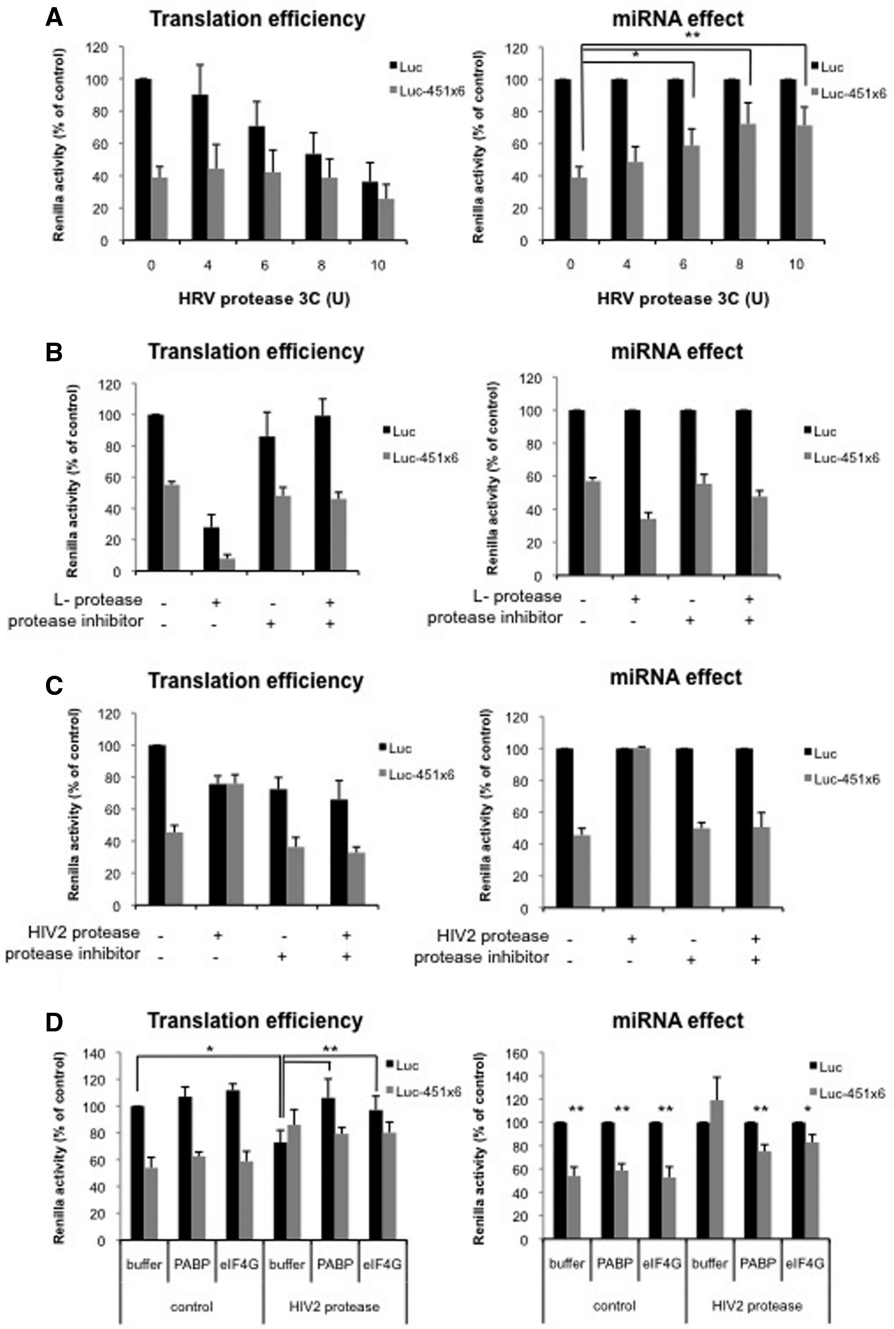

Figure 3. PABP and eIF4G are required for miRNA-mediated repression independently from their physical interaction. (**A**) Translation of Luc and Luc-451X6 RNAs was carried out in untreated RRL after addition of HRV 3C protease as indicated. (**B**) Translation of Luc and Luc-451X6 RNAs was carried out in untreated RRL after addition of 2 µl *in vitro* translated L-protease, E64 protease inhibitor (10 µM) or both as indicated. (**C**) Translation of Luc and Luc-451X6 RNAs was carried out in untreated RRL after addition of 2 µl recombinant HIV-2 protease, the palinavir protease inhibitor (10 µM) or both as indicated. (**D**) Translation of Luc and Luc-451X6 RNAs was carried out in RRL and treated with 2 µl HIV-2 protease for 10 min. The reaction was then stopped by addition of the palinavir protease inhibitor (10 µM) and the recombinant PABP (500 ng) or eIF4G (1 µg) were added to the mixture for a further 50 min before luciferase analysis. Results are shown as translation efficiency (left panels) and miRNA effect (right panels), as described in 'Materials and Methods' section. Error bars correspond to SD obtained from three independent experiments; * corresponds to a *P*-value <0.05; ** corresponds to a *P*-value <0.01; (non directional *t*-test).

miRNA-mediated repression is modulated by the composition of the 5′-UTR

Ribosomal scanning is a difficult process to study, as it involves many factors and it is hard to distinguish from other translational steps, such as ribosomal binding or AUG recognition (51). Nevertheless, both 5′-UTR length and structure have been shown to modulate ribosomal scanning rate. We thus decided to investigate the influence of 5′-UTR composition on miRNA effect. For this we cloned different human 5′-UTR in our Luc and Luc-451X6 vectors (Figure 4A). In addition to the 5′-UTR

Downloaded from https://academic.oup.com/nar/article-abstract/41/1/586/1159551 by guest on 08 May 2020

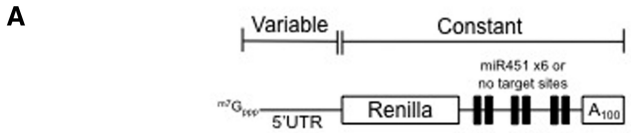

5'UTR	Length (nt)	GC content (%)	ΔG (kcal.mol^{-1})
Globin	53	45	-11
BCL3	75	81	-31
GAPDH	102	61	-22
Hsp70	243	63	-86
Cyclin D2	269	62	-139
Line 1	909	58	-350

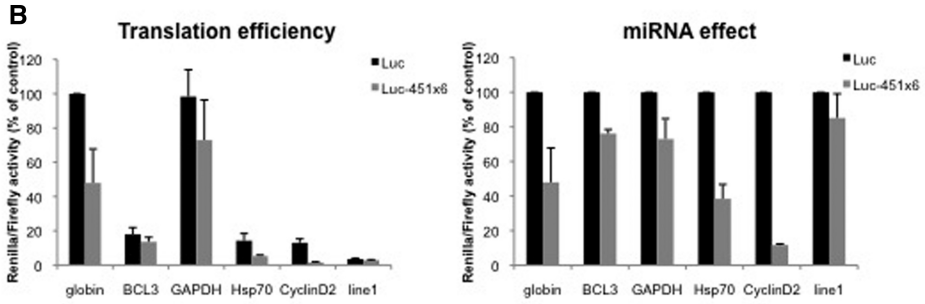

Figure 4. miRNA-mediated translation inhibition is affected by 5′-UTR composition. (**A**) Schematic representation of the Renilla luciferase RNA used, which contains either no target sites (Luc) or six target sites for miR-451 (Luc-451) at the 3′-end. Expression of this construct was driven by various 5′-UTR that were derived from cellular transcripts as shown on the table (stability of the 5′-UTR was predicted using the mfold program). (**B**) Translation of Luc and Luc-451X6 RNAs driven by different 5′-UTR was carried out in untreated RRL. Results are shown as translation efficiency (left panel) and miRNA effect (right panel), as described in 'Materials and Methods' section. Error bars correspond to SD obtained from three independent experiments.

of β-globin which was used as a positive control in the system, we have deliberately chosen genes harboring complex and structured 5′-UTRs such as BCL3 (75 nt., 81% GC rich), GAPDH (102 nt., 61% GC rich), Hsp70 (243 nt., 63% GC rich), Cyclin D2 (269 nt., 62% GC rich) and Line-1 (909 nt., 58% GC rich) (Figure 4A). As expected (Figure 4B, left panel), the efficiency of translation strongly differed between the different 5′-UTR tested, with β-globin and GAPDH driving translation at similar rates, while translation driven by BCL_3, Hsp70, Cyclin D2 and Line-1 5′-UTRs was significantly less important. Interestingly, the nature of the 5′-UTR considerably influenced the level of miRNA-mediated inhibition (Figure 4B, right panel). However, we were surprised to observe that we could not draw any linear correlation between the complexity of the 5′-UTR and the level of miRNA repression (Line-1 mRNA being only slightly affected by miRNAs although its 5′-UTR corresponds to the longest tested). Nevertheless, it is noteworthy that no linear correlation could be drawn either between the complexity of the 5′-UTR structure and the overall translational efficiency (compare translational efficiency for GAPDH with the others).

A possible explanation for these rather puzzling results is to consider that the structure of the 5′-UTR does not only influence ribosomal scanning but also initial binding of the ribosome. Thus, we may have combined two effects, binding and scanning, that could explain this lack of correlation. Alternatively, it has recently been shown that a specific subset of mRNAs with complex RNA structures can recruit additional RNA helicases such as DHX29 and DDX3 to facilitate the progression of the 43S complex (52,53). Therefore, complex-structured 5′-UTR may be better translated because they have the ability to recruit additional RNA helicases. Taken together these data suggest that the structure of the 5′-UTR plays a role in the magnitude of the miRNA response but the mechanism by which this occurs needs to be investigated further.

Ribosomal scanning is required for miRNA-mediated inhibition

As stated earlier, the 5′-UTR corresponds to the region where ribosomes initially contact the mRNA (via a large number of eIFs) and is also the place where linear scanning of the 43S pre-initiation complex takes place. Therefore, to distinguish which one of these two

Downloaded from https://academic.oup.com/nar/article-abstract/41/1/586/1159551 by guest on 08 May 2020

mechanisms (binding or scanning) is targeted by miRNAs, we have used the well-characterized IRESes from the encephalomyelocarditis virus (EMCV) and poliovirus (PV) viruses. These two IRESes are known to recruit the 40S ribosomal subunit in a similar way with entry being some 25 nt downstream the conserved polypyrimidine rich tract at the vicinity of an AUG codon (54). However, once bound to the EMCV mRNA, the 40S ribosome recognizes the AUG codon and initiate translation exclusively from this point with limited ribosome scanning, whereas, in the case of PV, the pre-initiation complex scans some 150 nt before it finds and recognizes the authentic AUG codon (54). Thus, we have exploited these differences to test whether miR-451 repression interferes with ribosome scanning. These IRESes have been inserted in front of the luciferase reporter gene (see Figure 5A) and reporter constructs were transcribed to create uncapped and polyadenylated RNAs as they are naturally found during the viral replication cycle. As observed (Figure 5B), translation mediated by these viral IRESes exhibited a different sensitivity to miRNA repression with the PV construct being repressed whereas function of the EMCV IRES was only slightly affected. Although a lack of effect of miRNAs on the EMCV IRES has been reported previously (14,16,17,22,45), the ability of miRNAs to repress translation driven by the PV IRES had never been tested so far. This most probably reflects differences in ribosomal movement and further supports the finding that miRNAs repress translation by interfering with ribosomal scanning with no, or little, effect on ribosomal attachment.

As it could be argued that the differences between PV and EMCV IRESes could also be explained by their relative different translational efficiency in the RRL, we have used the L protease to enhance translation of the PV IRES as previously reported (55). This is presented in Supplementary Figure S3 and nicely shows that the magnitude of miRNA repression does not vary upon stimulation of the PV IRES by the L protease.

To further confirm these data, we have used a chimeric IRES made between EMCV and PV (Figure 5A); interestingly, it has been shown that switching the 3′IRES boundaries between PV and EMCV was sufficient to induce ribosomal scanning on EMCV (33). We therefore tested the impact of miRNA activity on this EMCV/PV chimera (Figure 5B). Interestingly, translation of the EMCV/PV chimeric IRES which contains the EMCV core and the PV 'scanning segment' became sensitive to miRNA binding (see EMCV/PV) further suggesting that ribosomal scanning is the step of translation that is regulated by miRNAs.

miRNAs have no effect on 'non scanning' mRNAs such as HCV and HCV-like IRESes

Data presented in this article suggest so far that translation inhibition induced by miR-451 requires ribosomal scanning. Thus, given these data, we made the assumption that a mRNA that could initiate translation independently from ribosomal scanning would not be affected by miR-451. Such an mRNA exists in the form of HCV and CSFV IRESes that are naturally uncapped and non-polyadenylated (56). Thus, HCV- and CSFV-luciferase were translated in their natural conformation with or without miR-451 target sites as shown in Figure 5A. As it was anticipated and previously shown for HCV (17,21,22), translation driven by both IRESes was not repressed by miR-451 (Figure 5C). We have recently shown that the presence of the poly(A) tail was absolutely required for miRNA-mediated translation repression (22). Thus, from the experiment carried out with HCV/CSFV, it could be argued that the lack of miRNA effect could be due to the physical absence of a poly(A) tail on these two mRNAs. To circumvent this problem, we next used the IRESes of two members of the *Picornaviridae* family that were shown to initiate translation in a way that is closely related to HCV and CSFV. These picornavirus are namely the AEV and SVV (35,36), for which the viral RNA is uncapped but it contains a poly(A) tail (Figure 5A); however, it does not functionally initiate translation in a poly(A)/PABP dependent manner but rather rely on an HCV- and CSFV-like mechanism for ribosome recruitment. Interestingly, translation of these constructs in our system was not inhibited at all by the binding of miR-451 and showed a very similar and comparable behavior to that obtained with the HCV and CSFV IRESes (Figure 5C). Thus, it confirms that miRNA repression cannot occur when translation initiation operates in the absence of ribosomal scanning even if the mRNA target harbors a poly(A) tail.

DISCUSSION

miRNA repression affects several stages of gene expression including translation (7,9,12–17,19,20), deadenylation and decay of target mRNAs (6,7,23,24). Although it has been shown that miRNA-mediated deadenylation is translation independent (6,57), recent data suggest that miRNA repression first occurs at the translational stage before it can undergo deadenylation (3,5,30,31). Differences in the mechanism by which miRNAs repress gene expression are likely to reflect the fact that several overlapping mechanisms are at use or that differences in experimental design may introduce bias. To support this latter hypothesis, important variations in the magnitude of miRNA repression have been reported with different methods of cell transfection such as cationic lipids versus electroporation or DNA versus RNA (58), but also in the composition of the intrinsic promoter (SV40 versus TK) (59) or even in the sequence of the miRNA itself (60). In order to minimize any experimental bias, we have chosen to study the effect of the most abundant endogenous miRNA (miR-451) contained in the RRL, which was shown to faithfully recapitulate translational repression without inducing deadenylation nor RNA degradation (22). This was further verified in this present article by using an internalized poly(A) tail and we could show that this did not change significantly the level of repression induced by miRNAs (Supplementary Figure S1). Using this system, our initial goal was to find which stage of translation was repressed. This is an important unresolved issue as several conflicting reports showed that it could

Downloaded from https://academic.oup.com/nar/article-abstract/41/1/586/1159551 by guest on 08 May 2020

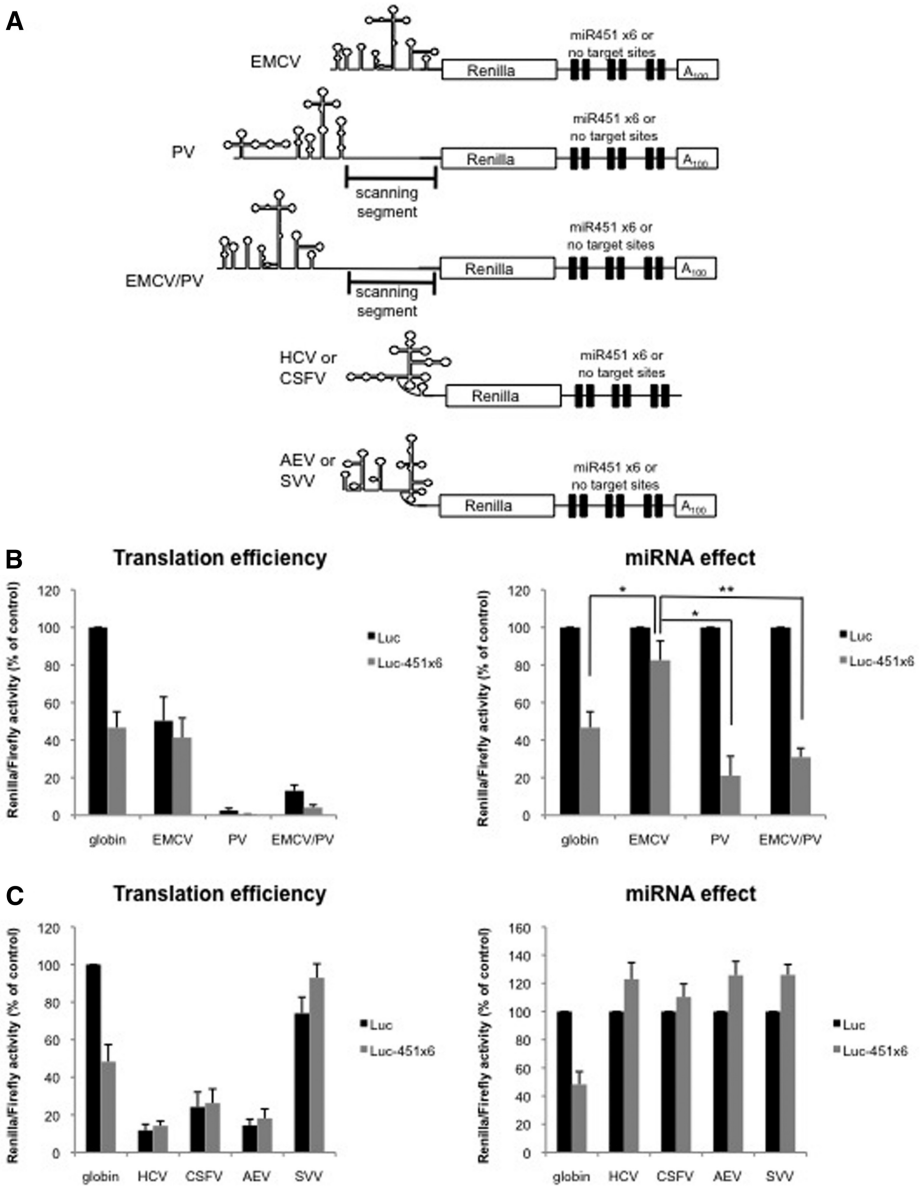

Figure 5. Ribosomal scanning is required for miRNA-mediated inhibition. (**A**) Schematic representation of the Renilla luciferase RNAs in which translation initiation was driven by EMCV, PV, the EMCV/PV chimera, HCV, CSFV, SVV or AEV IRES. (**B**) Translation of Luc or Luc-451X6 constructs containing the EMCV, PV, EMCV/PV IRES or globin 5′-UTR as a control, in the untreated RRL. (**C**) Translation of Luc or Luc-451X6 constructs containing the HCV, CSFV, SVV, AEV IRES or globin 5′-UTR as a control in the untreated RRL. Results are shown as translation efficiency (left panels) and miRNA effect (right panels), as described in 'Materials and Methods' section. Error bars correspond to SD obtained from three independent experiments; * corresponds to a *P*-value <0.05; ** corresponds to a *P*-value <0.01; (non directional *t*-test).

occur at initiation or elongation steps (7,9,12–17,19,20) or even by inducing proteolytic cleavage of nascent peptides through a, yet, uncharacterized machinery (11).

Our experimental strategy consisted of using a spectrum of natural or chemical molecules that are specifically targeting different stages of translation. By using puromycin and cycloheximide, we showed that the relative level of miRNA repression was not affected suggesting a mode of action upstream from the elongation step (Figure 1). This result is consistent with type I miRNA-repressed mRNAs, defined by Kong and coworkers, for which miRNA repression takes place at translation initiation and are not affected by the addition of low amounts of cycloheximide (59). Furthermore, it also confirms that miRNA-targeted mRNAs are undergoing active translocation of elongating ribosomes as previously suggested (12,59). Addition of the proteasome inhibitor MG132 showed that miRNA did not induce neo-synthesized peptide degradation (Figure 1) and the use of both MDMP and GMP-PNP ruled out any involvement of miRNAs in the control of 60S ribosome subunit joining (Figure 2). This suggests that repression induced by miR-451 happens at an early stage of translation, pointing out to an effect on the initiation stage of protein synthesis. Translational inhibition by miRNAs has already been shown to require both eIF4F and

Downloaded from https://academic.oup.com/nar/article-abstract/41/1/586/1159551 by guest on 08 May 2020

PABP in cell extracts (6,16). We thus wanted to test whether this is also the case in RRL. To this end, we tested a combination of proteins that cleave either PABP or eIF4G or both (Figure 3). We found that PABP and eIF4G are both required but this is not due to their physical interaction. Rather we observed that an RNA binding motif of eIF4G implicated in scanning may be important. We thus tested whether the composition of the 5′-UTR, which is known to modulate ribosomal scanning, could also exert an effect on RISC activity (Figure 4). Although we did not find any linear correlation between 5′-UTR structure and the magnitude of miRNA repression, we observed strong variations among the different 5′-UTR tested. This simply indicates a strong relationship between the composition of the 5′-UTR and the level of repression by miRNAs. Since the 5′-UTR controls translation initiation in eukaryotes both by modulating ribosomal binding and scanning (61), we then wanted to investigate further which of these two steps was involved in the repression mediated by miRNAs.

For this, we used an experimental approach consisting of testing the EMCV and PV IRESes that are known to bind and recruit the ribosome in a similar manner but are very different in terms of ribosome scanning (62). Interestingly, we found that miR-451 massively repressed PV-driven translation with only marginal effects on EMCV (Figure 5), suggesting that interference did not occur at the ribosome binding step but rather during ribosome scanning. Finally, the use of pestivirus and pestivirus-like IRESes confirmed the lack of miRNA repression in the absence of ribosomal scanning despite the physical presence of the poly (A) tail (Figure 6).

Although our results show the implication of ribosomal scanning and the involvement of both PABP and eIF4G in this mechanism, we are still lacking the exact molecular mechanistic. In a recent report by Zekri *et al.* (28), *Drosophila* GW182 (a RISC associated factor) was shown to bind PABP and to impair its interaction with eIF4G therefore disrupting the closed-loop structure and inducing translation inhibition. While this work was in progress, Fukaya and Tomari (37) showed by using a Drosophila based *in vitro* system that the PABP was neither required for translational repression nor deadenylation. Our data show that, both eIF4G and PABP are required for miRNA-mediated inhibition (Figure 3) but this would not be due to their physical interaction. Consistent with this is the fact that PABP cleavage mediated by 3C or HIV-2 protease does not separate the eIF4G binding domain from poly(A) binding activity (46). Indeed, both eIF4G and poly(A) interact specifically with the N-terminal part of PABP, while proteases rather cleave the C-terminal domain (46). Interestingly, PABP cleavage by HRV 3C protease has been shown to eliminate its interaction with other factors implicated in translation, such as Paip1, Paip2, eRF3 and eIF4B (46,63,64). Strikingly, PAM2 domain of GW182 has also been shown to interact with the C-terminal domain of PABP (6,28,65). GW182 may thus interfere with PABP association with one of those important translation factors. The understanding of how miRNAs and GW182 can interfere with PABP function and ribosomal scanning will be a very interesting challenge for future work.

SUPPLEMENTARY DATA

Supplementary Data are available at NAR Online: Supplementary Figures 1–3.

ACKNOWLEDGEMENTS

We would like to thank S. Morley for PABP and eIF4G antibodies. We thank the NIH for the HIV-2 protease. We thank Dr Lisa O. Roberts for the kind gift of the AEV and SVV IRES constructs, Dr Martin Bushell for pET15b-PABP plasmid and Dr C. Fraser for the gift of eIF4G. We also thank Dr H. Ougham (Aberystwyth University, UK) for providing L- and D-MDMP. Finally, we thank Pr Melissa Moore for critical reading of the article.

FUNDING

ANRS; ANR; Ministère de la Recherche et de la Technologie (to E.P.R.); Fondation pour la Recherche Medicale (FRM) fellowships (to E.P.R. and T.L.); Région Rhône-Alpes fellowship (to T.L.); Conicyt-Chile fellowship (to R.S.R.); Agence Nationale de Recherche sur le SIDA et les Hepatites Virales fellowship (to R.S.R.); Becas Chile/Conicyt fellowship (to P.S.R.). Funding for open access charge: INSERM.

Conflict of interest statement. None declared.

REFERENCES

1. Bartel,D.P. (2009) MicroRNAs: target recognition and regulatory functions. *Cell*, **136**, 215–233.
2. Friedman,R.C., Farh,K.K.-H., Burge,C.B. and Bartel,D.P. (2009) Most mammalian mRNAs are conserved targets of microRNAs. *Genome Res.*, **19**, 92–105.
3. Bazzini,A.A., Lee,M.T. and Giraldez,A.J. (2012) Ribosome profiling shows that miR-430 reduces translation before causing mRNA decay in zebrafish. *Science*, **336**, 233–237.
4. Bethune,J., Artus-Revel,C.G. and Filipowicz,W. (2012) Kinetic analysis reveals successive steps leading to miRNA-mediated silencing in mammalian cells. *EMBO Rep.*, **13**, 716–723.
5. Djuranovic,S., Nahvi,A. and Green,R. (2012) miRNA-mediated gene silencing by translational repression followed by mRNA deadenylation and decay. *Science*, **336**, 237–240.
6. Fabian,M.R., Mathonnet,G., Sundermeier,T., Mathys,H., Zipprich,J.T., Svitkin,Y.V., Rivas,F., Jinek,M., Wohlschlegel,J., Doudna,J.A. *et al.* (2009) Mammalian miRNA RISC recruits CAF1 and PABP to affect PABP-dependent deadenylation. *Mol. Cell*, **35**, 868–880.
7. Zdanowicz,A., Thermann,R., Kowalska,J., Jemielity,J., Duncan,K., Preiss,T., Darzynkiewicz,E. and Hentze,M.W. (2009) Drosophila miR2 primarily targets the m7GpppN cap structure for translational repression. *Mol. Cell*, **35**, 881–888.
8. Kim,J., Krichevsky,A., Grad,Y., Hayes,G.D., Kosik,K.S., Church,G.M. and Ruvkun,G. (2004) Identification of many microRNAs that copurify with polyribosomes in mammalian neurons. *Proc. Natl Acad. Sci. USA*, **101**, 360–365.
9. Maroney,P.A., Yu,Y., Fisher,J. and Nilsen,T.W. (2006) Evidence that microRNAs are associated with translating messenger RNAs in human cells. *Nat. Struct. Mol. Biol.*, **13**, 1102–1107.

Downloaded from https://academic.oup.com/nar/article-abstract/41/1/586/1159551 by guest on 08 May 2020

10. Nelson,P.T., Hatzigeorgiou,A.G. and Mourelatos,Z. (2004) miRNP: mRNA association in polyribosomes in a human neuronal cell line. *RNA*, **10**, 387–394.
11. Nottrott,S., Simard,M.J. and Richter,J.D. (2006) Human let-7a miRNA blocks protein production on actively translating polyribosomes. *Nat Struct. Mol. Biol.*, **13**, 1108–1114.
12. Petersen,C.P., Bordeleau,M.-E., Pelletier,J. and Sharp,P.A. (2006) Short RNAs repress translation after initiation in mammalian cells. *Mol. Cell*, **21**, 533–542.
13. Chendrimada,T.P., Finn,K.J., Ji,X., Baillat,D., Gregory,R.I., Liebhaber,S.A., Pasquinelli,A.E. and Shiekhattar,R. (2007) MicroRNA silencing through RISC recruitment of eIF6. *Nature*, **447**, 823–828.
14. Humphreys,D.T., Westman,B.J., Martin,D.I. and Preiss,T. (2005) MicroRNAs control translation initiation by inhibiting eukaryotic initiation factor 4E/cap and poly(A) tail function. *Proc. Natl Acad. Sci. USA*, **102**, 16961–16966.
15. Iwasaki,S., Kawamata,T. and Tomari,Y. (2009) Drosophila argonaute1 and argonaute2 employ distinct mechanisms for translational repression. *Mol. Cell*, **34**, 58–67.
16. Mathonnet,G., Fabian,M.R., Svitkin,Y.V., Parsyan,A., Huck,L., Murata,T., Biffo,S., Merrick,W.C., Darzynkiewicz,E., Pillai,R.S. *et al.* (2007) MicroRNA inhibition of translation initiation in vitro by targeting the cap-binding complex eIF4F. *Science*, **317**, 1764–1767.
17. Pillai,R.S., Bhattacharyya,S.N., Artus,C.G., Zoller,T., Cougot,N., Basyuk,E., Bertrand,E. and Filipowicz,W. (2005) Inhibition of translational initiation by Let-7 MicroRNA in human cells. *Science*, **309**, 1573–1576.
18. Thermann,R. and Hentze,M.W. (2007) Drosophila miR2 induces pseudo-polysomes and inhibits translation initiation. *Nature*, **447**, 875–878.
19. Wang,B., Love,T.M., Call,M.E., Doench,J.G. and Novina,C.D. (2006) Recapitulation of short RNA-directed translational gene silencing in vitro. *Mol. Cell*, **22**, 553–560.
20. Wang,B., Yanez,A. and Novina,C.D. (2008) MicroRNA-repressed mRNAs contain 40S but not 60S components. *Proc. Natl Acad. Sci. USA*, **105**, 5343–5348.
21. Walters,R.W., Bradrick,S.S. and Gromeier,M. (2010) Poly(A)-binding protein modulates mRNA susceptibility to cap-dependent miRNA-mediated repression. *RNA*, **16**, 239–250.
22. Ricci,E.P., Limousin,T., Soto-Rifo,R., Allison,R., Poyry,T., Decimo,D., Jackson,R.J. and Ohlmann,T. (2011) Activation of a microRNA response in trans reveals a new role for poly(A) in translational repression. *Nucleic Acids Res.*, **39**, 5215–5231.
23. Eulalio,A., Huntzinger,E., Nishihara,T., Rehwinkel,J., Fauser,M. and Izaurralde,E. (2009) Deadenylation is a widespread effect of miRNA regulation. *RNA*, **15**, 21–32.
24. Wu,L., Fan,J. and Belasco,J.G. (2006) MicroRNAs direct rapid deadenylation of mRNA. *Proc. Natl Acad. Sci. USA*, **103**, 4034–4039.
25. Braun,J.E., Huntzinger,E., Fauser,M. and Izaurralde,E. (2011) GW182 proteins directly recruit cytoplasmic deadenylase complexes to miRNA targets. *Mol. Cell*, **44**, 120–133.
26. Huntzinger,E., Braun,J.E., Heimstadt,S., Zekri,L. and Izaurralde,E. (2010) Two PABPC1-binding sites in GW182 proteins promote miRNA-mediated gene silencing. *EMBO J.*, **29**, 4146–4160.
27. Jinek,M., Fabian,M.R., Coyle,S.M., Sonenberg,N. and Doudna,J.A. (2010) Structural insights into the human GW182-PABC interaction in microRNA-mediated deadenylation. *Nat. Struct. Mol. Biol.*, **17**, 238–240.
28. Zekri,L., Huntzinger,E., Heimstadt,S. and Izaurralde,E. (2009) The silencing domain of GW182 interacts with PABPC1 to promote translational repression and degradation of microRNA targets and is required for target release. *Mol. Cell. Biol.*, **29**, 6220–6231.
29. Kiriakidou,M., Tan,G.S., Lamprinaki,S., De Planell-Saguer,M., Nelson,P.T. and Mourelatos,Z. (2007) An mRNA m7G cap binding-like motif within human Ago2 represses translation. *Cell*, **129**, 1141–1151.
30. Mishima,Y., Fukao,A., Kishimoto,T., Sakamoto,H., Fujiwara,T. and Inoue,K. (2012) Translational inhibition by deadenylation-independent mechanisms is central to microRNA-mediated silencing in zebrafish. *Proc. Natl Acad. Sci. USA*, **109**, 1104–1109.
31. Moretti,F., Kaiser,C., Zdanowicz-Specht,A. and Hentze,M.W. (2012) PABP and the poly(A) tail augment microRNA repression by facilitated miRISC binding. *Nat. Struct. Mol. Biol.*, **19**, 603–608.
32. Soto Rifo,R., Ricci,E.P., Décimo,D., Moncorgé,O. and Ohlmann,T. (2007) Back to basics: the untreated rabbit reticulocyte lysate as a competitive system to recapitulate cap/poly(A) synergy and the selective advantage of IRES-driven translation. *Nucleic Acids Res.*, **35**, e121.
33. Ohlmann,T. and Jackson,R.J. (1999) The properties of chimeric picornavirus IRESes show that discrimination between internal translation initiation sites is influenced by the identity of the IRES and not just the context of the AUG codon. *RNA*, **5**, 764–778.
34. Fletcher,S.P. and Jackson,R.J. (2002) Pestivirus internal ribosome entry site (IRES) structure and function: elements in the 5′ untranslated region important for IRES function. *J. Virol.*, **76**, 5024–5033.
35. Bakhshesh,M., Groppelli,E., Willcocks,M.M., Royall,E., Belsham,G.J. and Roberts,L.O. (2008) The picornavirus avian encephalomyelitis virus possesses a hepatitis C virus-like internal ribosome entry site element. *J. Virol.*, **82**, 1993–2003.
36. Willcocks,M.M., Locker,N., Gomwalk,Z., Royall,E., Bakhshesh,M., Belsham,G.J., Idamakanti,N., Burroughs,K.D., Reddy,P.S., Hallenbeck,P.L. *et al.* (2011) Structural features of the Seneca Valley virus internal ribosome entry site (IRES) element: a picornavirus with a pestivirus-like IRES. *J. Virol.*, **85**, 4452–4461.
37. Fukaya,T. and Tomari,Y. (2011) PABP is not essential for microRNA-mediated translational repression and deadenylation in vitro. *EMBO J.*, **30**, 4998–5009.
38. Eulalio,A., Huntzinger,E. and Izaurralde,E. (2008) GW182 interaction with Argonaute is essential for miRNA-mediated translational repression and mRNA decay. *Nat. Struct. Mol. Biol.*, **15**, 346–353.
39. Baxter,R., Knell,V.C., Somerville,H.J., Swain,H.M. and Weeks,D.P. (1973) Effect of MDMP on protein synthesis in wheat and bacteria. *Nat. New Biol.*, **243**, 139–142.
40. Gay,A., Thomas,H., Roca,M., James,C., Taylor,J., Rowland,J. and Ougham,H. (2008) Nondestructive analysis of senescence in mesophyll cells by spectral resolution of protein synthesis-dependent pigment metabolism. *New Phytol.*, **179**, 663–674.
41. Jackson,R.J., Hellen,C.U. and Pestova,T.V. (2010) The mechanism of eukaryotic translation initiation and principles of its regulation. *Nat. Rev. Mol. Cell Biol.*, **11**, 113–127.
42. Chakravarty,I., Bagchi,M.K., Roy,R., Banerjee,A.C. and Gupta,N.K. (1985) Protein synthesis in rabbit reticulocytes. Purification and properties of an Mr 80,000 polypeptide (Co-eIF-2A80) with Co-eIF-2A activity. *J. Biol. Chem.*, **260**, 6945–6949.
43. Parsyan,A., Svitkin,Y., Shahbazian,D., Gkogkas,C., Lasko,P., Merrick,W.C. and Sonenberg,N. (2011) mRNA helicases: the tacticians of translational control. *Nat. Rev. Mol. Cell Biol.*, **12**, 235–245.
44. Pause,A., Methot,N., Svitkin,Y., Merrick,W.C. and Sonenberg,N. (1994) Dominant negative mutants of mammalian translation initiation factor eIF-4A define a critical role for eIF-4F in cap-dependent and cap-independent initiation of translation. *EMBO J.*, **13**, 1205–1215.
45. Yoda,M., Kawamata,T., Paroo,Z., Ye,X., Iwasaki,S., Liu,Q. and Tomari,Y. (2009) ATP-dependent human RISC assembly pathways. *Nat. Struct. Mol. Biol.*, **17**, 17–23.
46. Bushell,M., Wood,W., Carpenter,G., Pain,V.M., Morley,S.J. and Clemens,M.J. (2001) Disruption of the interaction of mammalian protein synthesis eukaryotic initiation factor 4B with the poly(A)-binding protein by caspase- and viral protease-mediated cleavages. *J. Biol. Chem.*, **276**, 23922–23928.
47. Imataka,H., Gradi,A. and Sonenberg,N. (1998) A newly identified N-terminal amino acid sequence of human eIF4G binds poly(A)-binding protein and functions in poly(A)-dependent translation. *EMBO J.*, **17**, 7480–7489.

Downloaded from https://academic.oup.com/nar/article-abstract/41/1/586/1159551 by guest on 08 May 2020

48. Ohlmann,T., Prevot,D., Decimo,D., Roux,F., Garin,J., Morley,S.J. and Darlix,J.L. (2002) In vitro cleavage of eIF4GI but not eIF4GII by HIV-1 protease and its effects on translation in the rabbit reticulocyte lysate system. *J. Mol. Biol.*, **318**, 9–20.
49. Prevot,D., Decimo,D., Herbreteau,C.H., Roux,F., Garin,J., Darlix,J.L. and Ohlmann,T. (2003) Characterization of a novel RNA-binding region of eIF4GI critical for ribosomal scanning. *EMBO J.*, **22**, 1909–1921.
50. Castello,A., Franco,D., Moral-Lopez,P., Berlanga,J.J., Alvarez,E., Wimmer,E. and Carrasco,L. (2009) HIV-1 protease inhibits Cap- and poly(A)-dependent translation upon eIF4GI and PABP cleavage. *PLoS One*, **4**, e7997.
51. Hinnebusch,A.G. (2011) Molecular mechanism of scanning and start codon selection in eukaryotes. *Microbiol. Mol. Biol. Rev.*, **75**, 434–467, first page of table of contents.
52. Pisareva,V.P., Pisarev,A.V., Komar,A.A., Hellen,C.U. and Pestova,T.V. (2008) Translation initiation on mammalian mRNAs with structured 5′UTRs requires DExH-box protein DHX29. *Cell*, **135**, 1237–1250.
53. Soto-Rifo,R., Rubilar,P.S., Limousin,T., de Breyne,S., Decimo,D. and Ohlmann,T. (2012) DEAD-box protein DDX3 associates with eIF4F to promote translation of selected mRNAs. *EMBO J.*, **31**, 3745–3756.
54. Jackson,R.J. (2005) Alternative mechanisms of initiating translation of mammalian mRNAs. *Biochem. Soc. Trans.*, **33**, 1231–1241.
55. Ziegler,E., Borman,A.M., Kirchweger,R., Skern,T. and Kean,K.M. (1995) Foot-and-mouth disease virus Lb proteinase can stimulate rhinovirus and enterovirus IRES-driven translation and cleave several proteins of cellular and viral origin. *J. Virol.*, **69**, 3465–3474.
56. Pestova,T.V., Shatsky,I.N., Fletcher,S.P., Jackson,R.J. and Hellen,C.U. (1998) A prokaryotic-like mode of cytoplasmic eukaryotic ribosome binding to the initiation codon during internal translation initiation of hepatitis C and classical swine fever virus RNAs. *Genes Dev.*, **12**, 67–83.
57. Wakiyama,M., Takimoto,K., Ohara,O. and Yokoyama,S. (2007) Let-7 microRNA-mediated mRNA deadenylation and translational repression in a mammalian cell-free system. *Genes Dev.*, **21**, 1857–1862.
58. Lytle,J.R., Yario,T.A. and Steitz,J.A. (2007) Target mRNAs are repressed as efficiently by microRNA-binding sites in the 5′UTR as in the 3′ UTR. *Proc. Natl Acad. Sci. USA*, **104**, 9667–9672.
59. Kong,Y.W., Cannell,I.G., de Moor,C.H., Hill,K., Garside,P.G., Hamilton,T.L., Meijer,H.A., Dobbyn,H.C., Stoneley,M., Spriggs,K.A. *et al.* (2008) The mechanism of micro-RNA-mediated translation repression is determined by the promoter of the target gene. *Proc. Natl Acad. Sci. USA*, **105**, 8866–8871.
60. Wu,E., Thivierge,C., Flamand,M., Mathonnet,G., Vashisht,A.A., Wohlschlegel,J., Fabian,M.R., Sonenberg,N. and Duchaine,T.F. (2010) Pervasive and cooperative deadenylation of 3′UTRs by embryonic microRNA families. *Mol. Cell*, **40**, 558–570.
61. Jackson,R.J. and Wickens,M. (1997) Translational controls impinging on the 5′-untranslated region and initiation factor proteins. *Curr. Opin. Genet. Dev.*, **7**, 233–241.
62. Jackson,R.J. and Kaminski,A. (1995) Internal initiation of translation in eukaryotes: the picornavirus paradigm and beyond. *RNA*, **1**, 985–1000.
63. Craig,A.W., Haghighat,A., Yu,A.T. and Sonenberg,N. (1998) Interaction of polyadenylate-binding protein with the eIF4G homologue PAIP enhances translation. *Nature*, **392**, 520–523.
64. Khaleghpour,K., Svitkin,Y.V., Craig,A.W., DeMaria,C.T., Deo,R.C., Burley,S.K. and Sonenberg,N. (2001) Translational repression by a novel partner of human poly(A) binding protein, Paip2. *Mol. Cell*, **7**, 205–216.
65. Kozlov,G., Safaee,N., Rosenauer,A. and Gehring,K. (2010) Structural basis of binding of P-body-associated proteins GW182 and ataxin-2 by the Mlle domain of poly(A)-binding protein. *J. Biol. Chem.*, **285**, 13599–13606.

Downloaded from https://academic.oup.com/nar/article-abstract/41/1/586/1159551 by guest on 08 May 2020

4932–4943 *Nucleic Acids Research, 2009, Vol. 37, No. 15* *Published online 15 June 2009*
doi:10.1093/nar/gkp497

Translation of intronless RNAs is strongly stimulated by the Epstein–Barr virus mRNA export factor EB2

Emiliano P. Ricci[1,2,3], Fabrice Mure[1,2,3], Henri Gruffat[1,2,3], Didier Decimo[1,2,3], Cahora Medina-Palazon[1,2,3], Théophile Ohlmann[1,2,3] and Evelyne Manet[1,2,3,*]

[1]INSERM U758, Unité de Virologie Humaine, [2]Ecole Normale Supérieure de Lyon, Lyon F-69007 and [3]IFR128 Biosciences Gerland-Lyon Sud, Lyon F-69364, France

Received November 28, 2008; Revised May 18, 2009; Accepted May 21, 2009

Downloaded from https://academic.oup.com/nar/article-abstract/37/15/4932/2410023 by guest on 08 May 2020

ABSTRACT

The Epstein–Barr virus protein (EB2) allows the nuclear export of a particular subset of early and late viral RNAs derived from intronless genes. EB2 is conserved among most herpesvirus members and its presence is essential for the production of infectious particles. Here we show that, besides its role as a nuclear export factor, EB2 strongly stimulates translation of unspliced mRNAs without affecting overall cellular translation. Interestingly, this effect can be reversed by the addition of an intron within the gene. The spliced mRNA is then efficiently exported and translated even in the absence of EB2. Moreover, we show that EB2 associates with translating ribosomes and increases the proportion of its target RNA in the polyribosomal fraction. Finally, testing of EB2 homolog proteins derived from EBV-related herpesviruses, shows that, even if they play similar roles within the replication cycle of their respective virus, their mechanisms of action are different.

INTRODUCTION

In eukaryotic cells, gene expression is tightly controlled from the biogenesis of messenger RNAs (mRNAs) within the cell nucleus, until their export and translation in the cytoplasm (1). In particular, the control of mRNA translation is a multi-step complex mechanism mediated by a large number of factors. Translation initiation appears to be the rate-limiting and most regulated step of the overall translation mechanism (2,3). Regulation of translation initiation is mediated mostly by initiation factors, which recruit the 40S ribosomal subunit to the 5′ cap of the mRNA, allow scanning to the initiation codon and then the recruitment of the 60S ribosomal subunit (4).

Even though maturation of pre-mRNAs occurs in a different cellular compartment than translation, proteins that participate in the former process can also play a role in the latter. Indeed, translation stimulation of intron-containing genes has been observed in several systems and is linked to proteins that participate either in splicing or in the export of spliced mRNAs (5–12). Among these, the exon junction complex (EJC), which is deposited during splicing and plays an important role in mRNA surveillance, is able to modulate translation of spliced mRNAs through the mTOR pathway (7). Other proteins involved in translation stimulation of spliced mRNAs comprise the Ser-Arg-rich (SR) proteins that play a role not only in pre-mRNA splicing and spliceosome assembly but also in splice-site recognition and selection (13,14). Conversely, recent data have also shown that some of the SR proteins, which shuttle from the nucleus to the cytoplasm together with the spliced mRNA, can be associated with translating ribosomes to stimulate the translation of spliced mRNAs (11,15). This would allow the cell to ensure that only fully spliced RNAs are expressed as opposed to unspliced or incompletely spliced RNAs that could result in translation of aberrant proteins.

Viruses have evolved different mechanisms to efficiently export and translate unspliced RNAs. One example is the constitutive transport element (CTE) present in simple retroviruses, such as the Mason–Pfizner monkey virus (MPMV), which interacts with the TAP/NXF1 export protein and the cellular protein NXT1/p15 to promote

*To whom correspondence should be addressed. Tel: +33 472 728 176; Fax: +33 472 728 137; Email: emanet@ens-lyon.fr
Present address:
Cahora Medina-Palazon, Westmead Institute for Cancer Research, University of Sydney, Westmead Millenium Institute, Westmead, New South Wales 2145, Australia.

The authors wish it to be known that, in their opinion, the first two authors should be regarded as joint First Authors.

© 2009 The Author(s)
This is an Open Access article distributed under the terms of the Creative Commons Attribution Non-Commercial License (http://creativecommons.org/licenses/by-nc/2.0/uk/) which permits unrestricted non-commercial use, distribution, and reproduction in any medium, provided the original work is properly cited.

export and translation of unspliced genomic RNA (15–18). Again, translation stimulation of unspliced RNAs containing the CTE seems to rely on SR proteins such as 9G8 (15). For complex retroviruses, such as lentiviruses, the unspliced genomic RNA is exported by the viral protein Rev which interacts with *cis*-acting sequences located within the envelope coding region of the RNA, allowing export and translation stimulation (19–22).

The Epstein–Barr virus (EBV) early protein EB2 (also known as BMFL1, Mta or SM) shares several features with mRNA export factors. It is able to interact with RNA both *in vitro* and *in vivo* (23–25), it shuttles between the nucleus and the cytoplasm and it allows the cytoplasmic accumulation of unspliced RNAs generated from intronless and intron-containing genes, probably by the recruitment of REF and TAP/NXF1 (24,26–28). EB2 is essential for the production of viral particles and promotes the nuclear export of some early and most late viral mRNAs generated from EBV intronless genes (28). Moreover, like EBV many other herpesviruses code for a protein similar to EB2, i.e. ICP27 from herpes simplex virus type 1 (HSV1) (29–31), UL69 from cytomegalovirus (CMV) (32) ORF57 from Kaposi's sarcoma-associated herpesvirus (KSHV) (33) and ORF57 from herpesvirus saimiri (HVS) (34). All these proteins act as nuclear mRNA export factors but surprisingly their function cannot be *trans*-complemented between each other (27,35).

As cellular mRNA export factors, EB2 shuttles from the nucleus to the cytoplasm, probably associated with its target mRNAs, suggesting that it could also affect their translation. We thus tested the effect of EB2 on translation from an intronless reporter construct coding for the Renilla luciferase. In this system, translation stimulation was measured by analyzing the expression levels of Renilla luciferase normalized to the amount of cytoplasmic mRNAs determined by quantitative PCR. Our results show that EB2 strongly and specifically stimulates translation of intronless mRNAs without affecting overall cellular translation or protein stability. Introduction of an intron in this construct stimulates the efficiency of export and translation of the luciferase mRNA and at the same time abrogates the effect of EB2. Interestingly, the increase in translation of the luciferase mRNA generated from the intronless construct in the presence of EB2, correlates with an increase in the proportion of luciferase mRNA associated with polyribosomes. Moreover, we show that EB2 itself is associated with polyribosomes. Finally, a comparison between EB2 homologs from EBV-related viruses (HSV-1, CMV, KSHV) led us to conclude that their mechanisms of action are different.

MATERIALS AND METHODS

Cell lines and transfections

HeLa and HEK293T cells were grown in Dulbecco's modified Eagle medium supplemented with penicillin, streptomycin and 5% fetal calf serum (Invitrogen). NIH3T3 PKR-deficient cells (36) and NIH3T3 wild-type cells were grown as described for HeLa cells. For experiments using EBV gene-derived constructs, transfections were performed in 100 mm plates using calcium phosphate with 15 μg of total DNA (0.5 μg of pTRE2-Flag.BDLF1, 0.25 μg of pCI-Flag.EB2 and 0.5 μg of pTet-On or pTet-Off expression vectors (Clontech) and pUC18 up to 15 μg). When necessary, doxycyclin was added at a concentration of 1 μg/ml. For experiments using the luciferase reporter plasmids, transfections were carried out in 60 mm plates using Lipofectamine 2000 (Invitrogen) following the manufacturer's protocol. For the metabolic labeling experiments, transfection of HeLa cells with the EB2 expression plasmid was carried out in six-well plates using Lipofectamine 2000 (Invitrogen). The efficiency of transfection was evaluated by transfecting the pEGFP-C1 plasmid (Clontech) in the same conditions and counting the number of green fluorescent cells by FACS. Over 60% of the cells expressed GFP. For polysomal fractionation, HEK293T cells were seeded at 2×10^6 on a 150 mm culture dish 3 days before polysomal fractionation. Forty-eight hours before harvesting, cells were transfected with 1.25 μg of luciferase-coding plasmid together or not with 6.25 μg of pCI-Flag.EB2, using PEI reagent.

Plasmids

The pCI-Flag.EB2 construct has been previously described (28). For pTRE2-Flag.BDLF1, the EBV BDLF1 open reading frame tagged with the Flag epitope was amplified by PCR and cloned into the BamHI and XbaI sites of the pTRE2 expression plasmid (Clontech). The pTet-On vector was supplied by Clontech (Tet-Off and Tet-On gene expression systems). The pcDNA GlobinRen reporter plasmid was constructed by cloning the human β-globin 5′UTR (with the authentic initiation codon) followed by the Renilla luciferase reporter gene, amplified by PCR from the p-Globin Renilla vector (37) into the double digested (XbaI/AflII) pcDNA3.1 expression vector. For the pcDNAIntron-GlobinRen, the sequence corresponding to the intron of the human β-globin gene was amplified by PCR and cloned into the pcDNAGlobinRen vector previously digested by XbaI. pCI-mycORF57 contained the complete ORF57 coding sequence (first exon included) cloned in frame with the myc epitope, in pCI (Promega). The expression plasmid for UL69 (pCMV-UL69) was kindly provided by T. Stamminger (38). The expression plasmid for ICP27 (pCI-FlagICP27) has been previously described (27).

RNA extraction and real-time quantitative PCR (RT-PCR) from cytoplasmic RNAs

Cells were first scraped from the dish and then resuspended in 200 μl of cold RLNa buffer (10 mM Tris–HCl (pH 8), 10 mM NaCl, 3 mM $MgCl_2$, 1 mM DTT, 0.5% NP40 and 10 U/ml of RNaseOUT (Invitrogen). After 5 min incubation on ice, lysed cells were centrifuged for 2 min at 400*g* at 4°C and the supernatant was then recovered. One milliliter of Trizol (Invitrogen) was then added to the supernatant and RNAs were extracted following the Trizol protocol provided by the manufacturer. Cytoplasmic RNAs (1 μg) were treated with RQ1 DNAse (Promega) to avoid DNA contamination and reversed

Downloaded from https://academic.oup.com/nar/article-abstract/37/15/4932/2410023 by guest on 08 May 2020

Table 1. PCR primers used in this study[a]

Primer name	Primer sequence
BDLF1 forward	CAGATTTGAAAGTGGTAGTGTC
BDLF1 reverse	TTATCTTAACCAGCAAGTGGCCG
β-actin forward (Human)	GCTGCGTGTGGCTCCCGAGGAG
β-actin reverse (Human)	ATCTTCATTGTGCTGGGTGCCAG
GAPDH forward (Human)	TCCACCACCCTGTTGCTGTAG
GAPDH reverse (Human)	ACCCACTCCTCCACCTTTGAC
HPRT forward (Mouse)	TCATTATGCCGAGGATTTGGA
HPRT reverse (Mouse)	CAGAGGGCCACAATGTGATG
Renilla forward	AGGTGAAGTTCGTCGTCCAACATTATC
Renilla reverse	GAAACTTCTTGGCACCTTCAACAATAGC
18S rRNA forward (Human)	GTGGAGCGATTTGTCTGGTT
18S rRNA reverse (Human)	CGCTGAGCCAGTCAGTGTAG
28S rRNA forward (Human)	TGGGTTTTAAGCAGGAGGTG
28S rRNA reverse (Human)	AACCTGTCTCACGACGGTCT
U6 forward (Human)	CGCTTCGGCAGCACATATAC
U6 reverse (Human)	AAAATATGGAACGCTTCACGA

[a]Primers for real-time PCR were designed using Beacon designer software (from PREMIER Biosoft).

transcribed with $(dT)_{16}$ and 1 µl of Superscript II enzyme (Invitrogen) in a 20 µl reaction mix at 42°C for 1 h.

PCRs were performed using a *Taq* core kit (Q-Biogen) with a set of specific primer pairs (BDLF1 forward/BDLF1 reverse: Table 1) on various amounts of the RT reaction mixtures (0.05, 0.4, 1 or 2 µl) to have a linearly increasing signal after 25 PCR cycles. The PCR-amplified fragments were then analyzed on 2% agarose gels. We evaluated the endogenous expression of β-actin mRNA by RT-PCR (β-actin forward/β-actin reverse: Table 1). Amplification of a 690-bp DNA fragment corresponding to the β-actin mature mRNA showed that no DNA contamination was present in our RNA preparations. We tested for the presence of U6 snRNA using RT-PCR (U6 forward/U6 reverse: Table 1).

For RT-qPCR, a 20 µl reaction was prepared with 5 µl of template cDNA (1/20 diluted), 10 µl of MESA green SYBR premix (Eurogentec), 0.2 µM of each primer and subjected to amplification using a fluorescence thermocycler (Applied Biosystems 7000 RT-PCR, Foster City, CA) under the following conditions: 10 min at 94°C for initial denaturation, followed by 40 cycles of denaturation at 95°C for 15 s, annealing at 60°C for 15 s and elongation at 72°C for 30 s. This program was followed by a melting curve analysis in order to verify the specificity of the PCR product. Renilla luciferase was amplified in parallel with the housekeeping gene GAPDH (for HeLa cells) or HPRT (for mouse cells) and relative copy numbers of Renilla cDNAs were compared to GAPDH using $x^{-\Delta Ct}$ (where x corresponds to the experimentally calculated amplification efficiency of each primer couple). The primer sequences used in this study (presented in Table 1) were designed using Beacon designer software (from PREMIER Biosoft).

Western blotting analysis

Cells were collected by centrifugation, lysed on ice for 30 min in 100 µl of HNTG buffer (50 mM HEPES pH 7.5; 150 mM NaCl; 1% Triton X-100; 10% glycerol; 1 mM EDTA; 1 mM phenylmethylsulfonyl fluoride). Proteins were separated on 10% sodium dodecyl sulfate-polyacrylamide electrophoresis gels and then transferred to a nitrocellulose membrane by electroblotting (Hybond-ECL; Amersham Biosciences). Membranes were incubated with, respectively, anti-Flag M2 (Sigma) or anti α-tubulin (T5168, Sigma) monoclonal antibodies or an anti-PABP (kind gift from S. Morley) rabbit polyclonal antibody (39). Goat anti-mouse horseradish peroxidase conjugate or goat anti-rabbit horseradish peroxidase conjugate (Amersham) were used at a dilution of 1:5000 as secondary antibodies. For immunoblot detection, the ECL system (Amersham) was used.

Luciferase assays

Renilla activity from transfected cells was measured in a Veritas™ Luminometer (Turner Biosystems) using the Renilla luciferase assay system (Promega Madison Co). Luciferase activity was measured for identical amounts of total protein as evaluated by Bradford assay.

Polyribosome fractionation

Polyribosome fractionation was performed essentially as described previously (40,41). Forty-eight hours after transfection, HEK293T cells were treated with 100 µg/ml cycloheximide at 37°C for 5 min and harvested by scraping from the plate. In some experiments, EDTA was added to the cell lysate at a final concentration of 15 mM to disrupt the polysomes. The gradient was collected from the top using a Piston Gradient Fractionator (BioComp, New Brunswick, Canada) with concomitant measurement of the absorbance at 254 nm using an AKTA purifier (GE Healthcare, Amersham Biosciences, Piscataway, NJ) coupled to a fraction collector. For western blotting, 20 µl of each fraction were separated on 12% sodium dodecyl sulfate-polyacrylamide electrophoresis gels and then transferred to a PVDF membrane (Amersham biosciences) by electroblotting. The membrane was then incubated with various antibodies as described above in the 'western blotting analysis' section. RNA extraction was performed as described (15). RNAs were then reverse transcribed and analyzed by quantitative PCR as described above.

RESULTS

EB2 stimulates protein expression from EBV-derived mRNAs

It has been shown that the EBV-encoded viral protein EB2 acts as a nuclear export factor for a particular subset of mRNAs generated from intronless genes and for some unspliced mRNAs derived from intron-containing genes (24,26–28). However, although EB2 probably shuttles from the nucleus to the cytoplasm together with the exported RNA, the effect of EB2 on mRNA translation has never been reported. This prompted us to test whether expression of EB2 could have an influence on translation of its target viral mRNAs. We thus tested the effect of EB2 on translation of an EBV-encoded mRNA whose cytoplasmic accumulation depends on EB2. In order to control

Downloaded from https://academic.oup.com/nar/article-abstract/37/15/4932/2410023 by guest on 08 May 2020

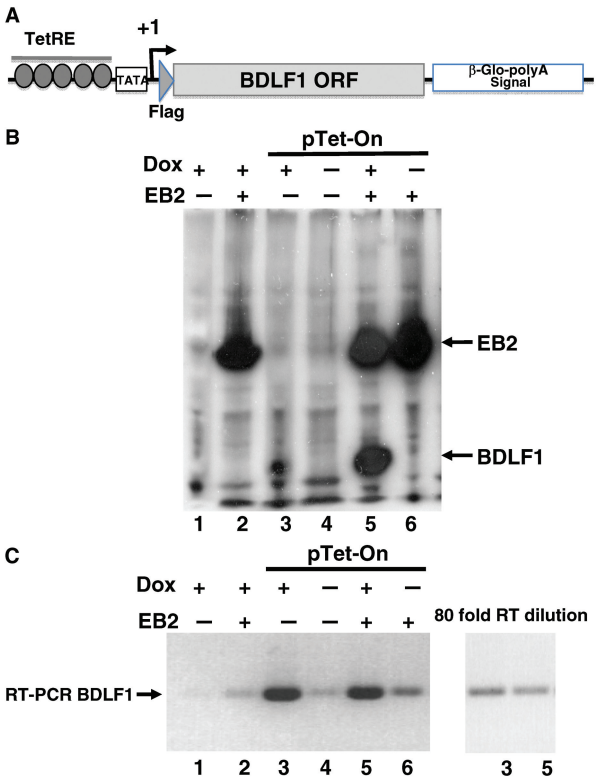

Figure 1. EB2 stimulates expression of the late EBV viral protein BDLF1. (**A**) Schematic representation of the BDLFI-encoding construct pTRE2-Flag-BDLF1. (**B**) Western analysis of Flag-BDLF1 expression in HeLa cells transfected with pTRE2-Flag-BDLF1, together with pTet-On and an expression plasmid for Flag-EB2 (pCI-FEB2) as indicated in the figure. Doxycycline was added as indicated. The M2 anti-Flag MAb was used to visualize both Flag-BDLF1 and Flag-EB2 proteins. (**C**) Quantification of the BDLF1 cytoplasmic RNA by semi-quantitative RT-PCR in HeLa cells transfected as described above.

transcription of the target mRNA, we used the Tet-On gene expression system (Clontech) to express the EBV BDLF1 late mRNA (Figure 1A). For this, the pTRE2-Flag-BDLF1 plasmid was transfected into HeLa cells together with the pTet-On vector (Clontech) and with or without the EB2 expression plasmid. Expression of EB2 and the BDLF1 protein was then monitored by western blotting using an anti-Flag antibody (Figure 1B). The amount of cytoplasmic BDLF1 mRNAs was quantified by semi-quantitative RT-PCR (Figure 1C). In cells cotransfected with the BDLF1 reporter plasmid and the pTet-On vector, in the absence of doxycycline, no BDLF1 protein was detected (Figure 1B, lane 4) and only a low amount of BDLF1 mRNAs were detected by RT-PCR (Figure 1C, lane 4). In these conditions, the expression of EB2 enhanced the cytoplasmic accumulation of the corresponding BDLF1 mRNA (Figure 1C, lane 6) but again no BDLF1 protein was detected (Figure 1B, lane 6). When doxycycline was added, the transcription of BDLF1 mRNAs was strongly stimulated (Figure 1C, lane 3) although only low levels of BDLF1 protein were detected by western blot in the absence of EB2 (Figure 1B, lane 3). However, in the presence of EB2 there was a large increase in the amount of BDLF1 protein expressed (Figure 1B, lane 5) although the amount of BDLF1 mRNA detected in the cytoplasm was comparable to that in the absence of EB2 (Figure 1C, compare lanes 3 and 5). Indeed, in these conditions, transcription of BDLF1 triggered by doxycycline was so strong that it appeared to compensate for the otherwise poor cytoplasmic accumulation observed in the absence of EB2. This allowed us to focus just on the effect of EB2 on BDLF1 translation without introducing a bias with the amount of mRNA. Finally, upon addition of doxycycline, only a weak signal corresponding to the BDLF1 mRNA expression was detected by RT-PCR in the absence or presence of EB2 (Figure 1C, lanes 1 and 2) and no BDLF1 protein expression was detected (Figure 1B, lanes 1 and 2) thus ruling out any non-specific effect of doxyxycline on BDLF1 expression in the absence of the pTet-On vector. Essentially similar results were obtained using the Tet-Off system for which transcription of BDLF1 was triggered by the absence of doxycycline (data not shown).

These results strongly suggest that EB2 is able to stimulate protein expression from EBV-derived mRNAs.

EB2 stimulates both export and translation independently of an EBV-specific sequence without affecting global mRNA translation

In order to quantify the relative effects of EB2 on mRNA export and translation we designed a reporter construct containing the 5′UTR of the human β-Globin gene followed by the Renilla luciferase coding region under the control of the cytomegalovirus (CMV) immediate early promoter (Figure 2A). It is important to note that this construct does not contain any EBV-related sequence. This construct was cotransfected together with the EB2 expression vector in HeLa cells and total luciferase activity was analyzed 24 h after transfection (Figure 2D, *top panel*), while expression of EB2 was measured by western blotting (Figure 2B). Cytoplasmic RNAs were extracted and we first quantified the amount of U6 snRNA in order to make sure that our cytoplasmic fractions were not contaminated by nuclear material (Figure 2C). Then cytoplasmic luciferase RNAs were quantified by relative quantitative RT-PCR using the housekeeping gene GAPDH as an internal control (Supplementary Figure 1). Interestingly, EB2 had no effect on GAPDH mRNA export thus ruling out any bias in the relative quantification of luciferase-coding mRNAs. As expected, expression of EB2 promoted the cytoplasmic accumulation of luciferase-coding RNAs in a dose-dependent manner (Figure 2D, *middle panel*) thus leading to a stimulation of luciferase expression (Figure 2D, *top panel*). The luciferase activity measured in each assay was then normalized to the amount of luciferase cytoplasmic RNAs. This gives an exact measure of the luciferase activity per RNA molecule, and thus can be considered as a quantitative representation of the translation rate. Interestingly, using this quantification we found that an average 7-fold stimulation of luciferase mRNA translation in the presence of EB2 was observed (Figure 2D, *bottom panel*).

Downloaded from https://academic.oup.com/nar/article-abstract/37/15/4932/2410023 by guest on 08 May 2020

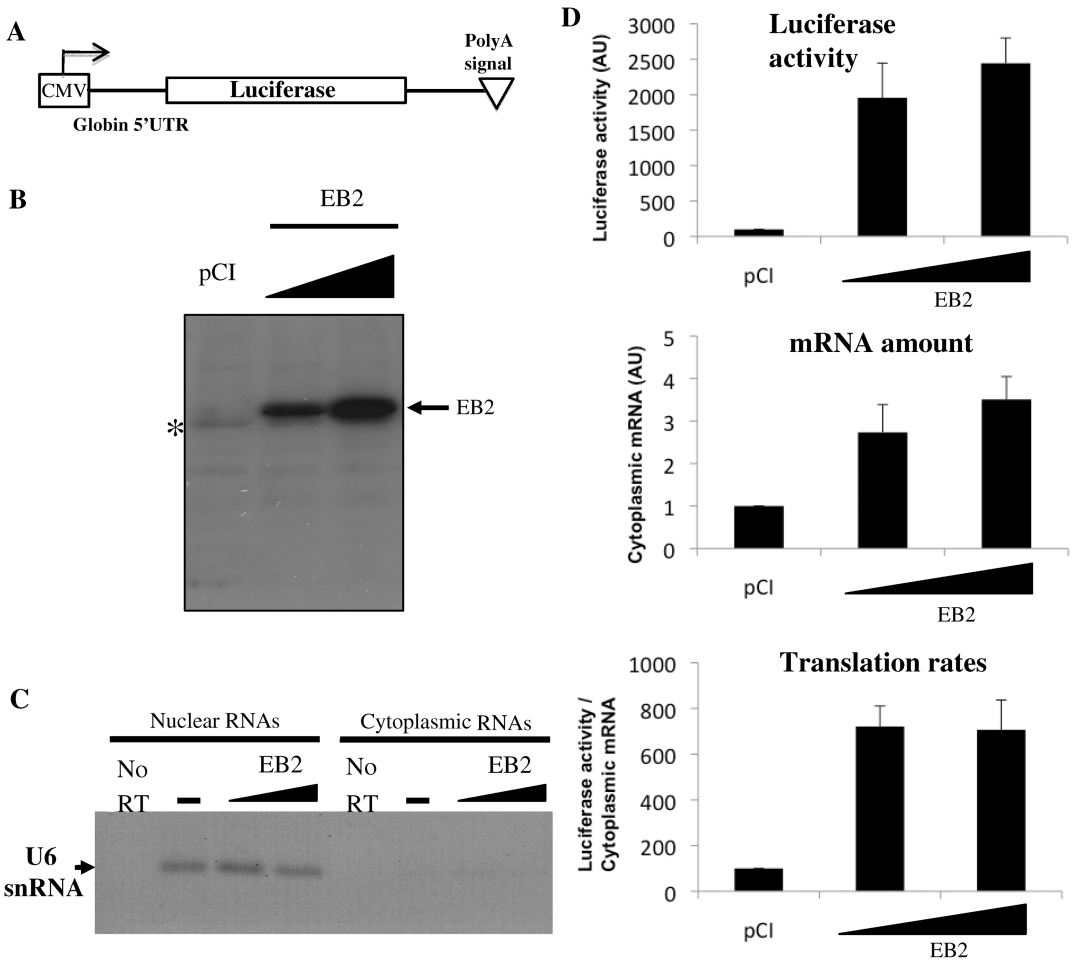

Figure 2. EB2 stimulates expression of a Renilla luciferase intronless gene at the translational level, independently of any viral-derived sequence. (**A**) Schematic representation of the luciferase intronless coding vector used in this study (pcDNAGlobinRen) showing positions of the CMV promoter and BGH polyadenylation signal. (**B**) Immunoblot of HeLa cells cotransfected with pcDNAGlobinRen together with the empty pCI vector or increasing amounts of the FlagEB2-encoding plasmid, pCI-FlagEB2 (250 and 500 ng). The M2 anti-Flag MAb was used to visualize Flag-EB2. Asterisk denotes an unspecific band detected by the M2 anti-Flag antibody. (**C**) Quantification of the amount of U6 snRNA present respectively in the nuclear and cytoplasmic fractions of cellular extracts used in D. U6 snRNA was amplified by RT-PCR using the specific primer set indicated in Table 1, and analyzed on a 2% agarose gel. (**D**) Measure of luciferase activity and quantification of cytoplasmic luciferase-encoding mRNAs by quantitative RT-PCR using GAPDH as an internal control. Total luciferase activity was measured 24 h post-transfection (top panel) and the amount of cytoplasmic luciferase coding mRNAs was quantified (middle panel). Translational efficiency (bottom panel) was calculated by normalizing the total luciferase activity by reference to the amount of cytoplasmic luciferase mRNA. AU: arbitrary units.

To test any impact EB2 could have on the stability of the neosynthesized luciferase protein we analyzed the stability of the luciferase protein in the absence and presence of EB2. For this, we blocked cellular translation by adding cycloheximide and measured luciferase decay activity over time on cells expressing, or not, EB2. As shown in Figure 3A, EB2 did not affect the stability of the Renilla luciferase protein, which had a 30-min half-life both in the absence and presence of EB2.

Furthermore, the lack of EBV-derived sequences on the luciferase reporter construct prompted us to test the effect of EB2 on global cellular mRNA translation. We thus performed a metabolic labeling of cells expressing (or not) EB2 (Figure 3B). For this, cells were pulsed in the presence of radiolabeled methionine for 30 min. Cells were then lysed and proteins resolved on SDS–PAGE to quantify the overall cellular translation rates. As shown in Figure 3B, we did not detect any significant difference in translation rates between cells expressing EB2 and those not expressing EB2.

We also wanted to exclude the possibility that translation stimulation driven by EB2 depends on protein kinase R (PKR). PKR is the principal cellular factor involved in the interferon-mediated inhibition of viral translation. This kinase is activated by double-stranded RNA and this activation leads to the phosphorylation of initiation factor eIF2α, thus inhibiting translation initiation of all cellular and viral RNAs (42,43). We thus monitored luciferase translation both in NIH3T3 PKR-deficient cells (36) and wt NIH3T3 in the presence or absence of EB2. We found that EB2 was able to stimulate translation of luciferase coding mRNAs even in the absence of PKR (Supplementary Data Figure 2), which argues for a mechanism of translation stimulation independent of the PKR pathway.

Finally, to rule out the possibility that translation rates were affected by the amount of cytoplasmic mRNAs, thus

Downloaded from https://academic.oup.com/nar/article-abstract/37/15/4932/2410023 by guest on 08 May 2020

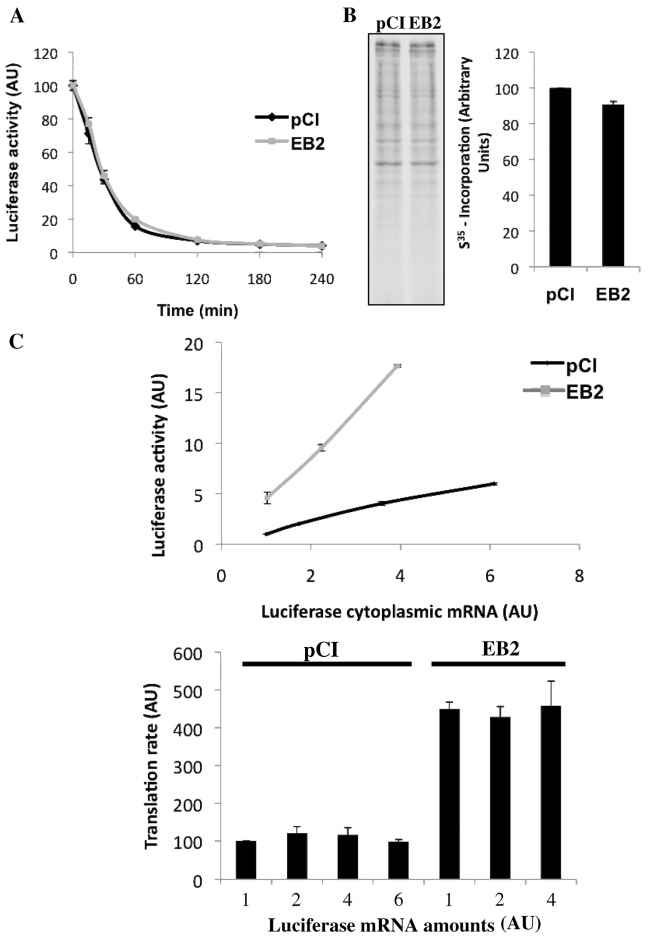

Figure 3. EB2 does not affect protein stability or global cellular mRNA translation and its effect on translation is independent of the amount of cytoplasmic luciferase coding mRNA. (**A**) Time-lapse measure of total luciferase activity from HeLa cells mock transfected (pCI) or transfected with an EB2 expression vector (pCI-FlagEB2) (250 ng) after addition of cycloheximide to block translation. Luciferase activity was measured 0, 15, 30, 60, 120, 180 and 240 min after addition of cycloheximide to the cell medium. (**B**) Metabolic labeling of HeLa cells mock transfected (pCI) or transfected with the EB2-encoding plasmid (250 ng), using ^{35}S-labeled methionine. After a 30-min pulse labeling, cells were lyzed and total cellular proteins resolved on 12% SDS-PAGE. Total translation was quantified by phosphorimaging using a Fujifilm FLA5100. (**C**) Top panel: Luciferase activity was plotted against the amount of cytoplasmic luciferase coding mRNAs in HeLa cells transfected with increasing amounts of luciferase-encoding plasmid in the absence (pCI) or presence (pCI-FlagEB2) of EB2 (250 and 500 ng). Bottom panel: Translation rates per unit of luciferase-encoding mRNAs (calculated by normalizing luciferase activity by reference to the amount of cytoplasmic luciferase-encoding mRNAs) in HeLa cells transfected with increasing amounts of luciferase-encoding plasmid in the absence or presence of EB2 expression plasmid. AU: arbitrary units.

leading to a stimulation of translation which would be independent of EB2, we transfected increasing amounts of luciferase expression vector in HeLa cells expressing, or not, EB2 (Figure 3C). As EB2 expression leads to a 4–5-fold increase of mRNA levels in the cytoplasm, it was of interest to test if increasing the amount of luciferase mRNAs in the absence of EB2 could lead to a stimulation of translation. For this, we measured luciferase translation rates (luciferase activity/amount of luciferase mRNA) for increasing amounts of cytoplasmic mRNAs either in the presence or absence of EB2 (Figure 3C). As presented in the *top panel*, luciferase expression increased proportionally with the amount of cytoplasmic mRNAs, both in the presence and absence of EB2. However, when luciferase activity was normalized to the amount of cytoplasmic mRNAs (which corresponds to the translation rate per arbitrary unit of mRNA) there was no significant change in luciferase translation rates for increasing amounts of cytoplasmic luciferase mRNAs in control (pCI) and EB2-expressing cells (*bottom panel*). Nevertheless, translation rates in the presence of EB2 were systematically 4–5-fold more than those in the absence of EB2, and this for identical mRNA amounts measured in the cytoplasm of the cells.

Taken together, these results show that EB2 stimulates translation of mRNAs without affecting the stability of the neosynthesized protein. Interestingly, EB2 expression does not affect global mRNA translation. Moreover, translation stimulation does not depend on the amount of cytoplasmic mRNA available for translation.

Addition of an intron within the reporter construct impairs translation stimulation driven by EB2

Our results show that EB2 is able to stimulate translation of viral genes and that of a non-related reporter gene without affecting global cellular translation. Consequently, we focused on understanding the lack of an effect of EB2 on cellular mRNA translation. Interestingly, EB2 has been shown to specifically stimulate the nuclear export of mRNA generated from intronless genes (23). This prompted us to test the translation of an mRNA generated from an intron-containing gene in the presence of EB2. We have thus introduced the β-globin intron within the 5′UTR of the luciferase reporter gene (Figure 4A). In order to test the efficiency of splicing of the corresponding mRNA, an RT-PCR from cytoplasmic mRNAs was performed using a forward and reverse primer flanking the intron (Figure 4B). We observed that transfection of the intronless construct in HeLa cells led to the expression of an unspliced mRNA which, upon RT-PCR, yielded a band of the same size to that from the control PCR, performed directly using the DNA plasmid as a template (Figure 4B, lanes 2, 3 and 4). On the contrary, transfection of the intron-containing construct led to the expression of an mRNA which, upon RT-PCR, yielded a band slightly longer than that of the intronless mRNA, but shorter than that of the control PCR obtained from the intron-containing DNA plasmid (Figure 4B, lanes 5–7). This band corresponds to the spliced form of the luciferase-coding mRNA. Thus the mRNA transcribed from this intron-containing reporter gene was efficiently spliced both in the presence or absence of EB2.

We then quantified the exact amount of cytoplasmic luciferase mRNA by quantitative RT-PCR and measured the corresponding luciferase activities (Supplementary Figure 3). When translation rates were calculated by normalizing the luciferase activity to the amount of

Downloaded from https://academic.oup.com/nar/article-abstract/37/15/4932/2410023 by guest on 08 May 2020

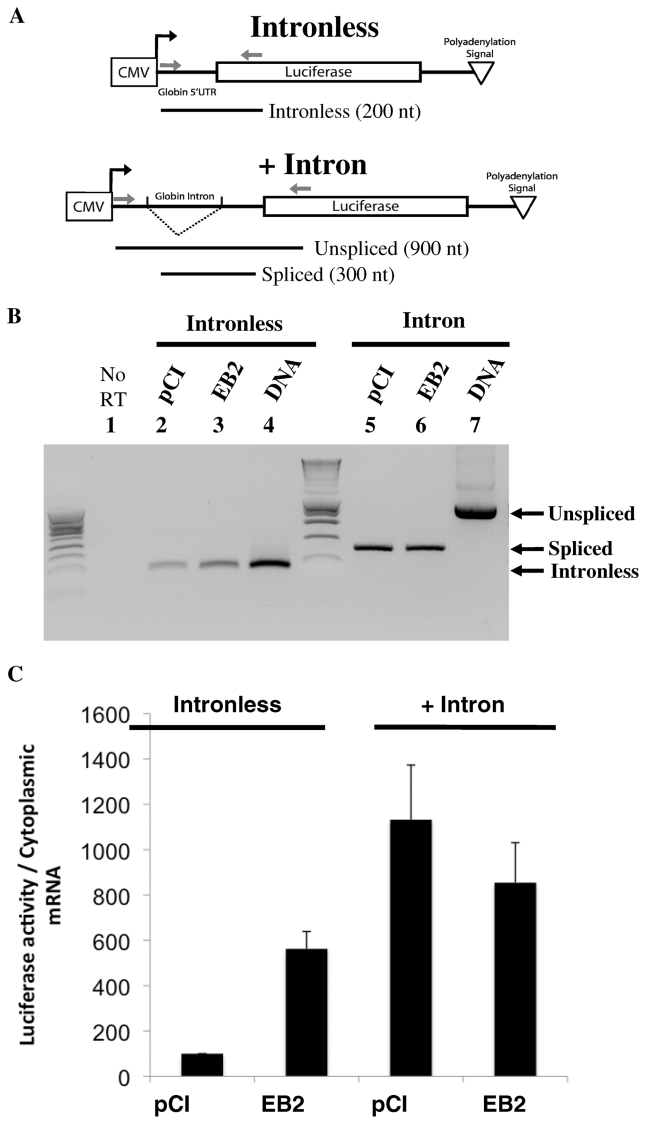

Figure 4. Translation stimulation does not occur with spliced mRNAs. (**A**) Schematic representation of the intronless (pcDNAGlobinRen) and the intron-containing (pcDNAIntronGlobinRen) vectors encoding the Renilla luciferase showing positions of the human β-globin intron within the 5′UTR of the luciferase construct (gray arrows correspond to positions of the PCR primers used to test efficient splicing of the intron). (**B**) RT-PCR (using primers shown in A) from cells cotransfected with pcDNAGlobinRen and pCI or the EB2-encoding plasmid pCI-FlagEB2 (lanes 2 and 3) or from cells cotransfected with pcDNAIntronGlobinRen and pCI or pCI-FlagEB2 (lanes 5 and 6), or directly from the purified DNA vector (lanes 4 and 7). (**C**) Luciferase activity normalized by reference to the amount of cytoplasmic luciferase-encoding mRNAs from HeLa cells cotransfected with pcDNAGlobinRen and pCI or pCI-FlagEB2, or pcDNAIntronGlobinRen and pCI or pCI-FlagEB2. The amount of luciferase-encoding mRNAs was monitored by quantitative RT-PCR.

luciferase-coding mRNA (Figure 4C), we observed a 10-fold more efficient translation of the spliced mRNA compared to unspliced in the absence of EB2. As expected, in the presence of EB2 the translation rate of the unspliced mRNA was increased by a factor 6. However, expression of EB2 did not further stimulate translation of the spliced luciferase mRNA but rather led to a mild inhibition. It is noteworthy, that we also observed an inhibitory effect of EB2 on the accumulation of luciferase mRNA generated from the intron-containing construct (Supplementary Figure 3) which corroborates previously published data from Ruvolo *et al.* (44).

These results indicate that EB2 specifically stimulates translation of intronless mRNAs without significantly affecting translation of spliced mRNAs.

EB2 co-sediments with polyribosomes and increases the utilization of reporter mRNA by the translation machinery

To determine whether EB2 is associated with the translation machinery and to find out whether it increases the association of its target mRNAs with polyribosomes, we performed sucrose gradient analysis to separate polyribosomes from monoribosomes and uncomplexed ribosomal subunits. HEK293T cells were transfected with pcDNAIntron-GlobinRen alone, pcDNAGlobinRen alone or pcDNAGlobinRen together with pCI-Flag.EB2. Cell extracts were prepared and fractionated on 10–50% sucrose gradients and fractions were first analyzed by western blotting. An example of the UV absorbance profile of the gradients is shown in Figure 5A and the corresponding 18S and 28S RNA profile, determined by RT-PCR, in Figure 5B. UV absorbance and the 18S/28S RNA profiles from all gradients were very similar. The polyribosome distribution of EB2 was compared with that of PABP, a general translation factor for polyA+ mRNA (45,46) (Figure 5A). As expected, PABP was present across the gradient from mRNPs to polyribosomal fractions. Interestingly, EB2 cosedimented with the 80S ribosome but was also found in the lighter polysomal fractions. As a control, α-tubulin was only found associated with the uncomplexed ribosomal subunit fractions. Furthermore, treatment of cytoplasmic extracts with EDTA, which is known to induce a dissociation of mono- and polyribosomes into ribosomal subunits, induced a redistribution of EB2 to the top of the gradient (Figure 5D and E).

We then analyzed the distribution of the reporter mRNAs throughout our sucrose gradients by quantitative RT-PCR (Figure 5C). Interestingly, the proportion of the Renilla luciferase mRNA generated from the intron-less construct, which is found associated with the polyribosomal fractions, is greatly increased in the presence of EB2 (compare the *middle* and *top panels*). Furthermore, in the latter case, the profile of repartition of the Renilla luciferase mRNA throughout the gradient is very similar to that obtained with the luciferase mRNA generated from the intron-containing construct (*bottom panel*). As expected, Renilla luciferase mRNA moved to the lighter fractions of the gradient following EDTA treatment (Figure 5F). Taken together, these data suggest that EB2 directly increases the utilization of its target reporter mRNA by the translation machinery.

EB2 viral homolog proteins exhibit different effects on mRNA generated from intronless genes

Herpesviruses code for EB2 homolog proteins that also serve as viral mRNA export factors. Interestingly, despite

Downloaded from https://academic.oup.com/nar/article-abstract/37/15/4932/2410023 by guest on 08 May 2020

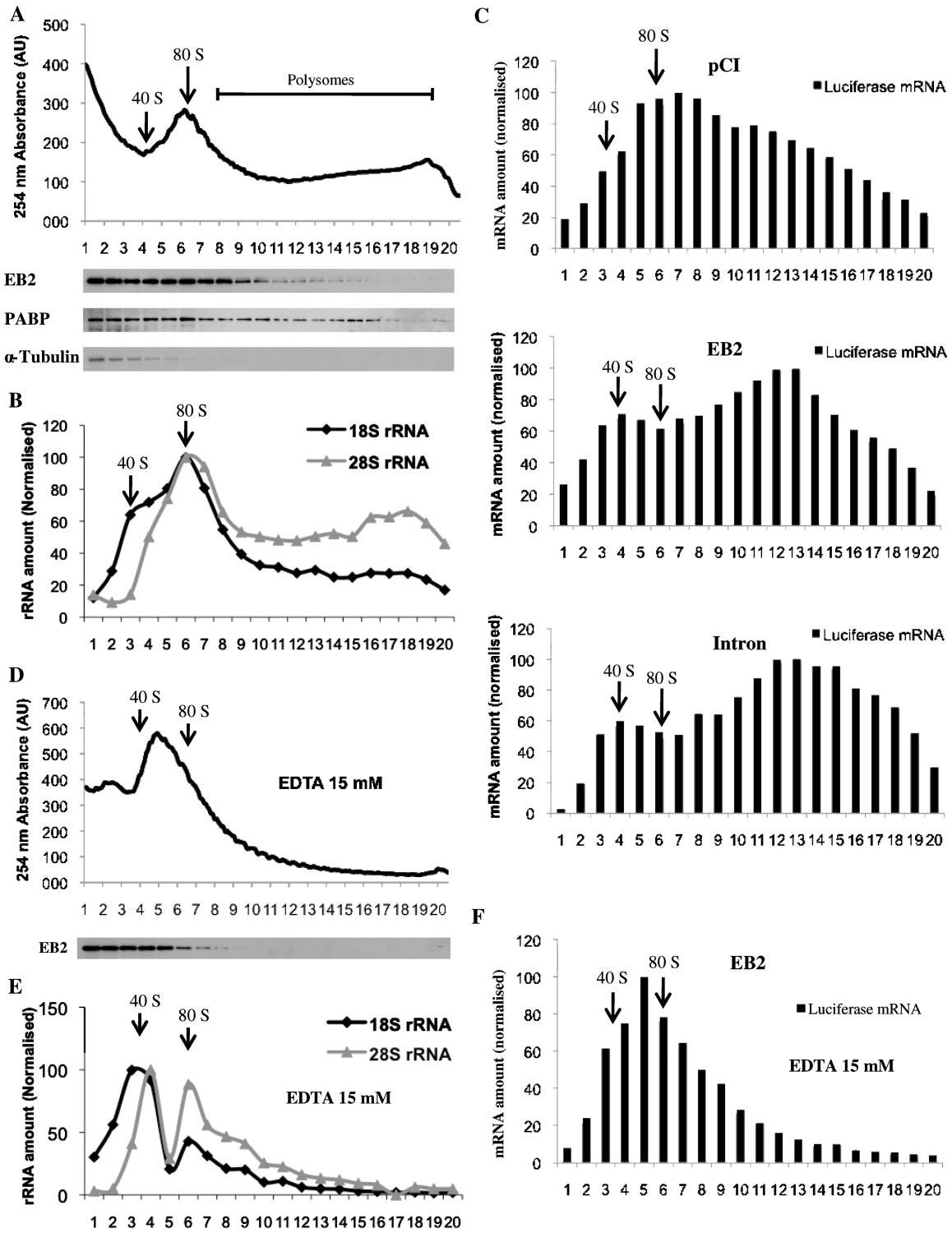

Figure 5. EB2 cosediments with polyribosomes and enhances utilization of its target mRNA by the translation machinery. (**A**, **B** and **C**) Cell cytosolic extracts of HEK293T transfected with pcDNAGlobinRen alone or pcDNAGlobinRen together with pCI-Flag.EB2 or pcDNAIntron-GlobinRen alone, were fractionated across 10–50% sucrose gradients. (A) Fractions from the gradient corresponding to HEK293T transfected with pcDNAGlobinRen together with pCI-Flag.EB2 were analyzed by western blotting with antibodies against the Flag epitope to detect Flag.EB2, poly(A)-binding protein (PABP) or α-tubulin. (Top) UV absorbance (254 nm) profile of cytoplasmic ribonucleoprotein complexes. (B) 18S and 28S RNA profile determined by quantitative RT-PCR. (C) Quantification of the Renilla luciferase reporter mRNA fractionated across 10–50% sucrose gradients by quantitative RT-PCR. (Top panel) HEK293T transfected with pcDNAGlobinRen. (Middle panel) HEK293T transfected with pcDNAGlobinRen together with pCI-Flag.EB2. (Bottom panel) HEK293T transfected with pcDNAIntron-GlobinRen. (**D**, **E** and **F**) An EDTA-treated cytoplasmic extract of HEK 293T cells transfected with pcDNAGlobinRen together with pCIF.EB2 was fractionated across a 10–50% sucrose gradients. (D) EB2 is relocalized to the top of the gradient. (Top) UV absorbance (254 nm) profile of cytoplasmic ribonucleoprotein complexes. (E) 18S and 28S RNA profile determined by quantitative RT-PCR. (F) Quantification of the Renilla luciferase reporter mRNA fractionated across a 10–50% sucrose gradient by quantitative RT-PCR.

Downloaded from https://academic.oup.com/nar/article-abstract/37/15/4932/2410023 by guest on 08 May 2020

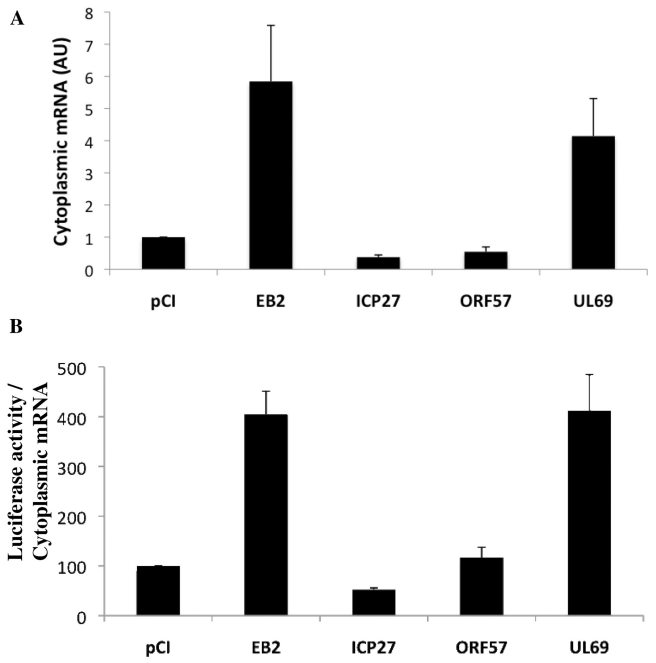

Figure 6. Differential effects on translation from EB2-related proteins derived from different herpesviruses. (**A**) Cytoplasmic luciferase mRNA levels monitored by quantitative PCR in HeLa cells mock transfected (pCI) or transfected with 500 ng of EBV EB2, HSV-1 ICP27, HKSV ORF57 and HCMV UL69-encoding plasmids. (**B**) Translation rate. Luciferase activity was normalized by the amount of cytoplasmic mRNAs from cells mock transfected (pCI) or transfected with EBV EB2, HSV-1 ICP27, HKSV ORF57 and HCMV UL69-encoding vectors, together with the reporter plasmid pcDNAGlobinRen. AU: arbitrary units.

their similarities, EB2 homolog proteins cannot *trans*-complement each other for viral production (35,47). Thus, it was of interest to test the effect of EB2-related proteins in our system. For this, we used proteins from each herpesvirus sub-family: ICP27 from HSV1 (herpes simplex virus 1), an α-herpesvirus, ORF57 from KSHV (Kaposi's sarcoma-associated herpesvirus), like EBV a γ-herpesvirus and UL69 from CMV (cytomegalovirus), a β-herpesvirus. Among these proteins, only ICP27 has been previously shown to stimulate translation of specific viral mRNAs (48,49). In order to monitor the effect of these proteins in our luciferase reporter system, we cotransfected HeLa cells with the intronless luciferase construct and expression plasmids for the different EB2-related herpesvirus proteins and we quantified both cytoplasmic mRNA accumulation (Figure 6A) and luciferase activity (not shown). Luciferase expression was again normalized to the amount of cytoplasmic luciferase-encoding mRNAs in order to specifically measure the impact of each viral protein on translation (Figure 6B). Expression of each of the viral proteins was verified by western blotting (data not shown). Unexpectedly, the effect observed with EB2 was not conserved for all of the homolog proteins. Indeed, only UL69 led to a strong luciferase translation stimulation similar to that of EB2 (i.e. 4–5-fold stimulation of translation), whereas ICP27 and ORF57 did not have a significant effect (Figure 6B). This was probably due to the fact that neither ICP27 nor ORF57 appear to export the luciferase mRNA (expression of ICP27 led in fact to a 40% reduction of the amount of luciferase cytoplasmic mRNA) contrary to EB2 and UL69, which provoked a 4–5-fold increase of luciferase cytoplasmic mRNA levels (Figure 6A).

This result shows that EB2 homologs derived from related viruses have differential effects on a heterologous mRNA and suggests that export of the mRNA and stimulation of its translation are strongly linked.

DISCUSSION

Although the role of EB2 in the nuclear export of unspliced RNAs has been extensively studied, its effect on translation has never been evaluated. With the growing evidence that cellular mRNA splicing and export factors are also able to modulate translation of spliced mRNAs, we decided to test whether the viral protein EB2 could also affect translation. Indeed, most of the EBV early and late genes do not contain any intron, suggesting that both export and translation of the corresponding mRNAs should be very inefficient. However, this defect is overcome by expression of the early viral protein EB2, which interacts with the viral mRNAs to facilitate their cytoplasmic accumulation. This tight interaction of EB2 with the exported mRNA and its transit to the cytoplasm strongly suggested that EB2 could also affect translation. In fact, expression of EB2 in cells coding for an EBV-derived unspliced RNA (BDLF1) led to a strong stimulation of BDLF1 accumulation that did not depend on an increase in cytoplasmic levels of the corresponding mRNA. This result indicates that, besides its role as a nuclear export factor, EB2 can also stimulate translation of EBV unspliced RNAs. Interestingly, the effect of EB2 on protein accumulation from unspliced mRNAs did not depend on any EBV-derived *cis*-acting sequence since expression of an artificial unspliced mRNA encoding for the Renilla luciferase was also strongly stimulated without affecting protein stability. Surprisingly, even though EB2 lacked a requirement for a specific RNA sequence, its expression did not affect global cellular mRNA translation suggesting a role for EB2 on translation of only a specific subset of mRNAs.

Since EB2 has been shown to export mostly mRNAs generated from intronless genes (23) including its specific EBV-encoded target genes we tested the effect of the introduction of intronic sequences within the 5′UTR of our reporter gene. Interestingly, we found that after addition of an intron within the luciferase reporter construct, EB2 was no longer able to stimulate translation, whereas it had a strong effect on the same RNA transcribed from an intronless construct.

These results together with previous results showing that EB2 can interact with mRNA independently of any specific sequence (50) suggest that EB2 can bind to both spliced and unspliced mRNAs. However, in the case of unspliced mRNAs, which do not recruit the normal set of splicing factors, EB2 would allow their export and stimulate their translation to levels similar to those of spliced mRNAs. In the case of intron-containing genes, EB2

Downloaded from https://academic.oup.com/nar/article-abstract/37/15/4932/2410023 by guest on 08 May 2020

could also bind to the mRNA but we suggest that either it is excluded from the mRNA by a cellular splicing or export factor, or it is exported to the cytoplasm with the spliced mRNA. In the latter case, its effect on translation would be redundant in the presence of splicing proteins. Indeed, it is possible that EB2 recruited cotranscriptionally to nascent mRNAs is able to interact with an as yet unknown cellular factor necessary for translation stimulation of spliced mRNAs. This would explain the stimulation of the translation of intronless mRNAs in the presence of EB2. On the contrary, if EB2 also interacts with spliced mRNAs, it could interfere with the cellular factors that normally stimulate their export and translation. This would explain the mild inhibition of export and translation that we observed upon addition of an intron in our luciferase reporter construct.

In accordance with the fact that EB2 specifically stimulates export and translation of mRNAs generated from intronless genes we have shown that cellular mRNAs, which are, in the majority, generated from intron-containing genes, are not globally affected by expression of EB2. There are however few cellular genes which are known for their absence of introns. It would be interesting to look at the effect of EB2 on the export and translation of mRNAs generated from such genes. In the case of EBV, most of the viral mRNAs of the productive cycle are intronless. We have previously shown that EB2 is necessary for the efficient export of the majority of these, but it is interesting to note that some are efficiently exported even in the absence of EB2, suggesting that they use an alternative export pathway, independent of splicing. Such an alternative pathway has been previously reported with the SR proteins, 9G8 and ASF/SF2, which have been found to promote the recruitment of TAP to mRNPs (51). Another interesting example of mRNA generated from an intronless gene and which is not affected by EB2 is the firefly luciferase mRNA expressed from an intronless construct (25). However, although there is no effect of EB2 on firefly luciferase expression, EB2 bound efficiently to its mRNA *in vivo* (25). Again, it is likely that this mRNA uses an alternative pathway for its export, independent of splicing. Thus, even if EB2 is associated with these mRNAs *in vivo*, its effect is probably redundant as discussed above in the case of spliced mRNAs.

In order to definitively conclude on a direct effect of EB2 on translation efficiency we studied the association of Renilla luciferase mRNAs with polyribosomes. The data clearly showed that the proportion of Renilla luciferase mRNAs associated with polyribosomes is largely increased in the presence of EB2. Moreover, we found that there is also an association of EB2 with polyribosomes, suggesting that EB2 binds the mRNPs in the nucleus, where it stimulates their export and then remains associated with the mRNPs as far as the polyribosomes. Taken together, these results argue for a role of EB2 in *cis* similar to that of the EJC proteins responsible for the translation stimulation of cellular mRNAs. One proposed mechanism involves an interaction between the EJC and the 48S preinitiation complex mediated by an interaction between Y14:Magoh and the protein PYM (52). Another mechanism involves the EJC-dependent recruitment of the 40S ribosomal protein S6 kinase 1 (S6K1) which is a central player in the TOR signaling cascade (7). When activated by the TOR pathway, S6K1 enhances translation initiation both by activating stimulatory factors and by inactivating inhibitory factors bound at the 5′ cap of mRNAs. The SR protein ASF/SF2 has also recently been reported to enhance translation initiation via recruitment of mTOR (8).

Finally, we tested several EB2 homologous proteins from other herpesviruses for their ability to stimulate translation of the intronless luciferase gene. Among the proteins tested, only UL69 from human cytomegalovirus (hCMV) behaves like EB2, while ICP27 and ORF57 were unable to stimulate luciferase translation. For UL69, this is the first report suggesting that this protein plays a role in stimulation of translation. On the contrary, it has been previously shown that ICP27 (from the herpes simplex virus type 1) plays a role in regulating translation of a subset of late viral mRNAs (48,49,53). However, the interaction between ICP27 and the viral mRNAs has been shown to depend on specific RNA sequences distributed along the viral genome (54). In addition, ICP27 has been shown to be able to stimulate translation of a luciferase mRNA only if it was previously tethered to it (53). Thus, it is not surprising that in our system, ICP27 does not stimulate Renilla luciferase mRNA translation nor cytoplasmic Renilla luciferase mRNA accumulation, suggesting that translation stimulation is probably dependent on the binding of the herpes simplex virus proteins to the mRNA. Since all the herpesvirus EB2 homologous proteins have been shown to shuttle from the nucleus to the cytoplasm (31,38,55) it is tempting to speculate that they first interact with their unspliced mRNA targets inside the nucleus, and then shuttle to the cytoplasm bound to these mRNAs where they play a role in translation. Accordingly, it is interesting to notice that ICP27 has also been shown to be associated with polyribosomes (53). Taken together, these results suggest firstly that both EB2 and the herpesvirus EB2 homologous proteins have a direct role on translation of the mRNA they interact with, and secondly that protein–mRNA interaction, mRNA export and translation stimulation are strongly linked.

EB2 expression is essential for viral particle production and its absence leads to very poor viral DNA replication probably because of the low expression of early viral mRNAs that depend on EB2 for their export (i.e. BALF5 and BALF2) (27). An even more drastic effect was seen on most of the late viral mRNAs (28,56). We have shown here that EB2 expression leads to a 25-fold stimulation of renilla luciferase reporter gene expression with a cytoplasmic accumulation of the corresponding mRNA stimulated 3.5-fold and the translation itself stimulated from 5- to 7-fold. This suggests that the essential role of EB2 during the EBV productive cycle could be explained by a combined role on mRNA export and translation stimulation.

SUPPLEMENTARY DATA

Supplementary Data are available at NAR Online.

Downloaded from https://academic.oup.com/nar/article-abstract/37/15/4932/2410023 by guest on 08 May 2020

ACKNOWLEDGEMENTS

We thank B. Blanquier from the 'Plateau d'analyse génétique' of IFR128 for advice on quantitative PCR. We thank A. Chaboud and Y. Tauran from the 'Plateau de production et d'analyse des protéines' of IFR 128 for use of the AKTA purifier. We thank Dr S. Morley for providing anti-human PABP antibodies and Dr D. Levy and S. Delpeut for providing PKR-deficient cells. We also thank the Réseau Herpesvirus and Cancer for its support. Finally, we thank Dr R. Buckland for reading the manuscript.

FUNDING

'Institut National de la Santé et de la Recherche Médicale' (INSERM), the 'Agence Nationale pour la Recherche' (ANR) [ANR MIME: grant number RPV06120CSA (to E.M.) and ANR blanche: grant number 06-0290-01 (to T.O.)] and the pole of competitivity Lyon Biopole. Fellowship from the 'Association pour la Recherche contre le cancer' (ARC) (to C.M.-P.); fellowship from the 'Ministère de la Recherche et de la Technologie' (MRT to E.R.). E.M. is a CNRS scientist. Funding for open access charge: INSERM.

Conflict of interest statement. None declared.

REFERENCES

1. Moore,M.J. and Proudfoot,N.J. (2009) Pre-mRNA processing reaches back to transcription and ahead to translation. *Cell*, **136**, 688–700.
2. Gingras,A.C., Raught,B. and Sonenberg,N. (1999) eIF4 initiation factors: effectors of mRNA recruitment to ribosomes and regulators of translation. *Annu. Rev. Biochem.*, **68**, 913–963.
3. Prevot,D., Darlix,J.L. and Ohlmann,T. (2003) Conducting the initiation of protein synthesis: the role of eIF4G. *Biol. Cell*, **95**, 141–156.
4. Pestova,T.V., Kolupaeva,V.G., Lomakin,I.B., Pilipenko,E.V., Shatsky,I.N., Agol,V.I. and Hellen,C.U. (2001) Molecular mechanisms of translation initiation in eukaryotes. *Proc. Natl Acad. Sci. USA*, **98**, 7029–7036.
5. Le Hir,H., Nott,A. and Moore,M.J. (2003) How introns influence and enhance eukaryotic gene expression. *Trends Biochem. Sci.*, **28**, 215–220.
6. Lu,S. and Cullen,B.R. (2003) Analysis of the stimulatory effect of splicing on mRNA production and utilization in mammalian cells. *RNA*, **9**, 618–630.
7. Ma,X.M., Yoon,S.O., Richardson,C.J., Julich,K. and Blenis,J. (2008) SKAR links pre-mRNA splicing to mTOR/S6K1-mediated enhanced translation efficiency of spliced mRNAs. *Cell*, **133**, 303–313.
8. Michlewski,G., Sanford,J.R. and Caceres,J.F. (2008) The splicing factor SF2/ASF regulates translation initiation by enhancing phosphorylation of 4E-BP1. *Mol. Cell*, **30**, 179–189.
9. Nott,A., Meislin,S.H. and Moore,M.J. (2003) A quantitative analysis of intron effects on mammalian gene expression. *RNA*, **9**, 607–617.
10. Pfeifer,I., Elsby,R., Fernandez,M., Faria,P.A., Nussenzveig,D.R., Lossos,I.S., Fontoura,B.M., Martin,W.D. and Barber,G.N. (2008) NFAR-1 and -2 modulate translation and are required for efficient host defense. *Proc. Natl Acad. Sci. USA*, **105**, 4173–4178.
11. Sanford,J.R., Gray,N.K., Beckmann,K. and Caceres,J.F. (2004) A novel role for shuttling SR proteins in mRNA translation. *Genes Dev.*, **18**, 755–768.
12. Wiegand,H.L., Lu,S. and Cullen,B.R. (2003) Exon junction complexes mediate the enhancing effect of splicing on mRNA expression. *Proc. Natl Acad. Sci. USA*, **100**, 11327–11332.
13. Sanford,J.R., Longman,D. and Caceres,J.F. (2003) Multiple roles of the SR protein family in splicing regulation. *Prog. Mol. Subcell Biol.*, **31**, 33–58.
14. Tacke,R. and Manley,J.L. (1999) Determinants of SR protein specificity. *Curr. Opin. Cell Biol.*, **11**, 358–362.
15. Swartz,J.E., Bor,Y.C., Misawa,Y., Rekosh,D. and Hammarskjold,M.L. (2007) The shuttling SR protein 9G8 plays a role in translation of unspliced mRNA containing a constitutive transport element. *J. Biol. Chem.*, **282**, 19844–19853.
16. Braun,I.C., Herold,A., Rode,M., Conti,E. and Izaurralde,E. (2001) Overexpression of TAP/p15 heterodimers bypasses nuclear retention and stimulates nuclear mRNA export. *J. Biol. Chem.*, **276**, 20536–20543.
17. Jin,L., Guzik,B.W., Bor,Y.C., Rekosh,D. and Hammarskjold,M.L. (2003) Tap and NXT promote translation of unspliced mRNA. *Genes Dev.*, **17**, 3075–3086.
18. Levesque,L., Guzik,B., Guan,T., Coyle,J., Black,B.E., Rekosh,D., Hammarskjold,M.L. and Paschal,B.M. (2001) RNA export mediated by tap involves NXT1-dependent interactions with the nuclear pore complex. *J. Biol. Chem.*, **276**, 44953–44962.
19. Hadzopoulou-Cladaras,M., Felber,B.K., Cladaras,C., Athanassopoulos,A., Tse,A. and Pavlakis,G.N. (1989) The rev (trs/art) protein of human immunodeficiency virus type 1 affects viral mRNA and protein expression via a *cis*-acting sequence in the env region. *J. Virol.*, **63**, 1265–1274.
20. Malim,M.H., Hauber,J., Le,S.Y., Maizel,J.V. and Cullen,B.R. (1989) The HIV-1 rev trans-activator acts through a structured target sequence to activate nuclear export of unspliced viral mRNA. *Nature*, **338**, 254–257.
21. Perales,C., Carrasco,L. and Gonzalez,M.E. (2005) Regulation of HIV-1 env mRNA translation by Rev protein. *Biochim. Biophys. Acta*, **1743**, 169–175.
22. Balvay,L., Lopez Lastra,M., Sargueil,B., Darlix,J.L. and Ohlmann,T. (2007) Translational control of retroviruses. *Nat. Rev. Microbiol.*, **5**, 128–140.
23. Buisson,M., Hans,F., Kusters,I., Duran,N. and Sergeant,A. (1999) The C-terminal region but not the Arg-X-Pro repeat of Epstein–Barr virus protein EB2 is required for its effect on RNA splicing and transport. *J. Virol.*, **73**, 4090–4100.
24. Hiriart,E., Farjot,G., Gruffat,H., Nguyen,M.V., Sergeant,A. and Manet,E. (2003) A novel nuclear export signal and a REF interaction domain both promote mRNA export by the Epstein–Barr virus EB2 protein. *J. Biol. Chem.*, **278**, 335–342.
25. Ruvolo,V., Gupta,A.K. and Swaminathan,S. (2001) Epstein–Barr virus SM protein interacts with mRNA in vivo and mediates a gene-specific increase in cytoplasmic mRNA. *J. Virol.*, **75**, 6033–6041.
26. Farjot,G., Buisson,M., Duc Dodon,M., Gazzolo,L., Sergeant,A. and Mikaelian,I. (2000) Epstein–Barr virus EB2 protein exports unspliced RNA via a Crm-1-independent pathway. *J. Virol.*, **74**, 6068–6076.
27. Gruffat,H., Batisse,J., Pich,D., Neuhierl,B., Manet,E., Hammerschmidt,W. and Sergeant,A. (2002) Epstein–Barr virus mRNA export factor EB2 is essential for production of infectious virus. *J. Virol.*, **76**, 9635–9644.
28. Batisse,J., Manet,E., Middeldorp,J., Sergeant,A. and Gruffat,H. (2005) Epstein–Barr virus mRNA export factor EB2 is essential for intranuclear capsid assembly and production of gp350. *J. Virol.*, **79**, 14102–14111.
29. Chen,I.H., Sciabica,K.S. and Sandri-Goldin,R.M. (2002) ICP27 interacts with the RNA export factor Aly/REF to direct herpes simplex virus type 1 intronless mRNAs to the TAP export pathway. *J. Virol.*, **76**, 12877–12889.
30. Koffa,M.D., Clements,J.B., Izaurralde,E., Wadd,S., Wilson,S.A., Mattaj,I.W. and Kuersten,S. (2001) Herpes simplex virus ICP27 protein provides viral mRNAs with access to the cellular mRNA export pathway. *EMBO J.*, **20**, 5769–5778.
31. Sandri-Goldin,R.M. (1998) ICP27 mediates HSV RNA export by shuttling through a leucine-rich nuclear export signal and binding viral intronless RNAs through an RGG motif. *Genes Dev.*, **12**, 868–879.

Downloaded from https://academic.oup.com/nar/article-abstract/37/15/4932/2410023 by guest on 08 May 2020

32. Lischka,P., Toth,Z., Thomas,M., Mueller,R. and Stamminger,T. (2006) The UL69 transactivator protein of human cytomegalovirus interacts with DEXD/H-Box RNA helicase UAP56 to promote cytoplasmic accumulation of unspliced RNA. *Mol. Cell Biol.*, **26**, 1631–1643.
33. Malik,P., Blackbourn,D.J. and Clements,B. (2004) The evolutionarily conserved Kaposi's sarcoma-associated herpesvirus ORF57 protein interacts with REF protein and acts as an mRNA export factor. *J. Biol. Chem.*, **279**, 33001–33011.
34. Williams,B.J.L., Boyne,J.R., Goodwin,D.J., Roaden,L., Hautbergue,G.M., Wilson,S.A. and Whitehouse,A. (2005) The prototype gamma 2 herpesvirus nucleocytoplasmic shuttling protein, ORF57, transports viral RNA through the cellular mRNA export pathway. *Biochem. J.*, **387**, 295–308.
35. Han,Z. and Swaminathan,S. (2006) Kaposi's sarcoma-associated herpesvirus lytic gene ORF57 is essential for infectious virion production. *J. Virol.*, **80**, 5251–5260.
36. Smith,E.J., Marie,I., Prakash,A., Garcia-Sastre,A. and Levy,D.E. (2001) IRF3 and IRF7 phosphorylation in virus-infected cells does not require double-stranded RNA-dependent protein kinase R or Ikappa B kinase but is blocked by Vaccinia virus E3L protein. *J. Biol. Chem.*, **276**, 8951–8957.
37. Soto Rifo,R., Ricci,E.P., Decimo,D., Moncorge,O. and Ohlmann,T. (2007) Back to basics: the untreated rabbit reticulocyte lysate as a competitive system to recapitulate cap/poly(A) synergy and the selective advantage of IRES-driven translation. *Nucleic Acids Res.*, **35**, e121.
38. Lischka,P., Rosorius,O., Trommer,E. and Stamminger,T. (2001) A novel transferable nuclear export signal mediates CRM1-independent nucleocytoplasmic shuttling of the human cytomegalovirus transactivator protein pUL69. *EMBO J.*, **20**, 7271–7283.
39. Fraser,C.S., Pain,V.M. and Morley,S.J. (1999) The association of initiation factor 4F with poly(A)-binding protein is enhanced in serum-stimulated Xenopus kidney cells. *J. Biol. Chem.*, **274**, 196–204.
40. Li,Y., Bor,Y.C., Misawa,Y., Xue,Y., Rekosh,D. and Hammarskjold,M.L. (2006) An intron with a constitutive transport element is retained in a Tap messenger RNA. *Nature*, **443**, 234–237.
41. Bor,Y.C., Swartz,J., Li,Y., Coyle,J., Rekosh,D. and Hammarskjold,M.L. (2006) Northern blot analysis of mRNA from mammalian polyribosomes. *Nat. Protoc.*, doi:10.1038/nprot.2006.216. Available at http://www.natureprotocols.com/2006/09/15/northern_blot_analysis_of_mrna.php.
42. Meurs,E.F., Watanabe,Y., Kadereit,S., Barber,G.N., Katze,M.G., Chong,K., Williams,B.R. and Hovanessian,A.G. (1992) Constitutive expression of human double-stranded RNA-activated p68 kinase in murine cells mediates phosphorylation of eukaryotic initiation factor 2 and partial resistance to encephalomyocarditis virus growth. *J. Virol.*, **66**, 5805–5814.
43. Barber,G.N., Wambach,M., Wong,M.L., Dever,T.E., Hinnebusch,A.G. and Katze,M.G. (1993) Translational regulation by the interferon-induced double-stranded-RNA-activated 68-kDa protein kinase. *Proc. Natl Acad. Sci. USA*, **90**, 4621–4625.
44. Ruvolo,V., Wang,E., Boyle,S. and Swaminathan,S. (1998) The Epstein–Barr virus nuclear protein SM is both a post-transcriptional inhibitor and activator of gene expression. *Proc. Natl Acad. Sci. USA*, **95**, 8852–8857.
45. Gorgoni,B. and Gray,N.K. (2004) The roles of cytoplasmic poly(A)-binding proteins in regulating gene expression: a developmental perspective. *Brief. Funct. Genomic Proteomic*, **3**, 125–141.
46. Mangus,D.A., Evans,M.C. and Jacobson,A. (2003) Poly(A)-binding proteins: multifunctional scaffolds for the post-transcriptional control of gene expression. *Genome Biol.*, **4**, 223.
47. Sergeant,A., Gruffat,H. and Manet,E. (2008) The Epstein–Barr virus (EBV) protein EB2 is an mRNA export factor essential for virus production. *Frontiers Biosci.*, **13**, 3798–3813.
48. Ellison,K.S., Maranchuk,R.A., Mottet,K.L. and Smiley,J.R. (2005) Control of VP16 translation by the herpes simplex virus type 1 immediate-early protein ICP27. *J. Virol.*, **79**, 4120–4131.
49. Fontaine-Rodriguez,E.C. and Knipe,D.M. (2008) Herpes simplex virus ICP27 increases translation of a subset of viral late mRNAs. *J. Virol.*, **82**, 3538–3545.
50. Hiriart,E., Bardouillet,L., Manet,E., Gruffat,H., Penin,F., Montserret,R., Farjot,G. and Sergeant,A. (2003) A region of the Epstein–Barr virus (EBV) mRNA export factor EB2 containing an arginine-rich motif mediates direct binding to RNA. *J. Biol. Chem.*, **278**, 37790–37798.
51. Huang,Y., Gattoni,R., Stevenin,J. and Steitz,J.A. (2003) SR splicing factors serve as adapter proteins for TAP-dependent mRNA export. *Mol. Cell*, **11**, 837–843.
52. Diem,M.D., Chan,C.C., Younis,I. and Dreyfuss,G. (2007) PYM binds the cytoplasmic exon-junction complex and ribosomes to enhance translation of spliced mRNAs. *Nat. Struct. Mol. Biol.*, **14**, 1173–1179.
53. Larralde,O., Smith,R.W., Wilkie,G.S., Malik,P., Gray,N.K. and Clements,J.B. (2006) Direct stimulation of translation by the multifunctional herpesvirus ICP27 protein. *J. Virol.*, **80**, 1588–1591.
54. Sokolowski,M., Scott,J.E., Heaney,R.P., Patel,A.H. and Clements,J.B. (2003) Identification of herpes simplex virus RNAs that interact specifically with regulatory protein ICP27 in vivo. *J. Biol. Chem.*, **278**, 33540–33549.
55. Bello,L.J., Davison,A.J., Glenn,M.A., Whitehouse,A., Rethmeier,N., Schulz,T. and Clements,J.B. (1999) The human ORF57 gene and its properties. *J. Gen. Virol.*, **80**, 3207–3215.
56. Han,Z., Marendy,E., Wang,Y.D., Yuan,J., Sample,J.T. and Swaminathan,S. (2007) Multiple roles of Epstein–Barr virus SM protein in lytic replication. *J. Virol.*, **81**, 4058–4069.

Downloaded from https://academic.oup.com/nar/article-abstract/37/15/4932/2410023 by guest on 08 May 2020

Staufen1 senses overall transcript secondary structure to regulate translation

Emiliano P Ricci[1–3], Alper Kucukural[1–3], Can Cenik[1–4], Blandine C Mercier[1–3], Guramrit Singh[1–3], Erin E Heyer[1–3], Ami Ashar-Patel[1–3], Lingtao Peng[1–3] & Melissa J Moore[1–3]

Human Staufen1 (Stau1) is a double-stranded RNA (dsRNA)-binding protein implicated in multiple post-transcriptional gene-regulatory processes. Here we combined RNA immunoprecipitation in tandem (RIPiT) with RNase footprinting, formaldehyde cross-linking, sonication-mediated RNA fragmentation and deep sequencing to map Staufen1-binding sites transcriptome wide. We find that Stau1 binds complex secondary structures containing multiple short helices, many of which are formed by inverted Alu elements in annotated 3′ untranslated regions (UTRs) or in 'strongly distal' 3′ UTRs. Stau1 also interacts with actively translating ribosomes and with mRNA coding sequences (CDSs) and 3′ UTRs in proportion to their GC content and propensity to form internal secondary structure. On mRNAs with high CDS GC content, higher Stau1 levels lead to greater ribosome densities, thus suggesting a general role for Stau1 in modulating translation elongation through structured CDS regions. Our results also indicate that Stau1 regulates translation of transcription-regulatory proteins.

© 2014 Nature America, Inc. All rights reserved.

Staufen proteins are highly conserved dsRNA-binding proteins (dsRBPs) found in most bilateral animals[1]. Mammals contain two Staufen paralogs encoded by different loci. Stau1, expressed in most tissues, has a microtubule-binding domain, a dimerization domain and four conserved dsRNA-binding domains (dsRBDs), only two of which (dsRBDs 3 and 4) are necessary for dsRNA binding[2]. Within cells, Stau1 can make direct interactions both with itself and with Stau2, the more tissue-specific paralog[3]. Functionally, Staufen proteins are involved in multiple post-transcriptional regulatory processes. In flies, 3′ UTR–bound Staufen is required for proper localization and translational control of bicoid and prospero mRNAs during oogenesis[4,5]. In mammals, Stau1 has been implicated in mRNA transport to neuronal dendrites[6], regulation of translation via physical interaction with the ribosome[7], a form of translation-dependent mRNA degradation known as Staufen-mediated decay (SMD)[8–11], regulation of stress-granule homeostasis[12], alternative splicing, nuclear export and translation of a gene containing 3′-UTR CUG-repeat expansions[13]. Although Stau1 is not essential for mammalian development, neurons lacking Stau1 have dendritic spine-morphogenesis defects *in vitro*, and knockout mice have locomotor-activity deficits[14].

Crucial for the understanding of how Stau1 regulates gene expression is comprehensive knowledge of its intracellular RNA-binding sites. Although mammalian Stau1- and *Drosophila* Staufen-associated mRNAs were identified by microarray analysis after native RNA immunoprecipitation (RIP)[15–18], those studies were unable to directly map any individual Stau1-binding site, and subsequent bioinformatics analysis yielded no clear consensus for identified mammalian targets[16]. Thus, with the exception of a few well-characterized binding sites validated by mutagenesis[19,20], the exact target sites and RNA structures recognized by mammalian Stau1 remain to be determined. To address this, we here undertook a tandem affinity purification strategy (RIPiT[21]) to map Stau1-binding sites transcriptome wide in human tissue-cultured cells. We also knocked down and overexpressed Stau1 to measure functional consequences on target-mRNA levels and translation efficiency. Our results revealed a new role for Stau1 in regulating translation of GC-rich mRNAs by 'sensing' overall transcript secondary structure.

RESULTS

Transcriptome-wide mapping of Stau1-binding sites

Using the Flp-In system and a tetracycline promoter, we generated HEK293 cells that inducibly expressed a single Flag-tagged copy of either the Stau1 65-kDa spliced isoform (Stau1-WT) or a mutant version (Stau1-mut) containing point mutations in dsRBDs 3 and 4 known to disrupt binding to dsRNA[2] (**Fig. 1a**). Consistently with its propensity to bind dsRNA through the sugar-phosphate backbone[22] and with a previous report suggesting poor UV-cross-linking ability[23], we found that Stau1 cross-linked with very poor efficiency to poly(A)$^+$ RNA upon shortwave UV irradiation of living cells (**Supplementary Fig. 1a**). Therefore we used a RIPiT approach wherein initial immunoprecipitation (IP) with anti-Flag antibody was followed by affinity elution with Flag peptide and then a second IP with a polyclonal anti-Stau1 antibody. RIPiT was performed under two different regimens: (i) To finely-map stable Stau1 footprints, we extensively digested samples

[1]Department of Biochemistry and Molecular Pharmacology, University of Massachusetts Medical School, Worcester, Massachusetts, USA. [2]RNA Therapeutics Institute, University of Massachusetts Medical School, Worcester, Massachusetts, USA. [3]Howard Hughes Medical Institute, University of Massachusetts Medical School, Worcester, Massachusetts, USA. [4]Present address: Department of Genetics, Stanford University School of Medicine, Stanford, California, USA. Correspondence should be addressed to M.J.M. (melissa.moore@umassmed.edu).

Received 8 August; accepted 19 November; published online 15 December 2013; doi:10.1038/nsmb.2739

with RNase I in between native anti-Flag and native anti-Stau1 IPs, generating 30- to 50-nt Stau1-bound RNA fragments (FOOT libraries; **Fig. 1b** and **Supplementary Fig. 1c**). However, many of these short reads derived from Alu repeat elements (described below) and so were not uniquely mappable. Further, under native conditions, Stau1 can make new dsRNA associations after cell lysis (**Supplementary Fig. 1b**). (ii) Therefore, we also subjected cells to formaldehyde cross-linking before lysis, extensively sonicated the lysates to shear long RNAs into 200- to 300-nt fragments (thereby increasing their ability to be mapped) and performed a denaturing anti-Flag IP and then a native anti-Stau1 IP (CROSS libraries; **Fig. 1b** and **Supplementary Fig. 1d**). Cross-linking and subsequent

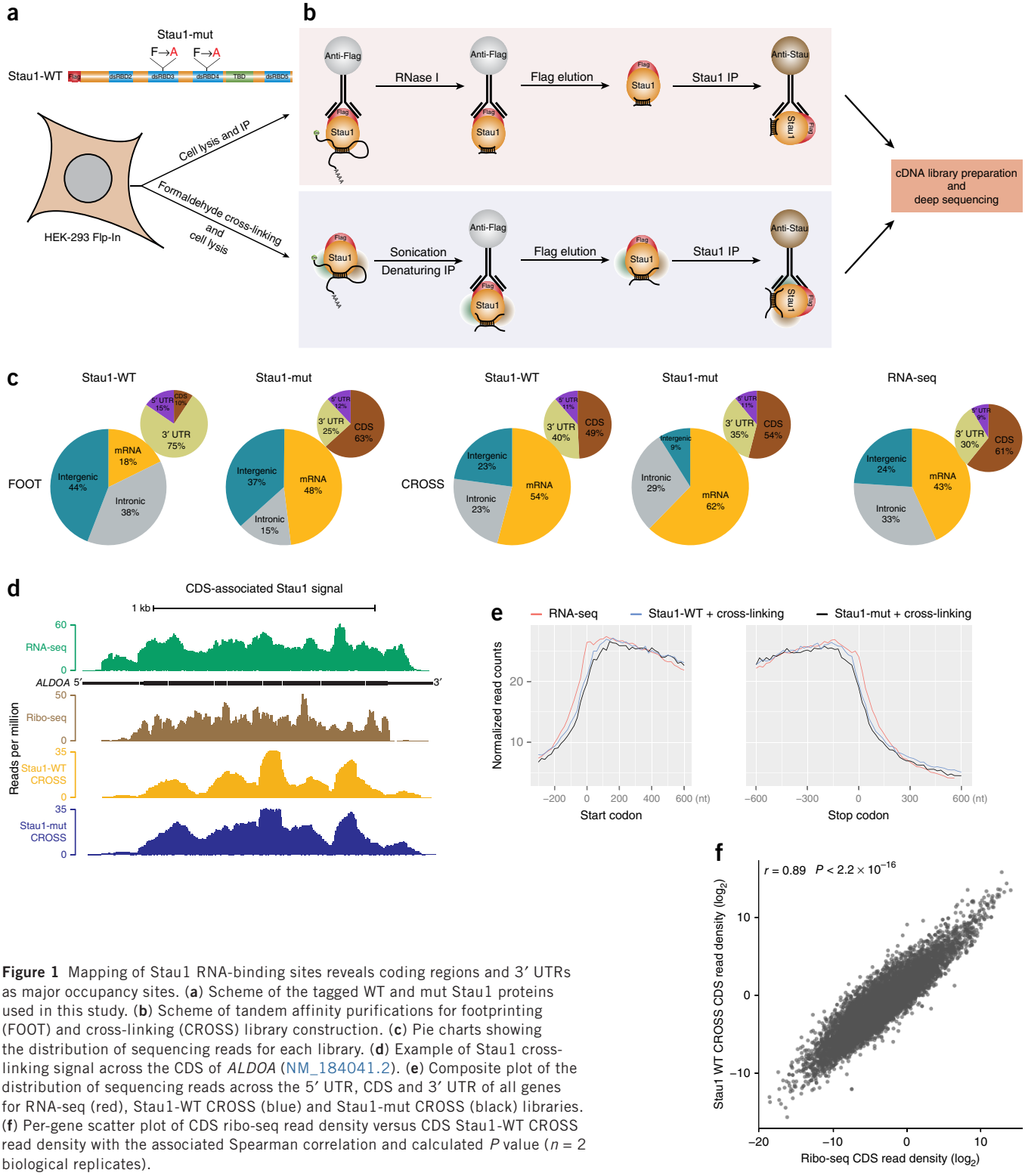

Figure 1 Mapping of Stau1 RNA-binding sites reveals coding regions and 3′ UTRs as major occupancy sites. (**a**) Scheme of the tagged WT and mut Stau1 proteins used in this study. (**b**) Scheme of tandem affinity purifications for footprinting (FOOT) and cross-linking (CROSS) library construction. (**c**) Pie charts showing the distribution of sequencing reads for each library. (**d**) Example of Stau1 cross-linking signal across the CDS of *ALDOA* (NM_184041.2). (**e**) Composite plot of the distribution of sequencing reads across the 5′ UTR, CDS and 3′ UTR of all genes for RNA-seq (red), Stau1-WT CROSS (blue) and Stau1-mut CROSS (black) libraries. (**f**) Per-gene scatter plot of CDS ribo-seq read density versus CDS Stau1-WT CROSS read density with the associated Spearman correlation and calculated *P* value ($n = 2$ biological replicates).

© 2014 Nature America, Inc. All rights reserved.

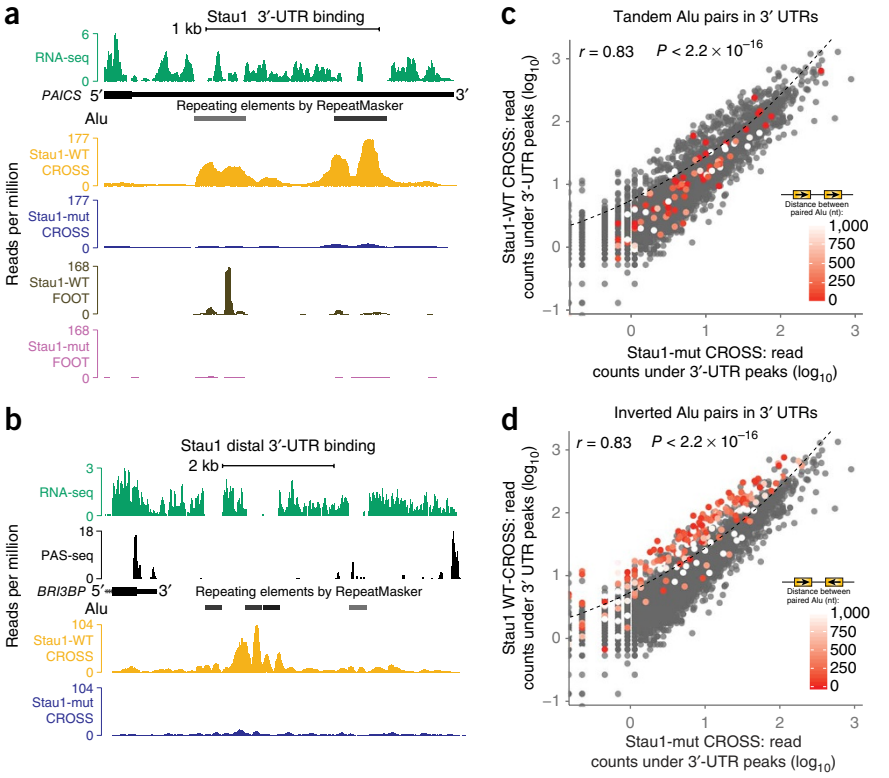

Figure 2 Inverted Alu pairs are an important class of Stau1-binding sites. (**a**,**b**) Distribution of sequencing reads obtained from RNA-seq (green), Stau1-WT CROSS (yellow), Stau1-mut CROSS (blue), Stau1-WT FOOT (brown), Stau1-mut FOOT (violet) and PAS-seq libraries (black) for the 3′ UTR of *PAICS* (NM_001079524) (**a**) and the strongly distal 3′ UTR of *BRI3BP* (NM_080626.5) (**b**). (**c**,**d**) Per-gene scatter plots of Stau1-WT CROSS and Stau1-mut CROSS read counts under called 3′-UTR Stau1-WT CROSS peak positions with associated Spearman correlation and calculated *P* values ($n = 2$ biological replicates). Genes containing a 3′ UTR Alu pair are colored with respect to the distance between each tandem Alu pair (**c**) or inverted Alu pair (**d**). The dashed line corresponds to the 2.7 cutoff in the ratio of Stau1-WT over mut read counts.

denaturation should both preserve weak *in situ* interactions that might otherwise dissociate during sample workup and prevent formation of any new interactions after cell lysis.

We sequenced all libraries constructed by 3′-adaptor ligation to RNA fragments, reverse transcription and circularization on GAII or HiSeq 2000 Illumina platforms and then mapped them to HG18 by using RefSeq gene annotations. Biological replicates of WT and mut CROSS and WT FOOT libraries exhibited extremely high correlations (r >0.98), thus indicating the reproducibility of the approach (**Supplementary Fig. 1e**).

Stau1 associates with translating ribosomes

In contrast to our previous exon junction complex (EJC) RIPiT libraries[24], all Stau1 FOOT libraries (WT and mut) were dominated by rRNA-mapping reads (14–30% versus 74–83%, respectively; **Supplementary Fig. 2**). Further, despite attempts to specifically deplete rRNA fragments during CROSS-library preparation, WT and mut CROSS libraries also contained abundant rRNA-mapping reads (**Supplementary Fig. 2**). These findings are consistent with a previous report that Stau1 cosediments with 60S ribosomal subunits via interactions independent of the functionality of dsRBDs 3 and 4 (ref. 2).

To further investigate this ribosome association, we performed sucrose sedimentation in the presence of inhibitors that either block elongation (cycloheximide) or initiation (harringtonine) (**Supplementary Fig. 3a**). In the presence of cycloheximide, both endogenous Stau1 and Flag–Stau1-WT cosedimented with 60S subunits, 80S monosomes and polysomes, with very little Stau1 observable in ribosome-free fractions at the top of the gradient. However, when lysates were treated with RNase before sedimentation, ~60% of Stau1 sedimented at the top of the gradient, with the remainder cosedimenting with 60S and 80S ribosomes (**Supplementary Fig. 3a**). This suggests that dsRBP-independent interactions with the ribosome are not the sole factor driving Stau1 polysome association. Finally, when translation initiation was blocked with harringtonine and elongating ribosomes allowed to complete translation (i.e., run off the mRNAs) before cell lysis, Stau1 sedimentation mirrored that of RPL26, an integral 60S protein. Both Stau1 and RPL26 rapidly shifted from heavy polysomal to 80S ribosome fractions upon inhibition of translation initiation (**Supplementary Fig. 3b**), suggesting that Stau1 associates with actively translating ribosomes.

Consistently with our ribosome-association data, approximately half of mRNA-mapping WT and mut CROSS reads (49% and 54%, respectively) mapped to coding exons (CDS regions; **Fig. 1c–e**). To test whether these CDS-mapping reads were due to Stau1 association with translating ribosomes, we compared their density to the density of ribosome footprints (ribo-seq; **Fig. 1f**). For both Stau1-WT (**Fig. 1f**; Spearman correlation = 0.89) and Stau1-mut (data not shown), CROSS read density strongly correlated with ribosome density in CDS regions. This correlation held for the entire gene population, thus suggesting that Stau1 generally associates with elongating ribosomes.

In sum, our data indicate that Stau1 is generally associated with the 60S ribosomal subunit, both on and off mRNA. Further, this ribosome association does not require dsRBD functionality but is partially dependent on RNA integrity. Last, Stau1 appears to associate with actively translating, not stalled, ribosomes.

Stau1 binds paired Alu elements in 3′ UTRs

Whereas WT and mut libraries were quite similar in their rRNA content, they were quite different with regard to Alu repeat–mapping reads. Alu repeats are ~300-nt primate-specific mobile elements in the short interspersed nuclear element family; the human genome contains ~1 million Alu elements, primarily in intergenic regions, introns and 3′ UTRs. Reads mapping to Alu repeats constituted 42% and 28% of non-rRNA–mapping reads in WT FOOT and CROSS libraries, respectively, but only 19% and 14% in the corresponding mut libraries (**Supplementary Fig. 2**). Greater Alu enrichment in WT libraries suggested that their interaction depended on Stau1's ability to bind dsRNA. Consistently with this, WT CROSS reads were often highly enriched over and adjacent to closely spaced Alu pairs likely to form dsRNA secondary structures. We detected such Alu-pair Stau1-binding sites on only two large

© 2014 Nature America, Inc. All rights reserved.

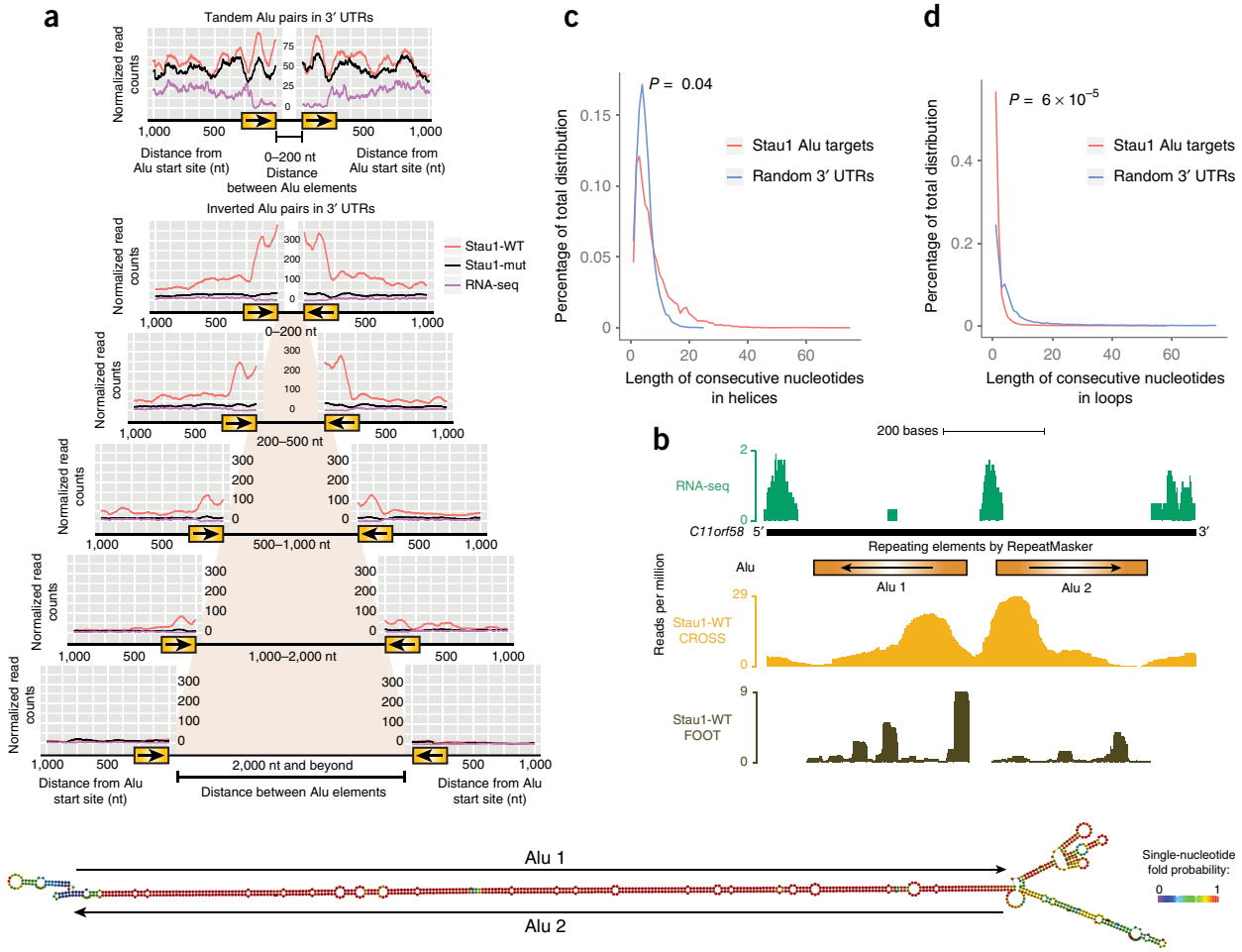

Figure 3 Characterization of the structural features of Stau1 Alu-binding sites. (**a**) Composite plot of Stau1-WT CROSS, Stau1-mut CROSS and RNA-seq read counts around tandem or inverted Alu pairs. Read counts normalized to host gene reads per kilobase per million mapped reads (RPKM) were determined for a region spanning 1 kb up- and downstream of the paired Alu elements separated by the indicated distance ($n = 2$ biological replicates). (**b**) Example of a 3′-UTR inverted Alu-binding site in *C11orf58* (NM_014267.5) showing read counts per million mapped (pmm) reads for RNA-seq, Stau1-WT CROSS and Stau1-mut CROSS libraries. The centroid secondary structure for this Alu pair predicted with the Vienna folding package[47] is shown below center. (**c**,**d**) Length distribution of predicted helices (**c**) and loop (**d**) regions within secondary structures of 3′-UTR inverted Alu pairs or 3′-UTR sequences of identical size randomly picked from nontarget genes. *P* values corresponding to the comparison of helix and loop length distributions between Stau1 Alu targets and random 3′ UTRs were calculated with the Wilcoxon rank-sum test ($n = 2$ biological replicates).

intergenic noncoding RNAs (NR_026757 and NR_026999) and minimally in introns (**Supplementary Fig. 4**). Conversely, they were highly enriched in 3′ UTRs (**Fig. 2a** and **Supplementary Fig. 4**) and in select 'intergenic' regions immediately 3′ to annotated 3′ UTRs (**Fig. 2b** and **Supplementary Fig. 4**). Polyadenylation-site sequencing (PAS-seq) revealed the intergenic regions to represent strongly distal 3′ UTRs[25] (**Fig. 2b**). Overall, we detected 515 strongly distal 3′ UTRs enriched for Stau1-WT CROSS reads (**Supplementary Table 1**), most of which contained multiple Alu pairs.

To identify those 3′ UTRs most enriched for dsRBD-dependent Stau1 binding, we called peaks in the WT CROSS libraries by using ASPeak (an expression-sensitive peak-calling algorithm[26]). We then compared, for each gene, the cumulative read counts under peak positions in the WT and mut CROSS libraries (**Fig. 2c**,**d**). Overall, the data sets were highly correlated ($r = 0.83$). Nonetheless, an outlier population ($n = 574$; **Supplementary Table 2**) exhibited much higher cross-linking (by a factor of 2.7) in WT than in mut (**Fig. 2c**,**d**); these outliers constitute a set of high-confidence 3′ UTRs displaying dsRNA-dependent Stau1 binding.

We next investigated the structural features of these targets. To identify those containing Alu pairs, we wrote an algorithm to identify, transcriptome wide, pairs of full-length Alu elements in the same (tandem) or opposite (inverted) orientation. Overlaying the inter-Alu distance for tandem Alu pairs on the WT versus mut CROSS scatter plot (**Fig. 2c**) revealed no specific relationship between tandem pairs and Stau1 cross-linking. However, the inverted Alu-pair overlay revealed a striking coincidence with the above outlier population (**Fig. 2d**). Further, inverted Alu elements separated by the least distance were the most outlying (**Fig. 2d**).

We confirmed the inverse relationship between dsRBD-dependent Stau1 cross-linking efficiency and inverted-pair inter-Alu distance in composite plots (**Fig. 3a** and **Supplementary Fig. 5**). We found similar, but less striking, results for inverted pairs containing partial Alu elements and for inverted pairs in introns and strongly distal 3′ UTRs (**Supplementary Fig. 5a**). As expected, we observed no specific mapping of WT reads on tandem Alu pairs or mapping of mut reads on Alu pairs in either orientation (**Fig. 3a**). The inverse correlation between Stau1-WT cross-linking efficiency and

© 2014 Nature America, Inc. All rights reserved.

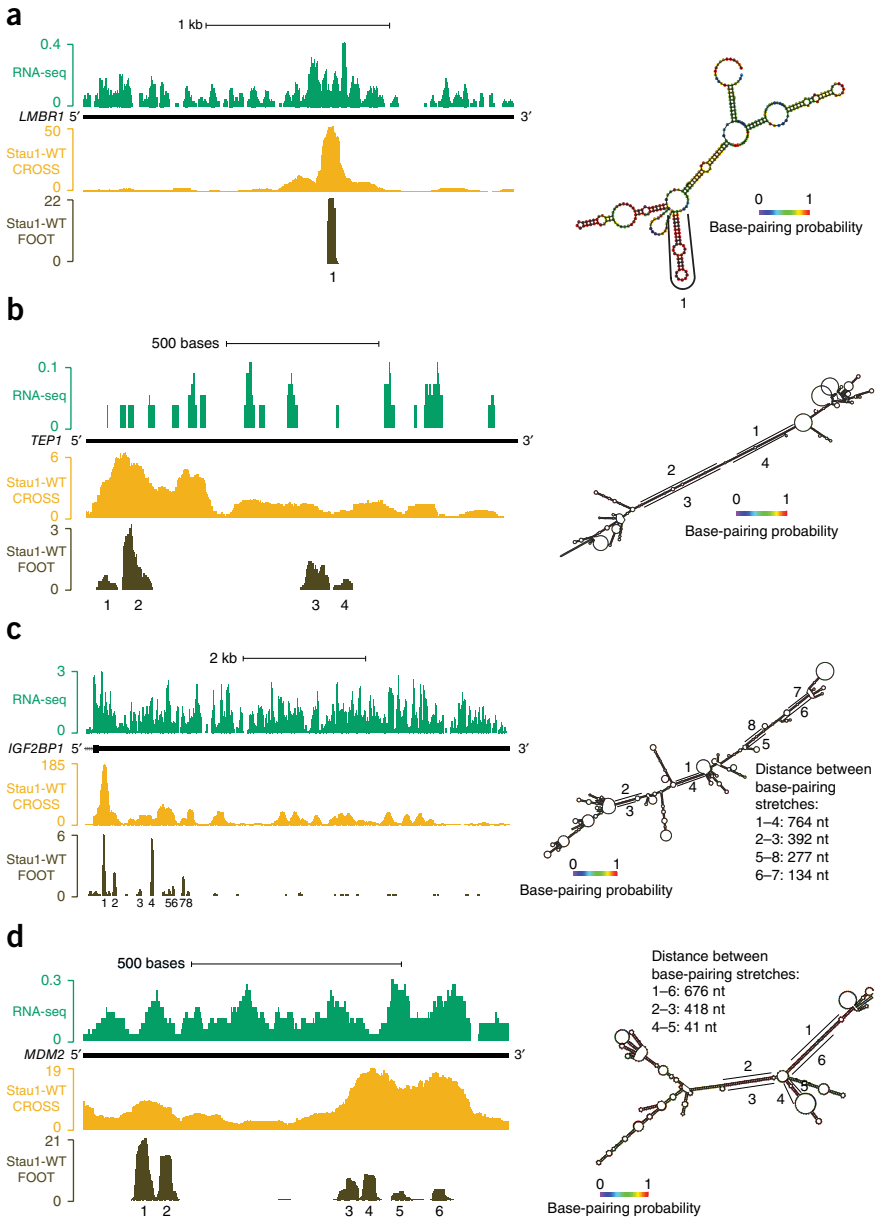

Figure 4 Examples of 3′-UTR non-Alu Staufen-binding sites. (**a**–**d**) Read distributions for RNA-seq (green), Stau1-WT CROSS (yellow) and Stau1-WT FOOT (brown) libraries on the 3′ UTRs of *LMBR1* (NM_022458.3) (**a**), *TEP1* (NM_007110.4) (**b**), *IGF2BP1* (NM_006546.3) (**c**) and *MDM2* (NM_002392) (**d**) (left) together with the corresponding centroid secondary structure colored for base-pairing probability as predicted by the Vienna folding package[47] (right). Numbers below the Stau1 WT FOOT track and in the predicted secondary structure correspond to Stau1-binding sites.

inverted-pair inter-Alu distance is consistent with the expectation that secondary-structure formation should inversely correlate with pairing-partner distance.

Because intact Alu elements are ~300 nt, inverted pairs containing full-length Alu elements could potentially form very long helices. However, individual elements in pairs exhibiting the highest WT cross-linking signal were often from different Alu families unlikely to be fully complementary. Consistently with this, *in silico* folding of an inverted Alu pair exhibiting one of the strongest Stau1-WT occupancies suggests the presence of many short helices interrupted by small loops (**Fig. 3b**). To assess the generalizability of this, we folded *in silico* all-full-length, 3′-UTR inverted Alu pairs highly enriched for Stau1-WT cross-linking and compared them to 3′-UTR sequences of similar length randomly chosen from nontarget genes. Histograms of predicted helix and loop lengths (**Fig. 3c**,**d**) revealed that Stau1-interacting Alu pairs tend to form structures with multiple helices containing <30 interrupted base pairs, spaced by 2- to 10-nt loops. Conversely, nontarget 3′ UTRs were predicted to have significantly shorter paired stretches (Wilcoxon rank-sum test, $P = 0.04$) interrupted by longer loops (Wilcoxon rank-sum test, $P = 6 \times 10^{-5}$).

Non-Alu 3′-UTR targets

Among the outlier population in **Figure 2d**, 201 of 574 contained clearly identifiable inverted Alu pairs (Alu targets), and 373 of 574 did not (non-Alu targets; **Supplementary Table 2**). Many of these non-Alu targets had clearly defined WT footprints in regions with high base-pairing probability (**Fig. 4**). A few contained a single strong footprint corresponding to a short stem-loop structure (**Fig. 4a**); others resembled inverted Alu pairs with many consecutive helices separated by short loops (**Fig. 4b**). The largest set, however, consisted of complex structures covering a few hundred nucleotides within which Stau1 footprints could be observed on multiple 7- to 40-bp helices (**Fig. 4c**,**d**). WT footprints were also present on the Arf1 3′ UTR, for which the precise Stau1-binding site was previously mapped by mutagenesis (**Supplementary Fig. 6a**)[20].

Comparison of FOOT and CROSS reads mapping to individual 3′ UTRs revealed that CROSS reads generally extended over much more of the 3′ UTR than did FOOT reads (for example, **Fig. 4c**). We could even observe extensive CROSS read coverage for many 3′ UTRs having no detectable footprints (**Supplementary Fig. 6b**). Greater abundance of such CROSS reads in WT libraries than in mut libraries indicated that they depended on Stau1's ability to bind dsRNA. This suggested that the kinetically stable Stau1-binding sites revealed by native footprinting represent only a small subset of RNA-interaction sites occurring within cells. Supporting the notion of many low-affinity Stau1-interaction sites *in vivo*, we observed a strong correlation ($r = 0.63$, $P < 2.2 \times 10^{-16}$) over all expressed genes between average per-nucleotide predicted secondary-structure strength (ΔG of the minimum free-energy structure/3′-UTR length) and the ratio of total WT/mut CROSS reads per 3′ UTR (**Fig. 5a**). We observed a similarly strong correlation ($r = 0.55$, $P < 2.2 \times 10^{-16}$) between this ratio and 3′-UTR GC content in all expressed genes (**Fig. 5b**).

We conclude that some Stau1-binding sites in 3′ UTRs consist of highly defined structures containing multiple short helices

© 2014 Nature America, Inc. All rights reserved.

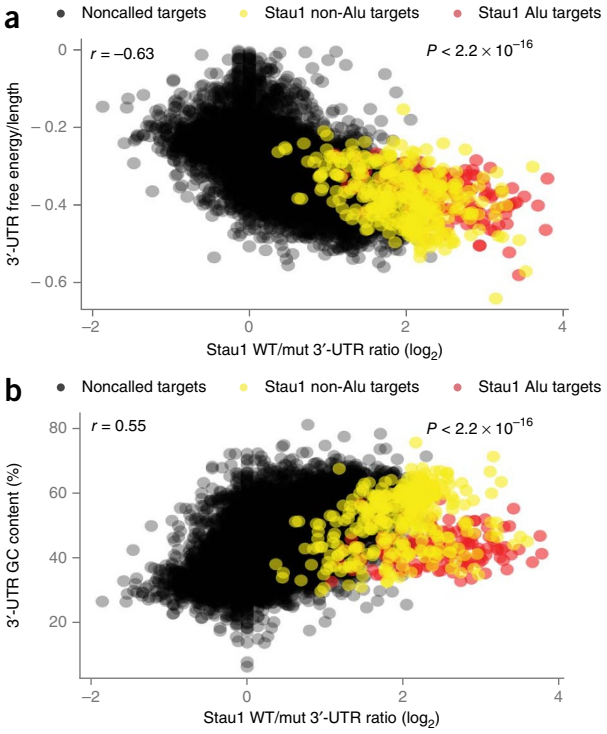

Figure 5 Stau1 binding to 3′ UTRs correlates with GC content and predicted secondary-structure free energy. (**a**) Per-gene scatter plot of 3′-UTR predicted secondary-structure free energy normalized by the length of the 3′ UTR (kcal/mol/nucleotide) against Stau1 WT/mut 3′-UTR ratio (log_2). (**b**) Per-gene scatter plot of 3′-UTR GC content (%) against Stau1 WT/mut 3′-UTR ratio (log_2) with associated Spearman correlation and calculated *P* values. Red and yellow dots correspond to called Alu and non-Alu binding sites, respectively ($n = 2$ biological replicates).

to which Stau1 binding is kinetically stable. Other binding sites, however, are more kinetically labile, and the extent of Stau1 occupancy on these sites is a function of overall 3′-UTR secondary structure–forming propensity, often driven by high GC content.

dsRBD-dependent binding of Stau1 to CDS regions

As previously discussed, both WT and mut CROSS reads mirrored ribosome density across CDS regions transcriptome wide (**Fig. 1f**). WT and mut reads were also similarly distributed relative to start and stop codons (**Fig. 1e**). In contrast to the general population, however, our 373 non-Alu 3′-UTR target genes had significantly greater CROSS reads in CDS regions for WT than for mut (**Fig. 6a**). This strong relationship between 3′ UTR and CDS WT/mut cross-linking initially suggested to us that dsRBD-dependent Stau1 binding within the 3′ UTR increases its association with CDS-bound ribosomes. Consistently with this, the correlation between preferential WT cross-linking in 3′-UTR and CDS regions held true for the entire mRNA population (**Fig. 6b**; $r = 0.61$, $P < 2.2 \times 10^{-16}$), with our identified 3′-UTR target genes simply being strongly skewed toward the higher end of both ratios. However, we also found that predicted per-nucleotide secondary structure–forming propensity and GC content were strongly correlated ($r = 0.55$ and 0.73, respectively, $P < 2.2 \times 10^{-16}$) between the 3′-UTR and CDS regions of individual genes (**Fig. 6c**,**d**); that is, the genes with high 3′-UTR secondary structure–forming propensity and GC content also tend to have high CDS secondary

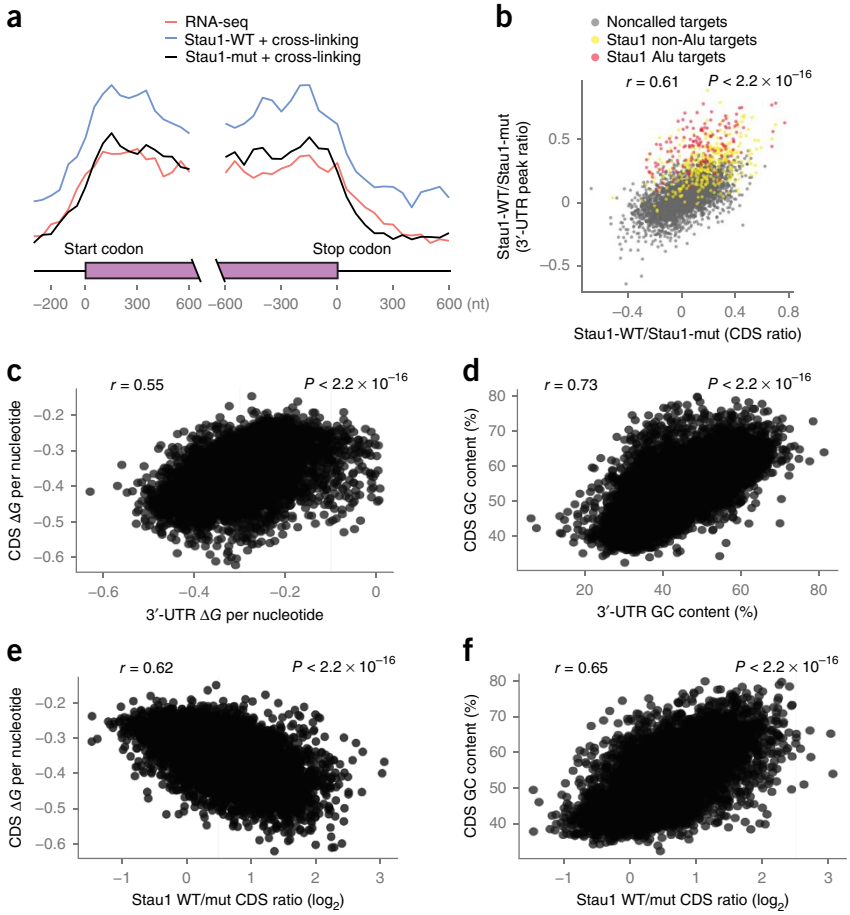

Figure 6 Stau1 occupancy on the CDS strongly correlates with GC content and predicted secondary-structure free energy. (**a**) Composite plot of the distribution of sequencing reads across the 5′ UTR, CDS and 3′ UTR of called Stau1-target genes for RNA-seq (red), Stau1-WT CROSS (blue) and Stau1-mut CROSS (black) libraries. (**b**) Per-gene scatter plot (log_{10}) of total CDS Stau1-WT CROSS read counts/total CDS Stau1-mut CROSS reads counts (CDS ratio) versus the ratio of Stau1-WT CROSS and Stau1-mut CROSS read counts under called 3′-UTR Stau1-WT CROSS peak positions (3′-UTR peak ratio). Red and yellow dots correspond to called Alu- and non-Alu–binding sites, respectively. (**c**) Per-gene scatter plot of 3′ UTR against CDS predicted secondary-structure free energy normalized by the length of the 3′ UTR (kcal/mol/nucleotide). (**d**) Per-gene scatter plot of 3′ UTR against CDS GC content (%). (**e**) Per-gene scatter plot of CDS predicted secondary-structure free energy normalized by the length of the CDS (kcal/mol/nucleotide) against Stau1 WT/mut 3′-UTR ratio (log_2). (**f**) Per-gene scatter plot of CDS GC content (%) against Stau1 WT/mut 3′-UTR ratio (log_2). All correlation coefficients and *P* values were calculated with the Spearman rank correlation ($n = 2$ biological replicates) throughout figure.

© 2014 Nature America, Inc. All rights reserved.

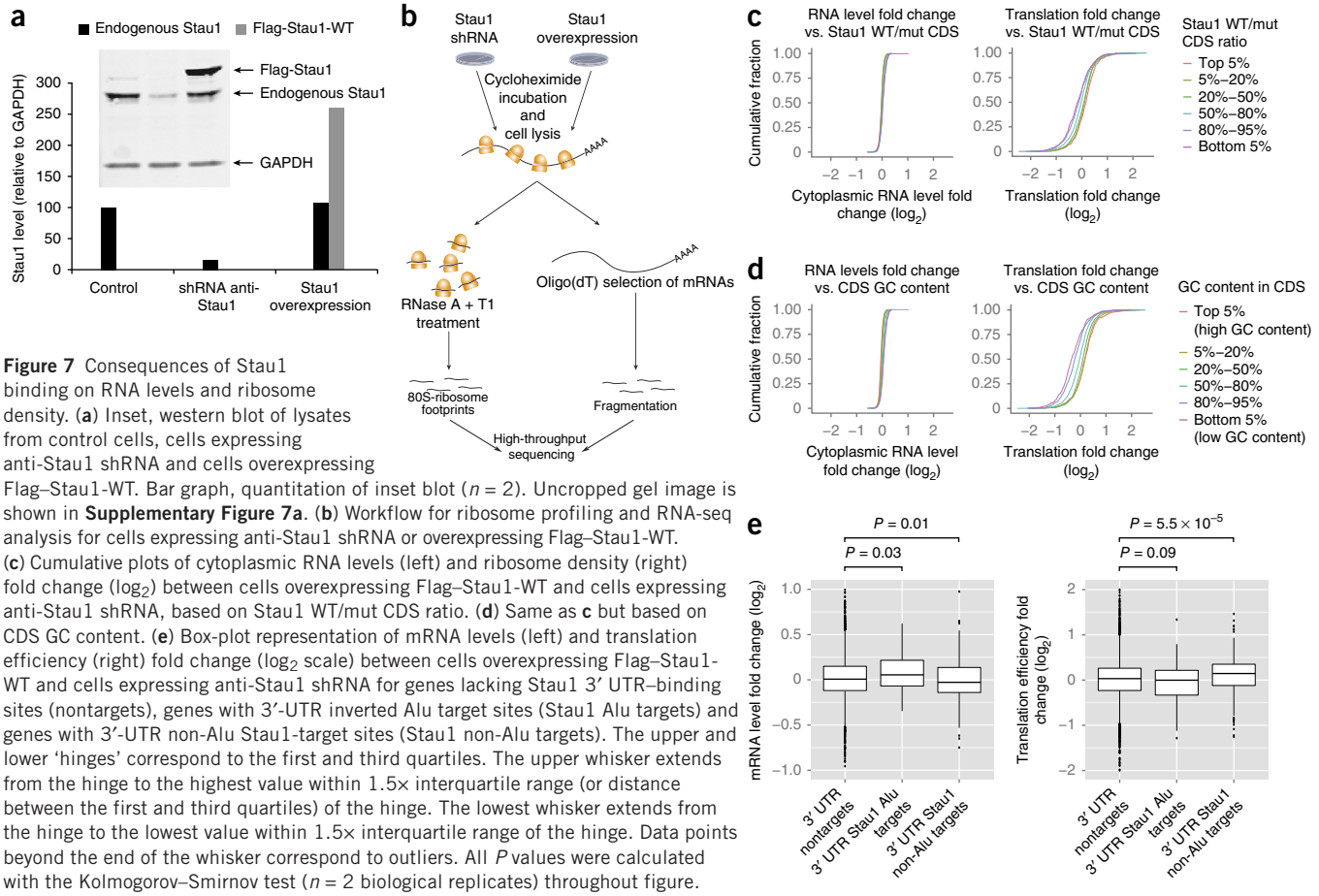

Figure 7 Consequences of Stau1 binding on RNA levels and ribosome density. (**a**) Inset, western blot of lysates from control cells, cells expressing anti-Stau1 shRNA and cells overexpressing Flag–Stau1-WT. Bar graph, quantitation of inset blot ($n = 2$). Uncropped gel image is shown in **Supplementary Figure 7a**. (**b**) Workflow for ribosome profiling and RNA-seq analysis for cells expressing anti-Stau1 shRNA or overexpressing Flag–Stau1-WT. (**c**) Cumulative plots of cytoplasmic RNA levels (left) and ribosome density (right) fold change ($\log_2$) between cells overexpressing Flag–Stau1-WT and cells expressing anti-Stau1 shRNA, based on Stau1 WT/mut CDS ratio. (**d**) Same as **c** but based on CDS GC content. (**e**) Box-plot representation of mRNA levels (left) and translation efficiency (right) fold change ($\log_2$ scale) between cells overexpressing Flag–Stau1-WT and cells expressing anti-Stau1 shRNA for genes lacking Stau1 3′ UTR–binding sites (nontargets), genes with 3′-UTR inverted Alu target sites (Stau1 Alu targets) and genes with 3′-UTR non-Alu Stau1-target sites (Stau1 non-Alu targets). The upper and lower 'hinges' correspond to the first and third quartiles. The upper whisker extends from the hinge to the highest value within 1.5× interquartile range (or distance between the first and third quartiles) of the hinge. The lowest whisker extends from the hinge to the lowest value within 1.5× interquartile range of the hinge. Data points beyond the end of the whisker correspond to outliers. All P values were calculated with the Kolmogorov–Smirnov test ($n = 2$ biological replicates) throughout figure.

© 2014 Nature America, Inc. All rights reserved.

structure–forming propensity and GC content. Consistently with this, preferential WT cross-linking in CDS regions strongly correlated with both predicted CDS secondary structure and GC content (**Fig. 6d** and **e**, $r = 0.62$ and 0.65, respectively, $P < 2.2 \times 10^{-16}$) and the 5′ UTR ($r = 0.2$; data not shown). These analyses suggest that enhanced Stau1-WT binding within CDS regions is primarily driven by GC content and secondary structure–forming propensity of the CDS itself, rather than by interactions of 3′ UTR–bound Stau1 with CDS-bound ribosomes.

From the above data, we conclude that Stau1 interacts to varying extents with the CDS and 3′-UTR regions of all cellular mRNAs in a manner dependent on their secondary structure–forming propensities. Further, the observed correlation between dsRBD-dependent Stau1 occupancy in CDS and 3′-UTR regions mainly reflects similar GC content between the CDS and 3′ UTR in individual genes rather than any direct effect of 3′-UTR binding on CDS binding. Instead, Stau1-WT occupancy on CDS regions appears to be driven by a combination of direct interactions with CDS secondary structures and its dsRBD-independent association with actively translating ribosomes.

Gene ontology analysis

To assess whether any particular gene classes were specifically enriched for dsRBD-dependent Stau1 binding, we performed gene ontology analysis using GeneCodis[27–29] (**Supplementary Table 3**). We obtained the most significant associations for the 469 genes having the highest WT/mut CDS cross-linking ratios (>1.9) and the 515 genes exhibiting high WT cross-linking to strongly distal 3′ UTRs. Both sets were highly enriched in transcription-regulatory proteins ($P = 7.1 \times 10^{-13}$ and $P = 1.1 \times 10^{-13}$, respectively). Among transcription-factor types, C2H2 zinc-finger proteins were the most enriched ($P = 4.5 \times 10^{-6}$), with homeobox and high-mobility group (HMG) proteins following close behind ($P = 1.3 \times 10^{-5}$ and 6.9×10^{-5}, respectively). Consistently with the strong correlation between Stau1 CDS and 3′-UTR occupancy, transcription-regulatory proteins were also highly enriched among our 373 non-Alu 3′-UTR targets ($P = 6.9 \times 10^{-7}$). Thus Stau1 may have a role in post-transcriptional regulation of transcription factors. Also enriched in the non-Alu and extended 3′-UTR targets ($P = 0.001$ and $P = 5.0 \times 10^{-5}$, respectively), but not in the 469 high CDS targets, were proteins involved in cell-cycle control.

Functional consequences of varying Stau1 protein levels

To directly test the functional consequences of Stau1 binding, we next varied intracellular Stau1 concentration (**Fig. 7a**,**b**). Transduction of HEK293 FLP-in cells with a lentivirus expressing an anti-Stau1 short hairpin RNA (shRNA) stably reduced endogenous Stau1 to ~20% normal levels (UNDER, **Fig. 7a**). Incubation of our stably integrated Flag–Stau1-WT cells overnight (16 h) with a high level of doxycycline induced transgene overexpression by 300–400% relative to endogenous Stau1 (OVER). We then assessed effects of Stau1 depletion or overexpression by preparing cytoplasmic poly(A)$^+$ RNA-seq and ribo-seq libraries.

RNA-seq and ribo-seq read counts on individual genes were highly correlated both between biological replicates ($r \geq 0.98$; E.P.R., unpublished data) and between UNDER and OVER samples ($r \geq 0.98$; **Supplementary Fig. 7**). Other than *STAU1* itself, there were no clear outlier genes between UNDER and OVER conditions for either

RNA-seq or ribo-seq. Further, no significant changes in alternative-splicing patterns could be detected (data not shown); thus, at least in HEK cells, binding of Stau1 in introns is of little apparent consequence for pre-mRNA splicing. However, small negative correlations between RNA levels and Stau1 levels could be detected when we ordered transcripts by CDS GC content or preferential Stau1-WT CDS cross-linking (**Fig. 7c**,**d**). That is, transcripts with high CDS GC content (which drives greater Stau1-WT CDS binding) exhibited slightly lower cytoplasmic mRNA abundances when Stau1 was overexpressed than underexpressed.

The strongest observable effect of varying Stau1 concentration was on ribosome occupancy. Cumulative histograms revealed positive relationships between ribosome occupancy and both Stau1-WT CDS cross-linking and CDS GC content across the entire transcriptome (**Fig. 7c**,**d**; Spearman correlation $r = 0.21$ and $r = 0.34$, respectively, $P < 2.2 \times 10^{-16}$). That is, genes with higher Stau1 CDS occupancy and higher CDS GC content exhibited increased ribosome occupancy upon Stau1 overexpression compared to Stau1 knockdown; conversely, genes with lower Stau1 CDS occupancy and CDS GC content exhibited decreased ribosome occupancy upon Stau1 overexpression compared to Stau1 knockdown. This suggests that higher Stau1 protein levels increase ribosome occupancy on high-GC-content transcripts at the expense of low-GC-content transcripts. Ontology analysis of the 400 genes exhibiting the greatest increase in ribosome occupancy between UNDER and OVER conditions revealed significant enrichments for transcription-regulatory proteins ($P = 0.004$) and zinc-binding proteins ($P = 1.1 \times 10^{-6}$; **Supplementary Table 3**), the same terms obtained above for genes exhibiting the highest CDS and extended 3′-UTR Stau1 occupancies.

Although we observed the strongest effects of varying Stau1 protein levels for genes with high Stau1 CDS occupancy, we also examined the effects of Stau1 over- and underexpression on our 3′-UTR non-Alu and Alu target sets. Ribosome occupancy increased slightly on non-Alu 3′-UTR targets (10% change from UNDER to OVER; $P = 0.00005$) when compared to the total population, whereas their mRNA levels decreased slightly (−2% change from UNDER to OVER; $P = 0.01$). Thus, non-Alu targets behaved like high-GC-content mRNAs. Conversely, Alu targets exhibited no significant change in ribosome occupancy, but their cytoplasmic mRNA levels increased upon Stau1 upregulation (+8% change from UNDER to OVER; $P = 0.03$; **Fig. 7e**). Therefore, mRNAs containing 3′-UTR inverted Alu pairs behave differently from other cellular mRNAs in response to Stau1 abundance. For the strongly distal 3′-UTR Stau1-binding sites, we detected no significant effect of Stau1 expression on either mRNA levels or ribosome occupancy (E.P.R., unpublished data), possibly because such isoforms represent only a minor fraction of transcripts from individual loci.

To confirm that changes in Stau1 levels are of little consequence for levels of mRNAs with 3′ UTR–binding sites, we performed quantitative reverse-transcription PCR (qRT-PCR) on several Alu and non-Alu 3′-UTR target mRNAs including Arf1, a previously identified SMD target (**Supplementary Fig. 8**). Consistently with our RNA-seq results, neither downregulation nor overexpression of Stau1 had a significant impact on the abundance of tested targets (**Supplementary Fig. 8a**). Experiments performed in two other cell lines (Huh7 and SK-Hep1) in which either Stau1 or Stau2 or both were downregulated yielded similar results (**Supplementary Fig. 8b**,**c**).

Taken together, our results indicate that Stau1 binding to the CDS results in increased ribosome occupancy and in decreased mRNA levels proportionate to both the amount of bound Stau1 and the GC content of the target mRNA. Further, at least in the cell lines we tested, Stau1 binding within the 3′ UTR appears to be of little or no consequence for translation efficiency or steady-state mRNA levels.

DISCUSSION

Like many RNA-binding factors, the *Drosophila* and mammalian Staufen proteins have been implicated in multiple post-transcriptional processes including alternative splicing[13], RNA localization[4,6,30–32], translational activation[7] and translation-dependent mRNA decay[8–11,14,20,33,34]. Which activity is observed depends on the cellular context, the identity of the bound RNA and the location of the binding site on the target RNA. Many of Staufen's previously documented activities parallel those of the EJC[7–11,19,20,33,35–38]. To better understand EJC function, we recently determined the complete EJC RNA-binding landscape in HEK293 cells[24]. Here we undertook the same analysis for Stau1.

Up to now, confirmed Staufen-binding sites were limited to a few well-characterized structures[19,20]. Broader identification of Staufen-associated mRNAs has been attempted in various organisms by combination of native RIP protocols with microarray analyses[15–18]. Unfortunately, however, such methodologies have yielded no consensus as to general features of Staufen targets. One recent study of Staufen-associated mRNAs from *Drosophila* oocytes reported enrichment of three different secondary-structural motifs that might explain Staufen binding specificity in flies[16]. However, the authors were unable to identify similar structural motifs among human Staufen-associated mRNAs from available native mammalian Stau1 and Stau2 RIP microarray data[15]. We show here that human Stau1 generally associates with actively translating ribosomes; therefore, it is impossible to discriminate between sites of direct Stau1-mRNA interaction via dsRNA binding and sites of indirect Stau1-mRNA association via elongating ribosomes without some sort of footprinting approach. Further, because of (i) Stau1's strong ribosome association, (ii) the prevalence of kinetically labile Stau1-binding sites *in vivo* and (iii) Stau1's ability to form new interactions with dsRNA after cell lysis, native RIP experiments are likely to be biased toward both highly translated mRNAs and RNAs containing the most stable sites of direct Stau1-dsRNA interaction. Our experimental design, which combined formaldehyde cross-linking and fragmentation of Stau1-associated RNAs, using both WT and mut proteins, allowed us to both avoid binding-site reassortment after cell lysis and discriminate between binding modes that do or do not require Stau1 dsRBD functionality.

The majority of non-rRNA reads in our cross-linked libraries mapped sense to 3′ UTRs and CDS regions. Within 3′ UTRs, we identified numerous high-occupancy Stau1-binding sites composed of either inverted Alu pairs (Alu targets) or sequences with extremely high secondary structure–forming propensity (non-Alu targets). Observable native Stau1 footprints showed that these structures often consist of several closely spaced helices separated by short loops. Bioinformatics analysis of the footprints, however, failed to identify any particular enriched motif (A.K. and E.P.R., unpublished data), results consistent with the idea that Staufen recognizes dsRNA in a sequence-independent manner[39–41].

Unexpectedly, in addition to detecting strong binding to large RNA secondary structures, we also detected extensive dsRBD-dependent Stau1 cross-linking extending throughout the entire length of 3′ UTRs and CDS regions. This cross-linking strongly correlated with both GC content and per-nucleotide predicted secondary-structure strength. Because GC content in CDS and 3′-UTR regions also correlate, mRNAs exhibiting preferential Stau1-WT 3′-UTR cross-linking also tend to exhibit preferential Stau1-WT CDS cross-linking. Inverted Alu pairs, the 3′ UTRs containing them and their associated CDS regions,

© 2014 Nature America, Inc. All rights reserved.

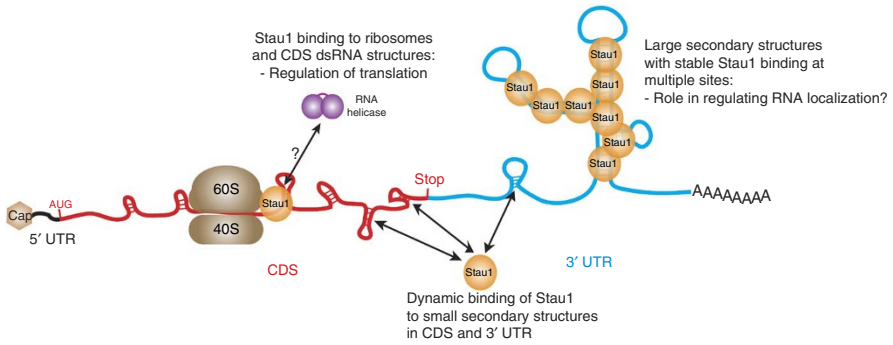

Figure 8 Model of Stau1 RNA binding and its functional role in translation. Stau1 interacts with both actively translating ribosomes and secondary structures in CDS and 3′-UTR regions. Some 3′ UTRs contain highly complex secondary structures (for example, inverted Alu pairs) that serve as kinetically stable Stau1-binding sites. However, Stau1 also makes transient interactions with smaller secondary structures throughout CDS and 3′-UTR regions. Formation of these structures is a function of overall CDS and 3′-UTR GC content. Whereas interaction of Stau1 with 3′-UTR Alu pairs has a small positive effect on cytoplasmic mRNA levels, high Stau1 CDS occupancy both increases ribosome density and slightly decreases cytoplasmic mRNA levels.

© 2014 Nature America, Inc. All rights reserved.

npg

however, exhibit average GC content. Despite high Stau1 occupancy on such 3′ UTRs, their CDS occupancies are close to levels that would be expected from their GC content alone. We therefore conclude that the strongest feature driving dsRBD-dependent Stau1 binding within CDS regions is the secondary structure–forming propensity of the CDS itself. Thus dsRBD-dependent Stau1 binding to 3′ UTRs appears to be functionally uncoupled from dsRBD-dependent Stau1 binding to CDS regions, with the correlation between 3′ UTR and CDS cross-linking driven primarily by GC-content similarity.

Our results suggest that endogenous Stau1 RNA targets can be divided into two broad classes dependent on their structural topology. One class corresponds to stable RNA secondary structures such as inverted Alu pairs and other sequences with extremely high secondary structure–forming propensity. Such elements are capable of simultaneously binding multiple Staufen molecules whose association may be further stabilized by multimerization. Close association of multiple Staufen-binding sites would assure continuous Staufen occupancy even though individual protein molecules might come and go. It is of note that we generally detected such binding sites in annotated 3′ UTRs and extended 3′ UTRs, the latter being particularly rich in inverted Alu pairs. Recently, extended 3′ UTRs were shown to be especially prevalent in the brain. Because Stau1 is known to have a role in dendritic mRNA targeting, these stable RNA secondary structures with their long-lived Stau1 associations could well be the functional binding sites through which Stau1 promotes proper subcellular mRNA localization in neurons.

The second class consists of smaller and more labile secondary structures as might occur in GC-rich CDS regions. Here our data indicate that transient Stau1 binding, perhaps by Stau1 molecules simultaneously interacting with elongating ribosomes, has a role in regulating translation. We arrived at this conclusion by analyzing cytoplasmic poly(A)$^+$ RNA-seq and ribo-seq data from cells under- and overexpressing Stau1. This allowed us to assess the effects of varying intracellular Stau1 concentration on both cytoplasmic mRNA levels and ribosome occupancy. Observable changes in mRNA levels were extremely subtle. Consistently with recent data indicating that Stau1 binding to mRNAs containing inverted Alu elements enhances their nucleocytoplasmic export[42], we did observe a small positive effect of increasing Stau1 on cytoplasmic mRNA levels for our 3′-UTR Alu targets. Conversely, for all other sets of mRNAs exhibiting preferential Stau1-WT cross-linking, Stau1 levels negatively influenced cytoplasmic mRNA levels proportionately to CDS Stau1 occupancy but not to 3′-UTR occupancy. Thus we could find little evidence for SMD driven by 3′ UTR–bound Stau1, either over the entire mRNA population or for previously identified SMD targets. Instead, higher Stau1 levels led to a preferential increase in ribosome density on high-GC-content mRNAs.

We propose a model (**Fig. 8**) based on these findings, wherein ribosome-bound Stau1 molecules transiently interact with short dsRNA helices throughout the CDS and 3′ UTR. In the CDS, such interactions somehow serve to increase ribosome density. Because Stau1 interacts with actively translating ribosomes, the increase in ribosome density may reflect increased translation efficiency. One possibility is that Stau1 helps ribosomes elongate through otherwise inhibitory secondary structures by recruiting factors such as RNA helicase A (RHA or DHX9) to disrupt them. RHA is a positive regulator of translation on mRNAs containing 5′-UTR secondary structures[43] and is known to copurify with Stau1 (ref. 44 and E.P.R., unpublished data). Another abundant translational-regulatory protein that binds ribosomes and cross-links throughout CDS regions is the fragile X protein, FMRP[45]. FMRP, however, is a negative regulator of translation. Whereas deletion of either FMRP or Stau1 causes neurological defects, the phenotypes are opposite: absence of FMRP leads to dendritic spine overgrowth[46], whereas absence of Stau1 results in fewer spines[14]. Thus it is possible that FMRP and Stau1 have opposing roles in synaptic protein production, with FMRP inhibiting translation and Stau1 promoting it.

Finally, mRNAs encoding transcription-regulatory proteins were recently reported as being enriched in *Drosophila* Staufen RIP samples[16]. Consistently with this, we found that mRNAs encoding transcription factors of the C2H2 zinc-finger, HMG and homeobox families were highly enriched among mRNAs exhibiting the highest preferential 3′-UTR and CDS Stau1-WT occupancy. Transcription factors and zinc-binding proteins were also highly enriched among the mRNAs whose ribosome density was most positively affected by Stau1 protein levels. Thus Stau1 may have a previously unrecognized role in the translational regulation of transcription-regulatory proteins.

METHODS

Methods and any associated references are available in the online version of the paper.

Accession codes. High-throughput sequencing data corresponding to native and cross-linked Stau1 RIPiT experiments as well as PAS-seq, RNA-seq and ribo-seq have been deposited in the GEO database under accession number GSE52447.

Note: Any Supplementary Information and Source Data files are available in the online version of the paper.

ACKNOWLEDGMENTS

We would like to acknowledge M. Garber, A. Bicknell, A. Noma and J. Braun for comments on the manuscript and the University of Massachusetts Medical School Deep Sequencing Core for technical advice. We thank P.S. Chen for technical help in preparing plasmids and cell lines. We also thank H. Ozadam for technical advice in using RNA structure–prediction tools. Finally, we thank M. Janas, R. Lakshmi

and D. Morrissey from Novartis for kindly sharing total RNA from Huh7 and HepG2 cells upon Stau1 and Stau2 knockdown. M.J.M. is supported as a Howard Hughes Medical Institute Investigator.

AUTHOR CONTRIBUTIONS

E.P.R. and M.J.M. conceived the study, designed the experiments and wrote the manuscript. E.P.R. performed the experiments. A.K. conducted most bioinformatics analyses. C.C. designed and implemented the ribo-seq analysis. E.P.R. and A.K. designed and performed GC-content and secondary structure–prediction analyses. B.C.M. and G.S. contributed with tandem-affinity purification of Stau1 complexes. E.E.H. contributed with cDNA library preparation for high-throughput sequencing. A.A.-P. prepared PAS-seq cDNA libraries. L.P. participated in quantitative PCR analysis.

COMPETING FINANCIAL INTERESTS

The authors declare no competing financial interests.

Reprints and permissions information is available online at http://www.nature.com/reprints/index.html.

1. Kerner, P., Degnan, S.M., Marchand, L., Degnan, B.M. & Vervoort, M. Evolution of RNA-binding proteins in animals: insights from genome-wide analysis in the sponge *Amphimedon queenslandica*. *Mol. Biol. Evol.* **28**, 2289–2303 (2011).
2. Luo, M., Duchaîne, T.F. & Desgroseillers, L. Molecular mapping of the determinants involved in human Staufen-ribosome association. *Biochem. J.* **365**, 817–824 (2002).
3. Martel, C. *et al.* Multimerization of Staufen1 in live cells. *RNA* **16**, 585–597 (2010).
4. St Johnston, D., Beuchle, D. & Nüsslein-Volhard, C. Staufen, a gene required to localize maternal RNAs in the *Drosophila* egg. *Cell* **66**, 51–63 (1991).
5. Ferrandon, D., Koch, I., Westhof, E. & Nüsslein-Volhard, C. RNA-RNA interaction is required for the formation of specific bicoid mRNA 3′ UTR–STAUFEN ribonucleoprotein particles. *EMBO J.* **16**, 1751–1758 (1997).
6. Köhrmann, M. *et al.* Microtubule-dependent recruitment of Staufen-green fluorescent protein into large RNA-containing granules and subsequent dendritic transport in living hippocampal neurons. *Mol. Biol. Cell* **10**, 2945–2953 (1999).
7. Dugré-Brisson, S. *et al.* Interaction of Staufen1 with the 5′ end of mRNA facilitates translation of these RNAs. *Nucleic Acids Res.* **33**, 4797–4812 (2005).
8. Kim, Y.K., Furic, L., Desgroseillers, L. & Maquat, L.E. Mammalian Staufen1 recruits Upf1 to specific mRNA 3′UTRs so as to elicit mRNA decay. *Cell* **120**, 195–208 (2005).
9. Gong, C. & Maquat, L.E. lncRNAs transactivate STAU1-mediated mRNA decay by duplexing with 3′ UTRs via Alu elements. *Nature* **470**, 284–288 (2011).
10. Gleghorn, M.L., Gong, C., Kielkopf, C.L. & Maquat, L.E. Staufen1 dimerizes through a conserved motif and a degenerate dsRNA-binding domain to promote mRNA decay. *Nat. Struct. Mol. Biol.* **20**, 515–524 (2013).
11. Park, E., Gleghorn, M.L. & Maquat, L.E. Staufen2 functions in Staufen1-mediated mRNA decay by binding to itself and its paralog and promoting UPF1 helicase but not ATPase activity. *Proc. Natl. Acad. Sci. USA* **110**, 405–412 (2013).
12. Thomas, M.G., Martinez Tosar, L.J., Desbats, M.A., Leishman, C.C. & Boccaccio, G.L. Mammalian Staufen 1 is recruited to stress granules and impairs their assembly. *J. Cell Sci.* **122**, 563–573 (2009).
13. Ravel-Chapuis, A. *et al.* The RNA-binding protein Staufen1 is increased in DM1 skeletal muscle and promotes alternative pre-mRNA splicing. *J. Cell Biol.* **196**, 699–712 (2012).
14. Vessey, J.P. *et al.* A loss of function allele for murine Staufen1 leads to impairment of dendritic Staufen1-RNP delivery and dendritic spine morphogenesis. *Proc. Natl. Acad. Sci. USA* **105**, 16374–16379 (2008).
15. Furic, L., Maher-Laporte, M. & Desgroseillers, L. A genome-wide approach identifies distinct but overlapping subsets of cellular mRNAs associated with Staufen1- and Staufen2-containing ribonucleoprotein complexes. *RNA* **14**, 324–335 (2008).
16. Laver, J.D. *et al.* Genome-wide analysis of Staufen-associated mRNAs identifies secondary structures that confer target specificity. *Nucleic Acids Res.* **41**, 9438–9460 (2013).
17. Maher-Laporte, M. & Desgroseillers, L. Genome wide identification of Staufen2-bound mRNAs in embryonic rat brains. *BMB Rep.* **43**, 344–348 (2010).
18. Kusek, G. *et al.* Asymmetric segregation of the double-stranded RNA binding protein Staufen2 during mammalian neural stem cell divisions promotes lineage progression. *Cell Stem Cell* **11**, 505–516 (2012).
19. Ferrandon, D., Elphick, L., Nüsslein-Volhard, C. & St Johnston, D. Staufen protein associates with the 3′UTR of bicoid mRNA to form particles that move in a microtubule-dependent manner. *Cell* **79**, 1221–1232 (1994).
20. Kim, Y.K. *et al.* Staufen1 regulates diverse classes of mammalian transcripts. *EMBO J.* **26**, 2670–2681 (2007).
21. Singh, G., Ricci, E.P. & Moore, M.J. RIPiT-Seq: a high-throughput approach for footprinting RNA:protein complexes. *Methods* doi:10.1016/j.ymeth.2013.09.013 (2 October 2013).
22. Ramos, A. *et al.* RNA recognition by a Staufen double-stranded RNA-binding domain. *EMBO J.* **19**, 997–1009 (2000).
23. Liu, Z.R., Wilkie, A.M., Clemens, M.J. & Smith, C.W. Detection of double-stranded RNA-protein interactions by methylene blue-mediated photo-crosslinking. *RNA* **2**, 611–621 (1996).
24. Singh, G. *et al.* The cellular EJC interactome reveals higher-order mRNP structure and an EJC-SR protein nexus. *Cell* **151**, 750–764 (2012).
25. Miura, P., Shenker, S., Andreu-Agullo, C., Westholm, J.O. & Lai, E.C. Widespread and extensive lengthening of 3′ UTRs in the mammalian brain. *Genome Res.* **23**, 812–825 (2013).
26. Kucukural, A., Özadam, H., Singh, G., Moore, M.J. & Cenik, C. ASPeak: an abundance sensitive peak detection algorithm for RIP-Seq. *Bioinformatics* **29**, 2485–2486 (2013).
27. Carmona-Saez, P., Chagoyen, M., Tirado, F., Carazo, J.M. & Pascual-Montano, A. GENECODIS: a web-based tool for finding significant concurrent annotations in gene lists. *Genome Biol.* **8**, R3 (2007).
28. Nogales-Cadenas, R. *et al.* GeneCodis: interpreting gene lists through enrichment analysis and integration of diverse biological information. *Nucleic Acids Res.* **37**, W317–W322 (2009).
29. Tabas-Madrid, D., Nogales-Cadenas, R. & Pascual-Montano, A. GeneCodis3: a non-redundant and modular enrichment analysis tool for functional genomics. *Nucleic Acids Res.* **40**, W478–W483 (2012).
30. Micklem, D.R., Adams, J., Grünert, S. & St Johnston, D. Distinct roles of two conserved Staufen domains in *oskar* mRNA localization and translation. *EMBO J.* **19**, 1366–1377 (2000).
31. Macchi, P. *et al.* The brain-specific double-stranded RNA-binding protein Staufen2: nucleolar accumulation and isoform-specific exportin-5-dependent export. *J. Biol. Chem.* **279**, 31440–31444 (2004).
32. Kiebler, M.A. *et al.* The mammalian staufen protein localizes to the somatodendritic domain of cultured hippocampal neurons: implications for its involvement in mRNA transport. *J. Neurosci.* **19**, 288–297 (1999).
33. Cho, H. *et al.* Staufen1-mediated mRNA decay functions in adipogenesis. *Mol. Cell* **46**, 495–506 (2012).
34. Kretz, M. *et al.* Control of somatic tissue differentiation by the long non-coding RNA TINCR. *Nature* **493**, 231–235 (2013).
35. Ghosh, S., Marchand, V., Gáspár, I. & Ephrussi, A. Control of RNP motility and localization by a splicing-dependent structure in *oskar* mRNA. *Nat. Struct. Mol. Biol.* **19**, 441–449 (2012).
36. Nott, A., Le Hir, H. & Moore, M.J. Splicing enhances translation in mammalian cells: an additional function of the exon junction complex. *Genes Dev.* **18**, 210–222 (2004).
37. Wiegand, H.L., Lu, S. & Cullen, B.R. Exon junction complexes mediate the enhancing effect of splicing on mRNA expression. *Proc. Natl. Acad. Sci. USA* **100**, 11327–11332 (2003).
38. Ivanov, P.V., Gehring, N.H., Kunz, J.B., Hentze, M.W. & Kulozik, A.E. Interactions between UPF1, eRFs, PABP and the exon junction complex suggest an integrated model for mammalian NMD pathways. *EMBO J.* **27**, 736–747 (2008).
39. Marión, R.M., Fortes, P., Beloso, A., Dotti, C. & Ortín, J. A human sequence homologue of Staufen is an RNA-binding protein that is associated with polysomes and localizes to the rough endoplasmic reticulum. *Mol. Cell Biol.* **19**, 2212–2219 (1999).
40. Wickham, L., Duchaîne, T., Luo, M., Nabi, I.R. & DesGroseillers, L. Mammalian staufen is a double-stranded-RNA- and tubulin-binding protein which localizes to the rough endoplasmic reticulum. *Mol. Cell Biol.* **19**, 2220–2230 (1999).
41. Monshausen, M. *et al.* Two rat brain staufen isoforms differentially bind RNA. *J. Neurochem.* **76**, 155–165 (2001).
42. Elbarbary, R.A., Li, W., Tian, B. & Maquat, L.E. STAU1 binding 3′ UTR IRAlus complements nuclear retention to protect cells from PKR-mediated translational shutdown. *Genes Dev.* **27**, 1495–1510 (2013).
43. Hartman, T.R. *et al.* RNA helicase A is necessary for translation of selected messenger RNAs. *Nat. Struct. Mol. Biol.* **13**, 509–516 (2006).
44. Villacé, P., Marión, R.M. & Ortín, J. The composition of Staufen-containing RNA granules from human cells indicates their role in the regulated transport and translation of messenger RNAs. *Nucleic Acids Res.* **32**, 2411–2420 (2004).
45. Darnell, J.C. *et al.* FMRP stalls ribosomal translocation on mRNAs linked to synaptic function and autism. *Cell* **146**, 247–261 (2011).
46. Comery, T.A. *et al.* Abnormal dendritic spines in fragile X knockout mice: maturation and pruning deficits. *Proc. Natl. Acad. Sci. USA* **94**, 5401–5404 (1997).
47. Gruber, A.R., Lorenz, R., Bernhart, S.H., Neuböck, R. & Hofacker, I.L. The Vienna RNA websuite. *Nucleic Acids Res.* **36**, W70–W74 (2008).

© 2014 Nature America, Inc. All rights reserved.

ONLINE METHODS

Plasmids and cell lines. pcDNA5-TetO-Flag was previously described[38]. A cDNA encoding Stau1 (HindIII-NotI) was inserted into the polylinker of pcDNA5-TetO-Flag. A cDNA encoding the Stau1 mutant lacking RNA-binding activity was created by PCR using primers carrying the mutations described in ref. 2, in which phenylalanines at position 216 in dsRBD3 and at position 319 in dsRBD4 were mutated into alanines.

Stable cell lines were generated as described in ref. 38. In these cells, the expression level of the stably integrated Flag-tagged protein was optimized by titration of doxycycline (Dox; 0–2,000 ng ml^{-1}) to determine a concentration at which exogenous protein expression levels were comparable to those of endogenous counterparts.

Generation of Stau1-knockdown cell line. HEK293T LentiX cells (Clontech) were transfected with pGIPZ encoding shRNAs directed against Stau1 (Open Biosystems, CloneID: V2LHS_42695), pPAX2 and pMD2.G at a 12:9:3 ratio with Lipofectamine 2000 (Invitrogen). 2 d after transfection, the supernatant of transfected cells was collected and passed through a 0.45-µm filter. To generate the Stau1-knockdown cell line, HEK293 TRex cells (Invitrogen) were transduced with 7 mL of the supernatant of lentiviral-producing cells in the presence of 10 µg ml^{-1} polybrene for 6 h. Transduced cells were then selected in the presence of puromycin (3 µg ml^{-1}) for 2 weeks.

Stau1 RIPiT. The procedure was performed essentially as described in (ref. 38). For each Staufen purification, TRex-HEK293 cells containing a stable copy of Flag-tagged Stau proteins (Stau1-WT and Stau1-mut) or control cells (expressing Flag tag only) were grown in four 15-cm plates. Expression of the Flag-tagged protein was induced with doxycycline for 16 h. 1 h before cell harvesting, cycloheximide (CHX) was added to 100 µg ml^{-1}. The monolayer was rinsed and harvested in phosphate-buffered saline (PBS) containing 100 µg ml^{-1} CHX. The cells were lysed in 3 ml hypotonic lysis buffer (20 mM Tris-HCl, pH 7.5, 15 mM NaCl, 10 mM EDTA, 0.5% NP-40, 0.1% Triton X-100, 1× EDTA-free protease inhibitor cocktail (ROCHE), and 100 µg ml^{-1} CHX) for 10 min on ice. The suspension was sonicated (Branson Digital Sonifier-250) at 40% amplitude with a Microtip for a total of 20 s (in 2-s bursts with 10-s intervals). NaCl was adjusted to 150 mM, and the lysate was cleared by centrifugation at 15,000*g* for 10 min at 4 °C. The lysate was incubated for 2 h at 4 °C with 420 µl of anti-Flag agarose beads (50% slurry, Sigma) prewashed twice with 10 ml isotonic wash buffer (IsoWB) (20 mM Tris-HCl, pH 7.5, 150 mM NaCl, and 0.1% NP-40). The RNA–protein (RNP) complexes captured on beads were washed four times (4 × 10 ml) with 10 ml IsoWB. After the fourth wash, bound RNP complexes were incubated with one bed volume of IsoWB containing 1 U $µl^{-1}$ of RNase I for 10 min at 37 °C with intermittent shaking. RNP complexes were again washed four times with 10 ml IsoWB. Flag epitope–containing complexes were affinity eluted from the beads in one bed volume of IsoWB containing 250 µg.ml^{-1} Flag peptide with gentle shaking at 4 °C for 2 h. To prepare the recovered elution for input into a second IP, its volume was adjusted to 400 µl and its composition adjusted to that of the lysis buffer above with NaCl at 150 mM. The suspension was incubated with 7 µg of anti-Stau1 antibody (ab105398, Abcam, validation of IP in **Supplementary Fig. 1c**,**d**) precoupled to 35 µl of Protein G Dynabeads (Invitrogen) according to the manufacturer's instructions. Immunoprecipitation was carried out at 4 °C for 2 h. Captured RNP complexes were washed six times with 1 ml of ice-cold IsoWB and eluted with 200 µl of clear sample buffer (100 mM Tris-HCl, pH 6.8, 4% SDS, 10 mM EDTA and 100 mM DTT) at 25 °C for 5 min and subsequently at 95 °C for 2 min.

For IPs under protein–cross-linking conditions, cells were collected and rinsed once in PBS + CHX and then resuspended in PBS + CHX. Formaldehyde was added to 0.1%, and the suspension was gently mixed at RT for 10 min. A one-tenth volume of quenching buffer (2.5 M glycine, and 25 mM Tris base) was added. Cells were pelleted and lysed in hypotonic lysis buffer supplemented with 0.1% SDS and 0.1% sodium deoxycholate. Sonication after cell lysis was performed at 40% amplitude with a Microtip for a total of 90 s (in 5-s bursts with 30-s intervals). After Flag IP as described above, IP samples were washed twice with IsoWB + 0.1% SDS and 0.1% sodium deoxycholate and then with IsoWB. All subsequent steps were as above with omission of RNase I treatment.

RIPiT RNA extraction. The volume of RIPiT elution was extracted as described in ref. 38. For Stau1 cross-linked RIPiT experiments, extracted RNAs were depleted of rRNA before cDNA library construction with the Ribozero rRNA-removal kit from Epicentre.

Preparation of samples for RNA-seq. 75 µg of total RNA were poly(A)-selected with the Dynabeads mRNA-purification kit (Invitrogen). After poly(A) selection, mRNAs were fragmented with RNA-fragmentation buffer (Ambion) for 4 min and 30 s at 70 °C to obtain fragments 100–125 nt long. After fragmentation, RNAs were precipitated in three volumes of 100% ethanol at −20 °C overnight. After a wash with 70% ethanol, RNA was resuspended in 5 µl of water and the 3′ ends dephosphorylated with PNK (New England BioLabs) for 1 h at 37 °C. After this, RNAs were subjected to cDNA library preparation.

Poly(A)-site sequencing (PAS-seq). 75 µg of total RNA were poly(A)-selected with the Dynabeads mRNA purification kit (Invitrogen). After poly(A) selection, mRNAs were fragmented with RNA fragmentation buffer (Ambion) for 5 min at 70 °C to obtain fragments 60–80 nt long. After fragmentation, RNAs were reverse transcribed with an anchored and barcoded oligo$(dT)_{21}$VN (where V corresponds to A, C or G residues) containing the sequences complementary to Illumina's paired-end primers (PE1.0 and PE2.0) separated by a polyethylene glycol (PEG) spacer. After reverse transcription (RT) with Superscript III (Invitrogen), cDNAs were size-selected and circularized with Circligase I (Epicentre) for 4 h at 60 °C. This was followed by inactivation at 80 °C for 10 min. After circularization, cDNAs were PCR-amplified with Illumina's PE1.0 and 2.0 primers for a total of 14 cycles. PCR products were size-selected on a nondenaturing polyacrylamide gel and sent for high-throughput sequencing on Illumina's HiSeq2000 platform.

Quantitative RT-PCR. Total RNA from HEK293, Huh7 and HepG2 cells transfected with control shRNA or a Stau1-targeting shRNA construct was reverse transcribed with the Vilo RT kit from Life Technologies. Obtained cDNAs were then used as input for quantitative PCR analysis as described in ref. 48 with the following primers: *GAPDH* forward, 5′ tccaccaccctgttgctgtag 3′ and reverse, 5′acccactcctccacctttgac3′; *Arf1* forward, 5′ atcttcgcctcccgactc 3′ and reverse, 5′atgcttgtggacaggtgga3′; *C11orf58* forward, 5′ cagacgacgatctgggatct 3′ and reverse, 5′ tgatctcctataacaagacgaccag 3′; *PAICS* forward, 5′ aaggaaaagctgcaatctcaa 3′ and reverse, 5′ ccccacattttctggtgaag 3′; *MDM2* forward, 5′ catgcctgcccactttaga 3′ and reverse, 5′ ggaggctcccaactgctt 3′; *MDM4* forward, 5′ agggatgaaatgcttcttgg 3′ and reverse, 5′ aaggttgctatgaggtctaccttg 3′.

Sucrose-gradient sedimentation of Flag–Stau1-WT cells. HEK293 cells were plated at 5 million in a 150-mm^2 plate and Flag–Stau1-WT expression induced overnight with doxycycline at 0.5 ng ml^{-1}. 16 h after induction, cells were either incubated with cycloheximide (100 µg ml^{-1}) for 10 min or with harringtonine (2 µg ml^{-1}) for either 3, 10 or 40 min. This was followed by incubation with cycloheximide (100 µg ml^{-1}) for 10 min. Cells were then washed in PBS + cycloheximide (100 µg ml^{-1}) or PBS + harringtonine (2 µg ml^{-1}) + cycloheximide (100 µg ml^{-1}) and scraped. Cells were then lysed in 1 ml of lysis buffer (10 mM Tris-HCl, pH 7.5, 5 mM $MgCl_2$, 100 mM KCl, 1% Triton X-100, 2 mM DTT, 100 µg/ml cycloheximide and 1× Protease-Inhibitor Cocktail EDTA-free (Roche). Lysate was homogenized by gentle pipetting up and down with a P1000 pipettor for a total of eight strokes and incubated at 4 °C for 10 min. The lysate was centrifuged at 1,300*g* for 10 min at 4 °C; the supernatant was recovered. After this, samples were loaded on top of a 10–50% (w/v) sucrose gradient (20 mM HEPES-KOH, pH 7.4, 5 mM $MgCl_2$, 100 mM KCl, 2 mM DTT, and 100 µg ml^{-1} cycloheximide) and centrifuged in a SW-40ti rotor at 35,000 r.p.m. for 2 h 40 min at 4 °C. Samples were fractionated into 14 individual samples that were subjected to SDS-PAGE to monitor Stau1 (ab105398, Abcam, 1:1,000 dilution) and Rpl26 (Bethyl, A300-685A, 1:1,000 dilution) levels by western-blotting. Experimental validation of antibodies used for western blots can be found at the manufacturers' websites.

Oligo(dT) pulldown of poly(A) RNAs after UV exposure of living cells. HEK293 Flp-In cells were exposed to 0, 0.2, 0.4 and 0.8 J cm^{-2} of 254-nm UV light. Cells were then scraped and lysed with binding buffer (0.5 M NaCl, 10 mM Tris-HCl, pH 7.5, 0.5% SDS, 0.1 mM EDTA and protease inhibitor cocktail). Cell lysates were passed through a 22-gauge syringe needle five times and spun at 15,000*g* for 10 min. Cleared cell lysates were added to oligo(dT) cellulose beads (Ambion, AM10020) previously washed in binding buffer. After 1 h of

© 2014 Nature America, Inc. All rights reserved.

doi:10.1038/nsmb.2739

incubation at room temperature, beads were washed three times with binding buffer and once with nondenaturing wash buffer (0.5 M NaCl, 10 mM Tris-HCl, pH 7.5, 0.1% NP-40, 0.1% Triton-X 100 and 0.2 mM EDTA). Finally, beads were resuspended in elution buffer (10 mM Tris-HCl, pH 7.5, and 1 mM EDTA) complemented with RNase A/T1 cocktail (Ambion AM2286) and incubated at 37 °C for 1 h. The supernatant was finally recovered and loaded on a 12% SDS-PAGE for western-blotting of hnRNPA1 and Stau1.

Stau1 RNA reassociation test. HEK293 Flp-In, Flag–Stau1-WT or Flag–Stau1-mut cells were harvested and lysed as described in the Stau1 RIPiT section (above). After cell lysis, 0.1 pmol of a radiolabeled *in vitro*–transcribed *Arf1* 3′-UTR sequence (labeled with [α-^{32}P]UTP) was added for each 150-mm^2 plate. The remaining procedure is identical to that described in the Stau1 RIPiT section until the Flag elution step. Flag eluates on each sample were monitored for radioactivity with liquid scintillation.

Ribosome profiling. HEK293 Flag–Stau1-WT cells incubated in the presence of 1 ng ml^{-1} of doxycycline (Stau1 overexpression) or not (control) as well as HEK293 cells expressing the shRNAs against Stau1 (Stau1 knockdown) were seeded at 5 million cells in a 150-mm dish. After 16 h of culture, cycloheximide was added to 100 μg ml^{-1} for 10 min. Cells were then washed two times in ice-cold PBS + cycloheximide (100 μg ml^{-1}) and scraped in 1 ml of PBS + cycloheximide (100 μg ml^{-1}). Cells were pelleted at 500*g* for 5 min at 4 °C and lysed in 1 ml of lysis buffer (10 mM Tris-HCl, pH 7.5, 5 mM $MgCl_2$, 100 mM KCl, 1% Triton X-100, 2 mM DTT, 100 μg/ml cycloheximide and 1× Protease-Inhibitor Cocktail EDTA-free (Roche)). Lysate was homogenized with a P1000 pipettor by gentle pipetting up and down for a total of eight strokes and incubated at 4 °C for 10 min. The lysate was centrifuged at 1,300*g* for 10 min at 4 °C, the supernatant recovered and the absorbance at 260 nm measured. For the footprinting, 5 A_{260} units of the cleared cell lysates were incubated with 300 units of RNase T1 (Fermentas) and 500 ng of RNase A (Ambion) for 30 min at RT. After this, samples were loaded on top of a 10–50% (w/v) linear sucrose gradient (20 mM HEPES-KOH, pH 7.4, 5 mM $MgCl_2$, 100 mM KCl, 2 mM DTT and 100 μg ml^{-1} of cycloheximide) and centrifuged in a SW-40ti rotor at 35,000 r.p.m. for 2 h 40 min at 4 °C.

Samples were then collected from the top of the gradient while absorbance was measured at 254 nm and the fraction corresponding to 80S monosomes recovered. The collected fraction was complemented with SDS to 1% final and proteinase K (200 μg ml^{-1}) and then incubated at 42 °C for 45 min. After proteinase K treatment, RNA was extracted with one volume of phenol (pH 4.5)/chloroform/isoamyl alcohol (25:24:1). The recovered aqueous phase was supplemented with 20 μg of glycogen, 300 mM sodium acetate, pH 5.2, and 10 mM $MgCl_2$. RNA was precipitated with three volumes of 100% ethanol at −20 °C overnight. After a wash with 70% ethanol, RNA was resuspended in 5 μl of water and the 3′ ends dephosphorylated with PNK (New England BioLabs) in MES buffer (100 mM MES-NaOH, pH 5.5, 10 mM $MgCl_2$, 10 mM β-mercaptoethanol and 300 mM NaCl) at 37 °C for 3 h. Dephosphorylated RNA footprints were then resolved on a 15% acrylamide (19:1), 8 M urea denaturing gel for 1 h 30 min at 35 W and fragments ranging from 26 nt to 32 nt size-selected from the gel. Size-selected RNAs were extracted from the gel slice by overnight nutation at RT in RNA elution buffer (300 mM NaCl, and 10 mM EDTA). The recovered aqueous phase was supplemented with 20 μg of glycogen, 300 mM sodium acetate, pH 5.2, and 10 mM $MgCl_2$. RNA was precipitated with three volumes of 100% ethanol at −20 °C overnight. After a wash with 70% ethanol, RNA was resuspended in 5 μl of water and subjected to cDNA library construction.

The remaining undigested cell lysates were extracted with an equal volume of phenol (pH 4.5)/chloroform/isoamyl alcohol (25:24:1). The recovered aqueous phase was supplemented with 20 μg of glycogen, 300 mM sodium acetate, pH 5.2, and 10 mM $MgCl_2$. RNA was precipitated with three volumes of 100% ethanol at −20 °C overnight. After a wash with 70% ethanol, RNA was resuspended in 9 μl of water and fragmented with RNA fragmentation buffer (Ambion) at 70 °C for 4 min 30 s in order to obtain RNA fragments of 100–150 nt. Fragmented RNAs were supplemented with 20 μg of glycogen, 300 mM sodium acetate, pH 5.2, and 10 mM $MgCl_2$ and precipitated with three volumes of 100% ethanol at −20 °C overnight. After a wash with 70% ethanol, RNA was resuspended in 5 μl of water and dephosphorylated as described above with PNK. After 3′-end dephosphorylation, RNA fragments were subjected to cDNA library construction.

Illumina cDNA library construction. cDNA libraries were prepared with a homemade kit (E.E.H., unpublished data). Briefly, RNA fragments with a 3′-OH were ligated to a preadenylated DNA adaptor. Following this, ligated RNAs were reverse transcribed with Superscript III (Invitrogen) with a barcoded reverse-transcription primer that anneals to the preadenylated adaptor. After reverse transcription, cDNAs were resolved in a denaturing gel (10% acrylamide and 8 M urea) for 1 h and 45 min at 35 W. Gel-purified cDNAs were then circularized with CircLigase I (Epicentre) and PCR-amplified with Illumina's paired-end primers 1.0 and 2.0 for 5 cycles (ribosome footprints), 12 cycles (Stau1 RIPiT) or 16 cycles (RNA-seq libraries). PCR amplicons were gel-purified and submitted for sequencing on the Illumina HiSeq 2000 platform.

Mapping of high-throughput sequencing reads. First, reads were split with respect to their 5′-barcode sequence. After this, 5′-barcode and 3′-adaptor sequences were removed from reads. Reads were then aligned to University of California, Santa Cruz (UCSC) human hg18 assembly with TopHat[49]. Unmapped reads from TopHat were then mapped with Bowtie[50] to a custom set of sequences including 18S, 28S, 45S, 5S and 5.8S rRNA, repeat elements, small-nuclear RNAs (snRNAs), tRNAs, microRNAs and pre-microRNAs.

Transcript-level quantification and normalization for all high-throughput sequencing libraries. Read counts from all high-throughput sequencing libraries were normalized to the total number of mapped reads. When a single read aligned across the boundary of two different regions (for example, CDS and 3′ UTR), the read was divided proportionally to the aligned length in the given region. To quantify gene expression, reads per kilobase per million of mapped reads (RPKM) were calculated for the most abundant isoform of each gene.

Transcriptome-wide pairing of inverted and tandem Alu elements. Genomic coordinates for all Alu elements were obtained from the repeat-masker track of the UCSC genome browser. With the BedTools[51] intersectBed function with –s(strand) option, we obtained coordinates of all Alu elements located in 3′ UTRs, distal 3′ UTRs and introns. After this step, Alu elements in Watson and Crick strands were separated. To pair inverted Alu elements, we used the ClosestBed function between Alu elements in the Watson and Crick strands. The same steps were also performed to detect same-strand pairs on Watson-Watson and Crick-Crick pairs. In this case, tandem pairs that had an inverted Alu pair less than 2,000 nt apart were excluded from the analysis.

Definition of distal 3′-UTR regions. To define distal 3′-UTR regions, we used PAS-seq mapped reads. For this, peaks were called from the PAS-seq library with ASPeak. With the BedIntersect function (BedTools) we found all genes that had a polyadenylation site within 10,000 nt of the canonical polyadenylation site, provided that they were upstream of the transcription start site of the downstream gene. If multiple peaks were called within that interval, the called peak most distal to the canonical polyadenylation site was selected.

Counting of sequencing reads for Alu pairs separated by different distances. With the genomic coordinates of tandem and inverted Alu pairs described above, we created a new file for each region (3′ UTR, distal 3′ UTR and introns) that contained the genomic coordinates of each Alu element within every pair in addition to 1,000 nt upstream of the 5′-most Alu element and 1,000 nt downstream of the 3′-most Alu element. After this, read counts from Stau1-WT CROSS, Stau1-mut CROSS and RNA-seq were obtained for each defined region within pairs and then normalized with RNA-seq RPKM value for the same interval. Normalized read counts for each interval were added for all Alu pairs located between 0 and 200 nt, 200 and 500 nt, 500 and 1,000 nt, 1,000 and 2,000 nt, and 2,000 nt and beyond.

Secondary-structure analysis of inverted Alu pairs. To analyze the secondary structure of inverted Alu pairs, we obtained the sequence of both Alu elements, including the region separating them. As a control, same-length sequences were randomly chosen from the list of genes devoid of Stau1-target sites. After the sequences were obtained, the Vienna Package RNAfold 2.1.1 (ref. 47) was used to predict secondary structures.

Analysis of ribosome-profiling reads. To calculate translational-efficiency changes upon knockdown or overexpression of Stau1, we used a generalized

© 2014 Nature America, Inc. All rights reserved.

linear model (GLM). We used the number of sequencing reads mapping to the annotated coding region (or ORF) for each RefSeq transcript. In the GLM, we used the cell type (overexpression of Stau1WT, Stau1-shRNA), sequence-library preparation batch and type of sequence data (RNA-seq or ribo-seq) as predictor variables of the number of mapped reads per transcript. We had two biological replicates for all conditions, which were used to estimate a biological variability in the number of counts. We used a trended dispersion estimation method, following ref. 52. To extract translation-efficiency changes upon a given treatment, we used the contrast between type of sequence data, ribo-seq versus RNA-seq, in each pair of conditions.

48. Ricci, E.P. *et al.* Translation of intronless RNAs is strongly stimulated by the Epstein-Barr virus mRNA export factor EB2. *Nucleic Acids Res.* **37**, 4932–4943 (2009).
49. Trapnell, C., Pachter, L. & Salzberg, S.L. TopHat: discovering splice junctions with RNA-Seq. *Bioinformatics* **25**, 1105–1111 (2009).
50. Langmead, B., Trapnell, C., Pop, M. & Salzberg, S.L. Ultrafast and memory-efficient alignment of short DNA sequences to the human genome. *Genome Biol.* **10**, R25 (2009).
51. Quinlan, A.R. & Hall, I.M. BEDTools: a flexible suite of utilities for comparing genomic features. *Bioinformatics* **26**, 841–842 (2010).
52. McCarthy, D.J., Chen, Y. & Smyth, G.K. Differential expression analysis of multifactor RNA-Seq experiments with respect to biological variation. *Nucleic Acids Res.* **40**, 4288–4297 (2012).

© 2014 Nature America, Inc. All rights reserved.

doi:10.1038/nsmb.2739

Post-transcriptional regulation of gene expression in innate immunity

Susan Carpenter[1], Emiliano P. Ricci[2*], Blandine C. Mercier[2*], Melissa J. Moore[2] and Katherine A. Fitzgerald[1,3]*

Abstract | Innate immune responses combat infectious microorganisms by inducing inflammatory responses, antimicrobial pathways and adaptive immunity. Multiple genes within each of these functional categories are coordinately and temporally regulated in response to distinct external stimuli. The substantial potential of these responses to drive pathological inflammation and tissue damage highlights the need for rigorous control of these responses. Although transcriptional control of inflammatory gene expression has been studied extensively, the importance of post-transcriptional regulation of these processes is less well defined. In this Review, we discuss the regulatory mechanisms that occur at the level of mRNA splicing, mRNA polyadenylation, mRNA stability and protein translation, and that have instrumental roles in controlling both the magnitude and duration of the inflammatory response.

A dynamic and coordinately regulated gene expression programme lies at the heart of the inflammatory process. This response endows the host with a first line of defence against infection and the capacity to repair and restore damaged tissues. However, unchecked, prolonged or inappropriately scaled inflammation can be detrimental to the host and lead to diseases such as atherosclerosis, arthritis and cancer[1,2].

The acute inflammatory programme is initiated when germline-encoded pattern recognition receptors (PRRs) that are present in distinct cellular compartments respond to signs of microbial infection[3,4]. Once activated, these receptors trigger signalling cascades that converge on well-defined transcription factors. Mobilization of these factors leads to rapid, dynamic and temporally regulated changes in the expression of hundreds of genes that are involved in antimicrobial defence, phagocytosis, cell migration, tissue repair and the regulation of adaptive immunity.

Multiple genes within distinct functional categories are coordinately and temporally regulated by transcriptional 'on' and 'off' switches that account for the specificity of gene expression in response to external stimuli. Multiple layers of regulation — including chromatin state, histone or DNA modifications, and the recruitment of transcription factors and of the basal transcription machinery — collaborate to control these pathogen-induced or danger signal-induced gene expression programmes[5,6], which vary depending on the cell lineage involved and the specific signal that is encountered. Although transcription is an essential first step, and certainly the most well-scrutinized area in studies of innate immunity[5,6], proper regulation of immune genes also involves a plethora of additional post-transcriptional checkpoints. These occur at the level of mRNA splicing, mRNA polyadenylation, mRNA stability and protein translation. Many of these mechanisms are particularly important for modulating the strength and duration of the response and for turning the system off in a timely and efficient manner. In this Review, we cover exciting recent developments in this underexplored area. We also highlight the emerging role of long non-coding RNAs (lncRNAs) in controlling the inflammatory response. A better understanding of these processes could facilitate the development of selective therapeutics to prevent damaging inflammation.

Alternative splicing in innate immunity

Although transcriptional regulation has been at the forefront of studies of innate immunity, the role of post-transcriptional regulation in controlling gene expression in macrophages and other innate immune cells is equally important. Almost one-fifth of the genes that are expressed in human dendritic cells (DCs) undergo alternative splicing upon bacterial challenge. Most of these genes are involved in general cellular functions but some participate directly in antimicrobial defence[7]. Furthermore, stimulation of human monocytes with the Toll-like receptor 4 (TLR4) ligand lipopolysaccharide

[1]*Program in Innate Immunity, Division of Infectious Diseases and Immunology, Department of Medicine, University of Massachusetts Medical School, Worcester, Massachusetts 01605, USA.*
[2]*Howard Hughes Medical Institute, University of Massachusetts Medical School, Worcester, Massachusetts 01605, USA.*
[3]*Centre of Molecular Inflammation Research, Department of Cancer Research and Molecular Medicine, Norwegian University of Science and Technology, 7491 Trondheim, Norway.*
**These authors contributed equally to this work.*
Correspondence to K.A.F.
e-mail: kate.fitzgerald@umassmed.edu
doi:10.1038/nri3682

© 2014 Macmillan Publishers Limited. All rights reserved

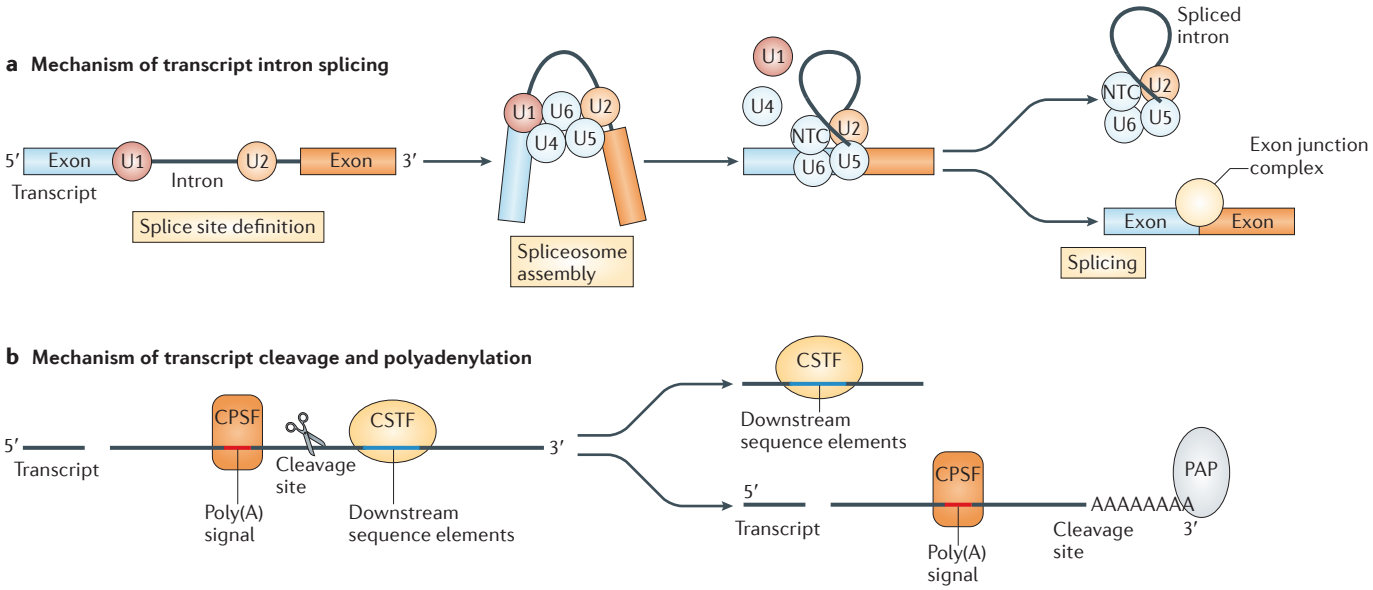

Figure 1 | **Pre-mRNA processing into mature mRNAs: intron splicing and polyadenylation. a** | Following transcription, pre-mRNA intronic sequences are removed by splicing. The 5′ and 3′ splice sites of introns are recognized by the small nuclear ribonucleoproteins (snRNPs) U1 and U2, respectively, then the spliceosome assembles and catalyses the excision of the introns and ligation of the flanking exons. A multi-protein complex, the exon junction complex, is deposited on exon–exon junctions. **b** | A poly(A) tail is also added to the 3′ end of transcripts. The poly(A) signal and nearby U-rich or GU-rich downstream sequence elements are recognized by two multi-protein complexes — namely, cleavage and polyadenylation specificity factor (CPSF) and cleavage stimulating factor (CSTF), respectively — that promote endonucleolytic cleavage of the transcript. Poly(A) polymerase (PAP) catalyses the subsequent addition of a stretch of adenosines from the cleavage site.

Pattern recognition receptors
(PRRs). Host receptors (such as Toll-like receptors (TLRs) or NOD-like receptors (NLRs)) that can sense pathogen-associated molecular patterns and initiate signalling cascades that lead to an innate immune response. These can be membrane-bound (for example, TLRs) or soluble cytoplasmic receptors (for example, retinoic acid-inducible protein I (RIG-I), melanoma differentiation-associated protein 5 (MDA5) and NLRs).

microRNA
(miRNA). Non-coding RNA (21 nucleotides in length) that is encoded in the genomes of animals and plants. miRNAs regulate gene expression by binding to the 3′ untranslated region of target mRNAs.

AU-rich elements
(AREs). Regulatory elements usually located in the 3′ untranslated regions of mRNAs that mediate the recognition of an array of RNA-binding proteins and determine RNA stability and translation.

(LPS) and with interferon-γ (IFNγ) causes the polyadenylation machinery to favour proximal poly(A) site use in terminal exons that contain two or more poly(A) sites[8]. This type of alternative polyadenylation leads to a global shortening of 3′ untranslated regions (UTRs) and a loss of key regulatory elements such as microRNA (miRNA) target sites and AU-rich elements (AREs).

Alternative pre-mRNA processing. Following transcription, pre-mRNA intronic sequences are removed by splicing. The 5′ and 3′ splice sites of introns are recognized by the small nuclear ribonucleic particles (snRNPs) U1 and U2, respectively, before the spliceosome assembles and catalyses excision of the introns and the ligation of flanking exons[9] (FIG. 1a). In addition, a poly(A) tail is added to the 3′ end of transcripts. A poly(A) signal and nearby U-rich or GU-rich downstream sequence elements (DSEs) are recognized by two multi-protein complexes — namely, cleavage and polyadenylation specificity factor (CPSF) and cleavage stimulation factor (CSTF), respectively — that promote endonucleolytic cleavage of the pre-mRNAs. Poly(A) polymerase (PAP; also known as PAPα and PAPOLA) subsequently catalyses the addition of a stretch of adenosines from the cleavage site[10] (FIG. 1b).

Remarkably, >94% of human genes are subject to alternative splicing and/or alternative polyadenylation[11]. Types of alternative splicing that alter the sequence of the encoded protein include mutually exclusive exons, exon skipping, intron retention and the alternative use of 5′ or 3′ splice sites at intron ends. Alternative polyadenylation within an intron can also generate an mRNA that encodes a truncated protein product. However, alternative processing is by no means limited to internal sites. Alternative promoter use results in alternative first exons, which changes the length and sequence of the 5′ UTR. Similarly, alternative polyadenylation within the last exon can shorten or extend the 3′ UTR[11] (FIG. 2a). Modifications to UTRs have important consequences because they can affect sequences that regulate subcellular mRNA localization, translation efficiency and mRNA stability[12].

Regulation of TLR signalling by alternative splicing and alternative polyadenylation. The TLR signalling pathway is subject to extensive post-transcriptional regulation, in which more than 256 alternatively processed transcripts encode variants of receptors, adaptors and signalling molecules[13]. Every *TLR* gene has numerous alternatively spliced variants[13–18], and *TLR1* to *TLR7* all have between two and four predicted alternative polyadenylation sites[16]. These variant transcripts have myriad effects on signal transduction. For example, an alternatively spliced form of mouse *Tlr4* mRNA includes an exon that is not present in the canonical mRNA[15]. An in-frame stop codon in this extra exon generates a secretable receptor isoform that lacks the transmembrane and intracellular domains that are present in the full-length protein. LPS stimulation enhances the expression of soluble TLR4 (smTLR4) by macrophages, and forced overexpression of smTLR4

© 2014 Macmillan Publishers Limited. All rights reserved

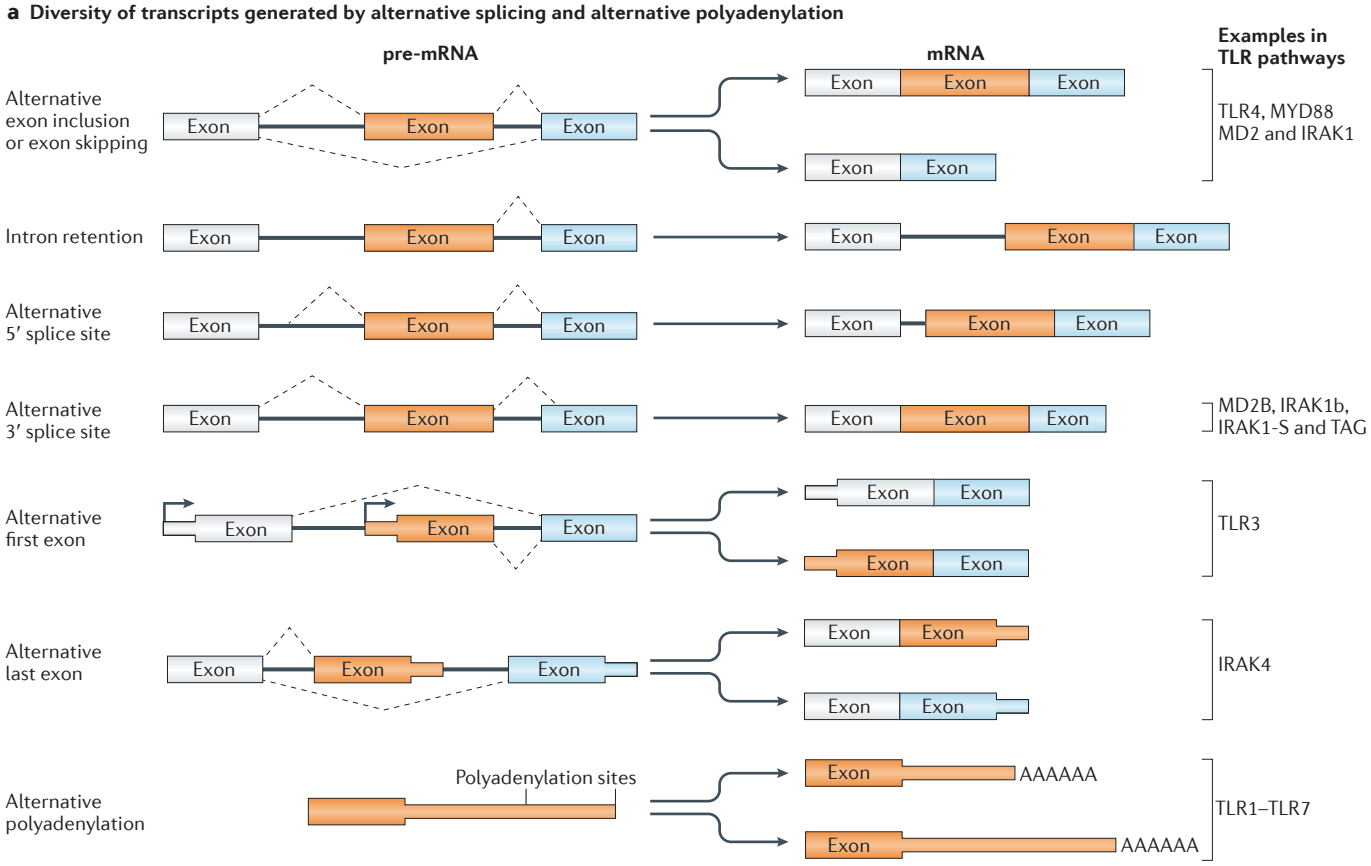

Figure 2 | **Regulation of Toll-like receptor signalling by alternative pre-mRNA processing.** **a** | Toll-like receptor (TLR) signalling pathways are regulated through diverse transcripts that are generated by alternative splicing and alternative polyadenylation. Dashed lines indicate spliced transcript. **b** | The TLR4 signalling pathway is markedly regulated by alternative splicing of mRNAs encoding the receptor (TLR4) and the co-receptor (MD2), the adaptor molecules (myeloid differentiation primary response protein 88 (MYD88) and TRIF-related adaptor molecule (TRAM)), as well as the IL-1R-associated kinases (IRAKs). Inhibitory isoforms are shown in red. AP-1, activator protein 1; IRF, interferon-regulatory factor; LPS, lipopolysaccharide; MD2B, splice variant of MD2; MYD88s, splice variant of MYD88; NF-κB, nuclear factor-κB; smTLR4, soluble TLR4 splice variant; TAG, splice variant of TRAM; TRAF, TNF receptor-associated factor; TRIF, TIR-domain-containing adaptor protein inducing IFNβ. Part **a** from REF. 11, Nature Publishing Group.

inhibits LPS-mediated activation of nuclear factor-κB (NF-κB) and the production of tumour necrosis factor (TNF)[15]. An analogous *TLR4* mRNA isoform that contains a premature stop codon is upregulated following LPS stimulation of human monocytes[14]. Induction of this isoform is significantly lower in monocytes from patients with cystic fibrosis who, compared with healthy controls, produce more TNF in response to LPS[14]. These results suggest that production of a truncated form of TLR4 generates a negative feedback loop that limits excessive inflammation. Another component of this negative feedback mechanism is the requisite TLR4 co-factor MD2 (which is encoded by *LY96*). Shortened MD2 isoforms have been described in both mouse macrophages[19] and human monocytic cell lines[20]. The mRNA encoding the mouse MD2B variant lacks the first 54 bases of exon 3 (REF. 19), whereas the mRNA encoding the human MD2s variant lacks all of exon 2 (REF. 20). MD2s expression is

© 2014 Macmillan Publishers Limited. All rights reserved

upregulated by LPS, as well as by IFNγ and interleukin-6 (IL-6)[20]. Both MD2B and MD2s proteins bind TLR4 as efficiently as full-length MD2 but they fail to mediate signalling. MD2B inhibits cell surface expression of mouse TLR4 (REF. 19), and MD2s inhibits the binding of full-length MD2 to TLR4 (REF. 20). Thus, these shortened forms of MD2 inhibit macrophage stimulation by LPS[19,20] by limiting productive interactions with full-length MD2. Together, these results suggest that the production of altered forms of either TLR4 or MD2 modulate macrophage responses to LPS and bacterial pathogens.

This idea that shorter protein isoforms fine-tune signalling is a common mechanism that occurs throughout the TLR signalling pathway. In response to LPS, myeloid differentiation primary response protein 88 (MYD88) enables the formation of multi-protein complexes that contain TLR4, MYD88, IL-1 receptor-associated kinase 1 (IRAK1) and IRAK4. IRAK1 is phosphorylated by IRAK4; phosphorylated IRAK1 binds to TNF receptor-associated factor 6 (TRAF6), and eventually NF-κB and activator protein 1 (AP-1) transcription factors are activated by IκB kinase (IKK) complexes (FIG. 2b). Stimulation of mouse monocytes with LPS or pro-inflammatory cytokines induces the expression of a splice variant of MYD88 — known as MYD88s — that lacks exon 2, which causes an in-frame deletion of the MYD88 intermediate domain[21–23]. Although MYD88s can still bind to TLRs and IRAK1, it cannot interact with IRAK4 (REF. 22). Consequently, MYD88s is unable to mediate IRAK1 phosphorylation and NF-κB activation[21]. MYD88s also acts as a dominant-negative inhibitor of NF-κB signalling by forming heterodimers with full-length MYD88 (REF. 21). By contrast, MYD88s does not impair LPS-induced AP-1 activation[23]. Thus, MYD88s production allows monocytes to differentially tune the NF-κB and AP-1 activation pathways.

Adding further complexity, IRAK1 is also subject to alternative splicing[24,25]. The IRAK1b[24] and IRAK1-S[25] variants result from the use of alternative 3′ splice sites in exon 12. Both proteins lack kinase activity[24,25] and IRAK1-S fails to bind TRAF6 (REF. 25). Nonetheless, both isoforms can induce NF-κB activation, possibly by forming functional heterodimers with full-length IRAK1 (REFS 24,25). Conversely, a third alternatively spliced variant that lacks exon 11, IRAK1c, has no kinase activity and acts as a dominant-negative inhibitor[26]. IRAK1c suppresses both NF-κB activation and TNF production in response to LPS[26]. IRAK2, another IRAK-like molecule, has four known alternatively spliced isoforms[27]. IRAK2a and IRAK2b potentiate NF-κB activation, whereas IRAK2c and IRAK2d act as inhibitors[27]. Finally (as reviewed in REF. 28), the NF-κB signalling cascade is tightly regulated by the expression of agonistic and antagonistic splice variants of inhibitor of NF-κB (IκB), IKK and the NF-κB transcription factor subunits RELA (also known as the p65 subunit), RELB and NF-κB2 (also known as the p100 subunit).

Regarding the MYD88-independent TLR pathway, TLR3 stimulation induces the association of the adaptor molecule TIR-domain-containing adaptor protein inducing IFNβ (TRIF) with TRIS, which is a shorter splice variant of TRIF that lacks the Toll/IL-1R (TIR) domain[29]. Overexpression of TRIS activates NF-κB and IFN-regulatory factor 3 (IRF3), whereas TRIS knockdown inhibits TLR3-mediated signalling[29]. These results suggest that the TLR3 signalling pathway involves the formation of heterocomplexes between TRIF and TRIS. TRIF-dependent TLR signalling also involves TRIF-related adaptor molecule (TRAM; also known as TICAM2) (FIG. 2b). In unstimulated cells, TRAM localizes to the plasma membrane where it interacts with TLR4 (REF. 30). In human mononuclear cells, a longer isoform of TRAM, known as TAG, results from the use of an alternative 3′ splice site in exon 4 of TRAM, and this variant contains an additional Golgi dynamics domain. Consequently, TAG localizes to the endoplasmic reticulum (ER)[30]. Following stimulation with LPS, TRAM and TAG colocalize to late endosomes where TAG displaces the adaptor TRIF from its productive association with TRAM. TAG expression also promotes TRAM degradation. As a result, TAG inhibits LPS-induced IRF3 activation[30]. Finally, IRF3 is also alternatively spliced, with eight different transcript variants described to date: IRF3, IRF3a to IRF3f, and IRF3CL[31–33]. Among them, only IRF3e is able to undergo cytoplasm-to-nuclear translocation in response to TLR3 ligands and bind to the *IFNB* promoter as full-length IRF3 does[32]. The other isoforms inhibit the transactivation potential of IRF3 to various degrees[31–33].

Together, these studies reveal how alternative splicing and alternative polyadenylation are exceedingly common events that occur throughout innate immunity and fine-tune almost all steps in the process (FIG. 2b). Nevertheless, surprisingly little is known about the mechanisms that drive this alternative processing. What is known is that bacterial challenge of human DCs changes the mRNA levels of >70 splicing factors[34] and LPS stimulation of mouse macrophages increases the mRNA and protein levels of CSTF64 (also known as CSTF2), which can favour the use of weak proximal polyadenylation sites[34]. Finally, two recent reports[35,36] indicate that the kinetics of pre-mRNA splicing itself might regulate gene expression during innate immune responses. Transcriptome-wide analysis of lipid A-stimulated macrophages revealed an accumulation of fully transcribed, but incompletely spliced, pre-mRNAs following TLR4 activation[35]. Similarly, TNF-induced splicing of intermediate and late transcripts is delayed compared with splicing of early gene pre-mRNAs[36]. These results suggest that not only are innate immune responses regulated by alternative pre-mRNA processing but the rate of such processing is also subject to variation, possibly to regulate the temporal order of gene expression in response to pro-inflammatory signals.

mRNA stability in innate immunity

Cellular mRNA levels are established by both mRNA production and degradation. Recently, *in vivo* labelling of newly synthesized RNAs using modified uridine (4-thiouridine (4sU)[37] or bromodeoxyuridine (BrU)[38]), or purification of chromatin-associated mRNAs[35] enabled the simultaneous assessment of total and

© 2014 Macmillan Publishers Limited. All rights reserved

nascent transcript levels in cells stimulated with LPS[35,37] or TNF[38]. As a result, both gene transcription and RNA decay rates could be evaluated for their respective contributions to cell responses. These analyses showed that increases in RNA levels that are induced by pro-inflammatory stimuli are mainly due to changes in the rate of transcription[35,37]. However, the duration of these responses — particularly those that are rapid and transient — is mainly determined by the rate of RNA decay[37]. In LPS-stimulated and TNF-stimulated macrophages, a negative correlation can be observed between the speed of transcript induction and intrinsic mRNA stability[39,40]. In addition, challenge with LPS[37], TNF[38] and *Mycobacterium tuberculosis*[17] modulates the stability of numerous transcripts. For example, stimulation of fibroblasts with TNF induces stabilization of 152 mRNAs and destabilization of 58 other transcripts[38]. Similarly, LPS treatment of DCs alters the stability of 6% of the expressed mRNAs[37]. Interestingly, the affected transcripts are enriched for inflammatory and immune signalling genes, as well as NF-κB targets[37]. Together, these results indicate that regulation of mRNA degradation is also essential for shaping innate immune responses.

ARE-mediated regulation of mRNA stability. In 1986, conserved AU-rich sequences were discovered in the 3′ UTR of the genes that encode the short-lived cytokines TNF[41] and granulocyte–macrophage colony-stimulating factor (GM-CSF; which is encoded by *CSF2*)[42]. Insertion of the *CSF2* AU-rich sequence into the 3′ UTR of the stable transcript encoding β-globin was shown to strongly induce its degradation[42]. These studies pioneered the discovery of AREs as major regulators of mRNA stability. Approximately 5–8% of all human transcripts contain AREs[43,44] and many of these ARE-containing mRNAs are involved in inflammation[43]. Consistent with rapid mRNA decay being essential for controlling response duration, early and transient transcripts that are induced in LPS-stimulated or TNF-stimulated macrophages contain significantly more AREs in their 3′ UTRs than intermediate and late transcripts[40]. Moreover, numerous pro-inflammatory factors, as well as anti-inflammatory cytokines, undergo ARE-mediated regulation, including IL-6, IL-8, TNF, IL-1β, GM-CSF, inducible nitric oxide synthase (iNOS; also known as NOS2), transforming growth factor-β (TGFβ) and IL-10 (REFS 45,46).

AREs consist of various large clusters of overlapping AUUUA pentamers and UUAUUUAUU nonamers that are specifically recognized by over 20 different ARE-binding proteins. Among them, tristetraprolin (TTP), butyrate response factor 1 (BRF1; also known as ZFP36L1), BRF2 (also known as ZFP36L2), KH-type splicing regulatory protein (KSRP; also known as KHSRP) and AU-rich element RNA-binding protein 1 (AUF1; also known as HNRNPD) stimulate target transcript decay by recruiting deadenylases and downstream degradation machineries[45,46]. By contrast, Y-box binding protein1 (YB1; also known as NSEP1) and the ELAV (embryonic lethal and abnormal vision) family members Hu-antigen R (HUR; also known as ELAVL1) and HUD (also known as ELAVL4) stabilize their targets by competing with the destabilizing ARE-binding proteins for ARE occupancy[45,46] (FIG. 3a). ARE-mediated regulation of *Tnf* and *Il1b* mRNA stability has been well studied. Notably, HUR initially stabilizes both transcripts in response to LPS[47]. LPS also induces TTP synthesis and phosphorylation[48,49], and phosphorylated TTP is sequestered by the chaperone protein 14-3-3 (REF. 49). When dephosphorylated by protein phosphatase 2A[50], TTP displaces HUR, binding the *Tnf* ARE with high affinity and the *Il1b* ARE with a lower affinity. TTP then recruits degradation factors to the *Tnf* transcript, but not to *Il1b*[48]. The destabilizing protein AUF1 also targets *Tnf* and *Il1b* mRNAs[51]. This regulation results in a rapid and transient induction of *Tnf* mRNA expression in response to LPS, whereas *Il1b* mRNA is induced more slowly and has a longer half-life[48]. Mice that are deficient in TTP[52,53] or AUF1 (REFS 51,54), or that express a mutant version of TNF that lacks its ARE[47], develop severe inflammatory diseases[52,53], including LPS-induced shock[51,54]. These symptoms, which result from excessive TNF and IL-1β production, illustrate the crucial role of ARE-mediated mRNA degradation in controlling inflammatory responses. Unexpectedly, mice that lack HUR expression in myeloid cells also show pathological exacerbation of their immune response[55]. This outcome might result from HUR-mediated stabilization of anti-inflammatory transcripts and/or inhibition of HUR-mediated translation in wild-type mice (see below). Together, these data highlight both the importance and the complexities of ARE-mediated post-transcriptional control of inflammation.

Non-ARE-mediated regulation of mRNA stability. The modulation of pro-inflammatory transcript stability also involves non-ARE regulatory elements. For example, a constitutive decay element (CDE) in the *TNF* 3′ UTR confers an intrinsic short half-life to the transcript that is independent of ARE-mediated decay[56]. Recognition of embryo deadenylation element (EDEN)-like sequences — which are rich in uridine–purine dinucleotides — by CUG triplet repeat RNA-binding protein 1 (CUGBP1; also known as CELF1) additionally induces *TNF* and *FOS* mRNA deadenylation[57]. By contrast, polypyrimidine tract-binding protein (PTB; also known as PTBP1), which is induced by pro-inflammatory cytokines, stabilizes iNOS transcripts through the recognition of a UC-rich sequence in the 3′ UTR[58] (FIG. 3b).

Among 3′ UTR regulatory elements, miRNAs have emerged as key modulators of mRNA decay and translation. They consist of ~21-nucleotide-long non-coding RNAs that base-pair to partially complementary sequences in the 3′ UTR of their target RNAs. miRNAs act as the nucleic acid core of the RNA-induced silencing complex (RISC), which inhibits mRNA translation and/or causes deadenylation and the subsequent decay of target transcripts[59] (FIG. 3c). More than 1,000 miRNAs have been identified in the human genome[60] and as many as 60% of all mRNAs are predicted to contain a miRNA target site (or multiple sites)[61]. Abundant evidence has revealed the importance of miRNAs in the development of immune cells, as well as in the initiation and termination of inflammation (reviewed in REFS 62,63).

© 2014 Macmillan Publishers Limited. All rights reserved

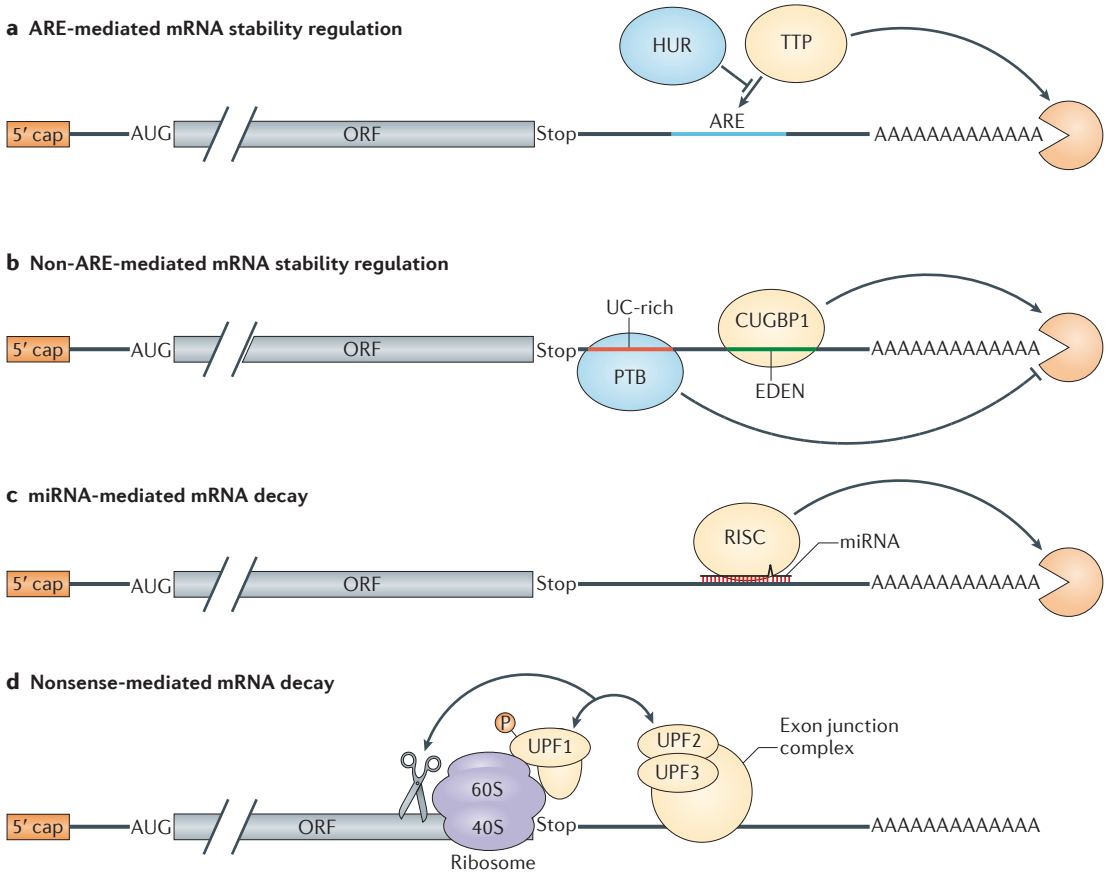

Figure 3 | **Regulation of mRNA stability during innate immune responses.** **a** | Many cytokine transcripts contain AU-rich elements (AREs) in their 3′ untranslated regions (3′ UTRs). The recognition of these motifs by destabilizing ARE-binding proteins, such as tristetraprolin (TTP), stimulates mRNA deadenylation and decay. Conversely, the binding of stabilizing proteins — such as Hu-antigen R (HUR) — that compete with destabilizing factors inhibits ARE-mediated RNA degradation. **b** | The recognition of other regulatory elements, such as embryo deadenylation element (EDEN)-like sequences by CUG triplet repeat RNA-binding protein 1 (CUGBP1) can additionally stimulate RNA deadenylation, whereas binding of polypyrimidine tract-binding protein (PTB) to UC-rich sequences stabilizes mRNAs. **c** | Numerous transcripts that are involved in innate immune responses also contain a microRNA (miRNA) target site (or multiple sites) in their 3′ UTRs. Specific recognition of these sites by the RNA-induced silencing complex (RISC) leads to deadenylation of the mRNA and its subsequent degradation. **d** | Finally, the presence of an exon junction complex downstream of a stop codon of a translated mRNA induces nonsense-mediated decay through interactions between regulator of nonsense transcripts (UPF) proteins, phosphorylation of UPF1 and endonucleolytic cleavage of the transcript. ORF, open reading frame.

Finally, transcripts that contain a very long 3′ UTR or an exon junction complex downstream of the translation termination codon can be degraded by nonsense-mediated decay (NMD) (FIG. 3d). This mechanism prevents the production of deleterious truncated proteins that are encoded by mutant or aberrantly spliced mRNAs containing premature termination codons. However, accumulating evidence shows that there is conserved expression of transcripts that are naturally spliced in their 3′ UTR[64], notably in haematopoietic cells. Inhibition of NMD impairs haematopoiesis[65] and deletion of the NMD factor regulator of nonsense transcripts 2 (UPF2) induces the upregulation of 186 genes in macrophages[65]. These results suggest that, in addition to its function as a quality control mechanism, NMD regulates gene expression in innate immune cells by controlling transcript stability.

Translation initiation in innate immunity

Many signalling events in innate immunity require gene expression changes that are too fast for new transcription or alternative pre-mRNA processing. In this case, changes in the translation of pre-existing mRNAs can allow for more rapid dynamic responses. Illustrating the importance of this post-transcriptional regulatory mechanism, LPS stimulation of DCs induces an immediate and massive increase in new protein synthesis within the first 60 minutes[66].

Regulation of translation initiation factor activity. Among all translation initiation factors, eukaryotic translation initiation factor 2 (eIF2) is the best studied regulator in innate immunity. eIF2 forms a ternary complex with the initiator methionyl-tRNA and a molecule of GTP, and this complex binds to the 40S ribosomal

© 2014 Macmillan Publishers Limited. All rights reserved

subunit where it is essential for start codon recognition and recruitment of the 60S ribosomal subunit. Upon positioning of the 40S subunit at the start codon, eIF2 hydrolyses its bound GTP, which causes the release of eIF2 from the ribosome (FIG. 4a). The resulting eIF2–GDP is then recycled by the guanine nucleotide exchange factor eIF2B to form a new ternary complex that is competent for a new round of translation. The activity of eIF2 is regulated by four different kinases that phosphorylate its α-subunit (eIF2α) and block its recycling by eIF2B. The phosphorylation of eIF2 can be triggered by double-stranded RNA (through protein kinase RNA-activated (PKR; also known as eIF2AK2)), ER stress (through PKR-like ER kinase (PERK; also known as eIF2AK3)), exposure to ultraviolet light (through GCN2; also known as eIF2AK4) or haem deficiency (through haem-regulated inhibitor (HRI; also known as eIF2AK1)). The phosphorylation of eIF2 leads to global translational repression of most cellular and viral mRNAs[67]. Suppression of translation mediated by eIF2 phosphorylation is beneficial during viral infection as it blocks the production of new viral proteins and limits viral spread. However, under the pathological chronic ER stress, prolonged eIF2 phosphorylation can be deleterious and lead to apoptosis[68]. Interestingly, TLR3 or TLR4 activation in macrophages and fibroblasts leads to the dephosphorylation of eIF2B via TRIF[69,70]. As a consequence, the guanine exchange activity of eIF2B is strongly stimulated and recycling of eIF2 occurs even though eIF2α remains phosphorylated (FIG. 4a). This allows the maintenance of efficient mRNA translation rates and an increase in cell survival upon prolonged ER stress, while still benefitting from the unfolded protein response (UPR) that is triggered by the ER stress and is essential to restore protein-folding homeostasis in the cell.

In addition to eIF2, the cap-binding protein eIF4E is highly regulated. eIF4E mediates the recruitment of the 40S ribosomal subunit by interacting both with the 5′ mRNA cap structure and the scaffold initiation factor eIF4G, which in turn contacts the 40S ribosome through eIF3 (FIG. 4b). In most cells, eIF4E levels are limiting, and thus the regulation of its activity has a strong impact on the translation efficiency of many mRNAs. Notably, eIF4E phosphorylation was recently shown to regulate the translation of pro-tumorigenic mRNAs[71], and eIF4E phosphorylation is usually altered in response to viral infection, which suggests a potential role in regulating innate immunity[72]. Consistent with this, mice that lack the two MAPK-interacting protein kinases (MNK1 and MNK2) that are responsible for eIF4E phosphorylation (FIG. 4b), or that express a mutant form of eIF4E that cannot be phosphorylated, have an enhanced type I IFN response that blocks infection by RNA viruses[73]. Surprisingly, although the lack of eIF4E phosphorylation does not affect global mRNA translation, it leads to specific translational downregulation of many mRNAs, including the mRNA that encodes IκBα. This increases NF-κB expression following RNA virus infection or specific TLR3 activation, which results in the induction of mRNAs that encode IFNβ and IRF7.

The phosphorylation of eIF4E is also regulated by IRAK2 and IRAKM (also known as IRAK3) (FIG. 4b). It has been shown that MNK1 and eIF4E were hypophosphorylated upon LPS stimulation in IRAK2-deficient mice compared with wild-type mice[74]. Consistent with low eIF4E phosphorylation levels, translation of several cytokines (including TNF and IL-6) was less efficient in IRAK2-deficient macrophages in response to LPS stimulation. Thus, in addition to its role in promoting NF-κB induction, IRAK2 promotes the translation of pro-inflammatory cytokines. Interestingly, IRAKM was recently shown to interact with IRAK2 and inhibit its ability to phosphorylate eIF4E (FIG. 4b), thereby preventing increased translation of cytokine mRNAs[75]. This inhibitory effect is thought to be important for downregulating TLR responses.

The activity of translation initiation factors is also subject to regulation by lipid mediators. In alveolar macrophages that are exposed to prolonged LPS treatment, 15-deoxy-Δ-12,14-prostaglandin J2 (15d-PGJ2) — a prostaglandin with anti-inflammatory activity — inhibits eIF4A activity and induces the formation of stress granules[76]. eIF4A is a DEAD-box RNA helicase that is required to unwind any RNA secondary structures that might otherwise block 40S ribosome progression through the 5′ UTR to find the start codon. Impairment of eIF4A activity by 15d-PGJ2 leads to translational repression of most cellular mRNAs, as well as sequestration of the pro-inflammatory TRAF2 protein into stress granules to resolve chronic inflammatory responses[76].

Together, these studies illustrate the diversity of mechanisms by which translation initiation factor activity is controlled by phosphorylation or direct interaction with small molecules to modulate both activation and resolution of inflammation.

Regulation by mTOR and 4EBPs. Mammalian target of rapamycin (mTOR) is a serine/threonine kinase that responds to many cellular stimuli, including TLR ligands. Its activation in macrophages occurs through MYD88–TRIF–phosphoinositide 3-kinase (PI3K)–AKT pathways[77]. In addition to regulating the transcription of immune genes, mTOR mediates the phosphorylation of eIF4E-binding proteins (4EBPs) (FIG. 4b). When hypophosphorylated, 4EBPs bind and sequester the translation initiation factor eIF4E to block its association with the scaffold initiation factor eIF4G and repress cap-dependent translation. Upon mTOR activation, 4EBPs become hyperphosphorylated and release eIF4E, which is then available to bind to eIF4G and participate in translation (FIG. 4b). The importance of 4EBPs in the translational control of innate immunity was revealed in mice that lack both 4EBP1 and 4EBP2 (*Eif4ebp1*$^{-/-}$*Eif4ebp2*$^{-/-}$ mice), which are refractory to RNA virus infection[78]. Further analysis revealed that 4EBP-depleted cells have increased type I IFN production following exposure to polyinosinic:polycytidylic acid (poly(I:C)) or in response to viral infection. Interestingly, although eIF4E is required for the translation of most cellular mRNAs, its sequestration by 4EBPs mainly affects the expression of those transcripts with

Unfolded protein response (UPR). A response that increases the ability of the endoplasmic reticulum (ER) to fold and translocate proteins, decreases the synthesis of proteins, degrades misfolded proteins and corrects disturbances in calcium and redox imbalance in the ER. If prolonged, the UPR can trigger apoptosis.

Stress granules
Cytoplasmic RNA–protein complexes that contain non-translating mRNAs, translation initiation components and other proteins that affect mRNA function. Stress granules are induced by stress and affect mRNA translation and stability.

© 2014 Macmillan Publishers Limited. All rights reserved

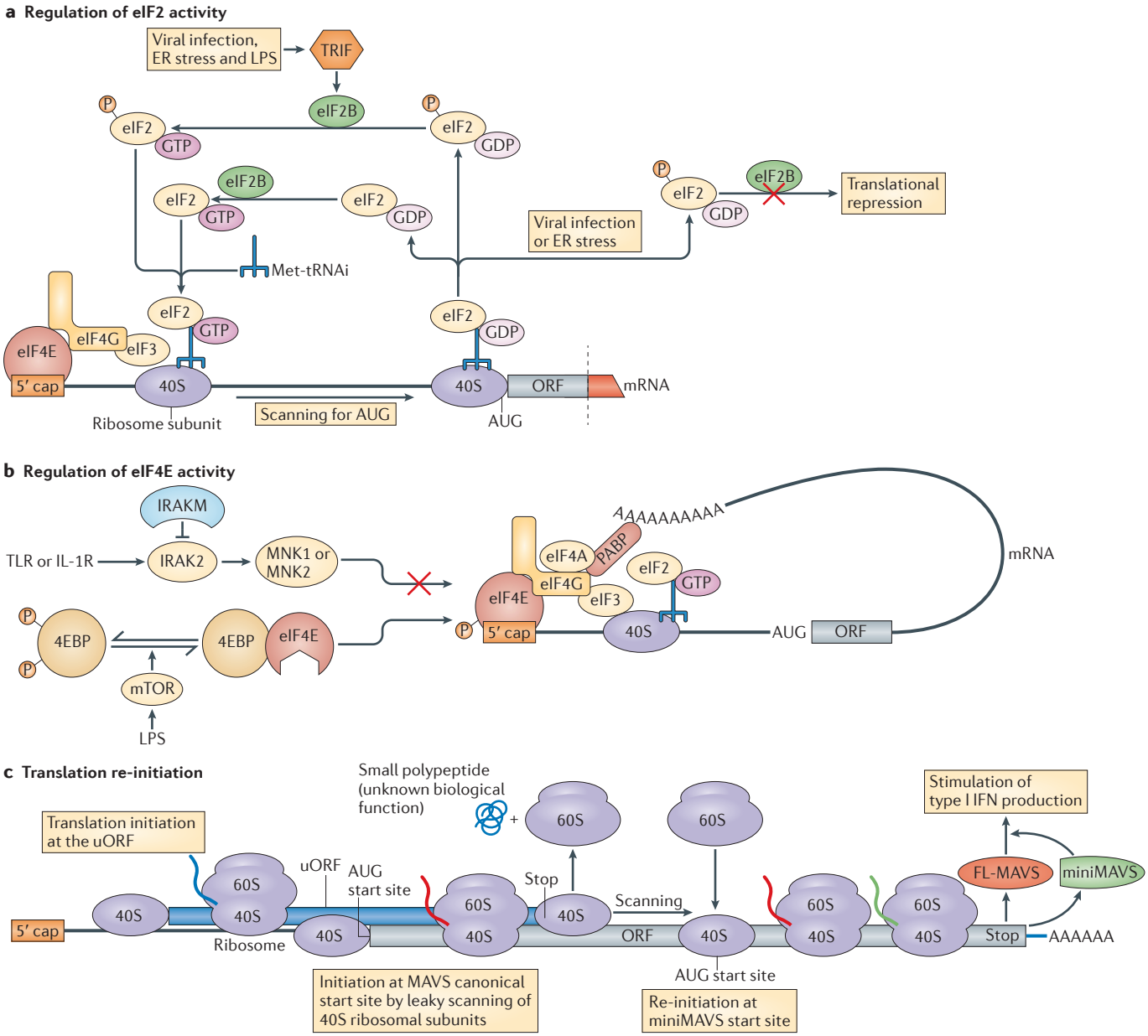

Figure 4 | **Translation initiation control of innate immunity.** **a** | Regulation of eukaryotic translation initiation factor 2 (eIF2) activity. Under normal conditions, eIF2 associates with a GTP molecule, a methionine-initiator tRNA (Met-tRNAi) and the 40S ribosome to participate in translation initiation. After initiation, the GTP molecule is hydrolysed and eIF2 is released from the 40S ribosome. The GDP-associated eIF2 is then recycled by eIF2B into a GTP-associated eIF2 that can re-engage in translation. During viral infection or endoplasmic reticulum (ER) stress, eIF2 can be phosphorylated, which impairs its recycling by eIF2B, leading to translational inhibition of most mRNAs. Toll-like receptor (TLR) engagement under ER stress conditions leads to eIF2B stimulation, which in turn is able to efficiently recycle eIF2, even in its phosphorylated form, to maintain translation. **b** | Regulation of eIF4E activity. TLR or interleukin-1 receptor (IL-1R) engagement induces the phosphorylation of eIF4E in an IL-1R-associated kinase 2 (IRAK2)-dependent and MAPK-interacting protein kinase 1 (MNK1)-dependent or MNK2-dependent manner to stimulate the translation of a subset of mRNAs. TLR engagement also activates the mammalian target of rapamycin (mTOR) pathway, which leads to eIF4E-binding protein (4EBP) phosphorylation, thus releasing the cap-binding protein eIF4E to stimulate the translation of mRNAs with highly structured 5′ untranslated regions (5′ UTRs). **c** | Translation re-initiation. A large proportion of cellular transcripts have predicted short upstream open reading frames (uORFs). When translated, these uORFs can affect the expression of the canonical ORF by different means. If the uORF overlaps with the main ORF, its translation will downregulate the translation of the main ORF, which will depend exclusively on leaky scanning of 40S ribosomal subunits that fail to recognize the start codon of the uORF and continue scanning the 5′ UTR until they reach the canonical ORF start codon — in this case the full-length mitochondrial antiviral signalling protein (FL-MAVS). Ribosomes that terminate translation of the uORF sometimes fail to dissociate from the mRNA, and the 40S ribosomal subunit might re-initiate scanning in a 5′ to 3′ direction until the ribosomes reach a new start codon situated in an optimal Kozak context. In this case, if the start codon is in the same reading frame as that of the canonical ORF, translation re-initiation will produce a truncated version of the canonical protein that is synthesized from the canonical ORF (in this case, the truncated version is called miniMAVS). If the internal start codon is not in the same reading frame, it can lead to the synthesis of a completely different protein. IFN, interferon; LPS, lipopolysaccharide; PABP, poly(A)-binding protein; TRIF, TIR-domain-containing adaptor inducing IFNβ.

© 2014 Macmillan Publishers Limited. All rights reserved

large secondary structures in their 5′ UTR and those that contain 5′ UTR oligopyrimidine tracts. Both of these UTR classes are highly dependent on eIF4E for efficient translation[79,80]. Among these genes, translation of *IRF7* — which has a long and highly structured 5′ UTR — is stimulated in cells in which 4EBP1 and 4EBP2 are depleted. Consistent with a role of 4EBPs in regulating innate immunity-related genes, LPS-mediated activation of macrophages leads to mTOR-dependent 4EBP phosphorylation, which activates the translation of TNF, IL-6 and CXC-chemokine ligand 1 (CXCL1)[79]. Thus, 4EBPs act as negative regulators of innate immunity in unstimulated cells and are required both for inducing efficient expression of IFN-regulatory genes as well as for avoiding an excessive innate immune response against pathogens. In agreement with such an important role, inactivation of mTOR by the *Leishmania* spp. protease GP63 (also known as leishmanolysin) leads to translational repression of macrophage transcripts and is required for pathogen survival[81].

In contrast to these findings, mTOR inactivation by rapamycin during the course of a bacterial infection has been shown to stimulate innate immunity by favouring the expression of pro-inflammatory genes[82]. Furthermore, infection of macrophages with a virulent strain of *Legionella pneumophilia* results in mTOR ubiquitylation and degradation, thereby suppressing its function[83]. Surprisingly, in this case, the resulting hypophosphorylation of 4EBPs leads to translational repression of low-abundance transcripts and activation of high-abundance transcripts. Among these abundant transcripts are those for pro-inflammatory cytokines. Interestingly, mTOR inactivation by *L. pneumophilia* requires the Dot/Icm secretion system, which suggests that triggering the innate immune system involves translational regulation following the detection of pathogen signatures.

The above data demonstrate the importance of translational regulation mediated by mTOR and 4EBPs in innate immunity. These data further illustrate the dual role of 4EBPs in restricting or promoting innate immunity depending on the nature of the pathogen.

Regulation of poly(A) length. The poly(A) tail located at mRNA 3′ ends has an essential role in translation by serving as a binding site for poly(A)-binding protein (PABP; also known as PABP1). Although recruited to the 3′ end, PABP interacts with multiple translation initiation factors and stimulates their activities (FIG. 4b). These interactions also bring the 5′ and 3′ ends into close proximity, thereby pseudo-circularizing the mRNA, which is thought to improve ribosome recycling and therefore translational efficiency[84]. Dynamic regulation of poly(A) tail length in numerous cell types has a strong impact on both translational efficiency and transcript stability[85].

In unstimulated macrophages, *TNF* mRNA is constitutively expressed but it lacks a poly(A) tail and so fails to engage the translation machinery and produce TNF protein[86]. However, following LPS stimulation, *TNF* transcripts gain poly(A) tails, which activates their translation and allows the rapid and abundant expression of TNF protein. Such regulation is similar to that occurring in resting memory $CD8^+$ T cells, in which constitutively expressed mRNA that encodes CC-chemokine ligand 5 (CCL5) lacks a poly(A) tail and so is translationally repressed until the T cell receptor is re-engaged. This re-engagement triggers polyadenylation of the pre-existing pool of *CCL5* mRNA, which facilitates rapid translation and CCL5 protein secretion[87]. Interestingly, although the mechanism responsible for the deadenylation and subsequent readenylation of *TNF* has not been elucidated, the AU-rich elements that are located within its 3′ UTR are very similar in sequence to the motif that is recognized by the cytoplasmic polyadenylation element binding protein (CPEB; also known as CPEBP1). CPEB has been shown to regulate the translation of mRNAs for many pro-inflammatory cytokines (including IL-6) in mouse embryonic fibroblasts[88]. It is therefore possible that, in addition to *TNF*, many other transcripts may be constitutively produced in resting macrophages and stored in a translationally silent state until TLR engagement triggers their rapid readenylation and translation.

Alternative translation initiation pathways

Although most mRNAs are translated through the classical cap-dependent mechanism, a subset of cellular mRNAs can also rely on alternative ways to initiate translation, such as leaky scanning, non-AUG translation initiation, translation re-initiation and internal ribosome entry sites (IRESs).

Recognition of the start codon by the scanning 43S ribosome is modulated by the nucleotide sequence surrounding the AUG, which is also known as the Kozak context[89]. The optimal sequence corresponds to a purine at position –3 and a guanosine at position +1. If the Kozak context is not optimal, the 43S ribosome fails to recognize the AUG codon and continues its 5′ to 3′ scanning until it reaches a downstream start codon — this mechanism is known as leaky scanning. Leaky scanning occurs in a variety of transcripts and allows the expression of multiple isoforms of the same protein without the requirement for alternative splicing. In DCs, translation of the transcript that encodes the secreted protein osteopontin (also known as SPP1) is controlled by leaky scanning to produce full-length secreted osteopontin and an amino-terminal truncated osteopontin isoform that is restricted to the cytoplasm[90]. Interestingly, translation of the N-terminal isoform is not initiated at an AUG codon but probably at a GCC codon (coding for aspartic acid) that is located downstream of the canonical AUG. Expression of this N-terminal truncated osteopontin isoform is required for efficient podosome formation upon DC activation by CpG-containing oligonucleotides[90].

Translation re-initiation occurs when an 80S ribosome that terminates translation at the stop codon is not completely recycled and the 40S ribosomal subunit is able to resume 5′ to 3′ scanning to reach a downstream initiation codon and re-initiate translation. The efficiency of re-initiation is linked to the length of the first open reading frame (ORF) that is translated, with shorter

Dot/Icm secretion system
A specialized bacterial secretion system that is encoded by 26 *Dot/Icm* (defect in organelle trafficking/intracellular multiplication) genes in *Legionella pneumophilia*. It is used to inject bacterial effector proteins into the host cell, which increase the ability of the bacteria to survive inside the host cell.

© 2014 Macmillan Publishers Limited. All rights reserved

ORFs allowing for a more efficient re-initiation[91]. Indeed, it is thought that translation initiation factors (which are required for translation re-initiation) remain associated with ribosomal subunits for some time after elongation begins and, therefore, ribosomes that are translating short ORFs will have more chance of carrying all of the factors that are necessary for re-initiation. Interestingly, more than 45% of mammalian mRNAs are predicted to contain small upstream ORF (uORF) in their 5′ UTR[92], which suggests that they could have a widespread role in regulating translation of the main ORF. In a recent report, two isoforms of the antiviral retinoic acid-inducible gene I (RIG-I) adaptor protein mitochondrial antiviral signalling protein (MAVS) — full length MAVS (FL-MAVS) and an N-terminal truncated isoform (miniMAVS) — were shown to be expressed from a single transcript species through the use of two in-frame start codons[93]. FL-MAVS is responsible for efficient type I IFN production during viral infection, whereas miniMAVS antagonizes FL-MAVS. Surprisingly, when dissecting the molecular mechanism responsible for miniMAVS translation, the authors revealed the presence of a short uORF in the 5′ UTR of the *MAVS* transcript that terminates downstream of the FL-MAVS start codon (FIG. 4c). Translation of this uORF allows ribosomes to bypass the FL-MAVS start codon. Then, through a mechanism of translation re-initiation, ribosomes can resume scanning and reach the start codon for translation of miniMAVS (FIG. 4c). By contrast, translation of FL-MAVS occurs through a leaky scanning mechanism whereby 40S ribosomal subunits fail to recognize the uORF start codon and continue scanning until they reach the start codon for FL-MAVS (FIG. 4c). The ratio of FL-MAVS and miniMAVS is dynamic during the course of viral infection, which suggests that leaky scanning and translation re-initiation can be differentially regulated. Finally, by performing genome-wide ribosome-footprinting experiments, numerous genes with multiple translation start sites have been identified, including genes that are involved in innate immunity, which demonstrates the widespread use of alternative translation initiation codons to increase the coding potential of mRNAs without involving alternative splicing.

In addition to translation re-initiation, some cellular transcripts rely on IRESs to initiate their translation. IRESs are RNA elements that can, through their secondary structure or primary sequence, recruit a 40S ribosomal subunit independently of the mRNA 5′ cap structure and the cap-binding factor eIF4E (reviewed in REF. 84). Ribosome recruitment occurs through direct interactions between components of the translation machinery (including translation initiation factors) and the RNA sequence or structure, and can be regulated by IRES *trans*-acting factors. Although translation that is mediated by cellular IRESs is usually inefficient under normal conditions, it allows translation to be sustained during conditions where cap-dependent translation is compromised. A few genes that are involved in innate immunity have been reported to contain IRESs in their 5′ UTR, including hypoxia-inducible factor 1α (HIF1α) and human surfactant protein A (SPA; also known as PSPA)[94,95]. However, IRES activity for these transcripts has not yet been monitored in the context of innate immunity. By contrast, polysome profiling of breast cancer cells that had been incubated with conditioned medium from activated macrophages revealed the genes for which translation was upregulated in the context of an inflammatory response[96]. Among these genes, early growth response gene 2 (*EGR2*) and 1,25-dihydroxyvitamin D3 24-hydroxylase (*CYP24A1*) were reported to depend on IRESs for their translation under inflammatory conditions[96,97]. As innate immunity is often associated with cellular stress conditions in which cap-dependent translation is highly regulated, it is tempting to speculate that IRES-mediated translation could have a role in allowing the translation of transcripts that are required to cope with such stresses.

Gene-specific regulation

Translation can be regulated in a transcript-specific manner through the recruitment of RNA-binding proteins, lncRNAs or small RNAs (FIG. 5a,b). Such interactions can occur on the 5′ UTR, the coding sequence or the 3′ UTR of target mRNAs and depend either on the transcript primary sequence or on particular RNA secondary structures.

Regulation by ARE-binding proteins. ARE-binding proteins are among the most important TLR-dependent regulators of translation. In addition to their role in modulating mRNA stability (see above), ARE-binding proteins have been reported to regulate the translation of key ARE-containing mRNAs following TLR engagement. Interestingly, because different ARE-binding proteins recognize similar sequence motifs, they can compete with one another for individual AREs and simultaneously occupy a single transcript that contains multiple AREs[98] (FIG. 5a). This results in complex and dynamic regulatory networks, which possibly involve multiple molecular mechanisms that affect both transcript translation and stability. Illustrating this, translation of *TNF* in resting macrophages is repressed by the ARE-binding protein TTP. However, following LPS stimulation, activation of the p38 mitogen-activated protein kinase (MAPK)–MAPK-activated protein kinase 2 (MAPKAPK2) pathway leads to TTP phosphorylation, which decreases its affinity for *TNF* AREs. As a consequence, TTP is replaced by HUR, which stimulates *TNF* translation[99].

The exact molecular mechanisms by which ARE-binding proteins regulate translation remain largely unexplored but most probably depend on the recruitment of additional proteins. In resting macrophages, TTP was shown to interact with DEAD-box protein 6 (DDX6; also known as RCK) and repress *TNF* translation, possibly by recruiting the mRNA to processing bodies (P-bodies)[100]. Nucleolysin TIA1 isoform p40 (TIA1), an ARE-binding protein that is required for translational regulation of *TNF* and other cytokines following TLR activation, has been shown to repress

Processing bodies
(P-bodies). These are identified as distinct foci within the cytoplasm. They are reversible non-membrane-bound structures that are involved in a number of processes, including mRNA decay, RNA-mediated silencing and translational control.

© 2014 Macmillan Publishers Limited. All rights reserved

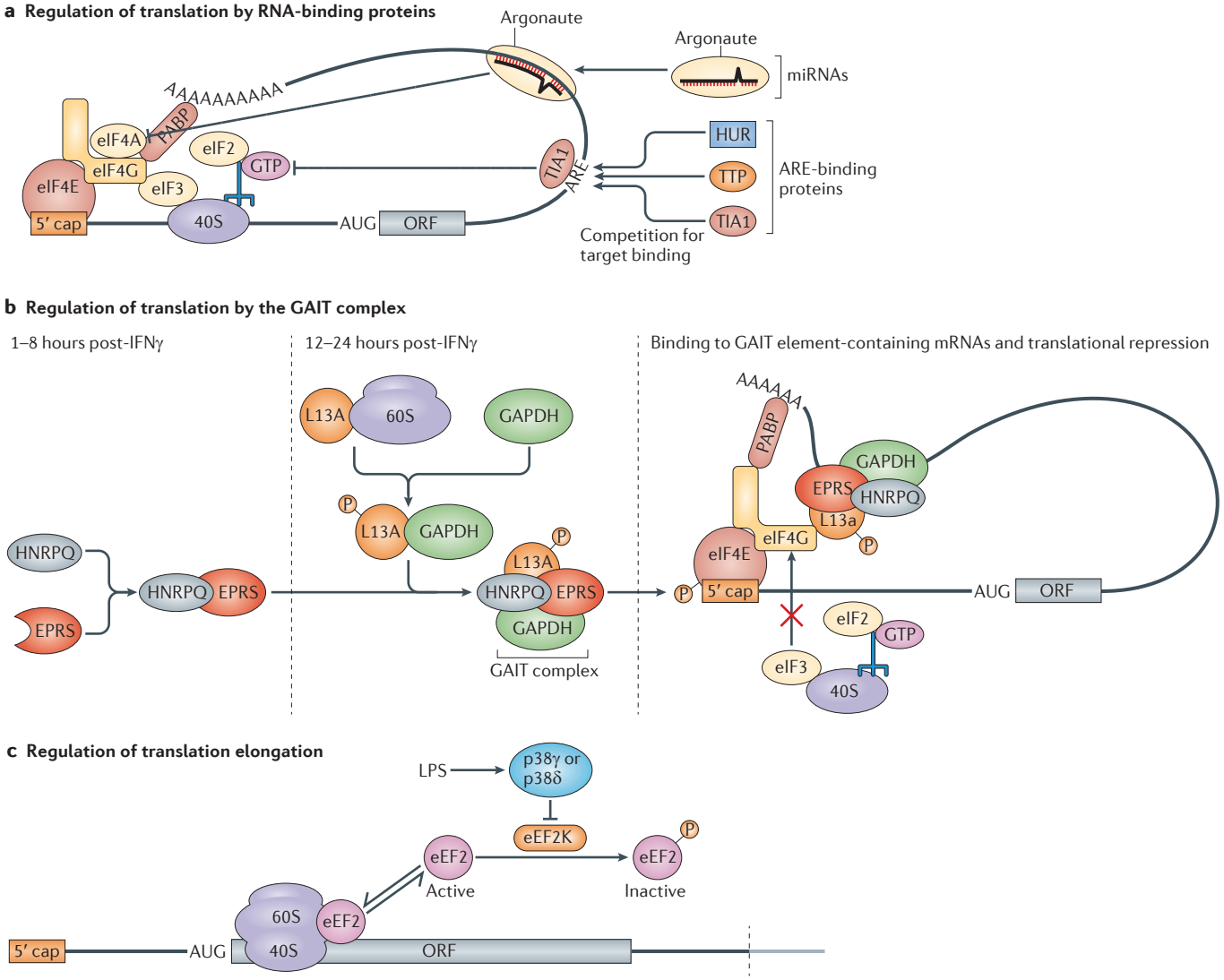

Figure 5 | **Translational control mediated by RNA-binding proteins and elongation factors.** **a** | Translational control through RNA-binding proteins. Differential expression of microRNAs (miRNAs) during Toll-like receptor (TLR) signalling can lead to translational repression of immune-related mRNAs. This inhibition is thought to occur mainly at the level of translation initiation through targeting of scanning by the 40S ribosomal subunit[125]. miRNAs can also lead to target transcript deadenylation to block translation initiation. TLR signalling regulates the levels and activity of many AU-rich element (ARE)-binding proteins, which are thought to regulate translation initiation through mechanisms that are still not fully elucidated. **b** | Interferon-γ (IFNγ) induces the multistep assembly of an IFNγ-activated inhibitor of translation (GAIT) complex through the association of glutamyl-prolyl tRNA synthetase (EPRS) and heterogeneous nuclear ribonucleoprotein Q (HNRPQ) 8 hours after IFNγ treatment, which is followed by the association of the large ribosomal subunit protein L13A with glyceraldehyde 3-phosphate dehydrogenase (GAPDH) and the formation of the fully functional GAIT complex. The GAIT complex binds to the 3′ untranslated region (UTR) of transcripts containing the GAIT element and represses their translation by abolishing the interaction between eukaryotic translation initiation factor 4G1 (eIF4G) and eIF3. **c** | Regulation of translation elongation. In macrophages, lipopolysaccharide (LPS) stimulation inhibits, in a mitogen-activated protein kinase (MAPK)-dependent manner, the kinase activity of eukaryotic elongation factor 2 kinase (eEF2K), thus increasing the pool of active eEF2 in the cell and stimulating translation elongation. HUR, Hu-antigen R; ORF, open reading frame; PABP, poly(A)-binding protein; TIA1, nucleolysin TIA1 isoform p40; TTP, tristetraprolin.

the translation of target mRNAs by preventing their engagement with polyribosomes[101]. Although the mechanism of this TIA1-dependent translational repression has not been fully elucidated, it has been suggested that TIA1 promotes the assembly of 48S-like ribosomes that lack eIF2 and are therefore unable to initiate translation[102]. This would be consistent with the known role of TIA1 in repressing the translation of mRNAs with 5′ UTR oligopyrimidine tracts under stress conditions — when eIF2α is phosphorylated and thus unavailable for translation — by relocalizing these mRNAs to stress granules[103].

© 2014 Macmillan Publishers Limited. All rights reserved

Regulation by the GAIT complex. In addition to ARE-binding proteins, the IFNγ-activated inhibitor of translation (GAIT) complex has an important role in gene-specific translational control in innate immunity. Evidence for the GAIT complex was first found in IFNγ-treated human monocytic U937 cells in which translation of the mRNA encoding ceruloplasmin (CP) was first stimulated and then strongly repressed after 16 hours of treatment[104]. Later, a 29-nucleotide bipartite stem–loop RNA structure that is located in the 3′ UTR of the *CP* transcript was reported to interact with a protein complex and shown to be sufficient to mediate translational repression of *CP* and that of reporter constructs expressed in IFNγ-treated cells[105]. Identification of the protein partners involved in GAIT — carried out using a yeast three-hybrid screen and affinity chromatography — revealed a 450 kDa complex that is composed of the large ribosomal subunit protein L13A (also known as RPL13A), glutamyl-prolyl tRNA synthetase (also known as EPRS and bifunctional glutamate/proline tRNA ligase), heterogeneous nuclear ribonucleoprotein Q (HNRPQ; also known as NSAP1) and glyceraldehyde-3-phosphate dehydrogenase (GAPDH)[106,107]. Interestingly, the GAIT complex is assembled in a two-step process in which, 8 hours after IFNγ treatment, EPRS and HNRPQ first assemble together but are unable to bind to GAIT element-containing mRNAs[106] (FIG. 5b). After 12 to 24 hours of treatment, L13A is phosphorylated and released from the 60S ribosomal subunit, which allows its interaction with GAPDH and with the EPRS–HNRPQ heterodimer[106,107] (FIG. 5b). The formed complex can then interact with the GAIT RNA element and drive translational repression by a mechanism that involves the direct interaction of L13A with the translation initiation factor eIF4G[108]. The L13A–eIF4G interaction interferes with the association of eIF4G with eIF3 and thus blocks the recruitment of the 40S ribosomal subunit to the target mRNA[108] (FIG. 5b).

In addition to regulating translation of the *CP* transcript, a polysome-profiling experiment combined with microarray analysis of IFNγ-treated cells revealed that many other mRNAs are also regulated by the GAIT complex, including chemokines and chemokine receptors[109], as well as genes that are involved in regulating GAIT complex assembly[110]. Among these genes, vascular endothelial growth factor A (*VEGFA*), which has a role in promoting angiogenesis during inflammation, was shown to contain a GAIT element in its 3′ UTR that was able to recruit the GAIT complex and repress *VEGFA* translation[111]. The GAIT RNA element that is located in the 3′ UTR of *VEGFA* is in close proximity to a binding site for the RNA-binding heterogeneous nuclear ribonucleoprotein L (HNRNPL) in complex with the double-stranded RNA-binding protein DRBP76 (also known as ILF3) and HNRNPA2/B1; this is also known as the HILDA complex. Binding of the GAIT complex and HNRNPL is mutually exclusive and mediated by a differential conformational change of the target RNA induced by each complex that, in turn, blocks the binding of the other complex[112,113]. This conformational switch allows the fine-tuning of *VEGFA* translation in the course of inflammation. Under normoxic conditions, IFNγ treatment activates the GAIT complex, which binds to the 3′ UTR of *VEGFA* to inhibit its translation. However, during hypoxia, HNRNPL is phosphorylated and relocalizes to the cytoplasm and binds to the 3′ UTR of *VEGFA*, thus impeding GAIT complex binding to allow for efficient VEGFA protein expression and to promote angiogenesis[113].

Together, available data exemplify the complexity and dynamic aspect of gene-specific translational control in innate immunity. Indeed, simultaneous binding and competition for binding sites between different RNA-binding proteins allows the cell to integrate multiple inputs at the same time and to differentially regulate gene expression in a target-specific manner as appropriate. Furthermore, it introduces the notion of a post-transcriptional code for regulating gene expression whereby the combinatorial binding of RNA-binding proteins to a particular transcript determines its expression level.

Regulation of translation elongation

Although most regulation of translation is thought to occur at the initiation step, translation can also be controlled at the elongation step. However, the mechanisms for regulating elongation, as well as their impact in physiological processes, are still poorly understood. It is known that translation elongation can be regulated by the mTOR and MAPK pathways in response to many stimuli[79]. Among these, TLR activation in macrophages that are deficient in MAPK kinase kinase 8 (MAP3K8; also known as COT and TPL2) results in reduced phosphorylation of eukaryotic elongation factor 2 kinase (eEF2K), which suggests a role for MAP3K8 in the regulation of translation elongation[79]. In its unphosphorylated form, eEF2K acts as a translational repressor by phosphorylating eEF2 (FIG. 5c). Confirming an involvement of eEF2 in innate immunity, activation of the MAPK proteins p38γ (also known as MAPK12) and p38δ (also known as MAPK13) in a model of LPS-induced hepatitis was shown to stimulate eEF2 activity in macrophages[114]. As a consequence, the translation of *TNF* is upregulated, which induces apoptosis and necrosis of hepatic cells. Interestingly, partial knockdown of eEF2 using small interfering RNAs blocked *TNF* expression by macrophages following LPS stimulation both *in vitro* and *in vivo*, and this blockade was sufficient to protect mice from liver failure. This result highlights the importance of the regulation of translation elongation in pro-inflammatory cytokine expression. As regulation of eEF2 activity should have an impact on the translation of most cellular mRNAs, it would be of interest to monitor its effect on additional cellular functions.

lncRNAs in innate immunity

Although miRNAs modulate inflammatory gene expression[62,63], exciting recent studies support important roles for additional non-coding RNAs in this setting. Although several lncRNAs were discovered and characterized prior to 2005 (REFS 115–117), advances in sequencing and array technologies over the past few years have led to the discovery of thousands of lncRNA

© 2014 Macmillan Publishers Limited. All rights reserved

Box 1 | **Emerging roles of long non-coding RNAs in immunity**

Recent studies have revealed functional roles for long non-coding RNAs (lncRNAs) in immunity. The lncRNA *Tmevpg1* (also known as NeST) controls Theiler's virus persistence in mice[126,127] by promoting the transcription of interferon-γ (*Ifng*) in $CD8^+$ T cells. The *Tmevpg1* lncRNA binds to WD repeat-containing protein 5 (WDR5), a histone-modifying complex, altering histone 3 (H3) lysine 4 trimethylation at the *Ifng* locus. Studies in macrophages have also revealed important roles for lncRNAs in controlling inflammatory gene expression. Many lncRNAs were found to be dynamically regulated in macrophages that were exposed to Toll-like receptor 2 (TLR2) ligands (see figure). One such transcript, long intergenic non-coding RNA (lincRNA)-*Cox2*, was found to act as a master regulator of gene expression. lincRNA-*Cox2* represses the basal expression of interferon-stimulated genes (ISGs) by partnering with the heterogeneous nuclear ribonucleoproteins (HNRNPs) HNRNPA/B and HNRNPA2/B1. Remarkably, lincRNA-*Cox2* was also essential for the TLR-induced expression of interleukin-6 (*Il6*) and more than 700 additional genes — many of which are secondary response genes[128] — through a mechanism that remains to be fully elucidated (indicated by a question mark in the figure). A pseudogene RNA named Lethe (also known as *Rps15a-ps4*) binds RELA — the p65 subunit of the nuclear factor-κB (NF-κB) heterodimeric complex — which prevents NF-κB from binding to promoter regions of target genes[129]. Finally, a lincRNA called TNF and HNRNPL-related immunoregulatory lincRNA (*THRIL*) was shown to regulate the expression of tumour necrosis factor (*TNF*) in human monocytes through its interactions with HNRNPL[130]. Collectively, these studies emphasize the importance of lncRNAs in regulating gene expression in macrophages and highlight yet another layer of complexity in gene regulation. Further analysis of their molecular functions could provide important insights into gene regulation, inflammation and human diseases.

lncRNAs can also act via post-transcriptional mechanisms altering mRNA splicing, turnover or translation. lncRNAs can act as microRNA (miRNA) sponges by preventing miRNA-mediated degradation of target mRNAs[131]. Metastasis-associated lung adenocarcinoma transcript 1 (MALAT1) controls alternative splicing of mRNA, whereas a newly defined class of lncRNAs (that is referred to as sno-lincRNAs) can affect RNA-binding protein fox-1 homologue 2 (FOX2)-mediated pre-mRNA splicing[132,133]. The lncRNA β-secretase 1 antisense transcript (*BACE1-AS*), which is upregulated in the brains of patients with Alzheimer's disease, stabilizes its protein-coding sense transcript *BACE1* by protecting it from RNase cleavage[134]. Hu-antigen R (HUR) can drive the translation of several mRNAs in a lncRNA-dependent manner. In HeLa cells, lincRNA-p21 (also known as *Trp53cor1*) can interact with several mRNAs through direct base-pairing at complementary regions, repressing translation in a mechanism that requires DEAD-box protein 6 (DDX6)[135]. The role of lncRNAs in post-transcriptional gene regulation has been reviewed extensively[136]. Whether lncRNAs control gene expression through these mechanisms in the context of innate immune signalling remains to be determined.

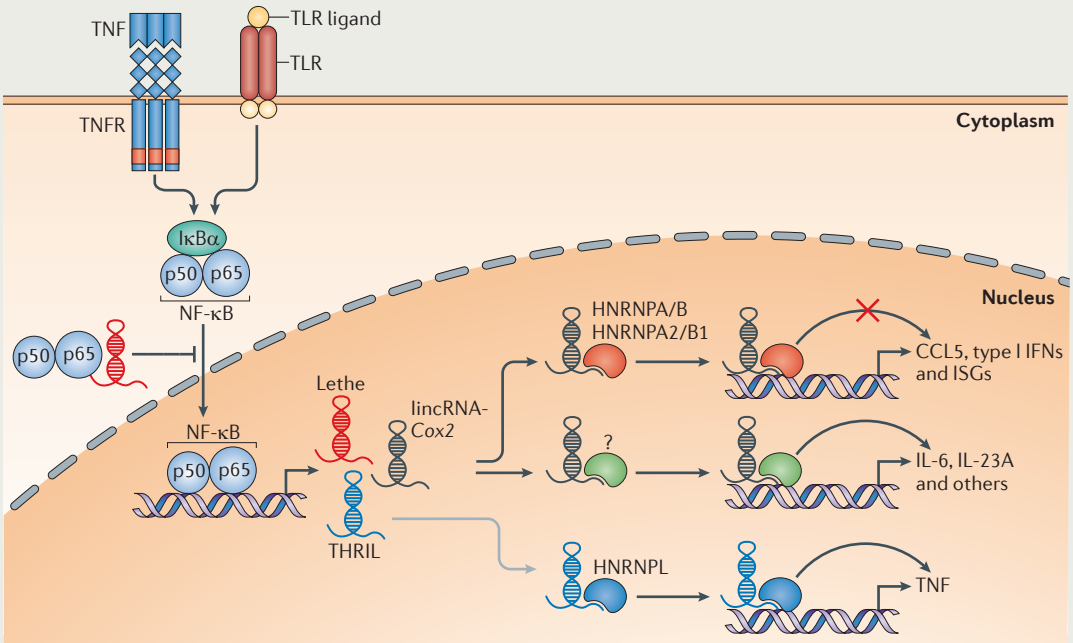

CCL5, CC-chemokine ligand 5; IκBα, NF-κB inhibitor-α; TNFR, TNF receptor.

transcripts in diverse cell types[118–124]. These lncRNAs have primarily been studied in the context of genomic imprinting, cancer and cell differentiation. More recently, however, their expression in immune cells has prompted investigation into their roles in transcriptional and post-transcriptional regulation of immune gene expression (BOX 1).

Conclusions and perspectives

This Review highlights the wealth of post-transcriptional mechanisms that control the expression levels of immune genes. Although transcriptional regulation has been the focus in this area, it is clear that splicing, polyadenylation, mRNA stability and protein translation all act in concert to fine-tune and modulate the initiation,

© 2014 Macmillan Publishers Limited. All rights reserved

duration and magnitude of inflammatory gene expression in innate immunity. The expression of inhibitory splice variants that are induced by inflammatory signals, as well as tight control of mRNA half-lives, enable rapid and transient responses. Furthermore, regulation of mRNA translation allows a rapid response that can be directed against a specific set of genes or against the entire transcript population. Although exuberant 'on' signals clearly contribute to chronic inflammation, dysregulation of the 'off' signals can be equally damaging to tissues. Turning off the system in a timely and efficient manner is essential. The existence of multiple and apparently non-redundant regulatory mechanisms raises an important question concerning the relative importance of these individual controls. Such control at multiple checkpoints suggests that, individually, these hurdles are not sufficient to modulate a particular response, and a concerted effort by multiple regulatory mechanisms is required. A broader understanding of all of the layers of regulation in this system can provide important information that could be harnessed in vaccine development to improve the efficacy and duration of vaccine-induced immunity. Additionally, these multiple layers could be modulated therapeutically to thwart chronic inflammation, which contributes to a growing array of human diseases.

1. Aringer, M., Gunther, C. & Lee-Kirsch, M. A. Innate immune processes in lupus erythematosus. *Clin. Immunol.* **147**, 216–222 (2013).
2. Moore, K. J., Sheedy, F. J. & Fisher, E. A. Macrophages in atherosclerosis: a dynamic balance. *Nature Rev. Immunol.* **13**, 709–721 (2013).
3. Kumar, H., Kawai, T. & Akira, S. Pathogen recognition by the innate immune system. *Int. Rev. Immunol.* **30**, 16–34 (2011).
4. Thompson, M. R., Kaminski, J. J., Kurt-Jones, E. A. & Fitzgerald, K. A. Pattern recognition receptors and the innate immune response to viral infection. *Viruses* **3**, 920–940 (2011).
5. Medzhitov, R. & Horng, T. Transcriptional control of the inflammatory response. *Nature Rev. Immunol.* **9**, 692–703 (2009).
6. Smale, S. T. Transcriptional regulation in the innate immune system. *Curr. Opin. Immunol.* **24**, 51–57 (2012).
7. Rodrigues, R., Grosso, A. R. & Moita, L. Genome-wide analysis of alternative splicing during dendritic cell response to a bacterial challenge. *PLoS ONE* **8**, e61975 (2013).
8. Sandberg, R., Neilson, J. R., Sarma, A., Sharp, P. A. & Burge, C. B. Proliferating cells express mRNAs with shortened 3′ untranslated regions and fewer microRNA target sites. *Science* **320**, 1643–1647 (2008).
9. Moore, M. J. & Proudfoot, N. J. Pre-mRNA processing reaches back to transcription and ahead to translation. *Cell* **136**, 688–700 (2009).
10. Elkon, R., Ugalde, A. P. & Agami, R. Alternative cleavage and polyadenylation: extent, regulation and function. *Nature Rev. Genet.* **14**, 496–506 (2013).
11. Wang, E. T. *et al.* Alternative isoform regulation in human tissue transcriptomes. *Nature* **456**, 470–476 (2008).
12. Miura, P., Shenker, S., Andreu-Agullo, C., Westholm, J. O. & Lai, E. C. Widespread and extensive lengthening of 3′ UTRs in the mammalian brain. *Genome Res.* **23**, 812–825 (2013).
13. Wells, C. A. *et al.* Alternate transcription of the Toll-like receptor signaling cascade. *Genome Biol.* **7**, R10 (2006).
14. Jarešová, I. *et al.* Kinetics of Toll-like receptor-4 splice variants expression in lipopolysaccharide-stimulated antigen presenting cells of healthy donors and patients with cystic fibrosis. *Microbes Infect.* **9**, 1359–1367 (2007).
15. Iwami, K. I. *et al.* Cutting edge: naturally occurring soluble form of mouse Toll-like receptor 4 inhibits lipopolysaccharide signaling. *J. Immunol.* **165**, 6682–6686 (2000).
16. Stevenson, B. J., Iseli, C., Beutler, B. & Jongeneel, C. V. Use of transcriptome data to unravel the fine structure of genes involved in sepsis. *J. Infect. Dis.* **187** (Suppl. 2), 308–314 (2003).
17. Chang, J.-S. *et al. Myobacterium tuberculosis* induces selective up-regulation of TLRs in the mononuclear leukocytes of patients with active pulmonary tuberculosis. *J. Immunol.* **176**, 3010–3018 (2006).
18. Haehnel, V., Schwarzfischer, L., Fenton, M. J. & Rehli, M. Transcriptional regulation of the human *Toll-like receptor 2* gene in monocytes and macrophages. *J. Immunol.* **168**, 5629–5637 (2002).
19. Ohta, S., Bahrun, U., Tanaka, M. & Kimoto, M. Identification of a novel isoform of MD-2 that downregulates lipopolysaccharide signaling. *Biochem. Biophys. Res. Commun.* **323**, 1103–1108 (2004).
20. Gray, P. *et al.* Identification of a novel human MD-2 splice variant that negatively regulates lipopolysaccharide-induced TLR4 signaling. *J. Immunol.* **184**, 6359–6366 (2010).
21. Burns, K. *et al.* Inhibition of interleukin 1 receptor/Toll-like receptor signaling through the alternatively spliced, short form of MyD88 is due to its failure to recruit IRAK-4. *J. Exp. Med.* **197**, 263–268 (2003).
This paper identifies MYD88s, which is a short dominant-negative inhibitor that is a splice variant of MYD88.
22. Janssens, S., Burns, K., Tschopp, J. & Beyaert, R. Regulation of interleukin-1- and lipopolysaccharide-induced NF-κB activation by alternative splicing of MyD88. *Curr. Biol.* **12**, 467–471 (2002).
23. Janssens, S., Burns, K., Vercammen, E., Tschopp, J. & Beyaert, R. MyD88S, a splice variant of MyD88, differentially modulates NF-κB-and AP-1-dependent gene expression. *FEBS Lett.* **548**, 103–107 (2003).
24. Jensen, L. E. & Whitehead, A. S. IRAK1b, a novel alternative splice variant of interleukin-1 receptor-associated kinase (IRAK), mediates interleukin-1 signaling and has prolonged stability. *J. Biol. Chem.* **276**, 29037–29044 (2001).
25. Yanagisawa, K. *et al.* A novel splice variant of mouse interleukin-1-receptor-associated kinase-1 (IRAK-1) activates nuclear factor-κB (NF-κB) and c-Jun N-terminal kinase (JNK). *Biochem. J.* **370**, 159–166 (2003).
26. Rao, N., Nguyen, S., Ngo, K. & Fung-Leung, W.-P. A novel splice variant of interleukin-1 receptor (IL-1R)-associated kinase 1 plays a negative regulatory role in Toll/IL-1R-induced inflammatory signaling. *Mol. Cell. Biol.* **25**, 6521–6532 (2005).
27. Hardy, M. P. & O'Neill, L. A. J. The murine IRAK2 gene encodes four alternatively spliced isoforms, two of which are inhibitory. *J. Biol. Chem.* **279**, 27699–27708 (2004).
28. Leeman, J. R. & Gilmore, T. D. Alternative splicing in the NF-κB signaling pathway. *Gene* **423**, 97–107 (2008).
29. Han, K.-J., Yang, Y., Xu, L.-G. & Shu, H.-B. Analysis of a TIR-less splice variant of TRIF reveals an unexpected mechanism of TLR3-mediated signaling. *J. Biol. Chem.* **285**, 12543–12550 (2010).
30. Palsson-McDermott, E. M. *et al.* TAG, a splice variant of the adaptor TRAM, negatively regulates the adaptor MyD88-independent TLR4 pathway. *Nature Immunol.* **10**, 579–586 (2009).
This paper identifies TAG, which is an inhibitory splice variant of the adaptor molecule TRAM.
31. Karpova, A. Y., Ronco, L. V. & Howley, P. M. Functional characterization of interferon regulatory factor 3a (IRF-3a), an alternative splice isoform of IRF-3. *Mol. Cell. Biol.* **21**, 4169–4176 (2001).
32. Li, C., Ma, L. & Chen, X. Interferon regulatory factor 3-CL, an isoform of IRF3, antagonizes activity of IRF3. *Cell. Mol. Immunol.* **8**, 67–74 (2011).
33. Li, Y. *et al.* Identification of novel alternative splicing variants of interferon regulatory factor 3. *Biochim. Biophys. Acta* **1809**, 166–175 (2011).
34. Shell, S. A., Hesse, C., Morris, S. M. & Milcarek, C. Elevated levels of the 64-kDa cleavage stimulatory factor (CstF-64) in lipopolysaccharide-stimulated macrophages influence gene expression and induce alternative poly(A) site selection. *J. Biol. Chem.* **280**, 39950–39961 (2005).
35. Bhatt, D. M. *et al.* Transcript dynamics of proinflammatory genes revealed by sequence analysis of subcellular RNA fractions. *Cell* **150**, 279–290 (2012).
This paper indicates that the kinetics of pre-mRNA splicing regulate the temporal order of pro-inflammatory gene expression.
36. Hao, S. & Baltimore, D. RNA splicing regulates the temporal order of TNF-induced gene expression. *Proc. Natl Acad. Sci. USA* **110**, 11934–11939 (2013).
37. Rabani, M. *et al.* Metabolic labeling of RNA uncovers principles of RNA production and degradation dynamics in mammalian cells. *Nature Biotech.* **29**, 436–442 (2011).
This paper analyses the respective contributions of gene transcription and RNA decay to the responses of DCs to LPS.
38. Paulsen, M. T. *et al.* Coordinated regulation of synthesis and stability of RNA during the acute TNF-induced proinflammatory response. *Proc. Natl Acad. Sci. USA* **110**, 2240–2245 (2013).
This paper analyses the respective contributions of gene transcription and RNA degradation to TNF-induced cell responses.
39. Elkon, R., Zlotorynski, E., Zeller, K. I. & Agami, R. Major role for mRNA stability in shaping the kinetics of gene induction. *BMC Genomics* **11**, 259 (2010).
40. Hao, S. & Baltimore, D. The stability of mRNA influences the temporal order of the induction of genes encoding inflammatory molecules. *Nature Immunol.* **10**, 281–288 (2009).
41. Caput, D. *et al.* Identification of a common nucleotide sequence in the 3′ untranslated region of mRNA molecules specifying inflammatory mediators. *Proc. Natl Acad. Sci. USA* **83**, 1670–1674 (1986).
This paper is the first to identify an ARE in *TNF* transcripts and its role in mRNA degradation.
42. Shaw, G. & Kamen, R. A conserved AU sequence from the 3′ untranslated region of GM-CSF mRNA mediates selective mRNA degradation. *Cell* **46**, 659–667 (1986).
This paper is the first to identify an ARE in *CSF2* transcripts and its role in mRNA degradation.
43. Bakheet, T., Williams, B. R. & Khabar, K. S. ARED 3.0: the large and diverse AU-rich transcriptome. *Nucleic Acids Res.* **34**, D111–114 (2006).
44. Halees, A. S., El-Badrawi, R. & Khabar, K. S. ARED Organism: expansion of ARED reveals AU-rich element cluster variations between human and mouse. *Nucleic Acids Res.* **36**, D137–D140 (2008).
45. Beisang, D. & Bohjanen, P. R. Perspectives on the ARE as it turns 25 years old. *Wiley Interdiscip. Rev. RNA* **3**, 719–731 (2012).
46. Ivanov, P. & Anderson, P. Post-transcriptional regulatory networks in immunity. *Immunol. Rev.* **253**, 253–272 (2013).
47. Kontoyiannis, D., Pasparakis, M., Pizarro, T. T., Cominelli, F. & Kollias, G. Impaired on/off regulation of TNF biosynthesis in mice lacking TNF AU-rich elements: implications for joint and gut-associated immunopathologies. *Immunity* **10**, 387–398 (1999).
48. Chen, Y.-L. *et al.* Differential regulation of ARE-mediated TNFα and IL-1β mRNA stability by lipopolysaccharide in RAW264.7 cells. *Biochem. Biophys. Res. Commun.* **346**, 160–168 (2006).
49. Stoecklin, G. *et al.* MK2-induced tristetraprolin:14-3-3 complexes prevent stress granule association and ARE-mRNA decay. *EMBO J.* **23**, 1313–1324 (2004).

© 2014 Macmillan Publishers Limited. All rights reserved

50. Sun, L. *et al.* Tristetraprolin (TTP)-14-3-3 complex formation protects TTP from dephosphorylation by protein phosphatase 2a and stabilizes tumor necrosis factor-α mRNA. *J. Biol. Chem.* **282**, 3766–3777 (2007).
51. Lu, J.-Y., Sadri, N. & Schneider, R. J. Endotoxic shock in *AUF1* knockout mice mediated by failure to degrade proinflammatory cytokine mRNAs. *Genes Dev.* **20**, 3174–3184 (2006).
52. Taylor, G. A. *et al.* A pathogenetic role for TNFα in the syndrome of cachexia, arthritis, and autoimmunity resulting from tristetraprolin (TTP) deficiency. *Immunity* **4**, 445–454 (1996).
53. Carballo, E., Lai, W. S. & Blackshear, P. J. Evidence that tristetraprolin is a physiological regulator of granulocyte-macrophage colony-stimulating factor messenger RNA deadenylation and stability. *Blood* **95**, 1891–1899 (2000).
54. Sadri, N. & Schneider, R. J. Auf1/*Hnrnpd*-deficient mice develop pruritic inflammatory skin disease. *J. Invest. Dermatol.* **129**, 657–670 (2009).
55. Yiakouvaki, A. *et al.* Myeloid cell expression of the RNA-binding protein HuR protects mice from pathologic inflammation and colorectal carcinogenesis. *J. Clin. Invest.* **122**, 48–61 (2012).
56. Stoecklin, G., Lu, M., Rattenbacher, B. & Moroni, C. A constitutive decay element promotes tumor necrosis factor alpha mRNA degradation via an AU-rich element-independent pathway. *Mol. Cell. Biol.* **23**, 3506–3515 (2003).
57. Moraes, K. C. M., Wilusz, C. J. & Wilusz, J. CUG-BP binds to RNA substrates and recruits PARN deadenylase. *RNA* **12**, 1084–1091 (2006).
58. Pautz, A. *et al.* The polypyrimidine tract-binding protein (PTB) is involved in the post-transcriptional regulation of human inducible nitric oxide synthase expression. *J. Biol. Chem.* **281**, 32294–32302 (2006).
59. Fabian, M. R. & Sonenberg, N. The mechanics of miRNA-mediated gene silencing: a look under the hood of miRISC. *Nature Struct. Mol. Biol.* **19**, 586–593 (2012).
60. Kozomara, A. & Griffiths-Jones, S. miRBase: integrating microRNA annotation and deep-sequencing data. *Nucleic Acids Res.* **39**, D152–D157 (2011).
61. Friedman, R. C., Farh, K. K.-H., Burge, C. B. & Bartel, D. P. Most mammalian mRNAs are conserved targets of microRNAs. *Genome Res.* **19**, 92–105 (2009).
62. O'Connell, R. M. & Rao, D. S. & Baltimore, D. microRNA regulation of inflammatory responses. *Annu. Rev. Immunol.* **30**, 295–312 (2012).
63. Li, Y. & Shi, X. MicroRNAs in the regulation of TLR and RIG-I pathways. *Cell. Mol. Immunol.* **10**, 65–71 (2013).
64. Bicknell, A. A., Cenik, C., Chua, H. N., Roth, F. P. & Moore, M. J. Introns in UTRs: why we should stop ignoring them. *Bioessays* **34**, 1025–1034 (2012).
65. Weischenfeldt, J. *et al.* NMD is essential for hematopoietic stem and progenitor cells and for eliminating by-products of programmed DNA rearrangements. *Genes Dev.* **22**, 1381–1396 (2008).
This paper indicates a role for NMD in gene expression regulation in macrophages.
66. Lelouard, H. *et al.* Regulation of translation is required for dendritic cell function and survival during activation. *J. Cell Biol.* **179**, 1427–1439 (2007).
67. Donnelly, N., Gorman, A. M., Gupta, S. & Samali, A. The eIF2α kinases: their structures and functions. *Cell. Mol. Life Sci.* **70**, 3493–3511 (2013).
68. He, B. Viruses, endoplasmic reticulum stress, and interferon responses. *Cell Death Differ.* **13**, 393–403 (2006).
69. Woo, C. W. *et al.* Adaptive suppression of the ATF4-CHOP branch of the unfolded protein response by toll-like receptor signalling. *Nature Cell Biol.* **11**, 1473–1480 (2009).
70. Woo, C. W., Kutzler, L., Kimball, S. R. & Tabas, I. Toll-like receptor activation suppresses ER stress factor CHOP and translation inhibition through activation of eIF2B. *Nature Cell Biol.* **14**, 192–200 (2012).
This paper shows that in ER-stressed macrophages the activity of eIF2B is stimulated to overcome translational repression caused by eIF2α phosphorylation.
71. Furic, L. *et al.* eIF4E phosphorylation promotes tumorigenesis and is associated with prostate cancer progression. *Proc. Natl Acad. Sci. USA* **107**, 14134–14139 (2010).
72. Kleijn, M., Vrins, C. L., Voorma, H. O. & Thomas, A. A. Phosphorylation state of the cap-binding protein eIF4E during viral infection. *Virology* **217**, 486–494 (1996).
73. Herdy, B. *et al.* Translational control of the activation of transcription factor NF-κB and production of type I interferon by phosphorylation of the translation factor eIF4E. *Nature Immunol.* **13**, 543–550 (2012).
This paper shows that eIF4E phosphorylation levels regulate the translation of IκBα to modulate type I IFN responses.
74. Wan, Y. *et al.* Interleukin-1 receptor-associated kinase 2 is critical for lipopolysaccharide-mediated post-transcriptional control. *J. Biol. Chem.* **284**, 10367–10375 (2009).
75. Zhou, H. *et al.* IRAK-M mediates Toll-like receptor/IL-1R-induced NFκB activation and cytokine production. *EMBO J.* **32**, 583–596 (2013).
76. Kim, W. J., Kim, J. H. & Jang, S. K. Anti-inflammatory lipid mediator 15d-PGJ2 inhibits translation through inactivation of eIF4A. *EMBO J.* **26**, 5020–5032 (2007).
77. Schmitz, F. *et al.* Mammalian target of rapamycin (mTOR) orchestrates the defense program of innate immune cells. *Eur. J. Immunol.* **38**, 2981–2992 (2008).
78. Colina, R. *et al.* Translational control of the innate immune response through IRF-7. *Nature* **452**, 323–328 (2008).
This paper shows that 4EBP-deficient mice have increased type I IFN responses and are less susceptible to viral infection.
79. López-Pelaéz, M. *et al.* Cot/tpl2–MKK1/2–Erk1/2 controls mTORC1-mediated mRNA translation in Toll-like receptor-activated macrophages. *Mol. Biol. Cell* **23**, 2982–2992 (2012).
This paper shows that 4EBP1 phosphorylation mediated by MAP3K8 (referred to as Cot/tpl2 above) upon TLR engagement stimulates cap-dependent translation.
80. Jefferies, H. B. *et al.* Rapamycin suppresses 5′TOP mRNA translation through inhibition of p70s6k. *EMBO J.* **16**, 3693–3704 (1997).
81. Jaramillo, M. *et al.* Leishmania repression of host translation through mTOR cleavage is required for parasite survival and infection. *Cell Host Microbe* **9**, 331–341 (2011).
82. Weichhart, T. *et al.* The TSC–mTOR signaling pathway regulates the innate inflammatory response. *Immunity* **29**, 565–577 (2008).
83. Ivanov, S. S. & Roy, C. R. Pathogen signatures activate a ubiquitination pathway that modulates the function of the metabolic checkpoint kinase mTOR. *Nature Immunol.* **14**, 1219–1228 (2013).
84. Jackson, R. J., Hellen, C. U. T. & Pestova, T. V. The mechanism of eukaryotic translation initiation and principles of its regulation. *Nature Rev. Mol. Cell. Biol.* **11**, 113–127 (2010).
85. Weill, L., Belloc, E., Bava, F.-A. & Méndez, R. Translational control by changes in poly(A) tail length: recycling mRNAs. *Nature Struct. Mol. Biol.* **19**, 577–585 (2012).
86. Crawford, E. K., Ensor, J. E., Kalvakolanu, I. & Hasday, J. D. The role of 3′ poly(A) tail metabolism in tumor necrosis factor-α regulation. *J. Biol. Chem.* **272**, 21120–21127 (1997).
87. Swanson, B. J., Murakami, M., Mitchell, T. C., Kappler, J. & Marrack, P. RANTES production by memory phenotype T cells is controlled by a posttranscriptional, TCR-dependent process. *Immunity* **17**, 605–615 (2002).
88. Groppo, R. & Richter, J. D. CPEB control of NF-κB nuclear localization and interleukin-6 production mediates cellular senescence. *Mol. Cell. Biol.* **31**, 2707–2714 (2011).
89. Kozak, M. An analysis of 5′-noncoding sequences from 699 vertebrate messenger RNAs. *Nucleic Acids Res.* **15**, 8125–8148 (1987).
90. Shinohara, M. L., Kim, H.-J., Kim, J.-H., Garcia, V. A. & Cantor, H. Alternative translation of osteopontin generates intracellular and secreted isoforms that mediate distinct biological activities in dendritic cells. *Proc. Natl Acad. Sci. USA* **105**, 7235–7239 (2008).
91. Kozak, M. Constraints on reinitiation of translation in mammals. *Nucleic Acids Res.* **29**, 5226–5232 (2001).
92. Calvo, S. E., Pagliarini, D. J. & Mootha, V. K. Upstream open reading frames cause widespread reduction of protein expression and are polymorphic among humans. *Proc. Natl Acad. Sci. USA* **106**, 7507–7512 (2009).
93. Brubaker, S. W., Gauthier, A. E., Mills, E. W., Ingolia, N. T. & Kagan, J. C. A bicistronic MAVS transcript highlights a class of truncated variants in antiviral immunity. *Cell* **156**, 800–811 (2014).
This paper shows that two isoforms of MAVS with antagonistic functions are produced from a single transcript through leaky scanning and translation re-initiation.
94. Lang, K. J. D., Kappel, A. & Goodall, G. J. Hypoxia-inducible factor-1α mRNA contains an internal ribosome entry site that allows efficient translation during normoxia and hypoxia. *Mol. Biol. Cell* **13**, 1792–1801 (2002).
95. Wang, G., Guo, X., Silveyra, P., Kimball, S. R. & Floros, J. Cap-independent translation of human SP-A 5′-UTR variants: a double-loop structure and *cis*-element contribution. *Am. J. Physiol. Lung Cell. Mol. Physiol.* **296**, L635–L647 (2009).
96. Rübsamen, D. *et al.* IRES-dependent translation of egr2 is induced under inflammatory conditions. *RNA* **18**, 1910–1920 (2012).
97. Rübsamen, D. *et al.* Inflammatory conditions induce IRES-dependent translation of cyp24a1. *PLoS ONE* **9**, e85314 (2014).
98. Leppek, K. & Stoecklin, G. An optimized streptavidin-binding RNA aptamer for purification of ribonucleoprotein complexes identifies novel ARE-binding proteins. *Nucleic Acids Res.* **42**, e13 (2013).
99. Tiedje, C. *et al.* The p38/MK2-driven exchange between tristetraprolin and HuR regulates AU-rich element-dependent translation. *PLoS Genet.* **8**, e1002977 (2012).
100. Qi, M.-Y. *et al.* AU-rich-element-dependent translation repression requires the cooperation of tristetraprolin and RCK/P54. *Mol. Cell. Biol.* **32**, 913–928 (2012).
101. Piecyk, M. *et al.* TIA-1 is a translational silencer that selectively regulates the expression of TNF-α. *EMBO J.* **19**, 4154–4163 (2000).
102. Anderson, P. & Kedersha, N. Visibly stressed: the role of eIF2, TIA-1, and stress granules in protein translation. *Cell Stress Chaperones* **7**, 213–221 (2002).
103. Damgaard, C. K. & Lykke-Andersen, J. Translational coregulation of 5′ TOP mRNAs by TIA-1 and TIAR. *Genes Dev.* **25**, 2057–2068 (2011).
104. Mazumder, B. & Fox, P. L. Delayed translational silencing of ceruloplasmin transcript in gamma interferon-activated U937 monocytic cells: role of the 3′ untranslated region. *Mol. Cell. Biol.* **19**, 6898–6905 (1999).
105. Sampath, P., Mazumder, B., Seshadri, V. & Fox, P. L. Transcript-selective translational silencing by gamma interferon is directed by a novel structural element in the ceruloplasmin mRNA 3′ untranslated region. *Mol. Cell. Biol.* **23**, 1509–1519 (2003).
106. Sampath, P. *et al.* Noncanonical function of glutamyl-prolyl-tRNA synthetase: gene-specific silencing of translation. *Cell* **119**, 195–208 (2004).
This paper describes the sequential assembly of the GAIT complex and the binding of the complex to its target mRNA upon IFNγ exposure.
107. Mazumder, B. *et al.* Regulated release of L13a from the 60S ribosomal subunit as a mechanism of transcript-specific translational control. *Cell* **115**, 187–198 (2003).
108. Kapasi, P. *et al.* L13a blocks 48S assembly: role of a general initiation factor in mRNA-specific translational control. *Mol. Cell* **25**, 113–126 (2007).
109. Vyas, K. *et al.* Genome-wide polysome profiling reveals an inflammation-responsive posttranscriptional operon in gamma interferon-activated monocytes. *Mol. Cell. Biol.* **29**, 458–470 (2008).
110. Mukhopadhyay, R. *et al.* DAPK-ZIPK-L13a axis constitutes a negative-feedback module regulating inflammatory gene expression. *Mol. Cell* **32**, 371–382 (2008).
111. Ray, P. S. & Fox, P. L. A post-transcriptional pathway represses monocyte VEGF-A expression and angiogenic activity. *EMBO J.* **26**, 3360–3372 (2007).
112. Ray, P. S. *et al.* A stress-responsive RNA switch regulates VEGFA expression. *Nature* **457**, 915–919 (2009).
113. Yao, P. *et al.* The HILDA complex coordinates a conditional switch in the 3′-untranslated region of the VEGFA mRNA. *PLoS Biol.* **11**, e1001635 (2013).
114. González-Terán, B. *et al.* Eukaryotic elongation factor 2 controls TNF-α translation in LPS-induced hepatitis. *J. Clin. Invest.* **123**, 164–178 (2013).
This paper shows that LPS-induced MAPK activation stimulates eEF2 activity to increase TNF translation elongation.

© 2014 Macmillan Publishers Limited. All rights reserved

115. Pachnis, V., Brannan, C. I. & Tilghman, S. M. The structure and expression of a novel gene activated in early mouse embryogenesis. *EMBO J.* **7**, 673–681 (1988).
116. Brannan, C. I., Dees, E. C., Ingram, R. S. & Tilghman, S. M. The product of the H19 gene may function as an RNA. *Mol. Cell. Biol.* **10**, 28–36 (1990).
117. Penny, G. D., Kay, G. F., Sheardown, S. A., Rastan, S. & Brockdorff, N. Requirement for Xist in X chromosome inactivation. *Nature* **379**, 131–137 (1996).
118. Guttman, M. *et al.* Chromatin signature reveals over a thousand highly conserved large non-coding RNAs in mammals. *Nature* **458**, 223–227 (2009).
119. Rinn, J. L. & Chang, H. Y. Genome regulation by long noncoding RNAs. *Annu. Rev. Biochem.* **81**, 145–166 (2012).
120. Mortazavi, A., Williams, B. A., McCue, K., Schaeffer, L. & Wold, B. Mapping and quantifying mammalian transcriptomes by RNA-Seq. *Nature Methods* **5**, 621–628 (2008).
121. Guttman, M. *et al. Ab initio* reconstruction of cell type-specific transcriptomes in mouse reveals the conserved multi-exonic structure of lincRNAs. *Nature Biotech.* **28**, 503–510 (2010).
122. Guttman, M. & Rinn, J. L. Modular regulatory principles of large non-coding RNAs. *Nature* **482**, 339–346 (2012).
123. Birney, E. *et al.* Identification and analysis of functional elements in 1% of the human genome by the ENCODE pilot project. *Nature* **447**, 799–816 (2007).
124. Peng, X. *et al.* Unique signatures of long noncoding RNA expression in response to virus infection and altered innate immune signaling. *mBio* **1**, e00206–e00210 (2010).
125. Ricci, E. P. *et al.* miRNA repression of translation *in vitro* takes place during 43S ribosomal scanning. *Nucleic Acids Res.* **41**, 586–598 (2013).
126. Gomez, J. A. *et al.* The NeST long ncRNA controls microbial susceptibility and epigenetic activation of the interferon-γ locus. *Cell* **152**, 743–754 (2013).
127. Collier, S. P., Collins, P. L., Williams, C. L., Boothby, M. R. & Aune, T. M. Cutting edge: influence of *Tmevpg1*, a long intergenic noncoding RNA, on the expression of *Ifng* by T_H1 cells. *J. Immunol.* **189**, 2084–2088 (2012).
128. Carpenter, S. *et al.* A long noncoding RNA mediates both activation and repression of immune response genes. *Science* **341**, 789–792 (2013).
129. Rapicavoli, N. A. *et al.* A mammalian pseudogene lncRNA at the interface of inflammation and anti-inflammatory therapeutics. *eLife* **2**, e00762 (2013).
130. Li, Z. *et al.* The long noncoding RNA *THRIL* regulates TNFα expression through its interaction with hnRNPL. *Proc. Natl Acad. Sci. USA* **111**, 1002–1007 (2014).
131. Salmena, L., Poliseno, L., Tay, Y., Kats, L. & Pandolfi, P. P. A ceRNA hypothesis: the Rosetta Stone of a hidden RNA language? *Cell* **146**, 353–358 (2011).
132. Zong, X., Tripathi, V. & Prasanth, K. V. RNA splicing control: yet another gene regulatory role for long nuclear noncoding RNAs. *RNA Biol.* **8**, 968–977 (2011).
133. Yin, Q. F. *et al.* Long noncoding RNAs with snoRNA ends. *Mol. Cell* **48**, 219–230 (2012).
134. Faghihi, M. A. *et al.* Expression of a noncoding RNA is elevated in Alzheimer's disease and drives rapid feed-forward regulation of β-secretase. *Nature Med.* **14**, 723–730 (2008).
135. Yoon, J.-H. *et al.* LincRNA-p21 suppresses target mRNA translation. *Mol. Cell* **47**, 648–655 (2012).
136. Yoon, J.-H., Abdelmohsen, K. & Gorospe, M. Posttranscriptional gene regulation by long noncoding RNA. *J. Mol. Biol.* **425**, 3723–3730 (2013).

Acknowledgements
This work is supported by the US National Institutes of Health (grant AI067497 to K.A.F) and the Howard Hughes Medical Institute, USA (M.J.M).

Competing interests statement
The authors declare no competing interests.

© 2014 Macmillan Publishers Limited. All rights reserved

nature COMMUNICATIONS

ARTICLE

https://doi.org/10.1038/s41467-018-07845-z OPEN

Genome editing in primary cells and in vivo using viral-derived Nanoblades loaded with Cas9-sgRNA ribonucleoproteins

Philippe E. Mangeot[1], Valérie Risson[2], Floriane Fusil[1], Aline Marnef[3], Emilie Laurent[1], Juliana Blin[1], Virginie Mournetas[4], Emmanuelle Massouridès[4], Thibault J.M. Sohier[1], Antoine Corbin[1], Fabien Aubé[5], Marie Teixeira[6], Christian Pinset[4], Laurent Schaeffer[2], Gaëlle Legube[3], François-Loïc Cosset[1], Els Verhoeyen[1,7], Théophile Ohlmann[1] & Emiliano P. Ricci[1,5]

Programmable nucleases have enabled rapid and accessible genome engineering in eukaryotic cells and living organisms. However, their delivery into target cells can be technically challenging when working with primary cells or in vivo. Here, we use engineered murine leukemia virus-like particles loaded with Cas9-sgRNA ribonucleoproteins (Nanoblades) to induce efficient genome-editing in cell lines and primary cells including human induced pluripotent stem cells, human hematopoietic stem cells and mouse bone-marrow cells. Transgene-free Nanoblades are also capable of in vivo genome-editing in mouse embryos and in the liver of injected mice. Nanoblades can be complexed with donor DNA for "all-in-one" homology-directed repair or programmed with modified Cas9 variants to mediate transcriptional up-regulation of target genes. Nanoblades preparation process is simple, relatively inexpensive and can be easily implemented in any laboratory equipped for cellular biology.

[1] CIRI, Centre International de Recherche en Infectiologie Univ Lyon, Inserm, U1111, Université Claude Bernard Lyon 1, CNRS, UMR5308, ENS de Lyon, F-69007 Lyon, France. [2] Institut NeuroMyoGène, CNRS 5310, INSERM U121, Université Lyon 1, Faculté de Médecine Lyon Est, Lyon 69008, France. [3] LBCMCP, Centre de Biologie Intégrative (CBI), CNRS, Université de Toulouse, UT3, 118 Route de Narbonne, 31062 Toulouse, France. [4] I-STEM/CECS, Inserm, UMR861 28 rue Henri Desbruères, 91100 Corbeil Essonnes, France. [5] LBMC, Laboratoire de Biologie et Modélisation de la Cellule Univ Lyon, ENS de Lyon, Université Claude Bernard Lyon 1, CNRS, UMR 5239, INSERM, U1210, Lyon 69007, France. [6] SFR BioSciences, Plateau de Biologie Expérimentale de la Souris (AniRA-PBES), Ecole Normale Supérieure de Lyon, Université Lyon1, CNRS UMS3444 INSERM US8, 69007 Lyon, France. [7] Present address: CIRI, Université Côte d'Azur, INSERM, C3M, 06204 Nice, France. These authors contributed equally: Valérie Risson, Floriane Fusil, Aline Marnef. Correspondence and requests for materials should be addressed to P.E.M. (email: philippe.mangeot@inserm.fr) or to E.P.R. (email: emiliano.ricci@ens-lyon.org)

Targeted genome editing tools, such as meganucleases (MGN), zinc-finger nucleases (ZFN), transcription activator-like effector nucleases (TALENs) and more recently the clustered regularly interspaced short palindromic repeats (CRISPR) have revolutionized most biomedical research fields. Such tools allow to precisely edit the genome of eukaryotic cells by inducing double-stranded DNA (dsDNA) breaks at specific loci. Relying on the cell endogenous repair pathways, dsDNA breaks can then be repaired by non-homologous end-joining (NHEJ) or homology-directed repair (HDR) allowing the removal or insertion of new genetic information at a desired locus.

Among the above-mentioned tools, CRISPR-Cas9 is currently the most simple and versatile method for genome engineering. Indeed, in the two-component system, the bacterial-derived nuclease Cas9 (for CRISPR-associated protein 9) associates with a single-guide RNA (sgRNA) to target a complementary DNA sequence and induce a dsDNA break[1]. Therefore, by the simple modification of the sgRNA sequence, users can specify the genomic locus to be targeted. Consistent with the great promises of CRISPR-Cas9 for genome engineering and gene therapy, considerable efforts have been made in developing efficient tools to deliver the Cas9 and the sgRNA into target cells ex vivo either by transfection of plasmids coding for the nucleases, transduction with viral-derived vectors coding for the nucleases or by direct injection or electroporation of Cas9-sgRNA complexes into cells.

Here, we have designed Nanoblades, a protein-delivery vector based on friend murine leukemia virus (MLV) that allows the transfer of Cas9-sgRNA ribonucleoproteins (RNPs) to cell lines and primary cells in vitro and in vivo. Nanoblades deliver the ribonucleoprotein cargo in a transient and rapid manner without delivering a transgene and can mediate knock-in in cell lines when complexed with a repair template. Nanoblades can also be programmed with modified Cas9 proteins to mediate transient transcriptional activation of targeted genes.

Results

Cas9-sgRNA RNP delivery through MLV virus-like particles (VLPs). Assembly of retroviral particles relies on the viral structural Gag polyprotein, which multimerizes at the cell membrane and is sufficient, when expressed in cultured cells, to induce release of VLPs into the cell supernatant[2]. When Gag is coexpressed together with a fusogenic viral envelope, pseudotyped VLPs are produced that lack a viral genome but still retain their capacity to fuse with target cells and deliver the Gag protein`into their cytoplasm. As previously investigated[3,4], we took advantage of the structural role of Gag and designed an expression vector coding for the MLV Gag polyprotein fused, at its C-terminal end, to a flag-tagged version of *Streptococcus pyogenes* Cas9 protein (Gag::Cas9, Fig. 1a). The two fused proteins are separated by a proteolytic site which can be cleaved by the MLV protease to release the Flag-tagged Cas9 (Fig. 1a). By cotransfecting HEK-293T cells with plasmids coding for Gag::Cas9, Gag-Pro-Pol, a sgRNA, and viral envelopes, fusogenic VLPs are produced and released in the culture medium (herein described as Nanoblades). Biochemical and imaging analysis of purified particles (Supplementary Figure 1a, 1b, 1c and 1d) indicates that Nanoblades (150 nm) are slightly larger than wild-type MLV (Supplementary Figure 1b) but sediment at a density of 1.17 g/ml (Supplementary Figure 1c) as described for MLV VLPs[5]. As detected by western blot, Northern blot, mass-spectrometry, and deep-sequencing, Nanoblades contain the Cas9 protein and sgRNA (Supplementary Figure 1 and 2 and Supplementary Data 1). In addition to Gag, Cas9 and envelope proteins, mass-spectrometry analysis of Nanoblades identified several cellular proteins, mostly membrane-associated proteins (Supplementary Figure 2a and Supplementary Data 1). Interestingly, the packaging of sgRNA depends on the presence of the Gag::Cas9 fusion protein, since Nanoblades produced from cells that only express the Gag protein fail to incorporate detectable amounts of sgRNA (Supplementary Figure 1d). Furthermore, Cas9-dependent loading of the sgRNA within Nanoblades is not limited by the efficiency of the interaction between the Cas9 and the sgRNA, since expressing an optimized version of the sgRNA that improves binding to Cas9[6] does not appear to increase sgRNA levels within purified VLPs (Supplementary Figure 1d see sgRNA(F+E)).

To assess for Cas9-sgRNA RNP delivery efficiency in target cells and induction of genomic dsDNA breaks, we designed Nanoblades with a sgRNA targeting the 45S rDNA loci. Human 45S rDNA genes are present in hundreds of tandem repeats across five autosomes, locate in the nucleolus and are transcribed exclusively by RNA polymerase (Pol) I[7]. Using immunofluorescence microscopy, it is therefore possible to follow the occurrence of dsDNA breaks at rDNA loci with single-cell resolution by monitoring the nucleolus using the nucleolar marker RNA Pol I and the well-established dsDNA break-marker, histone variant γ-H2AX[8], that localizes at the nucleolar periphery after dsDNA break induction within rDNA[9]. U2OS (osteosarcoma cell line) cells transduced for 24 h with Nanoblades programmed with a sgRNA targeting rDNA display the typical γ-H2AX distribution at the nucleolar periphery with RNA Pol I, indicative of rDNA breaks, whilst cells transduced with Nanoblades with control sgRNAs do not (Fig. 1b, top panel). Interestingly, this distribution of γ-H2AX at the nucleolar periphery can be observed as early as 4 h after transduction in 60% of cells with a maximum effect observed at 16 h after transduction, where almost 100% of observed cells display this γ-H2AX distribution (Fig. 1b, bottom panel and quantification below). In comparison, only 60% of cells transfected with a plasmid coding for Cas9 and the sgRNA display the perinucleolar γ-H2AX/RNA Pol I localization 24 h after transfection. Similar results were obtained in human primary fibroblasts with more than 85% cells displaying this distribution after 16 h (Supplementary Figure 1e). These results suggest that Nanoblade-mediated delivery of the Cas9-sgRNA RNP is both efficient and rapid in cell lines and primary human cells. To further confirm these results, we designed and dosed Nanoblades (by ELISA assay using anti-Cas9 antibodies) programmed with a sgRNA widely used in the literature[10] that targets the human *EMX1* gene to induce dsDNA cleavage at a single locus. HEK-293T cells were then transduced with increasing amounts of Nanoblades and gene editing was measured from the bulk population 48 h after transduction (Fig. 1c). Under these conditions, we observed a dose-dependent effect of Nanoblades ranging from 35% of *EMX1* (at 4 pmol of Cas9) editing to 77% of editing at the highest dose (20 pmol) of Cas9 (Fig. 1c).

Because Nanoblades carry cellular proteins from producer cells in addition to Cas9 (Supplementary Data 1), we tested whether these proteins could also be delivered to recipient cells. For this, we over-expressed the firefly luciferase in producer cells and collected Nanoblades targeting *EMX1* from the supernatant. Luciferase-loaded Nanoblades were then used to transduce HEK293T cells for 24 h. Cells were then washed twice in PBS and incubated in fresh medium for 4, 8, 24, and 48 h. Luciferase activity was measured at each time point, as well as in input Nanoblades (Supplementary Figure 2c). As observed, we could detect a mild luciferase signal (4–6% of input) at 4 and 8 h upon transduction. However, the signal rapidly faded at 24 h (2% of input) and

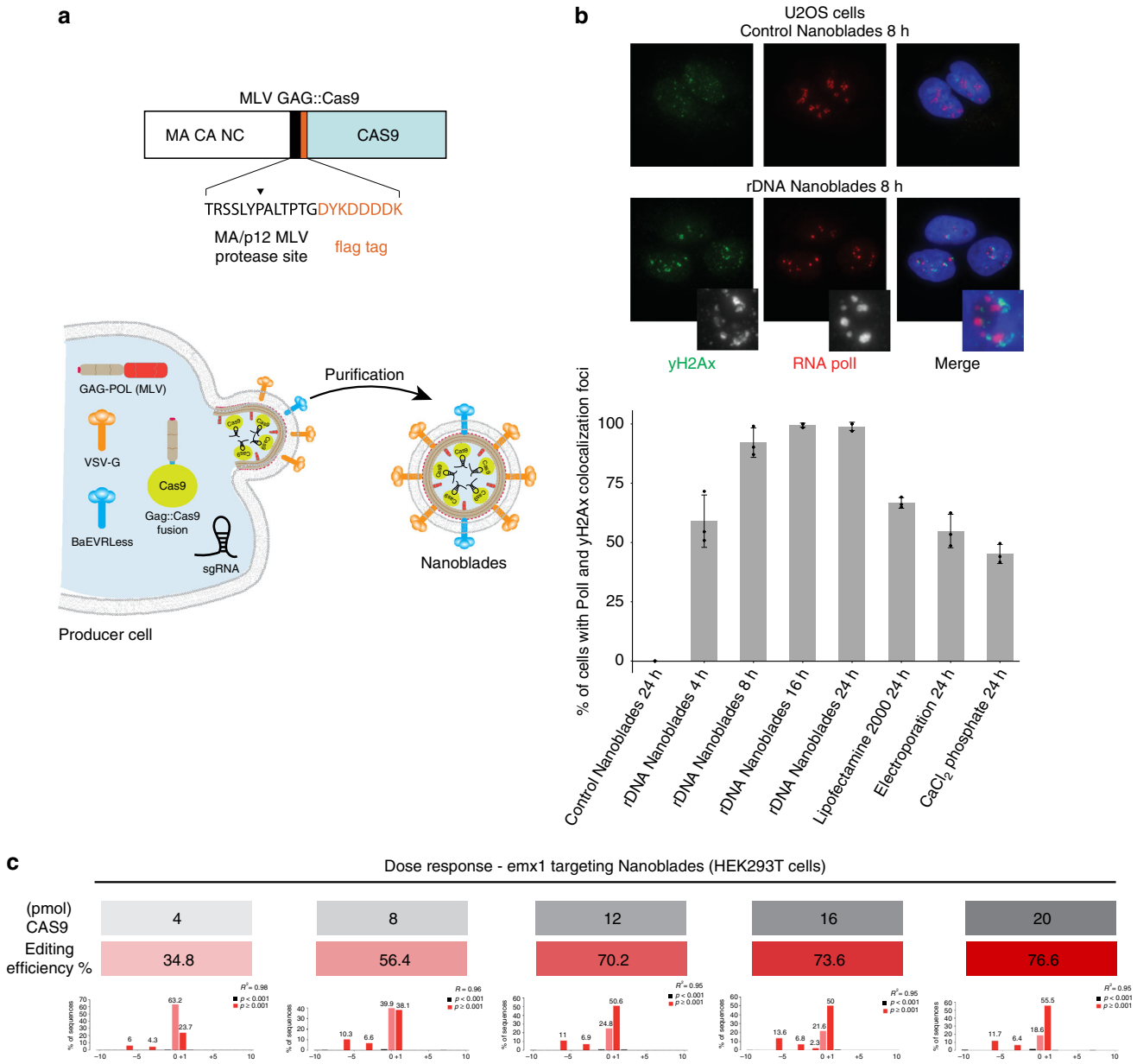

Fig. 1 Nanoblade-mediated genome editing. **a** Scheme describing the MLV Gag::Cas9 fusion and the Nanoblade production protocol based on the transfection of HEK-293T cells by plasmids coding for Gag-Pol, Gag::Cas9, VSV-G, BaEVRLess, and the sgRNA. **b** Top panel, immunofluorescence analysis of γ-H2AX (green), RNA poll (red) in U2OS cells 8 h after being transduced with control Nanoblades or with Nanoblades targeting ribosomal DNA genes. Bottom panel, quantification of γ-H2AX and RNA poll colocalization foci in U2OS cells at different times after Nanoblades transduction or after classical DNA transfection methods ($n = 3$, error bars correspond to standard deviation). **c** Dose response of Nanoblades. HEK-293T cells were transduced with increasing amounts of Nanoblades targeting human *EMX1* ($n = 1$ displayed). The exact amount of Cas9 used for transduction was measured by dot blot (in gray). Genome editing was assessed by Sanger sequencing and Tide analysis (in red)

was almost undetectable at 48 h (Supplementary Figure 2c). In addition to the ectopically expressed firefly luciferase, we also investigated transmission of the CD81 cell-surface protein, which is highly expressed in HEK293T producer cells and is present in Nanoblades as revealed by mass spectrometry (Supplementary Data 1). HepG2 cells, a hepatic cell line that lacks CD81 expression[11], were transduced for 24 h with Nanoblades targeting *EMX1* and then washed twice with PBS before monitoring CD81 residual signal immediately after the washes or 8 and 48 h after incubation with fresh medium (Supplementary Figure 2d). As observed, even though CD81 was very abundant at the cell surface of producer cells and completely absent in recipient cells (Supplementary Figure 2d, left and middle panels), we could only detect a mild CD81 signal immediately after transduction (see Supplementary Figure 2d, right panel). Later time points (8 and 48 h) did not show any specific CD81 labeling in recipient HepG2 cells. The impact of cellular proteins delivered by Nanoblades into recipient cells appears therefore limited and restricted to a short time frame.

Taken together, our results indicate that Nanoblades can be efficiently used to mediate genome editing in a rapid and dose-dependent manner with limited impact on the proteome of target cells.

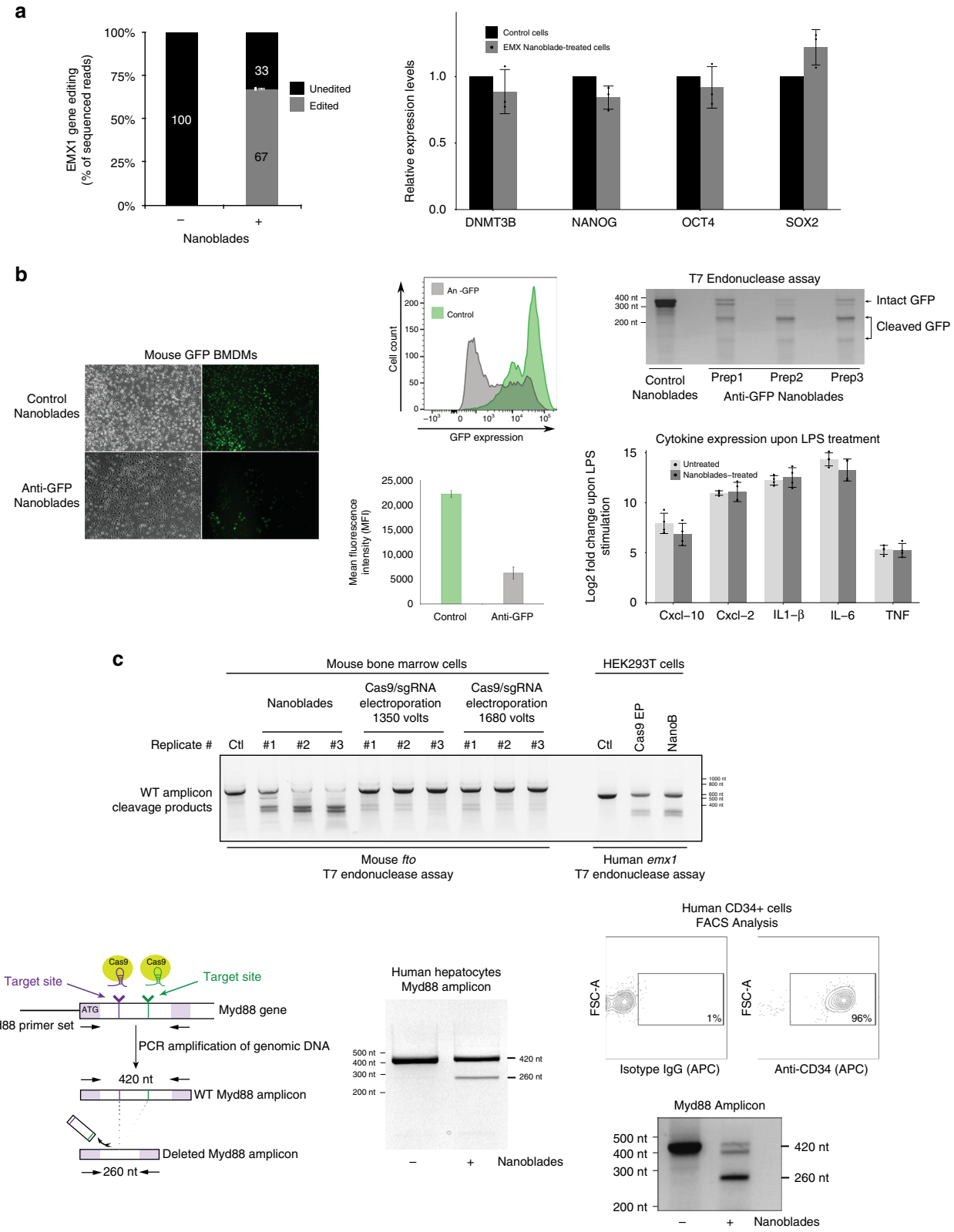

Nanoblades-mediated genome editing in primary cells. Genome editing in primary cells and patient-derived pluripotent cells represents a major interest both for basic science and therapeutical applications. However, primary cells are often refractory to DNA transfection and other gene delivery methods. Because Nanoblades were capable of efficient delivery of functional Cas9-sgRNA RNPs into primary fibroblasts, we tested whether they were effective in other primary cells for genome editing. To this aim, Nanoblades targeting *EMX1* were used to transduce human-induced pluripotent stem cells (hiPSCs). Genome editing at the *EMX1* locus was assessed in the bulk cellular population 48 h after transduction by deep-sequencing of the *EMX1* locus (Fig. 2a, left panel). As observed, Nanoblades were capable of mediating 67% genome editing at the *EMX1* locus in hiPSCs. Notably, hiPSCs

Fig. 2 Genome editing in primary cells transduced with Nanoblades. **a** Left panel, editing efficiency at the *EMX1* locus (measured by high-throughput sequencing on the Illumina Miseq platform) of human-induced pluripotent stem cells (hiPSCs) transduced with Nanoblades targeting human *EMX1* ($n = 3$). Right panel, expression of pluripotency markers measured by qPCR in control cells and cells transduced with Nanoblades targeting *EMX1* ($n = 3$). **b** Left and middle panels, fluorescence microscopy and FACS analysis of GFP expressing BMDMs transduced at the bone marrow stage (day 0 after bone marrow collection) with control Nanoblades or Nanoblades targeting the *GFP*-coding sequence ($n = 3$). Right top panel, T7 endonuclease assay against the GFP sequence from Nanoblades-treated BMDMs. Right bottom panel, cytokine expression levels (measured by qPCR) in untreated or Nanoblade-treated cells upon LPS stimulation ($n = 4$). **c** T7 endonuclease assay against mouse *Fto* or human *EMX1* genomic sequences amplified by PCR from primary mouse bone marrow cells transduced with Nanoblades or electroporated with recombinant Cas9-sgRNA RNPs. For bone marrow cells, two electroporation settings were tested. Lanes numbered #1–#3 correspond to biological replicates. Editing efficiencies were calculated by TIDE[13] analysis of the Sanger sequencing electropherograms for each PCR amplicon **d** Left panel, excision of a 160 bp DNA fragment of *MYD88* using Nanoblades. Middle panel PCR results obtained in human primary hepatocytes transduced with Nanoblades. Right-panel (top), FACS analysis of CD34+ cells purified from human cord-blood. Bottom, genome editing at the *MYD88* locus assessed by PCR in untreated and Nanoblades-treated CD34+ cells. Error bars in all figures correspond to standard deviation

treated with *EMX1* Nanoblades maintained constant levels of pluripotency markers compared to control cells (Fig. 2a, right panel) thus indicating that their multipotent status did not appear to be affected.

Similarly to hiPSCs, mouse bone marrow (BM) cells can be collected and differentiated in vitro into various hematopoietic cell types, such as macrophages (bone marrow-derived macrophages or BMDMs) and dendritic cells. Efficient genome editing of specific genes in BM cells would therefore allow for the corresponding pre-existing protein to be degraded during differentiation and obtain a functional knockout. To test this hypothesis, BM cells obtained from GFP transgenic mice[12] were transduced with Nanoblades programmed with a sgRNA targeting the *GFP* coding sequence. 6 h after transduction, cells were washed and incubated in presence of macrophage colony-stimulating factor (MCSF) for 1 week. After this, cells were collected to monitor GFP levels by fluorescence microscopy, FACS and genome editing by T7 endonuclease assay (Fig. 2b). We consistently obtained close to 75% reduction of GFP expression as measured by FACS analysis and around 60–65% genome editing at the *GFP* locus as measured by T7 endonuclease assays (Fig. 2b). Importantly, genome editing through Nanoblades did not affect the capacity of BMDMs to respond to LPS as their cytokine expression remains identical to that of untreated control cells (Fig. 2b bottom right panel). Nanoblades can therefore be used to inactivate genes in BM cells and study their function in differentiated cells. To further complement these results, we compared the efficiency of Nanoblades to that of recombinant Cas9-sgRNA RNP electroporation in targeting an endogenous gene in primary mouse BM cells. For this, Nanoblades or Cas9-sgRNA RNPs programmed to target the *Fto* gene were used, respectively, to transduce or electroporate primary BM cells freshly extracted from mice. As a control, Nanoblades or Cas9-sgRNA RNPs programmed to target human *EMX1* were also tested in HEK293T cells. In both cases, the efficiency of genome editing was assessed 24 h after transduction or electroporation. As observed (Fig. 2c), both Nanoblades and Cas9-sgRNA electroporation mediate efficient genome editing in HEK293T at 71% (Nanoblades) and 44% (Electroporation) of editing efficiency at the *EMX1* locus. Interestingly, in primary BM cells, while Nanoblades achieve highly efficient genome editing of the *Fto* locus (up to 76% as measured by TIDE[13] analysis), Cas9 electroporation was much less efficient at both conditions that we tested (1350 and 1680 V) yielding a mild but visible signal in the T7 endonuclease assay which was nevertheless below the detection limit for TIDE analysis. Interestingly both protocols (Nanoblades and protein electroporation) did not have an important impact on cell viability 24 h after Cas9 delivery (Supplementary Figure 2e).

Nanoblades efficiency was also investigated in human cells that represent a major interest in research and gene therapy like human primary hepatocytes and human hematopoietic stem cells (HSCs) that both have the capacity to colonize and regenerate fully functional tissues. For both these cell types, Nanoblades programmed with two sgRNAs targeting the human *Myd88* gene were prepared and achieved significant cleavage efficiencies, as revealed by flanking PCR assays (Fig. 2d). Interestingly, HSCs are difficult to transduce with classic VSV-G pseudotyped lentiviral vectors (LVs) because they lack the LDL receptor[14], a limitation that can be alleviated by the use of the baboon retroviral envelope glycoprotein (BaEV)[15]. This prompted us to equip Nanoblades with both BaEV and VSV G-envelopes for these cells and finally in all our study as the combination of both envelopes improved Cas9 delivery in most cells (Supplementary Figure 6a and b). As observed, Nanoblades were also able to induce genome editing in these cells (50% genome editing based on T7 endonuclease assay, Fig. 2d) thus expanding the catalog of primary cells that can be edited using Nanoblades.

Taken together, our results indicate that Nanoblades are an efficient delivery system to induce rapid and effective genome editing in murine and human primary cells of high therapeutic value that are notoriously difficult to transfect.

"All-in-one" Nanoblades for homology directed repair. Precise insertion of genetic material (also known as Knock-in) using CRISPR-Cas9 can be achieved through HDR. This occurs when a donor DNA template with sequence homology to the region surrounding the targeted genomic locus is provided to cells together with the Cas9-sgRNA RNP. Based on a previous finding showing that retroviral-particles can be complexed with DNA in the presence of polybrene to allow for virus-dependent DNA transfection[16], we tested whether Nanoblades could be directly complexed with a DNA template to mediate HDR in target cells. To test this approach, Nanoblades programmed to target a locus close to the AUG start codon of the human *DDX3* gene were complexed to a single-stranded DNA oligomer bearing the FLAG-tag sequence flanked with 46 nucleotide (nt) homology arms corresponding to the region surrounding the start-codon of *DDX3* (Fig. 3a, left panel). HEK293T were transduced with these "All-in-one" Nanoblades and passed 6 times before assessing HDR efficiency in the bulk cellular population both by PCR and by Flag-immunoprecipitation followed by western-blotting (using a DDX3 and FLAG-antibody). As observed (Fig. 3a, right panel), cells transduced with "All-in-one" Nanoblades showed incorporation of the FLAG-tag at the *DDX3* locus both genetically and at the level of protein expression (Fig. 3a right panel, see Flag-IP elution and Genotyping panels). In parallel, single-cell

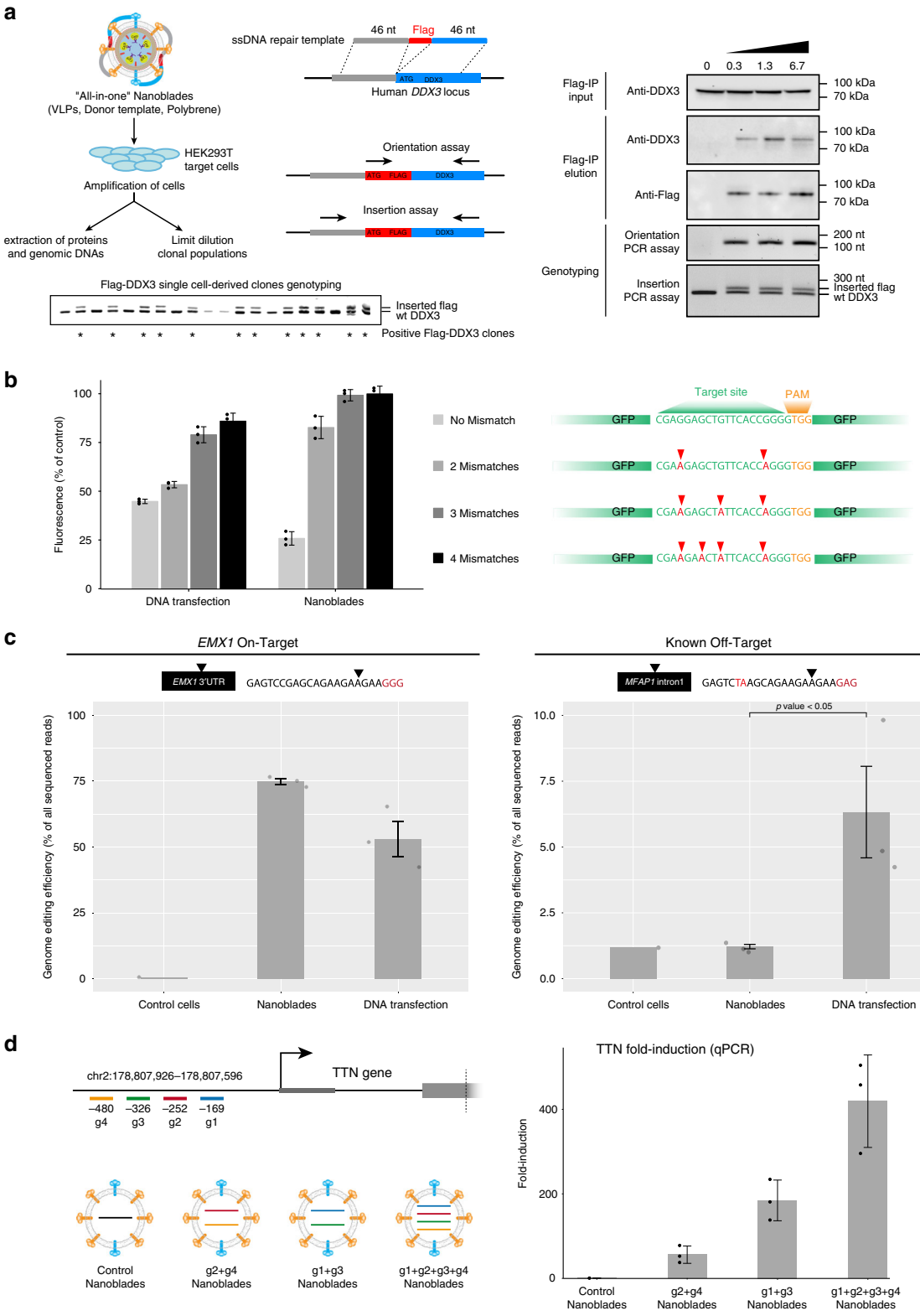

clones were derived from the Flag-DDX3 bulk population and tested for Flag incorporation by PCR. As shown (Fig. 3a left bottom panel), 12 out of 20 isolated clones displayed incorporation of the Flag-sequence at the DDX3 locus thus suggesting a knock-in efficiency of more than 50% of cells using "all-in-one" Nanoblades.

Knock-in assisted by "All-in-one" Nanoblades was also obtained at the AAVS1 locus which has been described as a safe harbor for transgene insertion[17]. For this we designed a dsDNA template of 4 kb bearing the puromycin resistance gene with homology arms to the AAVS1 locus. After transduction of HEK-293T cells with Nanoblades complexed with this template using polybrene, single-cell-derived clones were selected with puromycin. Out of 1×10^5 transduced cells, we obtained 47 puromycin-resistant clones (Supplementary Figure 3b, c and d). A PCR-assay revealed that 42 out of 47 puromycin-resistant clones tested had

Fig. 3 "All-in-one" Nanoblades for knock-in experiments and assessment of Nanoblades off-target activity. **a** Left panel, Nanoblades targeting human *DDX3* close to its start codon were complexed with a donor ssDNA bearing homology arms to the targeted locus and a Flag-tag sequence in the presence of polybrene. HEK293T cells were then transduced with these "All-in-one" Nanoblades. After cell amplification, a fraction of cells were collected to extract genomic DNA and total proteins while the remaining cells were cultured to obtain single-cell clonal populations. Right panel, insertion of the Flag-tag in HEK-293T cells transduced with "all-in-one" Nanoblades complexed with increasing amounts of donor ssDNA was assessed by Flag-immunoprecipitation followed by western-blot using anti-flag or anti-DDX3 antibodies in the input and Flag-immunoprecipitation elution fractions. Flag insertion was also assessed by PCR using a forward primer in the flag-sequence and a reverse primer in the DDX3 locus (Orientation PCR assay) or using primers flanking the Flag sequence (Insertion PCR assay). Bottom panel, Flag-insertion in 20 different single-cell-derived clones was assessed by PCR using primers flanking the Flag-sequence. **b** Left panel, off-target monitoring in immortalized mouse macrophages stably expressing *GFP* transgenes bearing silent mutations in the region targeted by the sgRNA. Right panel, cells were transfected with plasmids coding for Cas9 and the sgRNA or transduced with Nanoblades. GFP expression was measured by FACS 72 h after transfection/transduction ($n = 3$). **c** Left and right panels, gene-editing at the *EMX1* on-target site and the *MFAP1* intronic off-target site measured by high-throughput sequencing in untreated cells (control cells) and cells transduced with *EMX1* Nanoblades (Nanoblades) or transfected with plasmids coding for Cas9 and the EMX1 sgRNA (DNA transfection) ($n = 3$). Statistical significance of the Nanoblades and DNA transfection comparison at the on-target site was computed using a two-tail Student test. **d** Left panel, position of sgRNAs targeting the promoter of *TTN* and VLPs with different combination of sgRNAs produced for the experiment. Right-panel, TTN mRNA expression levels (normalized to Control) as measured by qPCR in MCF7 transduced with VLPs ($n = 3$). Error bars in all figures correspond to standard deviation

the puromycin cassette inserted at the AAVS1 locus (Supplementary Figure 3d).

Taken together, our results show that Nanoblades can be used for the precise insertion of genetic material through HDR both with ssDNA and dsDNA donor DNA template and no requirement for any transfection reagent.

Nanoblades confer low off-target genome-editing. A major concern related to the use of CRISPR/Cas9-mediated gene editing are the potential off-target effects that can occur at genomic loci that are similar in sequence to the original target. Interestingly, several reports have shown that transient delivery of the Cas9-sgRNA complex by injection or RNP transfection generally leads to reduced off-target effects as compared to constitutive expression of Cas9 and sgRNA from DNA transfection experiments[18]. Since Nanoblades deliver the Cas9-sgRNA complex in a dose-dependent and transient fashion, we tested whether they could also lead to reduced off-target effects when compared to classical DNA transfection. For this, we developed an approach similar to that described by Fu and colleagues[19] by creating a series of HEK-293T reporter cell lines transduced with different versions of a *GFP* transgene bearing silent point mutations located in the sgRNA target site (Fig. 3b, right panel). These cells were either transfected with plasmids coding for Cas9 and the sgRNA targeting the *GFP* or transduced with Nanoblades programmed with the same sgRNA. 96 h after transfection/transduction, cells were collected and GFP expression was monitored by FACS (Fig. 3b, left panel). As expected, GFP expression from cells bearing the wild-type *GFP* sequence (No Mismatch) was efficiently repressed both after Nanoblades transduction (close to 80% repression) and DNA transfection (close to 60% repression) (Fig. 3b, left panel "No Mismatch"). When two mismatches were introduced in the target site, Nanoblades were no longer able to efficiently repress GFP expression (20% compared to control) while GFP expression from transfected cells was still reduced to levels similar to that of the *GFP* bearing a perfect match with the sgRNA. Interestingly, the presence of three or four mismatches completely abolished *GFP* editing in Nanoblades-treated cells while cells transfected with the Cas9 and sgRNA plasmids still displayed a mild inhibition of GFP expression (Fig. 3b see 3 and 4 Mismatches).

To complement these results, we further tested for genomic off-target effects using the well-characterized sgRNA targeting human *EMX1*. Off-targets for this sgRNA have been extensively studied using T7 endonuclease assays and high-throughput sequencing approaches[10]. We PCR-amplified the *EMX1* locus and one of the previously described *EMX1* genomic off-target loci occurring at the intron of *MFAP1*[10] in cells treated for 72 h with Nanoblades programmed with the *EMX1* sgRNA or transfected with a DNA construct coding for Cas9 and the *EMX1* sgRNA. We then assessed genome-editing on each sample by high-throughput sequencing (Fig. 3c)[13]. Editing at the on-target site was efficient in Nanoblade-treated cells (75% in average) and to a less extent in cells transfected with the DNA coding for Cas9 and the sgRNA (53% in average) (Fig. 3c, left panel). As expected, small INDELs (insertions and deletions) occurred close to the expected Cas9 cleavage site located 3nt upstream the PAM sequence both in Nanoblades treated and in DNA-transfected cells (Supplementary Figure 4). Surprisingly, in spite of the higher editing efficiency at the on-target site, we could not detect any significant editing at the *MFAP1* off-target site in Nanoblades-treated cells (Fig. 3c, right panel). In contrast, cells transfected with the DNA coding for Cas9 and the sgRNA displayed significant editing (close 6%) at the off-target site (Fig. 3c, right panel) and had INDELs at the expected cut site (Supplementary Figure 4).

Taken together, our results indicate that similarly to other protocols that lead to transient delivery of the Cas9-sgRNA RNP, Nanoblades display low off-target effects.

Targeted transcriptional activation through Nanoblades. Having shown efficient genome editing using Nanoblades loaded with the catalytically active Cas9, we tested whether Nanoblades could also deliver Cas9 variant proteins for applications, such as targeted transcriptional activation. To this aim, we fused the Cas9-derived transcriptional activator (SP-dCas9-VPR)[20] to Gag from MLV and expressed the fusion protein in producer cells together with a control sgRNA or different combinations of sgRNAs targeting the promoter region of human Titin (*TTN*) as previously described[20] (Fig. 3d, left panel). Nanoblades loaded with SP-dCas9-VPR were then incubated with MCF-7 cells and induction of TTN measured by quantitative RT-PCR (normalized to GAPDH expression). As observed (Fig. 3d, right panel), when two different sgRNAs were used in combination, TTN transcription was stimulated from 50 to 200 fold compared to the control situation. Interestingly, when combining the four different sgRNAs in a single VLP, we obtained up to 400-fold transcription stimulation of TTN after 4 h of transduction. Our results therefore suggest that in spite of the large molecular size of the SP-dCas9-VPR (predicted at 224 kDa alone and 286 kDa when fused to MLV Gag), neither its encapsidation within VLPs nor its delivery and function within target cells are impaired. The use of Cas9 variants could therefore expand the toolbox of potential applications of Nanoblades in immortalized and primary cells.

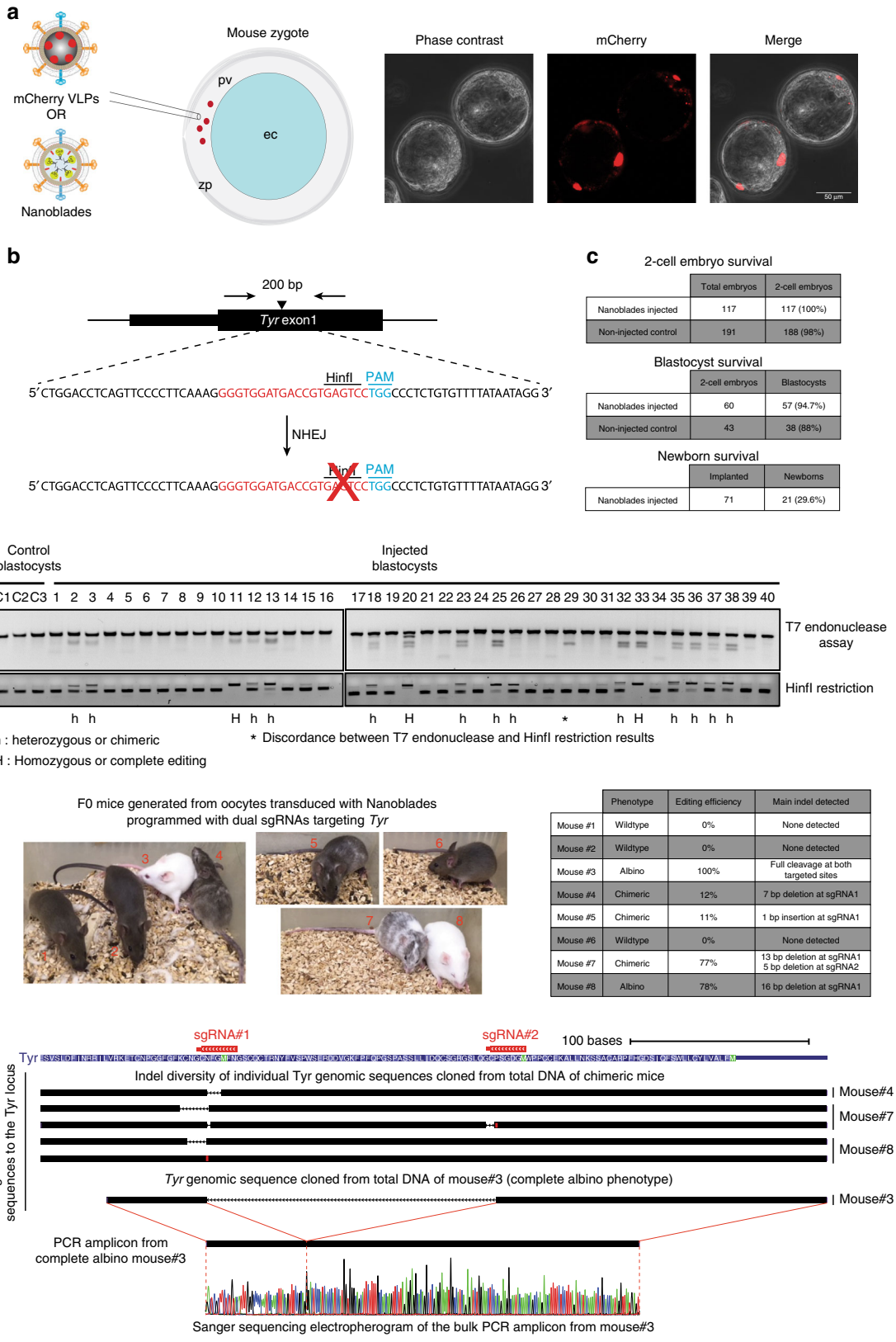

Nanoblades-mediated transduction of mouse zygotes. CRISPR-Cas9 has been extensively used to generate transgenic animals through microinjection of zygotes with DNA coding for Cas9 and the sgRNA or with the synthetic sgRNA and a Cas9 coding mRNA or directly with the preassembled Cas9-sgRNA RNP[21]. However, some of these options usually require injection into the pronucleus or the cytoplasm of zygotes, which can significantly impact their viability. Moreover, in some species, pronucleus and even cytoplasmic microinjection can be technically challenging.

Because Nanoblades are programmed to fuse with their target cells, we reasoned that they could also transduce murine zygotes without requiring intracellular microinjection. To test this

Fig. 4 Generation of transgenic mice using Nanoblades. **a** Left panel, scheme describing injection of mCherry VLPs or Nanoblades in the perivitelline space of mouse 1-cell embryos. Right panel, fluorescence microscopy of mouse blastocysts injected with mCherry VLPs at the single-cell stage. **b** Scheme of the design strategy to target the mouse *Tyr* locus (adapted from ref. [22]). Upon editing and NHEJ repair, the HinfI restriction site becomes inactive. **c** Survival rates of injected embryos at two-cell, blastocyst, and newborn stage (the latter obtained from experiments presented in Supplementary figure 5). **d** T7 endonuclease (top panel) and HinfI restrictions (bottom panel) assays on PCR fragments amplified from the *Tyr* locus of Control or Nanoblades-injected embryos. **e** Top left panel, photographs of F0 mice generated from embryos injected with Nanoblades programmed with two sgRNAs targeting the *Tyr* locus. Top-right panel, phenotype, editing efficiency (as measured by TIDE analysis of the Sanger-sequencing electropherograms) and the main INDEL type as detected by Sanger sequencing of individual PCR clones. Bottom-panel, alignment of individual PCR clones obtained from the *Tyr* locus of F0 mice against the mouse mm10 genome indicating the main observed INDELs in chimeric mice (mouse #4, #7, and #8) and total excision of the *Tyr* sequence between the sgRNA1 and sgRNA2 targeting loci for the complete albino mouse (mouse #3). The Sanger sequencing electropherogram from the bulk PCR amplicon obtained from mouse #3 indicates complete editing at both targeted sites

hypothesis, VLPs loaded with the mCherry protein (instead of Cas9) were produced and injected in the perivitelline space of mouse zygotes (Fig. 4a, top panel). Embryos were harvested 80 h after injection (blastocyst stage) and visualized by fluorescence microscopy, showing mCherry protein delivery within embryo cells (Fig. 4a, right panel).

Nanoblades programmed with a sgRNA targeting the first exon of the tyrosinanse (*Tyr*) gene previously described in ref. [22] were produced and injected in the perivitelline space of mouse zygotes. This particular sgRNA was specifically designed to target a HinfI restriction site in the *Tyr* gene that should be disrupted upon dsDNA cleavage and NHEJ repair[22] (Fig. 4b). 80 h after injection, blastocysts were harvested and genomic DNA extracted to monitor genome-editing by PCR amplification followed by T7 endonuclease assay or HinfI restriction. As observed (Fig. 4d), 16 out of 40 blastocysts were positive for genome-editing at the *Tyr* gene both for the T7 endonuclease and the HinfI restriction assays. Interestingly, three blastocysts (#11, #20, and #33) appeared to bear complete *Tyr* editing as we could not detect any residual HinfI restriction products (Fig. 4d). In the remaining 13 blastocysts that were positive for genome editing at the *Tyr* locus, we observed different editing efficiencies thus arguing for variable levels of mosaicism between individuals (Fig. 4d). Interestingly, injection of Nanoblades in the perivitelline was not associated with embryo mortality as we did not obtain any significant difference in survival rates between injected and non-inject embryos (Fig. 4c). To further validate these results, we produced Nanoblades programmed with two sgRNAs targeting the *Tyr* locus (see Fig. 4e bottom scheme) that were injected in the perivitelline space of single-cell embryos, which were then implanted into pseudopregnant females and carried to term. In this case, five out of eight F0 mice obtained carried detectable *Tyr* editing both at the phenotype and genotype level as assayed by PCR amplification of the *Tyr* locus from genomic DNA extracted from the fingers of each animal (Fig. 4e). Interestingly, one of the two fully albino mice carried a complete deletion of the DNA segment between the two sgRNA-targeted loci in all tested cells (as assayed by Sanger sequencing of the bulk PCR product and Sanger sequencing of single clone PCR fragments (Fig. 4e bottom panels)). The remaining F0 mice that displayed a partial *Tyr* disruption phenotype had an editing efficiency ranging from 11% up to 78% of all *Tyr* alleles (Fig. 4e see table). Sanger sequencing of individual PCR clones amplified from these mice indicated that one of the two sgRNAs (sgRNA1) was more efficient in inducing INDELs (Fig. 4e bottom scheme). Moreover, we also detected some degree of mosaicism within each individual mouse (with the exception of mouse #3 which had complete bi-allelic excision of the *Tyr* sequence between the two target loci) with at least two types of INDELs detected in mice 7 and 8 (Fig. 4e, see genomic alignment scheme). This, however, is very similar to the degree of mosaicism found in other approaches[22,23]. Taken together, these results validate the use of Nanoblades to generate transgenic mice upon perivitelline injection of single-cell embryos.

To further confirm the ability of Nanoblades to mediate genome-editing in mouse embryos and transmission of the edited locus to the offspring, we designed a sgRNA targeting the loxP sequence that could mimic the action of the Cre recombinase by removing a loxP flanked cassette (Supplementary Figure 5, left panel). These Nanoblades were first tested in primary BM cells derived from R26R-EYFP transgenic mice bearing a single-copy of the YFP transgene under control of a "lox-stop-lox" cassette[24] (Supplementary Figure 5, top right panel). Nanoblades were then injected in the perivitelline space of heterozygous R26R-EYFP 1-cell embryos which were then implanted into pseudopregnant females and carried to term. In this case, 1 out of 14 founder animals was YFP positive under ultraviolet (UV) light and displayed efficient excision of the "lox-stop-lox" cassette as confirmed by PCR[25] (Supplementary Figure 5, bottom left panel). Consistent with our previous results, the F1 progeny obtained after mating the loxed F0 mouse with a wild-type mouse contained the "loxed" version of the YFP allele and displayed YFP expression in tails and muscle fibers (Supplementary Figure 5, bottom right panel), indicating efficient transmission of the loxed allele from the F0 founder to its progeny.

Taken together, Nanoblades can represent a viable alternative to classical microinjection experiments for the generation of transgenic animals, in particular for species with fragile embryos or with poorly visible pronuclei.

In vivo editing of *Hpd* in the liver of tyrosinaemic FRG mice. Hereditary tyrosinemia type I (HT1) is a metabolic disease caused by disruption of fumarylacetoacetate hydrolase (*Fah*), which is an enzyme required in the tyrosine catabolic pathway. Fah-/- mice recapitulate many phenotypic characteristics of HT1 in humans, such as hypertyrosinemia and liver failure and have to be treated with nitisinone for their survival. Disruption of hydroxyphenylpyruvate dioxigenase (HPD, the enzyme targeted by nitisinone) through hydrodynamic tail vein injection in Fah-/- mice was recently shown to restore their survival in the absence of nitisinone thanks to the selective advantage of Hpd negative hepatocytes[26]. We therefore reasoned that Nanoblades could represent a non-invasive method to inactivate the *Hpd* gene in NRG (NODFah-/-/Rag2-/-/Il2rg-/-) mice[27]. To this aim, we designed a sgRNA directed against the fourth exon of *Hpd*, which should disrupt the reading frame through the INDELs caused by NHEJ (see Methods section for the sequence). Nanoblades directed against *Hpd* or against human *EMX1* (control) were introduced in NRG mice through retro-orbital injection (Fig. 5a). Upon injection, mice were weaned off nitisinone until they reached a 20% loss of their body weight, in which case nitisinone was subsequently administered punctually. Two weeks after injection, all mice injected with Nanoblades targeting *Hpd* displayed detectable editing in the liver (between 7% and 13%

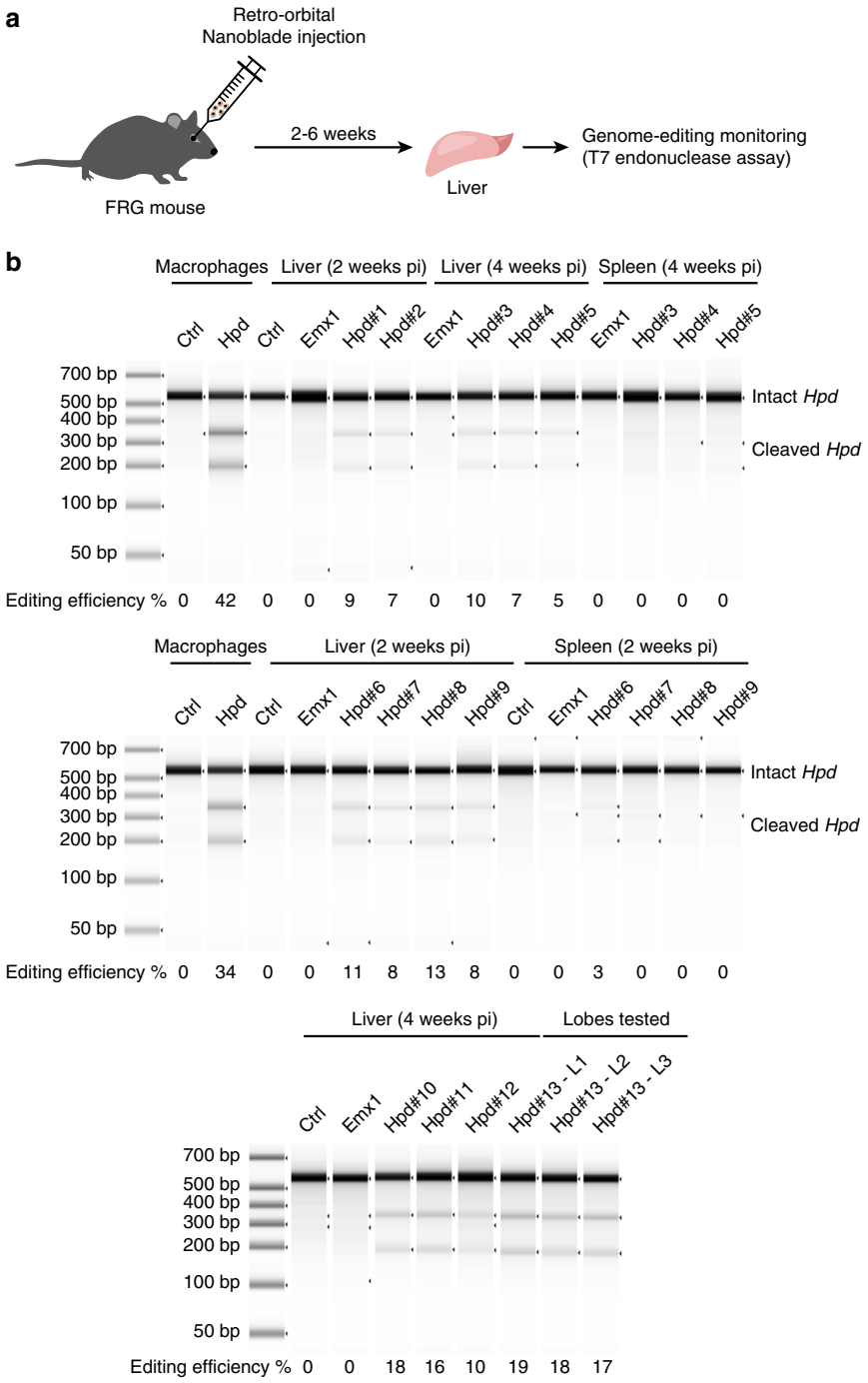

Fig. 5 Inactivation of *Hpd* in the liver of tyrosinaemic FRG mice. **a** Scheme of the experimental approach to target the liver of FRG mice. **b** T7 endonuclease assay to monitor genome editing at the *Hpd* gene in immortalized mouse macrophages and in the liver or spleen of injected mice. Samples were quantified using a Tapestation chip

efficiency, Fig. 5b). On the contrary, no editing was detected in control (uninjected) mice or in mice injected with Nanoblades targeting human *EMX1* (Fig. 5b). Similar results were obtained 4 weeks post-injection where all mice injected with Nanoblades targeting *Hpd* displayed genome editing in the liver (Fig. 5b). Furthermore, genome-editing occurred in a homogenous fashion across the liver as shown by T7 endonuclease assay from biopsies recovered from three different lobes of a single animal (Fig. 5b, bottom panel). In contrast, editing in other organs, such as spleen was weak or not detectable (Fig. 5b).

Interestingly, we observed a small overall increase in editing levels at 4 weeks post-injection compared to 2 weeks post-injection suggesting that cells with Hpd editing could have a selective advantage over non-edited cells (Fig. 5b compare middle and bottom panel). Because we did not monitor genome editing earlier than 2 weeks post injection, we cannot rule out that a similar selective advantage of edited cells might have occurred during this incubation time. Nevertheless, based on the weak increase of the editing efficiency observed between 2 and 4 weeks after injection, we do not expect this selective advantage to significantly improve the observed editing efficiency during the first 2 weeks after injection. Importantly, Nanoblades injection was not associated with any signs of morbidity.

Discussion

Genome editing should ideally be achieved in a fast and precise fashion to limit toxicity and possible off-target effects due to a sustained expression of effectors. In this regard, extensive efforts have been recently described to vehicle Cas9-sgRNA RNPs in cultured cells and in vivo by non-coding material including Nanocarriers[28], optimized transfection reagents[18], or lentivirus-derived particles[29].

This work describes and characterizes VLPs to efficiently vectorize the CRISPR-Cas9 system into primary cells, embryos, and animals. These non-coding agents—we called herein Nanoblades—incorporate the Cas9 endonuclease into their internal structure. The molecular basis of this technology is the fusion of Cas9 from *Streptococcus pyogenes* to Gag from MLV. Expressed with other components of viral assembly and construct encoding gRNA(s), this molecule can bind sgRNAs into producer cells, forms RNP complexes and cohabit with Gag and Gag-Pol within particles. We indeed show that robust packaging of sgRNAs into Nanoblades depends on their interaction with Gag::Cas9 (Supplementary Figure 1d).

When compared to other methods of delivery such as lipofection or electroporation, Nanoblades were more efficient and rapid in inducing dsDNA breaks both in immortalized U2OS cells, primary fibroblasts (Fig. 1b, Supplementary Figure 1e). Nanoblades are also functional in primary cells that are known to be difficult to transfect and transduce using classical delivery methods, such as human iPS cells, human CD34+ and primary mouse bone-marrow cells (Fig. 2) reaching efficiencies comparable or even superior to other recent methods[30,31], such as Cas9-sgRNA ribonucleoprotein electroporation (Fig. 2c), together with low off-target effects (Fig. 3b and c). Furthermore, Nanoblades achieve genome editing in a dose-dependent manner (Fig. 1c). Beyond delivery of Cas9-sgRNA complexes, we also show that Nanoblades can be complexed with DNA repair templates to mediate homologous recombination-based knock-in cultured cells in the absence of any transfection reagent. Our results also validate the use of Nanoblades in vivo for generating transgenic mice upon embryo injection in the perivitelline space (Fig. 4 and Supplementary Figure 5) or in the liver of injected animals (Fig. 5). Although, other recent methods for in vivo genome editing of zygotes and animals have reached higher editing rates[22,23,32–34], Nanoblades represent a viable, inexpensive, and accessible alternative that can still benefit from further improvements.

Similarly to other cell-derived particles (including most viral vectors), Nanoblades incorporate RNAs and proteins from producer cells that could be responsible for the transmission of undesired effects. Mass spectrometry analysis of the content of Nanoblades revealed that plasma membrane terms were particularly enriched, which is consistent with the vesicular nature of Nanoblades (Supplementary Figure 2a and Supplementary Data 1). As previously described for retroviral-VLPs[35], characterization of the RNA content revealed that Nanoblades contain thousands of individual cellular mRNA species, most of these being encapsidated stochastically, in proportion to their abundance in the producer cell. We found that transcripts overexpressed for production purposes (GAG, VSV-G, etc.) represent <0.4% of Nanoblades RNAs (Supplementary Figure 2b) supporting the notion that their delivery to recipient cells is marginal. Confirming this observation, transfer of cellular proteins loaded in Nanoblades from producer cells to recipient cells appears to be minimal and restricted to a short time window between 8 and 24 h after transduction (Supplementary Figure 2c and d). While we cannot exclude the fact that VLPs may be responsible for some cellular responses, depending on the nature of recipient cells, efficient doses of Nanoblades were globally harmless for most primary cells we tested and in injected animals. In our effort to exploit the retroviral nature of Nanoblades, we explored diverse pseudotyping options (Supplementary Figure 6) and finally focused on the use of an original mixture of two envelopes (VSV-G plus BRL), a recipe that we have optimized (Supplementary Figure 6) and which systematically displayed the best cleavage results in most recipient cells. Depending on the cellular target, it may be possible to pseudotype Nanoblades with envelopes from Measles virus[36], influenza virus[37], or other targeting systems[38,39] to restrict or improve Cas9 delivery to certain cell types (Supplementary Figure 6a).

Next generation Nanoblades may also benefit from the continual evolutions of Cas9-derivatives that can support fusion with Gag from MLV (Fig. 3) and could be adapted to other gene-editing targetable nucleases like Cpf1 nucleases[40] or even the latest generation of programmable base editors[41]. We also noted that Nanoblades can be engineered to accommodate other proteins/RNAs in addition to Cas9-RNPs and serve as multifunctional agents. Nanoblades capable of delivering both Cas9-RNPs and a reverse-transcribed template that can serve for reparation by homologous-recombination could therefore be envisioned. Furthermore, multiple sgRNAs can be incorporated within Nanoblades thus allowing gene excisions or multiple genes to be targeted. Multiplexing of sgRNAs may also allow the introduction of an additional sgRNA targeting a specific gene that will allow selection of cells efficiently edited by Nanoblade-mediated CRISPR[42].

This versatility allows any laboratory equipped with BSL2 facilities to generate its own batches of particles. Beyond cell lines, our VLP-based technique provides a powerful tool to mediate gene editing in hiPSCs and primary cells including macrophages, human hematopoietic progenitors and primary hepatocytes. We have shown that Nanoblades injection into the perivitelline space of mouse-zygotes was particularly harmless for the recipient cells, since none of the injected zygotes were affected in their development after treatment. Generation of transgenic animals upon perivitelline space injection of VLPs could be adapted to other species, including larger animals for which the number of zygotes is limited. Finally, we achieved significant gene-editing in the liver of injected adult mice with no consequences on their viability. Nanoblades, could therefore represent an interesting route for the delivery of Cas9 in vivo to inactivate gene expression but also used in combination with other viral delivery tools carrying a donor DNA template (such as Adeno-associated virus (AAV)) to perform in vivo HDR experiments as recently shown[32].

Considering the examples provided in our work, we believe that the Nanoblade technology will facilitate gene editing in academic laboratories working with primary cells and could represent a viable alternative for therapeutical purposes and the rapid generation of primary cell-types harboring genetic diseases, humanized-liver mouse models and transgenic animal models.

Methods

Plasmids. SP-dCas9-VPR was a gift from George Church (Addgene plasmid #63798). Lenti CRISPR was a gift from F. Zhang (Addgene plasmid #49535). The GagMLV-CAS9 fusion was constructed by sequential insertions of PCR-amplified fragments in an eukaryotic expression plasmid harboring the human cytomegalovirus early promoter (CMV), the rabbit Beta-globin intron and polyadenylation signals. The MA-CA-NC sequence from Friend MLV (Accession Number: M93134) was fused to the MA/p12 protease-cleavage site (9 aa) and the Flag-nls-spCas9 amplified from pLenti CRISPR.

Cell culture. Gesicle Producer 293T (Clontech 632617), U2OS cells, and primary human fibroblasts (Coriell Institute, GM00312) were grown in DMEM supplemented with 10% fetal calf serum (FCS).

hiPSCs were obtained and cultured as described in ref. [43].

Bone marrow-derived macrophages (BMDMs) were differentiated from BM cells obtained from wild-type C57BL/6 mice. Cells were grown in DMEM

supplemented with 10% FCS and 20% L929 supernatant containing MCSF as described in ref. [44]. Macrophages were stimulated for the indicated times with LPS (Invivogen) at a final concentration of 100 ng/ml.

CD34+-cell sample collection, isolation, and transduction. Cord blood (CB) samples were collected in sterile tubes containing the anti-coagulant, citrate-dextrose (ACD, Sigma, France) after informed consent and approval was obtained by the institutional review board (Centre international d'infectiologie (CIRI), Lyon, France) according to the Helsinki declaration. Low-density cells were separated over, Ficoll-Hypaque. CD34+ isolation was performed by means of positive selection using magnetic cell separation (Miltenyi MACs) columns according to the manufacturer's instructions (Miltenyi Biotec, Bergisch Gladbach, Germany). Purity of the selected CD34+ fraction was assessed by FACS analysis with a phycoerythrin (PE)-conjugated anti-CD34 antibody (Miltenyi Biotec, Bergisch Gladbach, Germany) and exceeded 95% for all experiments. Human CD34+ cells were incubated for 18–24 h in 24-well plates in serum-free medium (CellGro, CellGenix, Germany) supplemented with human recombinant: SCF (100 ng/ml), TPO (20 ng/ml), Flt3-L (100 ng/ml) (Myltenyi, France). 5×10^4 prestimulated CD34+ cells were then incubated with nanoblades in 48-well plates in serum-free medium.

sgRNA design and sequences (+PAM). sgRNAs targeting *MYD88*, *DDX3*, *GFP*, *Hpd, Fto, Tyr,* and the *LoxP* sequence were designed using CRISPRseek[45].
Human *AAVS1:* 5′ ACCCCACAGTGGGGCCACTAggg 3′
Human *DDX3*: 5′ AGGGATGAGTCATGTGGCAGtgg 3′
Human *EMX1*: 5′ GAGTCCGAGCAGAAGAAGAAggg 3′
Human *MYD88* #1: 5′ GAGACCTCAAGGGTAGAGGTggg 3′
Human *MYD88* #2: 5′ GCAGCCATGGCGGGCGGTCCtgg 3′
Human rDNA: 5′ CCTTCTCTAGCGATCTGAGagg 3′
Human *TTN* -169: 5′ CCTTGGTGAAGTCTCCTTTGagg 3′
Human *TTN* -252: 5′ ATGTTAAAATCCGAAAATGCagg 3′
Human *TTN* -326: 5′ GGGCACAGTCCTCAGGTTTGggg 3′
Human *TTN* -480: 5′ ATGAGCTCTCTTCAACGTTAagg 3′
Mouse *Fto:* 5′ CATGAAGCGCGTCCAGACCGcgg 3′
Mouse *Hpd*: 5′ GAGTTTCTATAGGTGGTGCTGGGTGggg 3′
Mouse *Tyr*: 5′ GGGTGGATGACCGTGAGTCCtgg 3′ obtained from Chen et al. [22]
Mouse Tyr: 5′ AACTTCATGGGTTTCAACTGcgg 3′ obtained from Yoon et al. [23]
Mouse *Tyr:* 5′ ATGGGTGATGGGAGTCCCTGcgg 3′ this study
LoxP: 5′ CATTATACGAAGTTATATTAagg 3′
GFP: 5′ CGAGGAGCTGTTCACCGGGGtgg 3′

Production of Nanoblades. Nanoblades were produced from transfected gesicles producer 293T cells plated at 5×10^6 cells/10 cm plate 24 h before transfection with the JetPrime reagent (Polyplus). Plasmids encoding the GagMLV-CAS9 fusion (1.7 µg), Gag-POLMLV (2.8 µg), gRNA expressing plasmid(s) (4.4 µg), VSV-G (0.4 µg), the Baboon Endogenous retrovirus Rless glycoprotein (BaEVRless)[15] (0.7 µg) were cotransfected and supernatants were collected from producer cells after 40 h. For production of serum-free particles, medium was replaced 24 h after transfection by 10 ml of Optimem (Gibco) supplemented with penicillin–streptomycin. Nanoblade-containing medium was clarified by a short centrifugation ($500 \times g$ 5 min) and filtered through a 0.8 µm pore-size filter before ultracentrifugation (1h30 at $96{,}000 \times g$). Pellet was resuspended by gentle agitation in 100 µl of cold 1X PBS. Nanoblades were classically concentrated 100-fold. X-Nanoblades referred as Nanoblades loaded with gRNA(s) targeting the x-gene.

To dose Cas9 packaged into particles, Nanoblades or recombinant Cas9 (New England Biolabs) were diluted in 1X PBS and serial dilutions were spotted onto a Nitrocellulose membrane. After incubation with a blocking buffer (nonfat Milk 5% w/v in TBST), membrane was stained with a Cas9 antibody (7A9-3A3 clone, Cell signaling) and revealed by a secondary anti-mouse antibody coupled to horseradish peroxidase. Cas9 spots were quantified by Chemidoc touch imaging system (Biorad).

Transduction procedure. Transductions with Nanoblades were performed in a minimal volume to optimize cell/particles interactions for at least 2 h before supplementing with fresh medium. When specified, polybrene was used at a final concentration of 4 µg/ml in the transduction medium. After dosing Cas9 amount in each Nanoblades preparation, we typically used 10 pmol of encapsidated Cas9 for 1×10^5 adherent cells.

sgRNA in vitro transcriptions. sgRNAs were in vitro transcribed using the EnGen sgRNA Synthesis kit, *S. pyogenes* (New England Biolabs; E3322S) following the manufacturer's protocol with the following oligonucleotides:
Human *EMX1*: 5′ TTCTAATACGACTCACTATAgagtccgag cagaagaagaaGTTTTAGAGCTAGA 3′
Mouse *Fto:* 5′ TTCTAATACGACTCACTATAgcatgaagcgcgtc cagaccgGTTTTAGAGCTAGA 3′
After transcription, sgRNAs were purified by acidic phenol/chloroform extraction and precipitated using 2.5 volumes of 100% ethanol. sgRNA integrity was then assessed by denaturing urea polyacrylamide gel electrophoresis.

Cas9-sgRNA RNP electroporation procedure. Cas9-sgRNA RNP electroporation was performed as described in the manufacturer's protocol. Briefly, 12 pmol of recombinant Cas9 (EnGen Cas9 NLS, S. pyogenes; New England Biolabs; M0646T) were incubated with 12 pmol of in vitro transcribed sgRNAs in the presence of Resuspension Buffer R (Neon Transfection System; ThermoFisher Scientific; MPK1025) for 20 min at room temperature. After this, 1×10^5 cells resuspended in 5 µl of resuspension buffer R (for HEK293T cells) or resuspension buffer T (for primary mouse BM cells) are added to the Cas9-sgRNA mix and the whole mixture electroporated with the following settings:
-1700 V, 20 ms, 1 pulse (HEK293T cells)
-1350 V, 10 ms, 4 pulses (mouse BM cells)
-1680 V, 20 ms, 1 pulse (mouse BM cells)
Upon electroporation, cells were incubated in their corresponding medium (DMEM complemented with 10% FCS for HEK293T cells and DMEM complemented with 10% FCS and 20% L929 supernatant containing MCSF for 24 h before extracting their genomic DNA to assess genome editing.

Combination of Nanoblades with ssDNA and dsDNA. Nanoblades programmed to target the AUG codon of *DDX3* were resuspended in PBS 2% FBS and combined with ssDNA donor repair template (see the sequence of "Flag-DDX3 primer" below) at a final concentration of 0.3, 1.3 or 6.7 µM in 30 µl of PBS supplemented with polybrene (Sigma) at 4 µg/ml. Complexes were let 15 min on ice before addition to 7×10^4 HEK293T cells plated 6 h before in 400 µl of complete medium supplemented with polybrene (4 µg/ml). 24 h latter, transduction medium was supplemented with 1 ml of fresh medium (10% FCS) and cells were passed the day after into six-well plates for amplification. Cells were amplified in 10 cm dishes and passed six times during 3 weeks before extraction of proteins and genomic DNAs.
Sequence of the Flag-DDX3 primer (HPLC-purified):
5′-ACTCGCTTAGCAGCGGAAGACTCCGagTTCTCGGTA CTCTTCAGGGATGGA
CTACAAGGACGACGATGACAAGagTCATGTGGCAGTG GAAAATGCGCTCGGGCTGGACCAGCAGGTGA-3’
DDX3 amplification was performed using the following primers: DDX3-Forward 5′-CTTCGCGGTGGAACAAACAC-3′ and DDX3-Reverse1 5′-CGCCATTAGCCAGGTTAGGT-3′ for the "Insertion PCR assay" and Flag-Forward 5′-GACTACAAGG ACGACGATGACAAG-3′ and DDX3-Reverse2 5′-CGCCATTA GCCAGGTTAGGT-3′ for the "Orientation PCR assay". PCR conditions were performed as follows: 94 °C 5 min, followed by three cycles (94 °C 30 s, 64 °C 30 s, 72 °C 30 s), followed by 25 cycles (94 °C 30 s, 57 °C 30 s, 72 °C 30 s), followed by 5 min at 72 °C.
dsDNA (AAVS1): 10 µl of concentrated Nanoblades were complexed with 650 ng of dsDNA in a total volume of 30 µl of PBS with polybrene at a final concentration of 4 µg/ml. After 15 min of incubation on ice, complexes were used to transduce 1×10^5 HEK293T cells in a 24-well plate containing medium supplemented with polybrene (4 µg/ml). Two days latter cells were reseeded in a 10 cm dish before puromycin selection (0.5 µg/ml). Single-cell-derived clones were next isolated and cultivated in a 12-well plates before PCR analysis performed on genomic DNAs (500 ng).
Primers used to assess the presence of the puromycin cassette are:
Puromycin-forward 1: 5′-GGCAGGTCCTGCTTTCTCTGAC-3′
Puromycin-reverse 1: 5′-GATCCAGATCTGGTGTGGCGCG TGGCGGGGTAG-3′
Followed by a nested-PCR using the following primers:
Puromycin-forward 2: 5′-GATATACGCGTCCCAGGGCCGG TTAATGTGGCTC-3′
Puromycin-reverse 1: 5′-GATCCAGATCTGGTGTGGCGCG TGGCGGGGTAG-3′
Primers used to assess correct integration of the cassette at the AAVS1 locus are:
AAVS1-forward: 5′-CGGAACTCTGCCCTCTAACGCTG-3′
Puromycin reverse 2: 5′-GATCCAGATCTGGTGTGGCGCG TGGCGGGGTAG-3′
Followed by a nested-PCR using the following primers:
AAVS1-forward: 5′-GGCAGGTCCTGCTTTCTCTGAC-3′
Puromycin reverse 3: 5′-CACCGTGGGCTTGTACTCGGT CAT-3′

Flag-immunoprecipitation and western-blotting. For Flag-immunoprecipitation, 5×10^6 cells were lysed in 500 µl of lysis buffer (NaCl 300 mM, $MgCl_2$ 6 mM, Tris–HCl 15 mM, 0.5% NP40). 250 µl of the cell lysate (1 mg of total proteins) was incubated with 40 µl of M2-antiFlag magnetic beads (Sigma M8823) equilibrated in TBS. After incubation for 2 h at 4 °C, beads were washed four times in lysis buffer and proteins eluted in 60 µl of TBS supplemented with Flag-peptide (120 µg/ml final) for 2 h at 4 °C. The supernatant (without beads) was then collected and used for western-blot analyses.
Western-blotting against Flag-DDX3 and endogenous DDX3 was performed using the following antibodies: anti-DDX3 (rabbit, Sigma 19B4, 1/1000 dilution), Flag-M2 Antibody (mouse, Sigma F3165, 1/2000 dilution), and actin antibody (mouse, Sigma A1978, 1/10,000 dilution). The uncropped images for

Supplementary Figs. 1a, 2d, 3d and 2b–d, 3a, 4d are provided in Supplementary Fig. 7.

T7 endonuclease assay. Genomic DNA was extracted from VLP-treated cells using the Nucleospin gDNA extraction kit (Macherey-Nagel). 150 ng of genomic DNA was then used for PCR amplification. PCR products were diluted by a factor 2 and complemented with Buffer 2 (New England Biolabs) to a final concentration of 1×. Diluted PCR amplicons were then heat denatured at 95 °C and cooled down to 20 °C with a 0.1 °C/s ramp. Heteroduplexes were incubated for 30 min at 37 °C in presence of 10 units of T7 Endonuclease I (NEB). Samples were finally run on a 2.5% agarose gel or on a BioAnalyzer chip (Agilent) to assess editing efficiency.

Reverse-transcription and quantitative PCR. Total RNAs were extracted using TriPure Isolation Reagent (Roche, 11667165001) following the manufacturer's instructions. 1.5 µg of total RNA was treated with DNase and reverse-transcribed using Maxima First Strand cDNA Synthesis Kit for RT-qPCR (Thermo Scientific, K1672) following the manufacturer's instructions. qPCR experiments were performed on a LightCycler 480 (ROCHE) in technical triplicates in 10 µl reaction volume as follows: 5 µl of 2X SYBR qPCR Premix Ex Taq (Tli RNaseH Plus) (TAKARA, TAKRR420W); forward and reverse primers (0.5 µM each final); 7.5 ng of cDNA.

Immunofluorescence and imaging. Cells were fixed in 1X PBS supplemented with 4% of paraformaldehyde (PFA) for 20 min, washed three times with 1X PBS and permeabilized with 0.5% Triton X-100 for 4.5 min. Cells were incubated with primary antibodies overnight at 4 °C. Primary antibodies used are: rabbit γH2AX (1:1000; Abcam 81299) and mouse RNA pol I RPA194 (1:500; Santacruz sc48385). Cells were washed three times in 1X PBS, followed by incubation of the secondary antibodies conjugated to Alexa 488 or 594 used at a 1:1000 dilution (Life Technologies) for 1 h at room temperature. After three 1X PBS washes, nucleus were stained with Hoechst 33342 at 1 µg/ml for 5 min. The coverslips were mounted in Citifluor medium (AF1, Citifluor, London, UK). Cells were observed under a Leica DM6000. At least 100 cells were counted in each indicated experiment. Averages and standard deviation values were obtained from three independent biological replicates.

Flow cytometry analysis of CD81 expression. 1×10^6 HepG2 or HEK293T cells were detached from the cell culture plate using Accutase (Stemcell technologies #07920) and washed twice in PBS + 2%BSA. Cells were then incubated in 100 µl of PBS + 2%BSA + Anti-CD81 (BD Biosciences #555675, clone JS-81, 1/200 dilution) for 30 min at 4 °C. Cells were then washed three times in PBS + 2% BSA and incubated in 100 µl of PBS + 2 %BSA + anti-mouse FITC (Biolegend # 406001, 1/2000 dilution) for 30 min at 4 °C in the dark. Cells were then washed three times in PBS + 2%BSA and fixed with 4% of paraformaldehyde (PFA) for 15 min and washed in PBS + 2%BSA before flow cytometry analysis on a BD FACSCanto II.

Northern-blot of sgRNAs. 2 µg of total RNA extracted from Nanoblades or Nanoblade-producing cells were run on a 10% acrylamide, 8 M Urea, 0.5X TBE gel for 1 h at 35 W. RNAs were then transferred onto a Nitrocellulose membrane (Hybond Amersham) by semi-dry transfert for 1 h at 300 mA in 0.5X TBE. The membrane was UV-irradiated for 1 min using a stratalinker 1800 and then baked at 80 °C for 30 min. The membrane was then incubated in 50 ml of Church buffer (125 mM Na_2HPO_4, 0.085% phosphoric acid, 1 mM EDTA, 7% SDS, 1% BSA) and washed twice in 10 ml of Church buffer. The 5′ P32-labeled (1×10^7 cpm total) and heat-denatured ssDNA probe directed against the constant sequence of the guideRNA (sequence of the sgRNA antisense probe: 5′GCACCGACTCGGTGCCACTTTTTCAAGTTGATAACGGACTAGCCTTATTTTAACTTGCTATTTCTAGCTCTA3′) was diluted in 10 ml of Church buffer and incubated with the membrane overnight at 37 °C. The membrane was washed four times in 50 ml of wash buffer (1X SSC + 0.1% SDS) before proceeding to phosphorimaging.

Transmission electron microscopy (TEM) and mass spectrometry (MS). Nanoblades programmed to target the YFP were prepared and processed for TEM and MS as previously described[46]. Briefly, Nanoblades were produced from transfected Gesicles Producer 293T cells plated at 5×10^6 cells/10 cm plate 24 h before transfection with the JetPrime reagent (Polyplus) and supernatants were collected from producer cells after 40 h, passed through a 0.45 µm filter and concentrated 100-fold by overnight centrifugation at 3800 × *g*. This preparation was next laid overlaid on a continuous optiprep gradient and ultracentrifuged to obtain density fractions. Fractions containing Nanoblades were next pooled and centrifuged overnight at 3800 × *g* before PBS resuspension to obtain a 6000×-concentrated sample.

For electron microscopy, after a flash-fixation in glutaraldehyde, staining was amplified using the R-Gent Kit (Biovalley, Marne-la-Vallee, France) before the negative coloration (phosphotungstic acid 2%). Specimen were observed under a JEM-1400 microscope (Jeol, Tokyo, Japan) coupled with the Orius-600 camera (Gatan, Pleasanton, CA).

High-troughput sequencing of RNAs extracted from Nanoblades. Total RNA was extracted from purified Nanoblades programmed to target the YFP using Trizol. RNAs were then fragmented to 100nt and used as input for the preparation of cDNA libraries following the protocol described in ref. [47]. Briefly, RNA fragments with a 3′-OH were ligated to a preadenylated DNA adaptor. Following this, ligated RNAs were reverse transcribed with Superscript III (Invitrogen) with a barcoded reverse-transcription primer that anneals to the preadenylated adaptor. After reverse transcription, cDNAs were resolved in a denaturing gel (10% acrylamide and 8 M urea) for 1 h and 45 min at 35 W. Gel-purified cDNAs were then circularized with CircLigase I (Epicentre) and PCR-amplified with Illumina's paired-end primers 1.0 and 2.0.

Analysis of high-troughput sequencing data was performed as previously described[48]. Briefly, reads were split with respect to their 5′-barcode sequence. After this, 5′-barcode and 3′-adaptor sequences were removed from reads. Reads were mapped to a custom set of sequences including 18S, 28S, 45S, 5S, and 5.8S rRNA, tRNAs, the sgRNA directed against the GFP sequence and all transcripts coding for Nanoblades components (Envelopes, Gag and Pol, Cas9) using Bowtie[49]. Reads that failed to map to this custom set of sequences were next aligned to University of California, Santa Cruz (UCSC) human hg18 assembly using TopHat2[50]. Read counts on all transcripts of interest were obtained using the HTSeq count package[51].

High-throughput sequencing of Emx1 On-target and Off-target loci. Genomic DNA was extracted from Nanoblades-treated cells using the Nucleospin gDNA extraction kit (Macherey-Nagel). 150 ng of genomic DNA was then used for PCR amplification using primers specific for the *EMX1* On-target locus (EMX1-Forward 5′-ACACTCTTTCCCTACACGACGCTCTTCCGATCTGGTTCCAGAACCGGAGGACAAAGTAC-3′ and EMX1-Reverse 5′-GTGACTGGAGTCCTCTCTATGGGCAGTCGGTGAAGCCCATTGCTTGTCCCTCTGTCAATG-3′) and the previously described Off-target locus in the intron of *MFAP1 (MFAP1*-Forward 5′-ACACTCTTTCCCTACACGACGCTCTTCCGATCTCCATCACGGCCTTTGCAAATAGAGCCC-3′ and MFAP1-Reverse 5′-GTGACTGGAGTCCTCTCTATGGGCAGTCGGTGACAGAGGGAACTACAAGAATGCCTGAGC-3′) bearing adapters sequencing for Illumina's Miseq platform. Obtained PCR products were purified and PCR amplified with a second set of primers bearing specific barcodes for multiplex sequencing. Final PCR products were sequenced on the Miseq platform using a custom sequencing primer (Miseq-Custom 1: 5′ ATCACCGACTGCCCATAGAGAGGACTCCAGTCAC 3′) and a custom index sequencing primer (Miseq-Custom 2: 5′ GTGACTGGAGTCCTCTCTATGGGCAGTCGGTGAT 3′).

Animal experimentation. All animal experiments were approved by a local ethics committee of the Université de Lyon (CECCAPP, registered as CEEA015 by the French ministry of research) and subsequently authorized by the French ministry of research (APAFIS#8154-2016l12814462837 v2 for the generation of transgenic animals and C 69 123 0303 for the usage of Nanoblades in vivo). All procedures were in accordance with the European Community Council Directives of September 22, 2010 (2010/63/EU) regarding the protection of animals used for scientific purposes.

Mouse oocyte injection. Four or five weeks old FVB/NRj female mice (Janvier Labs, France) were superovulated by intraperitoneal (i.p.) administration of 5 IU of pregnant mare serum gonadotropin (PMSG, Alcyon, France), followed by an additional i.p. injection of 5 IU human chorion gonadotropin 48 h later (hCG, Alcyon, France). Superovulated females were mated with B6D2F1 adult males (1 male/2 females) and euthanatized at 0.5 day post coitum (usually between 10 and 11 a.m.). Oviduct were dissected, and the ampulla nicked to release zygotes associated with surrounding cumulus cells into a 200 µl droplet of hyaluronidase (Sigma) in M2 solution (300 µg/ml, Sigma) under a stereomicroscope (Olympus SZX9). Zygotes were incubated for 1 min at room temperature and passed with a mouth pipette through three washes of M2 medium to remove cumulus cells. Zygotes were kept in M16 medium (Sigma) in a water jacketed CO_2 incubator (5% CO_2, 37 °C) until microinjection with Nanoblades. Micro-injection were carried-out under a stereomicroscope (Olympus SZX9) using a FemtoJet 4i (Eppendorf) microinjecter. Briefly, 1 pl of Nanoblades were injected in the perivitelline space of oocytes. Zygotes were then transferred into M16 medium and kept overnight in incubator. The embryos that reached the two-cell stage were transferred into the oviduct of B6CBAF1 (Charles River, France) pseudopregnant females (15–20 embryos per female).

Retro-orbital injection of Nanoblades. All experiments were performed in accordance with the European Union guidelines for approval of the protocols by the local ethics committee (Authorization Agreement C2EA 15, "Comité Rhône-Alpes d'Ethique pour l'Expérimentation Animale", Lyon, France). The highly Immunosuppressed NOD FRG mice (Fah-/-/Rag2-/-/Il2rg-/-) (Yecuris cooration), deficient for T-cell, B-cell, and NK-cell are maintained in pathogen-free facility. Retro-orbital injection (SRO) were performed under isoflurane anesthésia.

Genomic DNA from each mouse (treated either by control or *Hpd* targeting Nanoblades) was extracted from three distinct liver lobes and pooled together.

Following this, a two-step PCR was performed on 300 ng of gDNA template, the first PCR using primers Hpd-Forward 1: 5′-CTTAGGAGGTTAGCCAAAGATG GGAG-3′ and Hpd-Reverse 1: 5′-TCTAGTCTCTATCCAGGGCTCCAGCC-3′ to amplify the *Hpd* gene (94 °C 5 min, 3 cycles 94 °C, 64 °C, 72 °C, and 20 cycles 94 °C, 58 °C, 72 °C, 5 min 72 °C). The second nested-PCR used primers Hpd-Forward 2: 5′-GAACTGGGATTGGCTAGTGCG-3′ and Hpd_Reverse 2: 5′-CACCCAG CACCACCTATAGAAACTC-3′ (94 °C 5 min, 3 cycles 94 °C, 64 °C, 72 °C and 30 cycles 94 °C, 57 °C, 72 °C, 5 min 72 °C). Amplicons were next analyzed by T7-endonuclease assay as described.

Raw data files. Uncropped scans of ethidium bromide gels and western-blotting figures are displayed in Supplementary Figure 7.

Data availability

Gene Expression Omnibus: GSE107035. The following plasmids will be available from Addgene: Gag::Cas9 fusion (BIC-Gag-CAS9, Plasmid ID: 119942), the Gag:: Cas9-VPR fusion (BICstim-Gag-dCAS9-VPR, Plasmid ID: 120922) and the Gag:: Cre fusion (GAG-CRErec, Plasmid ID: 119971).

Received: 11 December 2017 Accepted: 30 November 2018
Published online: 03 January 2019

References

1. Jinek, M. et al. A programmable dual-RNA-guided DNA endonuclease in adaptive bacterial immunity. *Sci. N. Y. NY* **337**, 816–821 (2012).
2. Gheysen, D., Jacobs, E., de Foresta, F. & Thiriart, C. Assembly and release of HIV-1 precursor Pr55gag virus-like particles from recombinant baculovirus-infected insect cells. *Cell* **59**, 103–112 (1989).
3. Kaczmarczyk, S. J., Sitaraman, K., Young, H. A., Hughes, S. H. & Chatterjee, D. K. Protein delivery using engineered virus-like particles. *Proc. Natl Acad. Sci. USA* **108**, 16998–17003 (2011).
4. Voelkel, C. et al. Protein transduction from retroviral Gag precursors. *Proc. Natl Acad. Sci. USA* **107**, 7805–7810 (2010).
5. O'connor, T. E., Rauscher, F. J. & Zeigel, R. F. Density gradient centrifugation of a murine leukemia virus. *Sci. N. Y. NY* **144**, 1144–1147 (1964).
6. Chen, B. et al. Dynamic imaging of genomic loci in living human cells by an optimized CRISPR/Cas system. *Cell* **155**, 1479–1491 (2013).
7. Gibbons, J. G., Branco, A. T., Yu, S. & Lemos, B. Ribosomal DNA copy number is coupled with gene expression variation and mitochondrial abundance in humans. *Nat. Commun.* **5**, 4850 (2014).
8. Kinner, A., Wu, W., Staudt, C. & Iliakis, G. Gamma-H2AX in recognition and signaling of DNA double-strand breaks in the context of chromatin. *Nucleic Acids Res.* **36**, 5678–5694 (2008).
9. van Sluis, M. & McStay, B. A localized nucleolar DNA damage response facilitates recruitment of the homology-directed repair machinery independent of cell cycle stage. *Genes Dev.* **29**, 1151–1163 (2015).
10. Tsai, S. Q. et al. GUIDE-seq enables genome-wide profiling of off-target cleavage by CRISPR-Cas nucleases. *Nat. Biotechnol.* **33**, 187–197 (2015).
11. Zhang, J. et al. CD81 is required for hepatitis C virus glycoprotein-mediated viral infection. *J. Virol.* **78**, 1448–1455 (2004).
12. Okabe, M., Ikawa, M., Kominami, K. & Nakanishi, T. Green mice'as a source of ubiquitous green cells. *FEBS Lett.* **407**, 313–319 (1997).
13. Brinkman, E. K., Chen, T., Amendola, M. & van Steensel, B. Easy quantitative assessment of genome editing by sequence trace decomposition. *Nucleic Acids Res.* **42**, e168 (2014).
14. Amirache, F. et al. Mystery solved: VSV-G-LVs do not allow efficient gene transfer into unstimulated T cells, B cells, and HSCs because they lack the LDL receptor. *Blood* **123**, 1422–1424 (2014).
15. Girard-Gagnepain, A. et al. Baboon envelope pseudotyped LVs outperform VSV-G-LVs for gene transfer into early-cytokine-stimulated and resting HSCs. *Blood* **124**, 1221–1231 (2014).
16. Okimoto, T., Friedmann, T. & Miyanohara, A. VSV-G envelope glycoprotein forms complexes with plasmid DNA and MLV retrovirus-like particles in cell-free conditions and enhances DNA transfection. *Mol. Ther. J. Am. Soc. Gene Ther.* **4**, 232–238 (2001).
17. Sadelain, M., Papapetrou, E. P. & Bushman, F. D. Safe harbours for the integration of new DNA in the human genome. *Nat. Rev. Cancer* **12**, 51 (2012).
18. Zuris, J. A., Thompson, D. B., Shu, Y. & Guilinger, J. P. Efficient delivery of genome-editing proteins in vitro and in vivo. *Nature* **33**, 73–80 (2015).
19. Fu, Y. et al. High-frequency off-target mutagenesis induced by CRISPR-Cas nucleases in human cells. *Nat. Biotechnol.* **31**, 822–826 (2013).
20. Chavez, A. et al. Highly efficient Cas9-mediated transcriptional programming. *Nat. Methods* **12**, 326–328 (2015).
21. Horii, T. et al. Validation of microinjection methods for generating knockout mice by CRISPR/Cas-mediated genome engineering. *Sci. Rep.* **4**, 4513 (2014).
22. Chen, S., Lee, B., Lee, A. Y.-F., Modzelewski, A. J. & He, L. Highly efficient mouse genome editing by CRISPR ribonucleoprotein electroporation of zygotes. *J. Biol. Chem.* **291**, 14457–14467 (2016).
23. Yoon, Y. et al. Streamlined ex vivo and in vivo genome editing in mouse embryos using recombinant adeno-associated viruses. *Nat. Commun.* **9**, 412 (2018).
24. Srinivas, S., Watanabe, T. & Lin, C. S. Cre reporter strains produced by targeted insertion of EYFP and ECFP into the ROSA26 locus. *BMC Ldots* **1**, 4 (2001).
25. Zhang, D. J. et al. Selective expression of the Cre Recombinase in late-stage thymocytes using the distal promoter of the Lck gene. *J. Immunol.* **174**, 6725–6731 (2005).
26. Pankowicz, F. P. et al. Reprogramming metabolic pathways in vivo with CRISPR-Cas9 genome editing to treat hereditary tyrosinaemia. *Nat. Commun.* **7**, 12642 (2016).
27. Azuma, H. et al. Robust expansion of human hepatocytes in Fah-/-/Rag2-/-/Il2rg-/- mice. *Nat. Biotechnol.* **25**, 903–910 (2007).
28. Qazi, S. et al. Programmed self-assembly of an active P22-Cas9 nanocarrier system. *Mol. Pharm.* **13**, 1191–1196 (2016).
29. Choi, J. G. et al. Lentivirus pre-packed with Cas9 protein for safer gene editing. *Gene Ther.* **23**, 627–634 (2016).
30. Wang, G. et al. Efficient, footprint-free human iPSC genome editing by consolidation of Cas9/CRISPR and piggyBac technologies. *Nat. Protoc.* **12**, 88–103 (2017).
31. Modarai, S. R. et al. Efficient delivery and nuclear uptake is not sufficient to detect gene editing in CD34+ cells directed by a ribonucleoprotein complex. *Mol. Ther.—Nucleic Acids* **11**, 116–129 (2018).
32. Yin, H. et al. Therapeutic genome editing by combined viral and non-viral delivery of CRISPR system components in vivo. *Nat. Biotechnol.* **34**, 328–333 (2016).
33. Lau, C.-H. & Suh, Y. In vivo genome editing in animals using AAV-CRISPR system: applications to translational research of human disease. *F1000Res.* **6**, 2153 (2017).
34. Yin, H. et al. Structure-guided chemical modification of guide RNA enables potent non-viral in vivo genome editing. *Nat. Biotechnol.* **35**, 1179–1187 (2017).
35. Rulli, S. J. et al. Selective and nonselective packaging of cellular RNAs in retrovirus particles. *J. Virol.* **81**, 6623–6631 (2007).
36. Frecha, C. et al. Stable transduction of quiescent T cells without induction of cycle progression by a novel lentiviral vector pseudotyped with measles virus glycoproteins. *Blood* **112**, 4843–4852 (2008).
37. Szécsi, J. et al. Targeted retroviral vectors displaying a cleavage site-engineered hemagglutinin (HA) through HA-protease interactions. *Mol. Ther. J. Am. Soc. Gene Ther.* **14**, 735–744 (2006).
38. Morizono, K. et al. Lentiviral vector retargeting to P-glycoprotein on metastatic melanoma through intravenous injection. *Nat. Med.* **11**, 346–352 (2005).
39. Morizono, K. et al. Redirecting lentiviral vectors pseudotyped with Sindbis virus-derived envelope proteins to DC-SIGN by modification of N-linked glycans of envelope proteins. *J. Virol.* **84**, 6923–6934 (2010).
40. Zetsche, B. et al. Cpf1 is a single RNA-guided endonuclease of a class 2 CRISPR-Cas system. *Cell* **163**, 759–771 (2015).
41. Gaudelli, N. M. et al. Programmable base editing of A•T to G•C in genomic DNA without DNA cleavage. *Nature* **551**, 464–471 (2017).
42. Agudelo, D. et al. Marker-free coselection for CRISPR-driven genome editing in human cells. *Nat. Methods* **14**, 615–620 (2017).
43. Massouridès, E. et al. Dp412e: a novel human embryonic dystrophin isoform induced by BMP4 in early differentiated cells. *Skelet. Muscle* **5**, 40 (2015).
44. Carpenter, S. et al. A long noncoding RNA mediates both activation and repression of immune response genes. *Sci. N. Y. NY* **341**, 789–792 (2013).
45. Zhu, L. J., Holmes, B. R., Aronin, N. & Brodsky, M. H. CRISPRseek: a bioconductor package to identify target-specific guide RNAs for CRISPR-Cas9 genome-editing systems. *PLoS ONE* **9**, e108424 (2014).
46. Mangeot, P.-E. et al. Protein transfer into human cells by VSV-G-induced nanovesicles. *Mol. Ther. J. Am. Soc. Gene Ther.* **19**, 1656–1666 (2011).
47. Heyer, E. E., Ozadam, H., Ricci, E. P., Cenik, C. & Moore, M. J. An optimized kit-free method for making strand-specific deep sequencing libraries from RNA fragments. *Nucleic Acids Res.* **43**, e2 (2015).
48. Ricci, E. P. et al. Staufen1 senses overall transcript secondary structure to regulate translation. *Nat. Struct. Mol. Biol.* **21**, 26–35 (2014).
49. Langmead, B., Trapnell, C., Pop, M. & Salzberg, S. L. Ultrafast and memory-efficient alignment of short DNA sequences to the human genome. *Genome Biol.* **10**, R25 (2009).

50. Kim, D. et al. TopHat2: accurate alignment of transcriptomes in the presence of insertions, deletions and gene fusions. *Genome Biol.* **14**, R36 (2013).
51. Anders, S., Pyl, P. T. & Huber, W. HTSeq—a Python framework to work with high-throughput sequencing data. *Bioinformatics* **31**, 166–169 (2015).

Acknowledgements

Sequencing was performed by the IGBMC Microarray and Sequencing platform, a member of the 'France Génomique' consortium (ANR-10-INBS-0009). We acknowledge the contribution of SFR Biosciences (UMS3444/CNRS, US8/Inserm, ENS de Lyon, UCBL) facilities: Platim and PBES (Celphedia, AniRA). We also thank J.F. Henry, N. Aguilera, and J.L. Thoumas from the animal facility (PBES, Plateau de Biologie Expérimentale de la Souris, ENS de Lyon), as well as A. Ollivier for their technical help in handling mice. We thank Claire Lionnet from Platim for technical assistance in taking confocal fluorescence images. We thank Elisabeth Errazuriz-Cerda and the CeCIL-facility (Lyon, France) for the preparation and the observation of samples by TEM and Yohann Couté and the edyp-service (Grenoble, France) for the proteomic analysis. We thank Gérard Benoît for his help in preparing final figures. This work was funded by Labex Ecofect (ANR-11-LABX-0048) of the Université de Lyon, within the program Investissements d'Avenir (ANR-11-IDEX-0007) operated by the French National Research Agency (ANR), Fondation FINOVI and Agence Nationale des Recherches sur le SIDA et les Hépatites Virales (ANRS—ECTZ3306) to E.P.R. Open access fees were funded by the European Research Council (ERC-StG-LS6-805500 to E.P.R.) under the European Union's Horizon 2020 research and innovation programs.

Author contributions

P.E.M. and E.P.R. conceived the study and designed most experiments. P.E.M., E.P.R., V.R., A.M., E.L., F.F., E.V., F.L.C., T.S. and F.A. designed experiments. P.E.M., E.P.R., E.L., V.R., A.M., F.F., T.S., F.A., J.B., E.V., V.M., M.T., and E.M. performed experiments and analyzed data. P.E.M. and E.P.R. wrote the paper with contributions from all authors.

Additional information

Supplementary Information accompanies this paper at https://doi.org/10.1038/s41467-018-07845-z.

Competing interests: P.E.M., T.O., and E.P.R. are named as inventors on a patent relating to the Nanoblades technology (patent applicants: Institut National de la Sante et de la Recherche Medicale (INSERM), Centre National de la Recherche Scientifique (CNRS), Ecole Normale Superieure de Lyon, Universite Claude Bernard Lyon 1, Villeurb-Anne Cedex; name of inventors: Theophile Ohlmann, Mathieu Misery, Philippe Mangeot, Emiliano Ricci; application number: WO 2017/068077 Al; patent status: published, 27th April 2017; all aspects of the manuscript are covered by the patent application. The remaining authors declare no competing interests.

Reprints and permission information is available online at http://npg.nature.com/reprintsandpermissions/

Journal peer review information: *Nature Communications* thanks the anonymous reviewers for their contribution to the peer review of this work. Peer reviewer reports are available.

Publisher's note: Springer Nature remains neutral with regard to jurisdictional claims in published maps and institutional affiliations.

Open Access This article is licensed under a Creative Commons Attribution 4.0 International License, which permits use, sharing, adaptation, distribution and reproduction in any medium or format, as long as you give appropriate credit to the original author(s) and the source, provide a link to the Creative Commons license, and indicate if changes were made. The images or other third party material in this article are included in the article's Creative Commons license, unless indicated otherwise in a credit line to the material. If material is not included in the article's Creative Commons license and your intended use is not permitted by statutory regulation or exceeds the permitted use, you will need to obtain permission directly from the copyright holder. To view a copy of this license, visit http://creativecommons.org/licenses/by/4.0/.

© The Author(s) 2019